Dissertation

SUBMITTED TO THE

Combined Faculties of the Natural Sciences and Mathematics
of the Ruperto-Carola-University of Heidelberg, Germany

FOR THE DEGREE OF

Doctor of Natural Sciences

Put forward by

Chunhai Lyu (吕纯海)

Born in: Guang'an, Sichuan/ People's Republic of China

(出生地:中华人民共和国四川省广安市邻水县合流镇绿化村)

Oral examination: 04.07.2018

Narrow-band hard-X-ray lasing

Referees: **Hon. Prof. Dr. Christoph H. Keitel**
Prof. Dr. Jörg Jäckel

Zusammenfassung

Die Erzeugung von schmalbandigen, vollständig kohärenten Röntgenlasern basierend auf stimulierter Emission in hochgeladenen Ionen, wird untersucht. Das hier vorgeschlagene Lasingschema führt zu Röntgenquellen mit hoher räumlicher und zeitlicher Kohärenz, die neue Anwendungen in der Röntgenquantenoptik ermöglichen. Hochgeladene Ionen können in Plasmen erzeugt werden, die durch linienfokussierte intensive optische Laser erzeugt werden. Die Besetzungsinversion zwischen den Zuständen $1s2l$ ($l = s, p$) und $1s^2$ in He-ähnlichen Ionen wird durch Innerschalen-Photoionisation von Li-ähnlichen Ionen mit intensiven Freie-Elektronen-Röntgenlaser-Pulsen erreicht. Wir zeigen, dass das Lasing in Elementen wie Ne, Ar, Kr und Xe durch $E1$-, $M1$- oder $M2$-Übergänge erfolgen kann. Die entsprechenden Maxwell-Bloch Gleichungen werden unter Einbeziehung von Multipol-Wechselwirkungen zwischen den Röntgenfeldern und den Ionen entwickelt. Numerische Simulationen zeigen, dass die auf diese Weise erzeugten Röntgenlaser durch hohe Intensitäten und Femtosekunden-Pulsdauern charakterisiert sind. Die relativen Bandbreiten von $\Delta\omega/\omega = 10^{-5} - 10^{-7}$ sind um bis zu 3 Größenordnungen kleiner als bei Pulsen von modernen Röntgenquellen bei Wellenlängen bis hinunter zum Sub-Ångström-Bereich. Analytische Lösungen der Maxwell-Bloch-Gleichungen in der "exponential-gain"-Näherung ergeben Ergebnisse, die mit numerischen Simulationen für die Puls- und Spektrumprofile konsistent sind.

Abstract

The generation of narrow-band fully coherent x-ray lasers based on stimulated emission in highly charged ions is investigated. The lasing scheme we put forward leads to x-ray sources with high spatial and temporal coherence, enabling new applications in x-ray quantum optics. Highly charged ions can be generated in plasmas created by line-focused intense optical lasers. Population inversion between the $1s2l$ ($l = s, p$) and $1s^2$ states in He-like ions is obtained by inner-shell photoionization of Li-like ions with intense x-ray free-electron laser pulses. We show that lasing can happen in elements such as Ne, Ar, Kr and Xe through $E1$, $M1$ or $M2$ transitions. The corresponding Maxwell–Bloch equations are developed with the inclusion of multipole interactions between the x-ray fields and the ions. Numerical simulations show that the x-ray lasers generated this way are characterized by high intensities and with femtosecond pulse durations. The relative bandwidths of $\Delta\omega/\omega = 10^{-5} - 10^{-7}$ achieved are by up to 3 orders of magnitude narrower than in pulses from state-of-art x-ray sources at wavelengths down to the sub-ångström regime. Analytical solutions of the Maxwell–Bloch equations in the exponential-gain approximation are found to give results consistent with numerical simulations for the pulse and spectral profiles.

Within the framework of this thesis, the following article was submitted to a refereed journal:

In Chapter 5:

- ***Narrow-band hard-X-ray lasing***
  Chunhai Lyu (吕纯海), Stefano M. Cavaletto, Christoph H. Keitel and Zoltán Harman. arXiv:1801.02503.

Articles in preparation:

In Chapter 3:

- ***Maxwell–Bloch theory for multipole radiation***
  Chunhai Lyu (吕纯海), Stefano M. Cavaletto, Christoph H. Keitel and Zoltán Harman.

In Chapter 6:

- ***Analytical solution to the Maxwell–Bloch equations describing transient lasing***
  Chunhai Lyu (吕纯海), Stefano M. Cavaletto, Christoph H. Keitel and Zoltán Harman.

Contents

Chapter 1

Introduction

History of X-ray lasers

In 1953, Charles Townes and his colleagues at Columbia University created the first *maser* (microwave amplification by stimulated emission of radiation), where microwave radiation is amplified through stimulated emission from excited ammonia molecules in a resonant cavity [1]. The generated coherent electromagnetic wave, with a wavelength of $\lambda = 1.25$ cm (24 GHz), triggered wide-ranging applications in microwave communication. Thereafter, a theoretical proposal to extend this technology to the optical regime was raised, in 1958, by Townes and his colleagues in Bell Laboratories [2]. This new concept known as *laser* (light amplification by stimulated emission of radiation), firstly demonstrated by Theodore Maiman with a ruby crystal medium ($\lambda = 694.3$ nm) in 1960 at Hughes Research Laboratories [3], was widely replicated in varieties of gain media in solid, gas and liquid states in the 1960s [4–6]. Compared to candles and light bulbs which emit random uncorrelated photons in all directions, a laser generates coherent photons propagating in a well-defined single direction. As a result, the intensity of a laser is more than 6 orders of magnitude higher than the light field generated by conventional light sources with the same emission power. The availability of intense coherent radiation at optical frequencies had a major impact, leading to revolutionary applications in scientific and industrial research, as well as in medicine.

Early X-ray sources were mostly based on X-ray tubes. Similarly to candles and light bulbs, these X-ray sources emit incoherent broadband radiation into a wide range of directions. Therefore, when the maser and laser were invented, great efforts were devoted to extending the stimulated-emission scheme to shorter wavelengths such as the soft and hard X-ray regime ($\lambda < 0.1$ nm). The laser was demonstrated only 8 years after the creation of the maser, achieving a reduction of the wavelength by 5 orders of magnitude. However, a further reduction of the working wavelength to XUV and X-ray frequencies was very challenging [7–12]. Difficulties in atom-based short-wavelength lasers mainly come from two aspects: firstly, the large transition energies for short-wavelength photons demand a huge amount of pump power which could only be achieved when intense laser pulses became available; secondly, the large penetration lengths of short-wavelength photons render it hard to fabricate high-reflectivity normal-incident cavity mirrors, as required for a laser to reach saturation intensity. This issue was partly solved after 1985, in a different way, by using plasmas as the gain medium to generate XUV and soft-X-ray lasers (soft-XRLs) at wavelengths around 20 nm [13–18]. Because the plasma produces a density of population inversion orders of magnitude higher than in solid state lasers, the corresponding soft-XRLs can reach the saturation intensity with single-pass or double-pass amplification [19].

Plasma-based soft-XRLs are mainly based on $3p \rightarrow 3s$ or $4d \rightarrow 4p$ transition in highly charged Ne- or Ni-like ions for elements varying from ${}_{14}$Si to ${}_{79}$Au (the atomic numbers for Ne and Ni are 10 and 28, respectively). The population inversion is achieved through

Sources	Wavelength	Pulse duration	Coherences	Spectral width $\delta\omega/\omega$	Repetition rate (Hz)	Brightness ph/s/mm^2/mrad^2/0.1%bw
X-ray tubes	fixed by discharge voltage	continuous	spatial: no temporal: no	broadband	continuous	10^6
Synchrotrons (storage rings)	down to 0.017 Å (up to 750 keV)	$\sim$ 100 ps	spatial: yes temporal: no	broadband	continuous	$10^{12} \sim 10^{24}$
Plasma-XRLs	down to 3.5 nm (up to 0.34 keV)	down to 450 fs	spatial: no temporal: yes	$\sim 10^{-4}$	1 – 10 Hz	$10^{26} \sim 10^{27}$
HHG	down to 0.33 nm (up to 3.8 keV)	attosecond	spatial: yes temporal: yes	$\sim 10^{-3}$	1 kHz	$\sim 10^{22}$
SASE XFELs	down to 0.04 nm (up to 30 keV)	2 – 200 fs	spatial: yes temporal: no	$10^{-3} \sim 10^{-4}$	60 Hz – 1 MHz	$10^{33} \sim 10^{34}$
Seeded XFELs	down to 0.13 nm (up to 9 keV)	25 fs	spatial: yes temporal: yes	$10^{-4} \sim 10^{-5}$	10 – 120 Hz	$10^{33} \sim 10^{35}$
Inner-shell XRLs	1.46 nm (0.85 keV) 0.15 nm (8 keV)	$<$ 20 fs	spatial: yes temporal: yes	$\sim 10^{-4}$	120 Hz	10^{29}
This thesis	down to 0.04 nm (up to 30 keV)	10 fs – 1 ps	spatial: yes temporal: yes	$10^{-5} \sim 10^{-7}$	120 Hz	$10^{31} \sim 10^{34}$

Table 1.1: Ranges of key parameters of different X-ray sources.

electron collisional excitation in a hot dense plasma produced either by high-peak-power lasers [9, 11, 20], or by fast high-voltage discharge in a capillary [8, 21]. Another mechanism based on recombination-assisted population inversion between the $n = 3 \rightarrow 2$ and $n = 2 \rightarrow 1$ transitions, in H-like Li created by optical-field-induced ionization, was also demonstrated and resulted in a laser at a wavelength of $\lambda = 13.5$ nm [22, 23]. Until now, the shortest wavelength reported with these methods is $\lambda = 3.56$ nm based on Ni-like Au [20]. Though the recombination scheme based on the $n = 2 \rightarrow 1$ transition can scale the wavelength down to $\lambda < 0.1$ nm for elements with high atomic numbers, population inversion can hardly be obtained for elements heavier than carbon [15]. Nonetheless, these soft X-ray sources have found versatile applications in X-ray microscopy, holography and plasma diagnostics [8, 9, 11].

The first hard-XRL was initially proposed through direct pumping of the $1s^{-1} \rightarrow 2p^{-1}$ transition via photoionization of a K-shell electron in 1967 by Duguay and Rentzepis [24]. The same photoionization pumping scheme was subsequently reintroduced by theorists based on different gain media and pump sources [25–29]. Limited by the high pump power required, however, this inner-shell XRL scheme was demonstrated in Ne (1.46 nm) [30] and Cu (0.15 nm) [31] only in recent years after high-flux X-ray free-electron lasers (XFELs) became available.

Free-electron lasers (FELs) belong to a separate class of coherent electromagnetic radiation sources compared to the bound-electron-based atomic lasers discussed above [32–35]. Initially introduced and demonstrated by John Madey at Stanford in the 1970s [36, 37], the mechanism is based on the stimulated emission of bremsstrahlung when free electrons pass through a periodic magnetic field. In the first demonstration of FELs in 1977, a 43-MeV electron beam from a superconducting accelerator was injected into a 5-m long wiggler, generating radiation at a wavelength $\lambda = 3.4$ μm [37]. Early research on FELs is based on theories in the small-gain regime where the radiation field is assumed to be constant during the whole interaction with electrons. When a self-consistent theory was formulated, a high-gain regime with exponential amplification of the radiation field was found by Saldin and Kondratenko in 1980 [38, 39]. Thereafter, the self-amplified spontaneous emission (SASE) mechanism, as well as the extension of the scheme for the generation of short-wavelength FELs using relativistic electron beams, were extensively studied in the 1980s [38, 40–42]. These theoretical considerations were followed by the first realization of the SASE-FEL concept in 1997, which demonstrated a gain of 10^5 at wavelengths around 12 μm [43] in the infrared regime. Several years later in 2000,

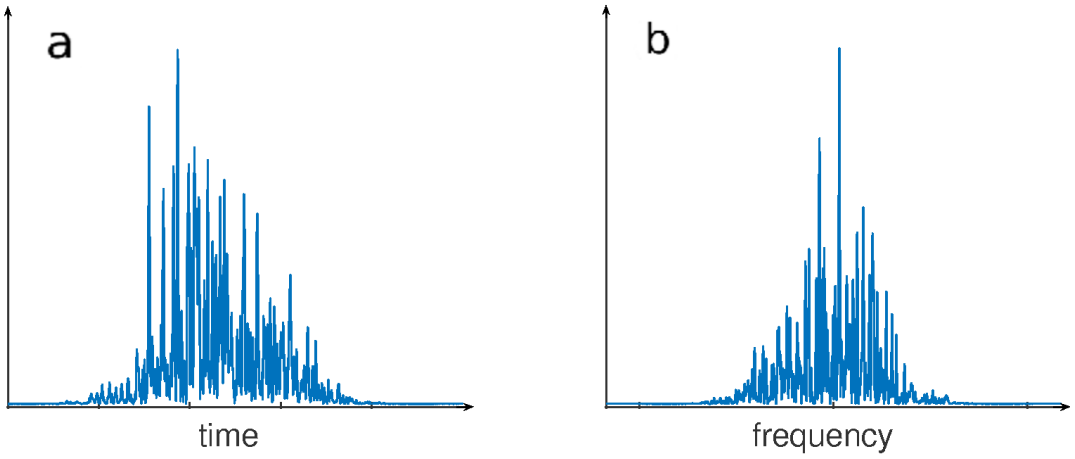

Figure 1.1: Typical pulse (a) and spectral (b) profiles for a single-shot SASE XFEL pulses. The behaviors of these profiles underly significant changes from shot to shot.

the first saturated SASE FEL was achieved at Argonne National Laboratory with visible (530 nm) and ultraviolet (UV) (390 nm) wavelengths [44]. Subsequently, similar saturation regimes were produced for FELs in the vacuum-UV (VUV) regime (98 nm) at DESY in 2001 [45, 46]. After this significant progress, the FELs can deliver high-brightness radiation in the far-infrared and VUV-frequency domain that can hardly be achieved with conventional atomic lasers.

The era of XFEL science started in 2005 when FLASH, the first soft X-ray FEL in the world, became accessible to the user community [47, 48]. This was then embraced by a worldwide construction of new XFEL facilities over the past decade [49]. This includes the first lasing of a hard X-ray FEL at LCLS in USA (2009, [50]), followed by SACLA in Japan (2011, [51]), the Fermi-FEL in Italy (2012, [52]), the PAL-XFEL in South Korea (2016, [53]), the SwissFEL in Switzerland (2016, [54]), the Shanghai-XFEL in China (2019, [55]) as well as the European-XFEL funded by the European Union (2016, [56]). By virtue of their spatial coherence, short pulse duration (femtosecod range), high peak brightness and broad wavelength tunability (0.04–52 nm), XFELs have found extensive applications in physics, chemistry and structural biology [57–62]. However, as shown in Fig. 1.1, the temporal coherence of the XFEL sources is rather poor [63–65]. Therefore, they are still limited in applications in X-ray quantum optics.

Besides these two types of X-ray lasers, there is another type of coherent X-ray source which is based on high-order harmonic generation (HHG) via free-bound transitions [66–69]. Though these sources enable the generation of fully coherent X-ray radiation at wavelengths as short as 0.33 nm [70–72], a high brightness only retains for wavelengths longer than 10 nm [73]. Nevertheless, this coherent radiation source is the only one that provides attosecond pulses which enable research on the ultrafast dynamics of electrons in atoms.

In this thesis, we put forward a scheme that combines the advantages of both plasma-based XRLs (good temporal coherence) and the high-brightness XFELs, to produce fully coherent high-intensity hard-X-ray lasers at wavelengths down to the sub-ångström regime [74]. Such XRLs may enable the study of X-ray quantum optics [75–78] and metrology [79], the investigation of nonlinear interactions between X rays and matter [80, 81], or high-precision spectroscopic studies in laboratory astrophysics [82].

Coherence properties of X-ray sources

Ever since its discovery in 1895 by Wilhelm Röntgen at the University of Würzburg, X-ray radiation has become a major tool triggering many ground-breaking discoveries in science. This includes the establishment of X-ray crystallography in 1912 by Laue and Braggs [83, 84] with the direct confirmation of the long-disputed periodic arrangement of atoms and molecules in crystals. When similar diffraction techniques were applied to non-crystalline materials, it resulted in the discovery of the double-helix structure of DNA by James Watson and Francis Crick in 1953 [85]. Furthermore, the first X-ray radiograms (1895) as well as the X-ray computed tomography (CT) developed in the 1970s [86] have found invaluable applications in medical imaging and industrial non-destructive testing [34].

These applications are successful because they rely on X-ray absorption or far-field diffraction that only require information on the intensity of the radiation. The next step of X-ray science would be to explore the applications based on the phase information of the X-ray photons [87]. To name a few, this includes X-ray holography [88–91], coherent diffraction imaging [73, 92] and quantum control in X-ray quantum optics [75, 79, 93]. For such techniques to work, it is essential to achieve a large number of coherent photons. Table 1.1 shows the ranges of the key parameters for different X-ray sources. The traditional X-ray tube source is characterized by poor coherence properties and small brightness. Though one can improve the degree of the temporal and the spatial coherence through monochromators and apertures, respectively [34], this leads to the reduction of the number of photons. Thus, sources with high brightness are demanded. As an example, when Hartmut Michel (Nobel laureate in chemistry in 1988) obtained the first diffraction pattern of single crystals of protein in 1981, the exposure times were typically several hours with a laboratory-based source (X-ray tubes). However, with synchrotrons, this can be achieved within minutes [94]. With XFEL pulses, their high brightness (10 orders of magnitude higher compared to synchrotron sources) even enables single-shot coherent imaging [95, 96]. Moreover, nonlinear interaction between X-rays and matter are also accessible [62, 80, 81, 97].

However, most of the XFEL facilities in operation or under construction generate X-ray pulses based on the SASE process. Despite their high peak brightness, these pulse are characterized by random spikes in both time and spectral domains. This results in a relative bandwidth of $\Delta\omega/\omega \sim 10^{-3}$. In order to improve the temporal coherence and frequency stability, different seeding schemes have been implemented successfully [52, 98–101]. In the hard-X-ray regime, the self-seeding mechanism has reduced the relative bandwidth to the level of 5×10^{-5} at photon energies of 8–9 keV [99]. However, at higher energies around 30 keV, the predicted relative bandwidth for seeded XFELs is still around 4×10^{-4} [35]. Further reduction of the bandwidth with low-gain XFEL oscillators (XFELOs) has also been proposed [102]. By recirculating the X-ray pulses through an undulator in a cavity, the output X-rays have an estimated relative bandwidth as small as 10^{-7}. To date, however, the XFELO scheme remains untested.

Motivation and structure of the thesis

The aim of this thesis is to explore an alternative scheme for generating fully coherent high-intensity X-ray pulses other than the inner-shell XRLs listed in Table 1.1. The inner-shell XRLs, as shown in Fig. 1.2a, are achieved by direct pumping of the K_α transitions through photoionization of K-shell electrons. However, due to the large

number of electrons in the outer shells, the upper-lasing state is dominated by Auger processes which limits the density and lifetime of population inversion. The XFEL-pumped plasma-XRLs put forward in Chapter 5 of this thesis exclude the fast Auger decay processes from the upper lasing levels, resulting in an X-ray laser with relative bandwidths of $\Delta\omega/\omega = 10^{-5} \sim 10^{-7}$, which are orders-of-magnitude smaller than in SASE XFELs, seeded XFELs, and inner-shell X-ray lasers with neutral atoms. This can be achieved without significantly decreasing the brightness (see Table 1.1).

The main discussion of our scheme is presented in Chapter 5. The gain medium is a laser-produced plasma consisting of Li-like ions in the $1s^2 2l$ state (Fig. 1.2b). K-shell photoionizations by the XFEL pulse generate population inversions in He-like ions between the $1s2l$ and $1s^2$ states. As there are only radiative processes, one can choose a long-lived state as the upper lasing state, resulting in a much narrower bandwidth of the output laser. In particular, when choosing heavier elements such as Kr and Xe, even magnetic quadrupole transitions become available for lasing. This provides a further reduction of the bandwidth in the output X-ray pulses.

In Chapters 2–4, we introduce the theoretical description of transient X-ray lasing based on stimulated emission in a laser-produced plasma, including also all relevant broadening effects. This is based on Maxwell–Bloch theory [103, 104], a self-consistent theory that describes the interaction between light and atomic matter. When light propagates in a medium, it populates excited states and generates coherences between different bound states in atoms or molecules. On the other hand, the response of the atoms or molecules induces a polarization field that, in turn, modifies the amplitude and phase of the light fields.

The propagation equations of the light field are derived in Sec. 2.1 from Maxwell's equations under the slowly varying envelope approximation, where the variations of the amplitude in time and space are assumed to be much slower than the scale of a single period and wavelength of the light. This condition is generally met in our consideration of narrow-band X-ray lasing. The Hamiltonian describing the dynamics of the atoms is presented in the electric-dipole approximation in Sec. 2.2. This leads to the formulation of density-matrix theory for two-level systems in Sec. 2.3, where von Neumann equations are obtained in different pictures, namely, the Schrödinger picture, the interaction picture

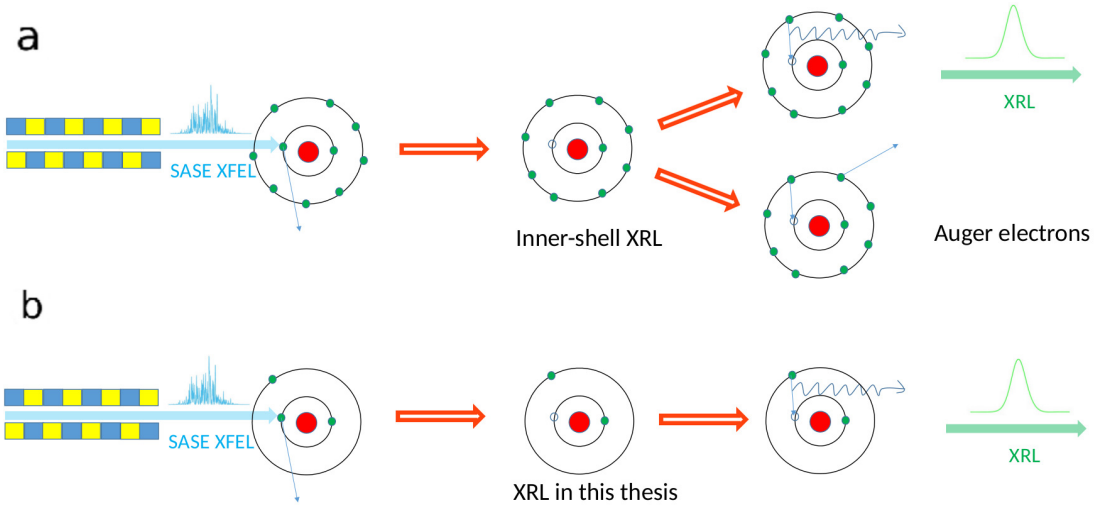

Figure 1.2: Inner-shell X-ray lasing with neutral atoms (a) and with HCIs (b). With a noisy XFEL pulse as an input, one obtains a coherent X-ray laser as output.

and the newly-defined rotating-phase picture. Connections between the polarization field and atomic coherence are discussed in detail in Sec. 2.3.2, based on which the Maxwell–Bloch equations are obtained in Sec. 2.4. Steady-state solutions to the Maxwell–Bloch equations are presented, by deriving the corresponding rate equations for describing light propagation in the medium. The rate-equation approach has been widely used in discussions of lasing processes, but our calculations show that this approach is only accurate for steady-state atomic systems, or, in other words, for the case where changes in the populations of atomic states are negligible during the presence of external fields. Otherwise, a more elaborate approach based on Maxwell–Bloch equations has to be used.

In Chapter 3, we extend the theory describing the electric-dipole transitions to multipole transitions. Our atomic calculation with the GRASP atomic structure code [105] shows that, for He-like ions, there are four main $K\alpha$ transitions, including two electric-dipole transitions, one magnetic-dipole transition and one magnetic-quadrupole transition. As all of them may have the chance to contribute to lasing, it is necessary to generalize the electric-dipole Hamiltonian to the case of a multipole Hamiltonian. Starting from the Dirac equation in the presence of a plane-wave electromagnetic field, we show that the light-matter interaction can be generally characterized by an effective dipole moment. General relationships between the effective dipole momenta and Einstein A coefficients are derived. In Sec. 3.2, based on the multipole expansion of the electromagnetic plane wave, the effective dipole momenta are expanded in series of multipole momenta. The corresponding relations between multipole momenta and Einstein A coefficients are also presented, which gives us the opportunity to obtain the value of multipole momenta from atomic codes, like GRASP for example. The Maxwell–Bloch equations are also generalized to include multipole radiations in Sec. 3.4.

In Chapter 4, different spectral broadening effects are considered. In order to produce highly charged ions, a hot dense plasma is necessary. This plasma is generally characterized by fast collisions (see also Appendix F) that may influence the bandwidth of the X-ray laser. Therefore, Doppler broadening is discussed in Sec. 4.1, and a formula for the electron impact broadening in the presence of a Coulomb scattering potential is derived in Sec. 4.2. The evaluation of this formula requires detailed calculations of atomic structures. However, we show how this formula can be approximately calculated with Einstein A coefficients and oscillator strengths from an atomic code. In the last section of this Chapter, the ionic Stark broadening of transitions in He-like ions is discussed.

The theoretical preparations in Chapters 2–4 provide the methods and formalism required to study X-ray lasing in realistic systems. Thus, in Chapter 5, numerical simulations of our lasing processes in He-like ions for noble-gas elements like Ne, Ar, Kr and Xe are performed. FLYCHK [106] simulations show that, under given densities and temperatures, significant fractions of Li- and He-like ions are obtained in laser-produced plasmas. The Chapter discusses the laser conditions needed to obtain the plasmas dominated by Li- and He-like ions. Atomic structure calculations for Einstein A coefficients, oscillator strengths and photoionization rates are also presented to obtain the associated parameters for the Maxwell–Bloch equations for realistic systems. As an exact solution of the Maxwell–Bloch equations is out of reach, we developed Fortran codes that can solve these equations numerically. This helped us to design the optimized temperatures, densities and plasma lengths needed to achieve narrow-band high-intensity X-ray lasers. The results of these simulations are discussed in Sec. 5.3–5.6. In particular, we use realistic noisy SASE-XFEL pulses to integrate the equations of motion, and show that fully coherent XRLs can be obtained with relative bandwidths of $10^{-5} \sim 10^{-7}$.

Stimulated by the numerical results above, in Chapter 6, analytical solutions to the

Maxwell–Bloch equations are presented by assuming that the laser field is underlying an exponential amplification in the gain medium. This intuitive hypothesis has also been confirmed by comparison with our numerical simulations. As a result, by introducing one parameter describing the effective gain coefficient, a relation between the laser field and the atomic coherence is obtained, which allows one to decouple the light propagation equations (Maxwell's equations) from the Bloch equations, and renders both of them analytically solvable. This analytical model allows us to predict a Gaussian X-ray laser profile, in good agreement with the numerical simulations presented in Chapter 5. Furthermore, this procedure can be generalized to different transient laser systems.

While analytical solutions of the Maxwell–Bloch equations under the assumption of exponential amplification were presented in Chapter 6 in the time domain, in Chapter 7, we study the amplification of a seeding pulse while propagating through the medium in the frequency space. In particular, we analyze two different conditions for the medium. In a steady state (or in perturbed systems), stimulated emission indicates that the photon emitted by the atom should have the same frequency, direction and polarization as the input photons. However, in a transient-gain medium, as discussed in this thesis, the populations of the atomic states feature fast modifications influencing the photons emitted by stimulation and, therefore, the photons occupy a broad frequency range.

Certain detailed calculations can be found in the appendices at the end of the thesis. Unless specifically stated, the international system of units (SI) is used.

Chapter 2

Maxwell–Bloch equations

In this Chapter, we introduce the semiclassical theories that are extensively used in Chapters 5–7 to describe light-matter interactions. For lasing, the atoms in the medium have to be treated in a quantum mechanical way, while the electromagnetic field may be described classically [107]. The propagation equations of the light field are derived in Sec. 2.1 from Maxwell's equations under the slowly varying envelope approximation, where the variations of the amplitude in time and space are assumed to be much slower than the scale of a single period and wavelength of the light. This condition is generally met in our consideration of narrow-band X-ray lasing. The Hamiltonian describing the dynamics of the atoms is presented in the electric-dipole approximation in Sec. 2.2. This leads to the formulation of density-matrix theory for two-level systems in Sec. 2.3, where von Neumann equations are obtained in different pictures, namely, the Schrödinger picture, the interaction picture and the newly-defined rotating-phase picture. Connections between the polarization field and atomic coherence are discussed in detail in Sec. 2.3.2, based on which the Maxwell–Bloch equations are obtained in Sec. 2.4. Steady-state solutions to the Maxwell–Bloch equations are presented, by deriving the corresponding rate equations for describing light propagation in the medium. The rate-equation approach has been widely used in discussions of lasing processes, but our calculations show that this approach is only accurate for steady-state atomic systems, or, in other words, for the case where changes in the populations of atomic states are negligible during the presence of external fields. Otherwise, a more elaborate approach based on Maxwell–Bloch equations has to be used.

2.1 Wave equation under slowly varying envelope approximation

In this Section, we will first review the Maxwell's equations in matter, then derive the propagation of the electromagnetic field both in time domain and in frequency domain.

2.1.1 Maxwell's equations

Microscopically, the Maxwell's equations are given as [108]

$$\nabla \cdot \mathbf{E} = \frac{\rho}{\varepsilon_0}, \tag{2.1}$$

$$\nabla \cdot \mathbf{B} = 0, \tag{2.2}$$

$$\nabla \times \mathbf{E} = -\frac{\partial \mathbf{B}}{\partial t}, \tag{2.3}$$

$$\nabla \times \mathbf{B} = \mu_0 \left(\mathbf{J} + \varepsilon_0 \frac{\partial \mathbf{E}}{\partial t} \right), \tag{2.4}$$

where $\mathbf{E}$ and $\mathbf{B}$ is the electric and magnetic field, respectively. ρ is the microscopic total charge density and $\mathbf{J}$ is the microscopic total current, including the charges and currents at the atomic level. Macroscopically, the total charge Q and total current I consists of free and bound parts:

$$Q = Q_\mathrm{b} + Q_\mathrm{f} = \iiint (\rho_\mathrm{b} + \rho_\mathrm{f})\, dV = \iiint \rho dV, \tag{2.5}$$

$$I = I_\mathrm{b} + I_\mathrm{f} = \iiint (\mathbf{J}_\mathrm{b} + \mathbf{J}_\mathrm{f}) \cdot d\mathbf{S} = \iiint \mathbf{J} \cdot d\mathbf{S}, \tag{2.6}$$

with

$$\rho = \rho_\mathrm{b} + \rho_\mathrm{f}, \tag{2.7}$$

$$\mathbf{J} = \mathbf{J}_\mathrm{b} + \mathbf{J}_\mathrm{f}, \tag{2.8}$$

where ρ_b and $\mathbf{J}_\mathrm{b}$ are the macroscopic bound charge density and bound current density, and ρ_f and $\mathbf{J}_\mathrm{f}$ are the macroscopic free charge density and free current density, respectively.

In order to treat the contributions of free charges and currents separately from the contributions of bound charges and currents, one introduces the displacement field $\mathbf{D}$ and the magnetizing field $\mathbf{H}$ with the definitions

$$\mathbf{D} = \varepsilon_0 \mathbf{E} + \mathbf{P}, \tag{2.9}$$

$$\mathbf{H} = \frac{1}{\mu_0}\mathbf{B} - \mathbf{M}. \tag{2.10}$$

Here, $\mathbf{P}$ is the polarization field and $\mathbf{M}$ is the magnetization field which are defined in terms of microscopic bound charges and currents, respectively. Macroscopically, These are given by

$$\rho_\mathrm{b} = -\nabla \cdot \mathbf{P}, \tag{2.11}$$

$$\mathbf{J}_\mathrm{b} = \nabla \times \mathbf{M} + \frac{\partial \mathbf{P}}{\partial t}. \tag{2.12}$$

This gives the macroscopic variant of Maxwell's equations

$$\nabla \cdot \mathbf{D} = \rho_\mathrm{f}, \tag{2.13}$$

$$\nabla \cdot \mathbf{B} = 0, \tag{2.14}$$

$$\nabla \times \mathbf{E} = -\frac{\partial \mathbf{B}}{\partial t}, \tag{2.15}$$

$$\nabla \times \mathbf{H} = \mathbf{J}_\mathrm{f} + \frac{\partial \mathbf{D}}{\partial t}. \tag{2.16}$$

In this set of equations, only free charges and currents are relevant.

For a source-free medium without free charges and currents, one has $\rho_\mathrm{f} = 0$ and $\mathbf{J}_\mathrm{f} = 0$. If the medium is also free of magnetization, $\mathbf{M} = 0$, then

$$\mathbf{H} = \frac{1}{\mu_0}\mathbf{B} - \mathbf{M} = \frac{1}{\mu_0}\mathbf{B}.$$

The corresponding Maxwell's equations are

$$\nabla \cdot \mathbf{D} = 0, \tag{2.17}$$
$$\nabla \cdot \mathbf{B} = 0, \tag{2.18}$$
$$\nabla \times \mathbf{E} = -\frac{\partial \mathbf{B}}{\partial t}, \tag{2.19}$$
$$\nabla \times \mathbf{B} = \mu_0 \frac{\partial \mathbf{D}}{\partial t}. \tag{2.20}$$

These equations, Eqs. (2.17-2.20), are widely used for the description of electromagnetic fields in media without magnetization effects [108]. In Chapter 3, we will generalize these equations to also include other couplings between the electromagnetic field and matter. However, within this Chapter, we only focus on the case where there is only electric dipole interaction between the field and matter. Based on Eqs. (2.17-2.20), we will derive how the electromagnetic wave may propagate in the medium.

2.1.2 Light propation in time domain

From Eqs. (2.20) and Eqs. (2.20), one obtains the relation between the electric field and the displacement field

$$\nabla \times (\nabla \times \mathbf{E}) = -\nabla \times \frac{\partial \mathbf{B}}{\partial t} = -\mu_0 \frac{\partial^2 \mathbf{D}}{\partial t^2}. \tag{2.21}$$

Using the formula

$$\nabla \times (\nabla \times \mathbf{E}) = \nabla (\nabla \cdot \mathbf{E}) - \nabla^2 \mathbf{E}, \tag{2.22}$$

one obtains

$$\nabla (\nabla \cdot \mathbf{E}) - \nabla^2 \mathbf{E} = -\mu_0 \frac{\partial^2 \mathbf{D}}{\partial t^2}. \tag{2.23}$$

Furthermore, from Eqs. (2.17) together with the definition of the displacement field in Eqs. (2.10), one has

$$\nabla \cdot \mathbf{D} = \varepsilon_0 \nabla \cdot \mathbf{E} + \nabla \cdot \mathbf{P} = 0. \tag{2.24}$$

If the polarization is uniform in space, one can take $\nabla \cdot \mathbf{P} = 0$ (discussions for the case $\nabla \cdot \mathbf{P} \neq 0$ can be found in Chapter G, or in reference [109]). This means that the divergence of the electric field is also zero, $\nabla \cdot \mathbf{E} = 0$. As a result, one has

$$\nabla \times (\nabla \times \mathbf{E}) = -\nabla^2 \mathbf{E}. \tag{2.25}$$

Accordingly, Eqs. (2.23) can be simplified to

$$\nabla^2 \mathbf{E} = \mu_0 \frac{\partial^2 \mathbf{D}}{\partial t^2}, \tag{2.26}$$

or

$$\nabla^2 \mathbf{E} - \frac{1}{c^2} \frac{\partial^2 \mathbf{E}}{\partial t^2} = \mu_0 \frac{\partial^2 \mathbf{P}}{\partial t^2}, \tag{2.27}$$

where $c = 1/\sqrt{\varepsilon_0\mu_0}$ is the velocity of light in vacuum. This equation can simply be written in a scalar form by multiplying it with the conjugate of the polarization vector of the electric field $\hat{\epsilon}^*$,

$$\nabla^2 \mathrm{E} - \frac{1}{c^2}\frac{\partial^2 \mathrm{E}}{\partial t^2} = \mu_0 \frac{\partial^2 (\mathbf{P}\cdot\hat{\epsilon}^*)}{\partial t^2}. \tag{2.28}$$

If $\mathbf{P}$ is parallel to the electric field, i.e. $\hat{\epsilon}$, one will have

$$\nabla^2 \mathrm{E} - \frac{1}{c^2}\frac{\partial^2 \mathrm{E}}{\partial t^2} = \mu_0 \frac{\partial^2 \mathrm{P}}{\partial t^2}. \tag{2.29}$$

This is always true for linearly polarized and circularly polarized light fields. For elliptical polarized light traveling through a nonlinear medium, a tensor relationship between the nonlinear polarization must be considered, and one must consider a vector wave equation.

2.1.3 Light propagation in the frequency domain

By introducing the Fourier transformation,

$$\hat{\mathbf{P}}(\mathbf{r},\omega) = \frac{1}{\sqrt{2\pi}}\int_{-\infty}^{\infty} \mathbf{P}(\mathbf{r},t)\mathrm{e}^{-i\omega t}dt, \tag{2.30}$$

$$\hat{\mathbf{E}}(\mathbf{r},\omega) = \frac{1}{\sqrt{2\pi}}\int_{-\infty}^{\infty} \mathbf{E}(\mathbf{r},t)\mathrm{e}^{-i\omega t}dt, \tag{2.31}$$

and substituting these relations into Eq. (2.27), one obtains the propagation equation in frequency domain as

$$\nabla^2 \hat{\mathbf{E}} + \frac{\omega^2}{c^2}\hat{\mathbf{E}} = -\mu_0\omega^2\hat{\mathbf{P}}. \tag{2.32}$$

Compared to Eq. (2.27), there are no time derivatives any more. This reduces the partial differential equation to an ordinary differential equation and simplifies the calculations if the expressions of polarization in frequency domain are known (Appx. G).

From the definition of Fourier transform we know that

$$\hat{F}(\omega) = \frac{1}{\sqrt{2\pi}}\int_{-\infty}^{\infty} f(t)\mathrm{e}^{-i\omega t}dt,$$

$$\hat{F}(-\omega) = \frac{1}{\sqrt{2\pi}}\int_{-\infty}^{\infty} f(t)\mathrm{e}^{i\omega t}dt.$$

When $f(t)$ is a real function, one will have

$$\hat{F}(\omega) = \hat{F}^*(-\omega).$$

The inverse Fourier transform gives

$$f(t) = \frac{1}{\sqrt{2\pi}}\int_{-\infty}^{\infty} \hat{F}(\omega)\mathrm{e}^{i\omega t}d\omega = \frac{2}{\sqrt{2\pi}}\mathrm{Re}\left\{\int_0^{\infty} \hat{F}(\omega)\mathrm{e}^{i\omega t}d\omega\right\}.$$

2.1.4 Slowly varying envelope approximation

The electric and polarization fields can be expressed as complex functions

$$\mathbf{E}(\mathbf{r},t) = \mathbf{E}^{(+)}(\mathbf{r},t) + \mathbf{E}^{(-)}(\mathbf{r},t), \tag{2.33}$$
$$\mathbf{P}(\mathbf{r},t) = \mathbf{P}^{(+)}(\mathbf{r},t) + \mathbf{P}^{(-)}(\mathbf{r},t), \tag{2.34}$$

with $\mathbf{E}^{(+)}$ being the positive-frequency part and $\mathbf{E}^{(-)}$ the negative-frequency part of the electric field, defined as

$$\mathbf{E}^{(+)}(\mathbf{r},t) = \sum_{\mathbf{k}} \hat{\epsilon}_{\mathbf{k}} \mathcal{E}_{\mathbf{k}} a_{\mathbf{k}} e^{i(\mathbf{k}\cdot\mathbf{r}-\omega_{\mathbf{k}}t+\phi_{\mathbf{k}})}, \tag{2.35}$$
$$\mathbf{E}^{(-)}(\mathbf{r},t) = \sum_{\mathbf{k}} \hat{\epsilon}^{*}_{\mathbf{k}} \mathcal{E}_{\mathbf{k}} a^{\dagger}_{\mathbf{k}} e^{-i(\mathbf{k}\cdot\mathbf{r}-\omega_{\mathbf{k}}t+\phi_{\mathbf{k}})}, \tag{2.36}$$

which is also an expansion of the electric field in different electromagnetic wave modes $\mathbf{k}$. With such a definition, the positive-frequency part $\mathbf{E}^{(+)}(\mathbf{r},t)$ only contains the annihilation operators $a_{\mathbf{k}}$ and the negative-frequency part only contains the creation operators $a^{\dagger}_{\mathbf{k}}$.

For a light wave propagating in a single direction, if the duration of the field is much longer than the period of the oscillating field, one can separate the fast oscillating component and the slowly varying component by introducing a carrier frequency ω_0 and the envelope function $\boldsymbol{\mathcal{E}}(\mathbf{r},t)$

$$\mathbf{E}^{(+)}(\mathbf{r},t) = \frac{1}{2}\boldsymbol{\mathcal{E}}(\mathbf{r},t)\, e^{i(\mathbf{k}_0\cdot\mathbf{r}-\omega_0 t+\phi(\mathbf{r},t))}, \tag{2.37}$$
$$\mathbf{E}^{(-)}(\mathbf{r},t) = \frac{1}{2}\boldsymbol{\mathcal{E}}^{*}(\mathbf{r},t)\, e^{-i(\mathbf{k}_0\cdot\mathbf{r}-\omega_0 t+\phi(\mathbf{r},t))}. \tag{2.38}$$

Similarly for the polarization field, one has

$$\mathbf{P}^{(+)}(\mathbf{r},t) = \frac{1}{2}\boldsymbol{\mathcal{P}}(\mathbf{r},t)\, e^{i(\mathbf{k}_0\cdot\mathbf{r}-\omega_0 t+\phi(\mathbf{r},t))}, \tag{2.39}$$
$$\mathbf{P}^{(-)}(\mathbf{r},t) = \frac{1}{2}\boldsymbol{\mathcal{P}}^{*}(\mathbf{r},t)\, e^{-i(\mathbf{k}_0\cdot\mathbf{r}-\omega_0 t+\phi(\mathbf{r},t))}. \tag{2.40}$$

Here, $\boldsymbol{\mathcal{E}}(\mathbf{r},t)\, e^{i\phi(\mathbf{r},t)}$ and $\boldsymbol{\mathcal{P}}(\mathbf{r},t)\, e^{i\phi(\mathbf{r},t)}$ stand for the envelope of the positive-frequency part of the electric and the polarization field, respectively. Because $\boldsymbol{\mathcal{E}}(\mathbf{r},t) = \hat{\epsilon}\mathcal{E}(\mathbf{r},t)$, in principle, $\hat{\epsilon}$ may be a complex vector (for circularly polarized light), one could always take $\mathcal{E}(\mathbf{r},t)$ and $\phi(\mathbf{r},t)$ as two real functions which refer to the amplitude and phase, respectively. For the polarization field, the relative phase with respect to the electric field is nonzero (see Sec. 2.4), therefore $\mathcal{P}(\mathbf{r},t)$ must be a complex function.

In the following, we assume that the light is propagating along the $\hat{x}$ direction. One would have

$$\mathbf{E}^{(+)}(\mathbf{r},t) = \frac{1}{2}\boldsymbol{\mathcal{E}}(x,t)\, e^{i(k_0 x-\omega_0 t+\phi(x,t))}, \tag{2.41}$$
$$\mathbf{P}^{(+)}(\mathbf{r},t) = \frac{1}{2}\boldsymbol{\mathcal{P}}(x,t)\, e^{i(k_0 x-\omega_0 t+\phi'(x,t))}. \tag{2.42}$$

where we also assume that the light field is uniform in the y–z plane, $\boldsymbol{\mathcal{E}}(\mathbf{r},t) = \boldsymbol{\mathcal{E}}(x,t)$.

These two assumptions yield

$$\nabla^2 \mathbf{E} = \frac{\partial^2 \mathbf{E}}{\partial x^2}. \tag{2.43}$$

By defining

$$Y = e^{i(k_0 x - \omega_0 t + \phi(x,t))}, \tag{2.44}$$

we first have

$$\begin{aligned}
\frac{\partial^2 \mathbf{E}^{(+)}}{\partial t^2} &= \frac{\partial^2}{\partial t^2}\left(\boldsymbol{\mathcal{E}} e^{i(k_0 x - \omega_0 t + \phi(x,t))}\right) \\
&= \frac{\partial}{\partial t}\left(\frac{\partial \boldsymbol{\mathcal{E}}}{\partial t} Y - i\omega_0 \boldsymbol{\mathcal{E}} Y + i\frac{\partial \phi}{\partial t}\boldsymbol{\mathcal{E}} Y\right) \\
&= \frac{\partial^2 \boldsymbol{\mathcal{E}}}{\partial t^2} Y - i\omega_0 \frac{\partial \boldsymbol{\mathcal{E}}}{\partial t} Y + i\frac{\partial \phi}{\partial t}\frac{\partial \boldsymbol{\mathcal{E}}}{\partial t} Y \\
&\quad -i\omega_0 \frac{\partial \boldsymbol{\mathcal{E}}}{\partial t} Y - \omega_0^2 \boldsymbol{\mathcal{E}} Y + \omega_0 \frac{\partial \phi}{\partial t}\boldsymbol{\mathcal{E}} Y \\
&\quad +i\frac{\partial^2 \phi}{\partial t^2}\boldsymbol{\mathcal{E}} Y + i\frac{\partial \phi}{\partial t}\frac{\partial \boldsymbol{\mathcal{E}}}{\partial t} Y + \omega_0 \frac{\partial \phi}{\partial t}\boldsymbol{\mathcal{E}} Y - \left(\frac{\partial \phi}{\partial t}\right)^2 \boldsymbol{\mathcal{E}} Y,
\end{aligned} \tag{2.45}$$

and

$$\begin{aligned}
\frac{\partial^2 \mathbf{E}^{(+)}}{\partial x^2} &= \frac{\partial^2}{\partial x^2}\left(\boldsymbol{\mathcal{E}} e^{i(k_0 x - \omega_0 t + \phi(x,t))}\right) \\
&= \frac{\partial}{\partial x}\left(\frac{\partial \boldsymbol{\mathcal{E}}}{\partial x} Y + ik_0 \boldsymbol{\mathcal{E}} Y + i\frac{\partial \phi}{\partial x}\boldsymbol{\mathcal{E}} Y\right) \\
&= \frac{\partial^2 \boldsymbol{\mathcal{E}}}{\partial x^2} Y + ik_0 \frac{\partial \boldsymbol{\mathcal{E}}}{\partial x} Y + i\frac{\partial \phi}{\partial x}\frac{\partial \boldsymbol{\mathcal{E}}}{\partial x} Y \\
&\quad +ik_0 \frac{\partial \boldsymbol{\mathcal{E}}}{\partial x} Y - k_0^2 \boldsymbol{\mathcal{E}} Y - k_0 \frac{\partial \phi}{\partial x}\boldsymbol{\mathcal{E}} Y \\
&\quad +i\frac{\partial^2 \phi}{\partial x^2}\boldsymbol{\mathcal{E}} Y + i\frac{\partial \phi}{\partial x}\frac{\partial \boldsymbol{\mathcal{E}}}{\partial x} Y - k_0 \frac{\partial \phi}{\partial x}\boldsymbol{\mathcal{E}} Y - \left(\frac{\partial \phi}{\partial x}\right)^2 \boldsymbol{\mathcal{E}} Y.
\end{aligned} \tag{2.46}$$

In the same way, we can write

$$\frac{\partial^2 \mathbf{P}^{(+)}}{\partial t^2} = \frac{\partial^2}{\partial t^2}\left(\boldsymbol{\mathcal{P}} e^{i(k_0 x - \omega_0 t + \phi(x,t))}\right)$$

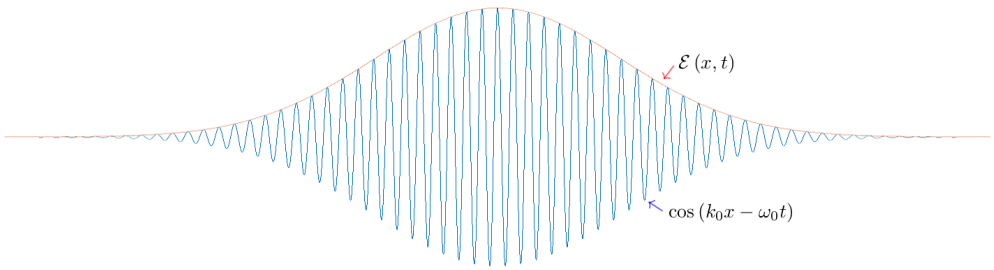

Figure 2.1: Schematic light pulse with envelope and fast oscillating term.

$$
\begin{aligned}
= \quad & \frac{\partial^2 \boldsymbol{\mathcal{P}}}{\partial t^2} Y - i\omega_0 \frac{\partial \boldsymbol{\mathcal{P}}}{\partial t} Y + i \frac{\partial \phi}{\partial t} \frac{\partial \boldsymbol{\mathcal{P}}}{\partial t} Y \\
& - i\omega_0 \frac{\partial \boldsymbol{\mathcal{P}}}{\partial t} Y - \omega_0^2 \boldsymbol{\mathcal{P}} Y + \omega_0 \frac{\partial \phi}{\partial t} \boldsymbol{\mathcal{P}} Y \\
& + i \frac{\partial^2 \phi}{\partial t^2} \boldsymbol{\mathcal{P}} Y + i \frac{\partial \phi}{\partial t} \frac{\partial \boldsymbol{\mathcal{P}}}{\partial t} Y + \omega_0 \frac{\partial \phi}{\partial t} \boldsymbol{\mathcal{P}} Y - \left(\frac{\partial \phi}{\partial t} \right)^2 \boldsymbol{\mathcal{P}} Y. \qquad (2.47)
\end{aligned}
$$

For a slowly varying envelope, both the amplitude $\boldsymbol{\mathcal{E}}$ and phase ϕ vary slowly compared to the fast oscillating terms. This means that

$$
\left| \frac{\partial^2 \boldsymbol{\mathcal{E}}}{\partial t^2} \right| \ll \left| \omega_0 \frac{\partial \boldsymbol{\mathcal{E}}}{\partial t} \right|, \quad \left| \frac{\partial^2 \boldsymbol{\mathcal{E}}}{\partial x^2} \right| \ll \left| k_0 \frac{\partial \boldsymbol{\mathcal{E}}}{\partial x} \right|, \qquad (2.48)
$$

$$
\left| \frac{\partial^2 \boldsymbol{\mathcal{P}}}{\partial t^2} \right| \ll \left| \omega_0 \frac{\partial \boldsymbol{\mathcal{P}}}{\partial t} \right| \ll \left| \omega_0^2 \boldsymbol{\mathcal{P}} \right|, \qquad (2.49)
$$

and

$$
\left| \frac{\partial^2 \phi}{\partial t^2} \right| \ll \left| \omega_0 \frac{\partial \phi}{\partial t} \right|, \quad \left| \frac{\partial^2 \phi}{\partial x^2} \right| \ll \left| k_0 \frac{\partial \phi}{\partial x} \right|. \qquad (2.50)
$$

Substituting the results of Eqs. (2.45–2.47) into Eq. (2.27) and, eliminating the exponent term Y on both sides of the equation, one obtains

$$
i \frac{\partial \boldsymbol{\mathcal{E}}}{\partial t} + ic \frac{\partial \boldsymbol{\mathcal{E}}}{\partial x} - \frac{\partial \phi}{\partial t} \boldsymbol{\mathcal{E}} - c \frac{\partial \phi}{\partial x} \boldsymbol{\mathcal{E}} = -\frac{\mu_0 \omega_0 c^2}{2} \boldsymbol{\mathcal{P}}, \qquad (2.51)
$$

where $\omega_0 = ck_0$ has been used.

Note that the electric field $\boldsymbol{\mathcal{E}}$ and the polarization field $\boldsymbol{\mathcal{P}}$ are still vectors in these evolution equations. Because $\boldsymbol{\mathcal{E}} = \mathcal{E}\hat{\epsilon}$, one can multiply with the conjugate of the polarization vector, $\hat{\epsilon}^*$, on each side of the equation to get the scalar variables:

$$
i \frac{\partial \mathcal{E}}{\partial t} + ic \frac{\partial \mathcal{E}}{\partial x} - \frac{\partial \phi}{\partial t} \mathcal{E} - c \frac{\partial \phi}{\partial x} \mathcal{E} = -\frac{\mu_0 \omega_0 c^2}{2} \boldsymbol{\mathcal{P}} \cdot \hat{\epsilon}^*. \qquad (2.52)
$$

As discussed above, with proper definition, $\mathcal{E}$ and ϕ are two real functions and $\boldsymbol{\mathcal{P}} \cdot \hat{\epsilon}^*$ is a complex function. Then, we obtain the approximate evolution of the slowly varying amplitude and slowly varying phase of the envelope as

$$
\frac{\partial \mathcal{E}}{\partial t} + c \frac{\partial \mathcal{E}}{\partial x} = -\frac{\mu_0 \omega_0 c^2}{2} \mathrm{Im}[\boldsymbol{\mathcal{P}} \cdot \hat{\epsilon}^*], \qquad (2.53)
$$

$$
\frac{\partial \phi}{\partial t} + c \frac{\partial \phi}{\partial x} = \frac{\mu_0 \omega_0 c^2}{2} \frac{1}{\mathcal{E}} \mathrm{Re}[\boldsymbol{\mathcal{P}} \cdot \hat{\epsilon}^*]. \qquad (2.54)
$$

Based on the definition of the phase in the complex form of electric field,

$$
\mathbf{E}^{(+)}(\mathbf{r}, t) = \boldsymbol{\mathcal{E}}(x, t)\, e^{i(k_0 x - \omega_0 t - \phi(x,t))}, \qquad (2.55)
$$

$$
\mathbf{P}^{(+)}(\mathbf{r}, t) = \boldsymbol{\mathcal{P}}(x, t)\, e^{i(k_0 x - \omega_0 t - \phi(x,t))}, \qquad (2.56)
$$

one can also have

$$
i \frac{\partial \boldsymbol{\mathcal{E}}}{\partial t} + ic \frac{\partial \boldsymbol{\mathcal{E}}}{\partial x} + \frac{\partial \phi}{\partial t} \boldsymbol{\mathcal{E}} + c \frac{\partial \phi}{\partial x} \boldsymbol{\mathcal{E}} Y = -\frac{\mu_0 \omega_0}{2} \boldsymbol{\mathcal{P}}, \qquad (2.57)
$$

which adds a negative sign to the equations of the phase evolution:

$$\frac{\partial \mathcal{E}}{\partial t} + c\frac{\partial \mathcal{E}}{\partial x} = -\frac{\mu_0\omega_0 c^2}{2}\mathrm{Im}[\boldsymbol{\mathcal{P}}\cdot\hat{\epsilon}^*], \tag{2.58}$$

$$\frac{\partial \phi}{\partial t} + c\frac{\partial \phi}{\partial x} = -\frac{\mu_0\omega_0 c^2}{2}\frac{1}{\mathcal{E}}\mathrm{Re}[\boldsymbol{\mathcal{P}}\cdot\hat{\epsilon}^*]. \tag{2.59}$$

These are the two equations describing the evolution of the amplitude and phase of the envelope of the electric field. Noticing that $\frac{\mu_0\omega_0 c^2}{2} = \frac{\omega_0}{2\varepsilon_0}$, Eq. (2.59) gives the same results as [107]. From the equations for the phase evolution one can see that there is a sudden change of phase at the point $\mathcal{E} \to 0$. To avoid this singularity, one should have $\mathrm{Re}[\boldsymbol{\mathcal{P}}\cdot\hat{\epsilon}^*] \to 0$ as $\mathcal{E} \to 0$ so that $\mathrm{Re}[\boldsymbol{\mathcal{P}}\cdot\hat{\epsilon}^*]/\mathcal{E}$ remains finite. Otherwise, the slowly varying approximation is not valid at this point.

2.1.5 Retarded time

As we will see in the later Chapters, to describe the light propagation in the slowly varying envelope approximation, there are several variants of Eq. (2.52) and Eq. (2.57). They are consistent with each other, but each with its own advantages for given applications. As an example, here we will show how those equations can be simplified by switching to the retarded-time coordinates

$$x \to x' = x, \tag{2.60}$$

$$t \to \tau = t - \frac{x}{c}. \tag{2.61}$$

Under this coordinate transformation, the derivatives can be calculated as

$$\frac{\partial \mathcal{E}(x,t)}{\partial x} = \frac{\partial \mathcal{E}(x',\tau)}{\partial x'}\frac{\partial x'}{\partial x} + \frac{\partial \mathcal{E}(x',\tau)}{\partial \tau}\frac{\partial \tau}{\partial x} = \frac{\partial \mathcal{E}(x',\tau)}{\partial x'} - \frac{1}{c}\frac{\partial \mathcal{E}(x',\tau)}{\partial \tau}, \tag{2.62}$$

and

$$\frac{\partial \mathcal{E}(x,t)}{\partial t} = \frac{\partial \mathcal{E}(x',\tau)}{\partial x'}\frac{\partial x'}{\partial t} + \frac{\partial \mathcal{E}(x',\tau)}{\partial \tau}\frac{\partial \tau}{\partial t} = \frac{\partial \mathcal{E}(x',\tau)}{\partial \tau}. \tag{2.63}$$

Therefore, one has the evolution of the envelope in the retarded-time coordinates as

$$\frac{\partial \mathcal{E}(x',\tau)}{\partial x'} = -\frac{\mu_0\omega_0 c}{2}\mathrm{Im}[\boldsymbol{\mathcal{P}}\cdot\hat{\epsilon}^*], \tag{2.64}$$

$$\frac{\partial \phi(x',\tau)}{\partial x'} = -\frac{\mu_0\omega_0 c}{2}\frac{1}{\mathcal{E}}\mathrm{Re}[\boldsymbol{\mathcal{P}}\cdot\hat{\epsilon}^*]. \tag{2.65}$$

The partial differential equations have been replaced by two ordinary differential equations, simplifying numerical simulations in Chapter 5.

Besides the discussions above, more details about of envelope propagation can be found in Appx. G.

2.2 Hamiltonian for light-matter interaction

For a particle with charge q moving in an electromagnetic field, the Hamiltonian is [107]

$$H = \frac{\left(\mathbf{p} - q\mathbf{A}\left(\mathbf{r}\right)\right)^2}{2m} + qV\left(\mathbf{r}\right), \tag{2.66}$$

with $\mathbf{p}$ being the canonical momentum, which satisfies the relation

$$\dot{x} = \frac{\partial H}{\partial p_x} \Rightarrow mv_x = p_x - qA_x. \tag{2.67}$$

The quantum operator for the canonical momentum is given as

$$\mathbf{p} = -i\hbar\nabla. \tag{2.68}$$

Therefore, one gets

$$H = \frac{\left(-i\hbar\nabla - q\mathbf{A}\left(\mathbf{r}\right)\right)^2}{2m} + qV\left(\mathbf{r}\right) \quad = \quad \frac{\left(i\hbar\nabla + q\mathbf{A}\left(\mathbf{r}\right)\right)^2}{2m} + qV\left(\mathbf{r}\right). \tag{2.69}$$

For an electron with $q = -e$ ($e = 1.6 \times 10^{-19}$ C being a positive value), then

$$\begin{aligned} H &= \frac{\left(\mathbf{p} + e\mathbf{A}\left(\mathbf{r}\right)\right)^2}{2m} + V\left(\mathbf{r}\right) \\ &= \frac{\left(-i\hbar\nabla + e\mathbf{A}\left(\mathbf{r}\right)\right)^2}{2m} + V\left(\mathbf{r}\right) \\ &= -\frac{\hbar^2}{2m}\left(\nabla + \frac{ie}{\hbar}\mathbf{A}\left(\mathbf{r}\right)\right)^2 + V\left(\mathbf{r}\right), \end{aligned} \tag{2.70}$$

where we have absorbed the charge into the potential term by renaming

$$-eV\left(\mathbf{r}\right) \rightarrow V\left(\mathbf{r}\right). \tag{2.71}$$

An atom consists of a nucleus and electrons.In the presence of an electromagnetic wave field, both the nucleus and the electrons interact with the field. However, the mass of the nucleus is much larger than the mass of the electrons, such that the former can hardly respond to the change of the field. Therefore, one can assume the coordinate of the nucleus, thus the coordinate of the atom, to be fixed. Only the dynamics of the electrons are taken into consideration. This is called the Born-Oppenheimer approximation. In this approximation, one can divide the coordinate of the electron into two parts: $\mathbf{r}_0 + \mathbf{r}$, with $\mathbf{r}_0$ being the coordinate of the atomic nucleus and $\mathbf{r}$ the coordinate of the electron relative to the nucleus. With $\mathbf{r}_0$ being a constant value for a given atom, the interaction between atom and electromagnetic field is reduced to be the interaction between the field and the electrons bound in the atom.

After the simplification of the atomic part of the Hamiltonian, we now apply further approximations to the electromagnetic wave field. We will follow the ideas used in reference [107] and generalize them to our case with a pulse light field:

$$\mathbf{A}\left(\mathbf{r}_0 + \mathbf{r}, t\right) \quad = \quad \frac{1}{2}\boldsymbol{\mathcal{A}}\left(\mathbf{r}_0 + \mathbf{r}, t\right) e^{i\omega_0 t - \left(\mathbf{k}_0 \cdot \left(\mathbf{r}_0 + \mathbf{r}\right) - \phi\left(\mathbf{r}_0 + \mathbf{r}, t\right)\right)}$$

$$
\begin{aligned}
& +\frac{1}{2}\boldsymbol{\mathcal{A}}^{*}\left(\mathbf{r}_0+\mathbf{r},t\right)e^{-i\omega_0 t-\left(\mathbf{k}_0\cdot\left(\mathbf{r}_0+\mathbf{r}\right)-\phi\left(\mathbf{r}_0+\mathbf{r},t\right)\right)} \\
\simeq\ & \frac{1}{2}\boldsymbol{\mathcal{A}}\left(\mathbf{r}_0,t\right)e^{i\left(\omega_0 t-\mathbf{k}_0\cdot\mathbf{r}_0-\phi\left(\mathbf{r}_0,t\right)\right)} \\
& +\frac{1}{2}\boldsymbol{\mathcal{A}}^{*}\left(\mathbf{r}_0,t\right)e^{-i\left(\omega_0 t-\mathbf{k}_0\cdot\mathbf{r}_0-\phi\left(\mathbf{r}_0,t\right)\right)} \\
=\ & \mathbf{A}\left(\mathbf{r}_0,t\right). \qquad (2.72)
\end{aligned}
$$

Here we have used three approximations:

$\boldsymbol{\mathcal{A}}\left(\mathbf{r}_0+\mathbf{r},t\right)\simeq\boldsymbol{\mathcal{A}}\left(\mathbf{r}_0,t\right)$	Slowly varying envelope approximation;
$\phi\left(\mathbf{r}_0+\mathbf{r},t\right)\simeq\phi\left(\mathbf{r}_0,t\right)$	Slowly varying phase approximation;
$\mathbf{k}_0\cdot\left(\mathbf{r}_0+\mathbf{r}\right)\simeq\mathbf{k}_0\cdot\mathbf{r}_0$	Dipole approximation.

In the dipole approximation, we have assumed that the carrier wavelength of the electromagnetic field is much larger than the size of the atom, which gives $\mathbf{k}_0\cdot\mathbf{r}\ll 1$. This approximation is more stringent than the other two approximations. Thus, as long as the dipole approximation holds, the other two approximations are also applicable subsequently. Under these field approximations, the electrons are assumed to be moving in a uniform field which only oscillates in time, with the Hamiltonian being

$$
H = \frac{\left(\mathbf{p}+e\mathbf{A}\left(\mathbf{r}_0,t\right)\right)^2}{2m}+V\left(\mathbf{r}\right)=-\frac{\hbar^2}{2m}\left(\nabla+\frac{ie}{\hbar}\mathbf{A}\left(\mathbf{r}_0,t\right)\right)^2+V\left(\mathbf{r}\right). \qquad (2.73)
$$

This represents a large simplification to the Hamiltonian given by Eq. (2.70): as $\mathbf{A}\left(\mathbf{r}_0,t\right)$ is independent of the electron's displacement $\mathbf{r}$, it commutes now with the canonical momentum operator:

$$
\mathbf{p}\cdot\mathbf{A}\left(\mathbf{r}_0,t\right)=\mathbf{A}\left(\mathbf{r}_0,t\right)\cdot\mathbf{p}. \qquad (2.74)
$$

In this dipole approximation, the dynamics of the wave function of the electron moving in the atom is given by the Schrödinger equation

$$
i\hbar\frac{\partial\Phi\left(\mathbf{r}_0,\mathbf{r},t\right)}{\partial t} = \left\{-\frac{\hbar^2}{2m}\left(\nabla+\frac{ie}{\hbar}\mathbf{A}\left(\mathbf{r}_0,t\right)\right)^2+V\left(\mathbf{r}\right)\right\}\Phi\left(\mathbf{r}_0,\mathbf{r},t\right). \qquad (2.75)
$$

As mentioned before, $\mathbf{r}_0$ is the coordinate of the atom and $\mathbf{r}$ is the coordinate of the electron moving around the atomic nucleus with respect to $\mathbf{r}_0$. Because the atoms are independent of each other, here in the Schrödinger equation, $\mathbf{r}_0$ is just a parameter and not a variable.

Eq. (2.75) is the equation describing the light-matter interaction in velocity gauge. By introducing a gauge transformation defined by

$$
\Phi\left(\mathbf{r}_0,\mathbf{r},t\right) = \exp\left[-\frac{ie}{\hbar}\mathbf{A}\left(\mathbf{r}_0,t\right)\cdot\mathbf{r}\right]\Psi\left(\mathbf{r}_0,\mathbf{r},t\right), \qquad (2.76)
$$

one can switch to the length gauge. Accordingly, the time derivative of the wave function $\Phi\left(\mathbf{r}_0,\mathbf{r},t\right)$ can be described in terms of the wave function $\Psi\left(\mathbf{r}_0,\mathbf{r},t\right)$ in the length gauge as

$$
\frac{\partial\Phi\left(\mathbf{r}_0,\mathbf{r},t\right)}{\partial t} = -\frac{ie}{\hbar}\dot{\mathbf{A}}\cdot\mathbf{r}\exp\left[-\frac{ie}{\hbar}\mathbf{A}\cdot\mathbf{r}\right]\Psi+\exp\left[-\frac{ie}{\hbar}\mathbf{A}\cdot\mathbf{r}\right]\dot{\Psi}. \qquad (2.77)
$$

Moreover, one can rewrite

$$\left(\nabla + \frac{ie}{\hbar}\mathbf{A}\right)^2 \Phi\left(\mathbf{r}_0, \mathbf{r}, t\right) = \left(\nabla + \frac{ie}{\hbar}\mathbf{A}\right)^2 \exp\left[-\frac{ie}{\hbar}\mathbf{A}\cdot\mathbf{r}\right]\Psi = \exp\left[-\frac{ie}{\hbar}\mathbf{A}\cdot\mathbf{r}\right]\nabla^2\Psi.$$

Thus, one obtains the Schrödinger equation in the length gauge:

$$i\hbar\frac{\partial\Psi\left(\mathbf{r}_0, \mathbf{r}, t\right)}{\partial t} = \left[-\frac{\hbar}{2m}\nabla^2 + V\left(\mathbf{r}\right) - e\frac{\partial\mathbf{A}}{\partial t}\cdot\mathbf{r}\right]\Psi\left(\mathbf{r}_0, \mathbf{r}, t\right). \tag{2.78}$$

Making use of the relation $\mathbf{E} = -\frac{\partial\mathbf{A}}{\partial t}$, one obtains the Schrödinger equation in the form of the electric field in the dipole approximation

$$i\hbar\frac{\partial\Psi\left(\mathbf{r}_0, \mathbf{r}, t\right)}{\partial t} = \left[-\frac{\hbar^2}{2m}\nabla^2 + V\left(\mathbf{r}\right) + e\mathbf{E}\left(\mathbf{r}_0, t\right)\cdot\mathbf{r}\right]\Psi\left(\mathbf{r}_0, \mathbf{r}, t\right), \tag{2.79}$$

or, equivalently

$$i\hbar\frac{\partial\Psi\left(\mathbf{r}_0, \mathbf{r}, t\right)}{\partial t} = \left[\frac{\mathbf{p}^2}{2m} + V\left(\mathbf{r}\right) + e\mathbf{E}\left(\mathbf{r}_0, t\right)\cdot\mathbf{r}\right]\Psi\left(\mathbf{r}_0, \mathbf{r}, t\right). \tag{2.80}$$

Thus, the Hamiltonian in the length gauge is

$$H = H_{\mathrm{A}} + H_{\mathrm{I}}, \tag{2.81}$$

with

$$H_{\mathrm{A}} = \frac{\mathbf{p}^2}{2m} + V\left(\mathbf{r}\right), \tag{2.82}$$

being the bare atomic Hamiltonian, and

$$H_{\mathrm{I}} = e\mathbf{E}\left(\mathbf{r}_0, t\right)\cdot\mathbf{r} \tag{2.83}$$

being the interaction Hamiltonian between the electric dipole moment of the atom and the electric field. Because the direction of the dipole moment is pointing from the negative charge to the positive charge, and $\mathbf{r}$ refers to the displacement of the electron, the dipole moment of the atom is defined as

$$\mathbf{d} = -e\mathbf{r}. \tag{2.84}$$

Accordingly, the interaction Hamiltonian is

$$H_{\mathrm{I}} = -\mathbf{d}\cdot\mathbf{E}. \tag{2.85}$$

This is exactly the Hamiltonian of a dipole in the electric field.

In addition, one also needs to include the Hamiltonian of the free electromagnetic field defined by

$$H_{\mathrm{EM}} = \sum_{\mathbf{k}}\hbar\omega_{\mathbf{k}}\left(a_{\mathbf{k}}^{\dagger}a_{\mathbf{k}} + \frac{1}{2}\right). \tag{2.86}$$

Therefore, the full Hamiltonian describing the light-atom interaction is given by

$$H = H_{\mathrm{A}} + H_{\mathrm{I}} + H_{\mathrm{EM}}. \tag{2.87}$$

When the photons in the light field are in a Fock state, one needs to treat the light field as photons, thus the **E** field in Eq. (2.85) must be written in terms of photon annihilation/creation operators. This corresponds to a full quantum theory of the light-atom interaction. However, if the photons are in a coherent state, the light can be treated as a classical electromagnetic field, and only the atoms are treated through quantum mechanics. This approach represents a semi-classical theory of the system.

As we discussed before, the full Hamiltonian can be divided into two parts, one is the Hamiltonian

$$H_0 = H_{\mathrm{A}} + H_{\mathrm{EM}} \tag{2.88}$$

describing a bare atom and free field which is exactly solvable, the other is the Hamiltonian H_{I} representing the interaction between the atom and light field. When the light can be treated as a classical field, one can drop the free electromagnetic energy H_{EM} from the bare Hamiltonian.

In principle, there is no exact solution to this problem. Nevertheless, one can still gain many important insights on this problem under some approximations. As a first step, we will define the Hilbert space based on the complete eigenvectors of the bare Hamiltonian. Then all the wave functions and operators (including the interaction Hamiltonian) can be represented by the basis of the Hilbert space. This procedure is important because it provides the mathematical foundations for further approximations to be introduced.

The Schrödinger equation of an atom without any external field is given by

$$i\hbar\frac{\partial\Psi_0\left(\mathbf{r}_0,\mathbf{r},t\right)}{\partial t} = \left[\frac{\mathbf{p}^2}{2m}+V\left(\mathbf{r}\right)\right]\Psi_0\left(\mathbf{r}_0,\mathbf{r},t\right). \tag{2.89}$$

After separation of variables, one arrives to the stationary Schrödinger equation

$$\left[\frac{\mathbf{p}^2}{2m}+V\left(\mathbf{r}\right)\right]\left|\psi_{nlm}^{(0)}\right\rangle = E_{nlm}^{(0)}\left|\psi_{nlm}^{(0)}\right\rangle, \tag{2.90}$$

where we assume the atom is a hydrogen-like system so that n, l, m are good quantum numbers to classify the complete eigenbasis. For many-electron systems, the procedures are similar but with different notifications of the orthonormal basis.

Solving this stationary Schrödinger equation one gets the eigenvectors which define the Hilbert space of this quantum system. Any wave function can be expanded in this eigenbasis as a vector

$$\left|\Psi^{(0)}\right\rangle = \sum_{k=\{nlm\}} c_k^{(0)}\left|\psi_k^{(0)}\right\rangle. \tag{2.91}$$

The operator $\hat{F}$ is represented in a matrix form

$$\hat{F} = \sum_{ij} F_{ij}\left|\psi_i^{(0)}\right\rangle\left\langle\psi_j^{(0)}\right|, \tag{2.92}$$

with each element given by

$$F_{ij} = \left\langle \psi_i^{(0)} \right| \hat{F} \left| \psi_j^{(0)} \right\rangle . \tag{2.93}$$

Dynamics of the wave function of this system are then just described by time-dependent coefficients for each eigenvector.

When interaction with an extra field is involved, its Hamiltonian can also be expressed in a matrix form

$$H_{\mathrm{I}} = \sum_{ij} H_{ij}^{1} \left| \psi_i^{(0)} \right\rangle \left\langle \psi_j^{(0)} \right| . \tag{2.94}$$

The Schrödinger equation can be expressed in a matrix form

$$i\hbar \frac{\partial}{\partial t} \left| \Psi \left(\mathbf{r}_0, \mathbf{r}, t \right) \right\rangle = \left[H_0 + H_{\mathrm{I}} \right] \left| \Psi \left(\mathbf{r}_0, \mathbf{r}, t \right) \right\rangle . \tag{2.95}$$

With

$$\left| \Psi \left(\mathbf{r}_0, \mathbf{r}, t \right) \right\rangle = \sum_{k=\{nlm\}} c_k(t) \left| \psi_k^{(0)} \right\rangle , \tag{2.96}$$

Due to the infinite number of eigenvectors, the matrix-form Schrödinger equation is actually a set of infinite number of coupled linear equations. An exact solution is not possible. Thus one needs to make approximations based on the problem of interest [110].

For instance, one can truncate the number of levels involved if H_{I} only has significant couplings between a finite number of eigenstates. As a result, one obtains a finite-dimensional matrix, thus a finite number of coupled linear equations. The simplest cases would be the two-level, three-level or four-level approximation, which will be discussed later in Sec. 2.3. This simplified problem can be either solved numerically (with an exact diagonalization method), or analytically. The accuracy of this method is limited by the truncation of levels.

Another way to gain insight into the coupled equations is based on a perturbation series [110]. This approach is applicable when the interaction Hamiltonian is perturbatively small, i.e. the magnitude of each coefficient $c_k(t)$ only deviates to a small extent from $c_k^{(0)}$ (more discussion can be found in Appx. A).

For the interaction between light and atoms, as an example, if the frequency of the light is tuned far from the resonance of the atom, it will have a negligible influence on the atomic state. Therefore, perturbation theory is applicable. When the light is close to resonance, singularities show up in perturbation series. One needs to use e.g. the two-level approximation instead of perturbation theory to resolve the problem. If the strength of the light field is low, stimulated emission/absorption would be much smaller compared to the decay of the atoms. In such case, rate equations are sufficient to describe the two-level system. However, when the field becomes strong enough, Rabi flopping will show up and the populations of the eigenstates will undergo fast changes. In this situation, a density-matrix theory [111] should be used for the two-level system. Until now, the light field is still perturbative compared to the static electric field of the atomic nucleus. Rabi oscillation in the populations is only a result of resonance (or in full quantum theory, a result of degenerate-state perturbation). When the light intensity becomes ultra-strong such that tunneling ionization becomes possible, both perturbative and level-truncation approaches fail to describe the problem, and some other treatment

should be used.

In this thesis, we will only focus on perturbative interaction. Therefore density matrix theory or perturbation theory is sufficient to analyze the physical situation. Moreover, in a full quantum mechanical treatment, the two-level approach represents a degenerate perturbation theory.

2.3 Density matrix for two-level atoms

As discussed in the previous Section, when the frequency of the light field is close to resonance with one of the atomic transitions, a two-level approximation on the infinite atomic levels is valid [107, 112]. Here, we introduce the density-matrix theory [111] to describe the dynamics of the two-level systems under interactions with an external field given by Eq. (2.85). By going from the Schrödinger picture to the interaction picture and then to the rotating-phase picture, the equation of motion for the density matrix is presented in Eq. (2.133). Furthermore, we deduce the calculation of the polarization field based on density matrix, resulting in a connection of Maxwell's equations and density-matrix theory.

2.3.1 Hamiltonian for two-level systems

Depending on the problems of interest, different pictures such as the Schrödinger picture, the Heisenberg picture and the interaction picture can be used to describe the time evolution of a quantum system [107]. Different pictures are related to each other by unitary transformations of the wave functions, density matrix as well as the Hamiltonian. In the following, we first give the expressions of the density matrix and the Hamiltonian in the Schrödinger picture and the interaction picture. After that, a new picture called rotating-phase picture is defined to simplify the discussions of atoms interacting with a detuned light field [113]. Details of the constructions of these pictures can be found in Appx. S-I-R-Picture.

2.3.1.1 The Schrödinger picture

For a two-level system with eigenstates $|\mathrm{g}\rangle$ and $|\mathrm{e}\rangle$ standing for ground state and excited state, respectively, the time-dependent wave function of the atomic state has the general form

$$|\psi(t)\rangle = c_{\mathrm{g}}(t)\,|\mathrm{g}\rangle + c_{\mathrm{e}}(t)\,|\mathrm{e}\rangle\,. \tag{2.97}$$

This pure state can also be represented by the corresponding density matrix [107, 112]

$$\rho = |\psi\rangle\langle\psi| = \begin{bmatrix} c_{\mathrm{g}}c_{\mathrm{g}}^{*} & c_{\mathrm{g}}c_{\mathrm{e}}^{*} \\ c_{\mathrm{e}}c_{\mathrm{g}}^{*} & c_{\mathrm{e}}c_{\mathrm{e}}^{*} \end{bmatrix} = \begin{bmatrix} \rho_{\mathrm{gg}} & \rho_{\mathrm{ge}} \\ \rho_{\mathrm{eg}} & \rho_{\mathrm{ee}} \end{bmatrix}. \tag{2.98}$$

According to the Schrödinger equation, one ccan derive the equation of motion for the density matrix (more details in Appx. C)

$$\dot{\rho} \;=\; i\,[\rho, H] = i\,[\rho, H_0 + H_{\mathrm{I}}]\,. \tag{2.99}$$

Here, Eq. (2.99) is called von Neumann equation, which is the starting point to study the dynamics of a quantum system in density matrix theory. Because we don't consider

any spatial variations for the atomic system we are interested in, the partial derivative with respect to time is changed to be total derivative.

With the eigenenergy of the ground state $|\mathrm{g}\rangle$ set to be zero, the bare atomic Hamiltonian for a two-level system is given by

$$H_0 = \begin{bmatrix} 0 & 0 \\ 0 & \omega_\mathrm{a} \end{bmatrix}. \tag{2.100}$$

Here we take $\hbar = 1$. Considering that it is interacting with an electric field as

$$\mathbf{E}(\mathbf{x},t) = \frac{1}{2}\left(\boldsymbol{\mathcal{E}}_\mathrm{m}(\mathbf{x},t)\, e^{-i\omega_0 t} + \boldsymbol{\mathcal{E}}_\mathrm{m}^*(\mathbf{x},t)\, e^{i\omega_0 t}\right) \tag{2.101}$$

with

$$\boldsymbol{\mathcal{E}}_\mathrm{m}(\mathbf{x},t) \;=\; \boldsymbol{\mathcal{E}}(\mathbf{x},t)\, e^{i(\mathbf{k}\cdot\mathbf{x}+\phi(\mathbf{x},t))}, \tag{2.102}$$

the interaction Hamiltonian is

$$H_\mathrm{I} \;=\; e\mathbf{r}\cdot\mathbf{E}(\mathbf{x},t) = \frac{e\mathbf{r}}{2}\left(\boldsymbol{\mathcal{E}}_\mathrm{m}(\mathbf{x},t)\, e^{-i\omega_0 t} + \boldsymbol{\mathcal{E}}_\mathrm{m}^*(\mathbf{x},t)\, e^{i\omega_0 t}\right). \tag{2.103}$$

Accordingly, the matrix form of the interaction Hamiltonian is

$$H_\mathrm{I} = \frac{e\mathbf{E}(\mathbf{x},t)}{2}\begin{bmatrix} \langle \mathrm{g}|\,\mathbf{r}\,|\mathrm{g}\rangle & \langle \mathrm{g}|\,\mathbf{r}\,|\mathrm{e}\rangle \\ \langle \mathrm{e}|\,\mathbf{r}\,|\mathrm{g}\rangle & \langle \mathrm{e}|\,\mathbf{r}\,|\mathrm{e}\rangle \end{bmatrix}. \tag{2.104}$$

Here we use the vector $\mathbf{x}$ instead of $\mathbf{r}_0$ as the coordinate of the atom and the electric field. The vector $\mathbf{r}$ corresponds to the relative coordinate of the electron in a specific atom. Considering the parity symmetry of the atomic wave function, one can see $\langle \mathrm{g}|\,\mathbf{r}\,|\mathrm{g}\rangle = \langle \mathrm{e}|\,\mathbf{r}\,|\mathrm{e}\rangle = 0$, therefore, the interaction Hamiltonian reduces to

$$H_\mathrm{I} = \frac{e\mathbf{E}(\mathbf{x},t)}{2}\begin{bmatrix} 0 & \langle \mathrm{g}|\,\mathbf{r}\,|\mathrm{e}\rangle \\ \langle \mathrm{e}|\,\mathbf{r}\,|\mathrm{g}\rangle & 0 \end{bmatrix}. \tag{2.105}$$

2.3.1.2 The interaction picture

In the Schrödinger picture presented above, both the bare Hamiltonian and the interaction Hamiltonian are involved in the dynamics of the density matrix. When switch to the interaction picture, the bare Hamiltonian will be absorbed into the density matrix and only the interaction Hamiltonian will play a role. With the unitary transformation

$$U_0 = e^{iH_0 t} = \begin{bmatrix} 1 & 0 \\ 0 & e^{i\omega_\mathrm{a} t} \end{bmatrix}, \tag{2.106}$$

the density matrix ρ^I in the interaction picture has the form

$$\rho^\mathrm{I} \;=\; U_0 \rho U_0^\dagger = \begin{bmatrix} \rho_\mathrm{gg} & \rho_\mathrm{ge}e^{-i\omega_\mathrm{a} t} \\ \rho_\mathrm{eg}e^{i\omega_\mathrm{a} t} & \rho_\mathrm{ee} \end{bmatrix}, \tag{2.107}$$

and the off-diagonal elements in the interaction picture can be regarded as the envelope function of the off-diagonal elements in Schrödinger picture:

$$\rho_{\mathrm{ge}}^{\mathrm{I}} = \rho_{\mathrm{ge}} e^{-i\omega_{\mathrm{a}}t} = \tilde{\rho}_{\mathrm{ge}}, \tag{2.108}$$
$$\rho_{\mathrm{eg}}^{\mathrm{I}} = \rho_{\mathrm{eg}} e^{i\omega_{\mathrm{a}}t} = \tilde{\rho}_{\mathrm{eg}}. \tag{2.109}$$

The corresponding interaction Hamiltonian $H^{\mathrm{I}} = U_0 H_{\mathrm{I}} U_0^{\dagger}$ becomes

$$H^{\mathrm{I}} = \frac{e}{2}\begin{bmatrix} 0 & \langle \mathrm{g}|\,\mathbf{r}\,|\mathrm{e}\rangle \left(\boldsymbol{\mathcal{E}}_{\mathrm{m}} e^{-i(\omega_0+\omega_{\mathrm{a}})t} + \boldsymbol{\mathcal{E}}_{\mathrm{m}}^{*} e^{i(\omega_0-\omega_{\mathrm{a}})t}\right) \\ \langle \mathrm{e}|\,\mathbf{r}\,|\mathrm{g}\rangle \left(\boldsymbol{\mathcal{E}}_{\mathrm{m}} e^{-i(\omega_0-\omega_{\mathrm{a}})t} + \boldsymbol{\mathcal{E}}_{\mathrm{m}}^{*} e^{i(\omega_0+\omega_{\mathrm{a}})t}\right) & 0 \end{bmatrix}.$$

In the rotating-wave approximation, where one neglects the fast oscillating term with $\omega_0 + \omega_{\mathrm{a}}$ in the exponent, one obtains

$$H^{\mathrm{I}} = \frac{1}{2}\begin{bmatrix} 0 & \Omega_{\mathrm{m}}^{*}(\mathbf{x},t)\, e^{i\Delta t} \\ \Omega_{\mathrm{m}}(\mathbf{x},t)\, e^{-i\Delta t} & 0 \end{bmatrix}, \tag{2.110}$$

where $\Delta = \omega_0 - \omega_{\mathrm{a}}$ refers to the detuning between the carrier frequency and the atom. The complex coupling function is given by

$$\Omega_{\mathrm{m}}(\mathbf{x},t) = e\,\langle \mathrm{e}|\,\mathbf{r}\,|\mathrm{g}\rangle\, \boldsymbol{\mathcal{E}}_{\mathrm{m}}(\mathbf{x},t), \tag{2.111}$$
$$\Omega_{\mathrm{m}}^{*}(\mathbf{x},t) = e\,\langle \mathrm{g}|\,\mathbf{r}\,|\mathrm{e}\rangle\, \boldsymbol{\mathcal{E}}_{\mathrm{m}}^{*}(\mathbf{x},t). \tag{2.112}$$

Explicitly, they can be written as

$$\Omega_{\mathrm{m}}(\mathbf{x},t) = \Omega(\mathbf{x},t)\, e^{i(\mathbf{k}\cdot\mathbf{x}+\phi(\mathbf{x},t)+\phi_0)}, \tag{2.113}$$
$$\Omega_{\mathrm{m}}^{*}(\mathbf{x},t) = \Omega(\mathbf{x},t)\, e^{-i(\mathbf{k}\cdot\mathbf{x}+\phi(\mathbf{x},t)+\phi_0)}, \tag{2.114}$$

with the amplitude $\Omega(\mathbf{x},t)$ being the Rabi frequency defined by

$$\Omega(\mathbf{x},t) = \left|e\,\langle \mathrm{e}|\,\mathbf{r}\,|\mathrm{g}\rangle \cdot \boldsymbol{\mathcal{E}}(\mathbf{x},t)\right| = \left|e\,\langle \mathrm{e}|\,\mathbf{r}\,|\mathrm{g}\rangle \cdot \hat{\epsilon}\right| \mathcal{E}(\mathbf{x},t) = \mu\mathcal{E}(\mathbf{x},t), \tag{2.115}$$

where $\boldsymbol{\mathcal{E}} = \hat{\epsilon}\mathcal{E}$ and

$$\mu = \left|e\,\langle \mathrm{e}|\,\mathbf{r}\,|\mathrm{g}\rangle \cdot \hat{\epsilon}\right| \tag{2.116}$$

have been introduced. The constant parameters μ and ϕ_0 are the magnitude and phase from the coupling between the light and atom,

$$e\,\langle \mathrm{e}|\,\mathbf{r}\,|\mathrm{g}\rangle \cdot \hat{\epsilon} = \mu e^{i\phi_0}. \tag{2.117}$$

In reality, μ is the magnitude of the dipole moment and ϕ_0 is the angle between the directions of the dipole moment and the direction $\hat{\epsilon}$ of the electric field. Both of them could be different for different transitions. Calculations for μ and ϕ_0 based on realistic atomic transitions can be found in Appx. B.

As shown in Appx. C, in the interaction picture, the von Neumann equation Eq. (2.99)

has been replaced by

$$\dot{\rho}^{\mathrm{I}} = i\left[\rho^{\mathrm{I}}, H^{\mathrm{I}}\right], \tag{2.118}$$

where only the interaction Hamiltonian remains.

2.3.1.3 The rotating-phase picture

Though the von Neumann equation given by Eq (2.118) in the interaction picture is simpler compared to Eq (2.99) in the Schrödinger picture, the exponential terms in the effective Hamiltonian in Eq (2.110) makes it difficult to analysis. Therefore, we introduce a new picture that can remove them from the off-diagonal elements of the Hamiltonian.

By defining a new phase function

$$\theta(\mathbf{x}, t) = \mathbf{k}\cdot\mathbf{x} - \Delta t + \phi(\mathbf{x}, t) + \phi_0, \tag{2.119}$$

one can rewrite the Hamiltonian in the interaction picture as

$$H^{\mathrm{I}} = \frac{\Omega(\mathbf{x}, t)}{2}\begin{bmatrix} 0 & e^{-i\theta(\mathbf{x},t)} \\ e^{i\theta(\mathbf{x},t)} & 0 \end{bmatrix}. \tag{2.120}$$

In form, the time-dependent exponential terms $e^{\pm i\theta(\mathbf{x},t)}$ are explicit. Thus, with another unitary transformation

$$U_\theta = \begin{bmatrix} 1 & 0 \\ 0 & e^{-i\theta(\mathbf{x},t)} \end{bmatrix}, \tag{2.121}$$

one can eliminate the exponential term and obtain

$$H^{\mathrm{M}} = U_\theta H^{\mathrm{I}} U_\theta^\dagger = \frac{1}{2}\begin{bmatrix} 0 & \Omega \\ \Omega & 0 \end{bmatrix}. \tag{2.122}$$

Correspondingly, after the U_θ transformation, the density matrix is changed to be

$$\rho^{\mathrm{M}} = U_\theta \rho^{\mathrm{I}} U_\theta^\dagger = \begin{bmatrix} \rho^{\mathrm{I}}_{\mathrm{gg}} & \rho^{\mathrm{I}}_{\mathrm{ge}} e^{i\theta} \\ \rho^{\mathrm{I}}_{\mathrm{eg}} e^{-i\theta} & \rho^{\mathrm{I}}_{\mathrm{ee}} \end{bmatrix}, \tag{2.123}$$

with the von Neumann equation being replaced by (see Appx. C)

$$\frac{\partial \rho^{\mathrm{M}}}{\partial t} = i\left[\rho^{\mathrm{M}}, H_{\mathrm{eff}}\right], \tag{2.124}$$

where the effective Hamiltonian H_{eff} is given by

$$H_{\mathrm{eff}} = \begin{bmatrix} 0 & \Omega/2 \\ \Omega/2 & \frac{\partial\theta}{\partial t} \end{bmatrix} = \begin{bmatrix} 0 & \Omega/2 \\ \Omega/2 & \frac{\partial\phi}{\partial t} - \Delta \end{bmatrix}. \tag{2.125}$$

We may call this *rotating-phase picture* as a different language compared to the interaction picture and the Schrödinger picture. Note that, by working in this picture, all the functions are real functions of the time t and the coordinate $\mathbf{x}$. From this effective Hamiltonian one can see that the change of the phase with time gives the time-dependent

instantaneous frequency detuning in this coupled system:

$$\Delta_\theta(t) = -\frac{\partial\theta}{\partial t}. \tag{2.126}$$

Because $\mathbf{k}\cdot\mathbf{x}$ and ϕ_0 are constant quantities which are independent of time for each atom, one could have

$$\Delta_\theta(t) = \Delta - \frac{\partial\phi}{\partial t}. \tag{2.127}$$

For the time-dependent phase function $\phi(\mathbf{x},t)$, one can write it in a polynomial form as

$$\phi(\mathbf{x},t) = \phi^{(0)}(\mathbf{x}) + \phi^{(1)}(\mathbf{x})\,t + \phi^{(2)}(\mathbf{x})\,t^2 + ... \tag{2.128}$$

One can notice that the first term $\phi^{(0)}$ refers to a constant phase which is independent of time. Because the derivative of this term gives zero in the rotating-phase picture, it does not change the physics in this case. One could also absorb the other two constant-phase terms $\mathbf{k}\cdot\mathbf{x}$ and ϕ_0 into $\phi^{(0)}$. The second term $\phi^{(1)}$ can be regarded as a frequency shift of the carrier frequency. If we take the reference carrier frequency to be resonant with the two-level system, $\Delta = 0$, and $\phi^{(1)}$ exactly refers to the detuning between the two-level system and the light field. For the third term, $\phi^{(2)}$ corresponds to a chirp in the light pulse. As a result, in principle, the detuning Δ, the constant phase ϕ_0 and the time-independent phase $\mathbf{k}\cdot\mathbf{x}$ can be absorbed into a single phase term ϕ.

$$\theta(\mathbf{x},t) = \theta^{(0)}(\mathbf{x}) + \theta^{(1)}(\mathbf{x})\,t + \theta^{(2)}(\mathbf{x})\,t^2 + ..., \tag{2.129}$$

with

$$\theta(\mathbf{x})^{(0)} = \phi(\mathbf{x})^{(0)} + \mathbf{k}\cdot\mathbf{x} + \phi_0, \tag{2.130}$$

$$\theta(\mathbf{x})^{(1)} = \phi(\mathbf{x})^{(1)} - \Delta, \tag{2.131}$$

$$\theta(\mathbf{x})^{(\mathrm{n})} = \phi(\mathbf{x})^{(\mathrm{n})} \qquad \text{for all } n \geq 2. \tag{2.132}$$

When the decay and decoherence processes are included, the full equations of motion for the density matrix are given by

$$\dot{\rho}^{\mathrm{M}} = i\left[\rho^{\mathrm{M}}, H_{\mathrm{eff}}\right] + \Gamma\begin{bmatrix} \rho^{\mathrm{M}}_{\mathrm{ee}} & -\frac{1}{2}\rho^{\mathrm{M}}_{\mathrm{ge}} \\ -\frac{1}{2}\rho^{\mathrm{M}}_{\mathrm{eg}} & -\rho^{\mathrm{M}}_{\mathrm{ee}} \end{bmatrix} + \beta\begin{bmatrix} 0 & -\frac{1}{2}\rho^{\mathrm{M}}_{\mathrm{ge}} \\ -\frac{1}{2}\rho^{\mathrm{M}}_{\mathrm{eg}} & 0 \end{bmatrix}. \tag{2.133}$$

With Γ being the decay rate of the excited state, the second term is the Lindblad Hamiltonian which is added phenomenologically to describe spontaneous emission (see Appx. B.3 and [112]). The third term with β is related to different decoherence process such as elastic collisions (see Chapter 4). Such collisions between the atoms and other particles lead to dephasing of the atomic state. As a result, it causes decay of the coherences (ρ_{eg} and ρ_{ge}) between the two states.

2.3.2 Polarization

In terms of the density matrix, one can calculate the expectation value of the dipole moment in the Schrödinger picture according to

$$\langle \mathbf{d} \rangle = \mathrm{Tr}\left\{\rho \mathbf{d}\right\} = -e\mathrm{Tr}\left\{\rho \mathbf{r}\right\}. \tag{2.134}$$

This gives

$$\begin{aligned} \langle \mathbf{d} \rangle &= -e\left[\langle \mathrm{g}| \rho \mathbf{r} |\mathrm{g}\rangle + \langle \mathrm{e}| \rho \mathbf{r} |\mathrm{e}\rangle\right] \\ &= -e\left[\langle \mathrm{g}| \rho |\mathrm{e}\rangle \langle \mathrm{e}| \mathbf{r} |\mathrm{g}\rangle + \langle \mathrm{e}| \rho |\mathrm{g}\rangle \langle \mathrm{g}| \mathbf{r} |\mathrm{e}\rangle\right] \\ &= -e\left[\rho_{\mathrm{ge}} \langle \mathrm{e}| \mathbf{r} |\mathrm{g}\rangle + \rho_{\mathrm{eg}} \langle \mathrm{g}| \mathbf{r} |\mathrm{e}\rangle\right]. \end{aligned} \tag{2.135}$$

Therefore, the polarization field induced by light when it propagates through the atomic medium can be calculated as

$$\mathbf{P} = n\langle \mathbf{d} \rangle = -ne\left[\rho_{\mathrm{ge}} \langle \mathrm{e}| \mathbf{r} |\mathrm{g}\rangle + \rho_{\mathrm{eg}} \langle \mathrm{g}| \mathbf{r} |\mathrm{e}\rangle\right], \tag{2.136}$$

where n is the number density of the atoms, and ρ_{ge} and ρ_{eg} are the density matrix elements in the Schrödinger picture. Recalling the relationships

$$\rho_{\mathrm{ge}} = \rho_{\mathrm{ge}}^{\mathrm{M}} e^{i\omega_{\mathrm{a}}t - i\theta} = \rho_{\mathrm{ge}}^{\mathrm{M}} e^{i(\omega_0 t - \mathbf{k}\cdot\mathbf{x} - \phi(\mathbf{x},t) - \phi_0)}, \tag{2.137}$$

$$\rho_{\mathrm{eg}} = \rho_{\mathrm{eg}}^{\mathrm{M}} e^{-i\omega_{\mathrm{a}}t + i\theta} = \rho_{\mathrm{eg}}^{\mathrm{M}} e^{-i(\omega_0 t - \mathbf{k}\cdot\mathbf{x} - \phi(\mathbf{x},t) - \phi_0)}, \tag{2.138}$$

one obtains the polarization in the rotating-phase picture

$$\begin{aligned} \mathbf{P} &= -ne \langle \mathrm{e}| \mathbf{r} |\mathrm{g}\rangle \rho_{\mathrm{ge}}^{\mathrm{M}} e^{i(\omega_0 t - \mathbf{k}\cdot\mathbf{x} - \phi(\mathbf{x},t) - \phi_0)} \\ &\quad -ne \langle \mathrm{g}| \mathbf{r} |\mathrm{e}\rangle \rho_{\mathrm{eg}}^{\mathrm{M}} e^{-i(\omega_0 t - \mathbf{k}\cdot\mathbf{x} - \phi(\mathbf{x},t) - \phi_0)} \\ &= \mathbf{P}^{(+)}(\mathbf{x},t) + \mathbf{P}^{(-)}(\mathbf{x},t), \end{aligned} \tag{2.139}$$

with

$$\mathbf{P}^{(+)}(\mathbf{x},t) = -ne \langle \mathrm{g}| \mathbf{r} |\mathrm{e}\rangle \rho_{\mathrm{eg}}^{\mathrm{M}} e^{-i(\omega_0 t - \mathbf{k}\cdot\mathbf{x} - \phi(\mathbf{x},t) - \phi_0)}, \tag{2.140}$$

$$\mathbf{P}^{(-)}(\mathbf{x},t) = -ne \langle \mathrm{e}| \mathbf{r} |\mathrm{g}\rangle \rho_{\mathrm{ge}}^{\mathrm{M}} e^{i(\omega_0 t - \mathbf{k}\cdot\mathbf{x} - \phi(\mathbf{x},t) - \phi_0)}. \tag{2.141}$$

By comparing these result with the definition of the positive and negative parts of the polarization field in Eq. (2.39) and Eq. (2.40)

$$\mathbf{P}^{(+)}(\mathbf{x},t) = \frac{1}{2}\boldsymbol{\mathcal{P}}(\mathbf{x},t)\, e^{i(\mathbf{k}\cdot\mathbf{x} - \omega_0 t + \phi(\mathbf{x},t))},$$

one immediately arrives at the atomic definition of the polarization envelope

$$\boldsymbol{\mathcal{P}}(\mathbf{x},t) = -2ne \langle \mathrm{g}| \mathbf{r} |\mathrm{e}\rangle \rho_{\mathrm{eg}}^{\mathrm{M}} e^{i\phi_0}. \tag{2.142}$$

To see how the atoms may affect the light field, we rewrite the propagation equation of the slowly varying envelope of the light field derived in Eq. (2.53) and Eq. (2.54)

$$\frac{\partial \mathcal{E}}{\partial t} + c\frac{\partial \mathcal{E}}{\partial x} = -\frac{\mu_0 \omega_0 c^2}{2}\mathrm{Im}[\boldsymbol{\mathcal{P}} \cdot \hat{\epsilon}^*],$$

$$\frac{\partial \phi}{\partial t} + c\frac{\partial \phi}{\partial x} = \frac{\mu_0 \omega_0 c^2}{2}\frac{1}{\mathcal{E}}\mathrm{Re}[\boldsymbol{\mathcal{P}} \cdot \hat{\epsilon}^*].$$

The term $\boldsymbol{\mathcal{P}} \cdot \hat{\epsilon}^*$ can be written as

$$\boldsymbol{\mathcal{P}} \cdot \hat{\epsilon}^* = -2ne\rho_{\mathrm{eg}}^{\mathrm{M}} e^{i\phi_0} \langle \mathrm{g}| \mathbf{r} |\mathrm{e}\rangle \cdot \hat{\epsilon}^*. \tag{2.143}$$

By using the relation

$$\langle \mathrm{g}| \mathbf{r} |\mathrm{e}\rangle \cdot \hat{\epsilon}^* = \Big(\langle \mathrm{e}| \mathbf{r} |\mathrm{g}\rangle \cdot \hat{\epsilon} \Big)^*, \tag{2.144}$$

one has

$$\langle \mathrm{g}| \mathbf{r} |\mathrm{e}\rangle \cdot \hat{\epsilon}^* = \Big| \langle \mathrm{e}| \mathbf{r} |\mathrm{g}\rangle \cdot \hat{\epsilon} \Big| e^{-i\phi_0} = \mu e^{-i\phi_0}, \tag{2.145}$$

and

$$\boldsymbol{\mathcal{P}} \cdot \hat{\epsilon}^* = -2n\mu\rho_{\mathrm{eg}}^{\mathrm{M}}. \tag{2.146}$$

Here, the magnitude of the coupling factor μ is given as

$$\mu = e\Big| \langle \mathrm{e}| \mathbf{r} |\mathrm{g}\rangle \cdot \hat{\epsilon} \Big|. \tag{2.147}$$

Finally, we arrive at the evolution equations of the magnitude and the phase of the electric field under interaction with two-level atoms:

$$\frac{\partial \mathcal{E}}{\partial t} + c\frac{\partial \mathcal{E}}{\partial x} = \mu_0 n\mu\omega_0 c^2 \mathrm{Im}[\rho_{\mathrm{eg}}^{\mathrm{M}}], \tag{2.148}$$

$$\frac{\partial \phi}{\partial t} + c\frac{\partial \phi}{\partial x} = -\mu_0 n\mu\omega_0 c^2 \frac{1}{\mathcal{E}}\mathrm{Re}[\rho_{\mathrm{eg}}^{\mathrm{M}}]. \tag{2.149}$$

2.4 Maxwell–Bloch equations

As we discussed in the previous Section, in the rotating-phase picture the magnitude and phase of the light envelope are directly coupled to the off-diagonal element of the density matrix. For two-level systems, the von Neumann equation in Eq. (2.133) describing the time evolution of each element in the density matrix is also called Bloch equation. Therefore, the light propagation equations together with the Bloch equations are called Maxwell–Bloch equations [103, 104]. They are the basic equations to describe the interaction between light and matter where both of the systems are affected by each other.

As we will work in the rotating-phase picture from now on, to simplify our notation we will remove the superscript 'M' for the density operator ρ^{M}. Without any specific note, ρ represents the density operator in the rotating-phase picture instead of the operator in Schrödinger picture:

$$\dot{\rho} = i\,[\rho, H_{\mathrm{eff}}] + \Gamma \begin{bmatrix} \rho_{\mathrm{ee}} & -\frac{1}{2}\rho_{\mathrm{ge}} \\ -\frac{1}{2}\rho_{\mathrm{eg}} & -\rho_{\mathrm{ee}} \end{bmatrix} + \beta \begin{bmatrix} 0 & -\frac{1}{2}\rho_{\mathrm{ge}} \\ -\frac{1}{2}\rho_{\mathrm{eg}} & 0 \end{bmatrix}. \tag{2.150}$$

The Bloch equations for the four matrix elements are given as

$$\dot{\rho}_{\mathrm{gg}} = \frac{i\Omega}{2}(\rho_{\mathrm{ge}} - \rho_{\mathrm{eg}}) + \Gamma\rho_{\mathrm{ee}}, \tag{2.151}$$

$$\dot{\rho}_{\mathrm{ge}} = -\frac{i\Omega}{2}(\rho_{\mathrm{ee}} - \rho_{\mathrm{gg}}) - i\Delta_\theta\rho_{\mathrm{ge}} - \frac{\gamma}{2}\rho_{\mathrm{ge}}, \tag{2.152}$$

$$\dot{\rho}_{\mathrm{eg}} = \frac{i\Omega}{2}(\rho_{\mathrm{ee}} - \rho_{\mathrm{gg}}) + i\Delta_\theta\rho_{\mathrm{eg}} - \frac{\gamma}{2}\rho_{\mathrm{eg}}, \tag{2.153}$$

$$\dot{\rho}_{\mathrm{ee}} = \frac{i\Omega}{2}(\rho_{\mathrm{eg}} - \rho_{\mathrm{ge}}) - \Gamma\rho_{\mathrm{ee}}, \tag{2.154}$$

with

$$\Omega = \mu\mathcal{E}, \quad \Delta_\theta = \Delta - \frac{\partial\phi}{\partial t} \quad \text{and} \quad \gamma = \Gamma + \beta, \tag{2.155}$$

and they are coupled to the light propagation equations

$$\frac{\partial\mathcal{E}}{\partial t} + c\frac{\partial\mathcal{E}}{\partial x} = \mu_0 n\mu\omega_0 c^2 \mathrm{Im}[\rho_{\mathrm{eg}}], \tag{2.156}$$

$$\frac{\partial\phi}{\partial t} + c\frac{\partial\phi}{\partial x} = -\mu_0 n\mu\omega_0 c^2 \frac{1}{\mathcal{E}}\mathrm{Re}[\rho_{\mathrm{eg}}]. \tag{2.157}$$

Thus, this set of equations is called *Maxwell–Bloch equations* [103, 104]. Through the Rabi frequency Ω and the detuning Δ_θ in Eq. (2.155), the amplitude $\mathcal{E}$ and phase ϕ of the light field are involved in the atomic populations and coherences in Eqs. (2.151-2.154). In return, the coherence ρ_{eg} (with $\rho_{\mathrm{eg}} = \rho^*_{\mathrm{eg}}$) acts as a dipole source to the light field in Eq. (2.156) and Eq. (2.157), which influences the propagation of the light. The newly defined parameter γ is the total decoherence rate of the atomic system.

There are different variants of Maxwell–Bloch equations (see Appx. D). As another form of the Maxwell–Bloch equations in Eqs. (2.151-2.157), one can explicitly separate the coherence terms ρ_{eg} (or ρ_{ge}) in real and imaginary parts

$$\rho_{\mathrm{eg}} = a + ib, \tag{2.158}$$

$$\rho_{\mathrm{ge}} = a - ib. \tag{2.159}$$

This gives a different form of the Bloch equations:

$$\dot{\rho}_{\mathrm{gg}} = \Omega b + \Gamma\rho_{\mathrm{ee}}, \tag{2.160}$$

$$\dot{a} = -\frac{\gamma}{2}a - \Delta_\theta b, \tag{2.161}$$

$$\dot{b} = \frac{\Omega}{2}(\rho_{\mathrm{ee}} - \rho_{\mathrm{gg}}) + \Delta_\theta a - \frac{\gamma}{2}b, \tag{2.162}$$

$$\dot{\rho}_{\mathrm{ee}} = -\Omega b - \Gamma\rho_{\mathrm{ee}}. \tag{2.163}$$

When the total population, $\rho_{\mathrm{ee}} + \rho_{\mathrm{gg}} = 1$ is conserved, one can define a new variable

$$N = \rho_{\mathrm{ee}} - \rho_{\mathrm{gg}}, \tag{2.164}$$

to represent the population difference (or population inversion) between the excited state

and the ground state. We have

$$\dot{a} = -\frac{\gamma}{2}a - \Delta_\theta b, \tag{2.165}$$

$$\dot{b} = \frac{\Omega}{2}N + \Delta_\theta a - \frac{\gamma}{2}b, \tag{2.166}$$

$$\dot{N} = -2\Omega b - \Gamma\left(N+1\right). \tag{2.167}$$

In this way, the evolution of the electric field becomes

$$\frac{\partial \mathcal{E}}{\partial t} + c\frac{\partial \mathcal{E}}{\partial x} = \mu_0 n \mu \omega_0 c^2 b, \tag{2.168}$$

$$\frac{\partial \phi}{\partial t} + c\frac{\partial \phi}{\partial x} = -\mu_0 n \mu \omega_0 c^2 \frac{1}{\mathcal{E}} a, \tag{2.169}$$

or in the retarded time coordinates

$$\frac{\partial \mathcal{E}\left(x,\tau\right)}{\partial x} = \mu_0 n \mu \omega_0 c b, \tag{2.170}$$

$$\frac{\partial \phi\left(x,\tau\right)}{\partial x} = -\mu_0 n \mu \omega_0 c \frac{1}{\mathcal{E}} a. \tag{2.171}$$

Because n, μ and ω are non-negative quantities, and the magnitude of the electric field $\mathcal{E}$ is also defined to be positive, one can see that the imaginary part b defines whether the light will be absorbed or amplified:

if	$b > 0$,	gain & emission,
if	$b < 0$,	attenuation & absorption.

The real part a is related to the phase of the light field, thus it determines the dispersion or refractive index when light propagates in the medium.

The Maxwell–Bloch equations do not have exact analytical solutions yet. Therefore we developed numerical codes that can solve this equation exactly. Besides that, one can also obtain analytical solutions based on further approximations and assumptions. One possible simplification is to assume that the atoms have evolved into a steady state, and then one can solve the equations explicitly.

2.4.1 Steady-state solutions and rate equations

When the density of the atoms is small such that the variation (absorption/amplification) of the light is negligible, the atoms will evolve into a steady state for times longer than the decoherence time of the atoms. If such conditions are met, one will have $\dot{\rho} = 0$ and all the derivatives of the density matrix elements can be taken to be zero

$$-\frac{\gamma}{2}a - \Delta_\theta b = 0, \tag{2.172}$$

$$\frac{\Omega}{2}N + \Delta_\theta a - \frac{\gamma}{2}b = 0, \tag{2.173}$$

$$-2\Omega b - \Gamma\left(N+1\right) = 0. \tag{2.174}$$

The differential equations for the density matrix are reduced to a set of algebraic equations that can be easily solved as

$$b = -\frac{\Omega\Gamma\gamma}{2\gamma\Omega^2+\Gamma\left(4\Delta_\theta^2+\gamma^2\right)}, \tag{2.175}$$

$$a = \frac{2\Delta_\theta\Omega\Gamma}{2\gamma\Omega^2+\Gamma\left(4\Delta_\theta^2+\gamma^2\right)}, \tag{2.176}$$

$$N = -\frac{\Gamma\left(4\Delta_\theta^2+\gamma^2\right)}{2\gamma\Omega^2+\Gamma\left(4\Delta_\theta^2+\gamma^2\right)}, \tag{2.177}$$

with the relation

$$a = -\frac{2\Delta_\theta}{\gamma}b. \tag{2.178}$$

Furthermore, from Eq. (2.175) and Eq. (2.177) one obtains the following relation between the coherence and population inversion:

$$b = \frac{\Omega\gamma}{\left(4\Delta_\theta^2+\gamma^2\right)}N. \tag{2.179}$$

Due to the fact that $\frac{\Omega\gamma}{\left(4\Delta_\theta^2+\gamma^2\right)} > 0$ always holds, the sign of the coherence b is only determined by the population inversion N. When $N > 0$, one has $b > 0$ and the light field is amplified, though it is negligibly small. This is true because $N > 0$ means that there are more atoms in the excited state than the atoms in the ground state. Therefore, stimulated emission would be larger than the stimulated absorption and the net effect is that the light field is amplified. On the other hand, if $N < 0$, the light will be attenuated as it propagates in the medium.

Another phenomenon revealed by Eq. (2.179) is that the absorption rate is frequency dependent. This can be clearly seen if we rewrite Eq. (2.179) as

$$b = \frac{\Omega}{\gamma}g\left(\omega\right)N, \tag{2.180}$$

with the dimensionless function $g\left(\omega\right)$ being a normalized Lorentzian function given by

$$g\left(\omega\right) = \frac{\gamma^2}{4\left(\omega-\omega_\mathrm{a}\right)^2+\gamma^2} = \frac{\left(\gamma/2\right)^2}{\left(\omega-\omega_\mathrm{a}\right)^2+\left(\gamma/2\right)^2}. \tag{2.181}$$

For simplicity, we have assumed the light to be a plane wave such that

$$\phi(x,t) = (k-k_0)x-(\omega-\omega_0)t, \tag{2.182}$$

and

$$\Delta_\theta = \Delta-\frac{\partial\phi}{\partial t} = \omega_0-\omega_\mathrm{a}+\omega-\omega_0 = \omega-\omega_\mathrm{a}. \tag{2.183}$$

We should mention that here, ω and ω_a are angular frequencies with dimensions of "rad s^{-1}". Therefore, the value of the decay rate Γ should also be given in units of angular frequency. For example, when we have Einstein A coefficient A_eg (in units of "s^{-1}") as the spontaneous decay rate from the excited state to the ground state, one will

have

$$\Gamma = \frac{A_{\mathrm{eg}}}{2\pi}. \tag{2.184}$$

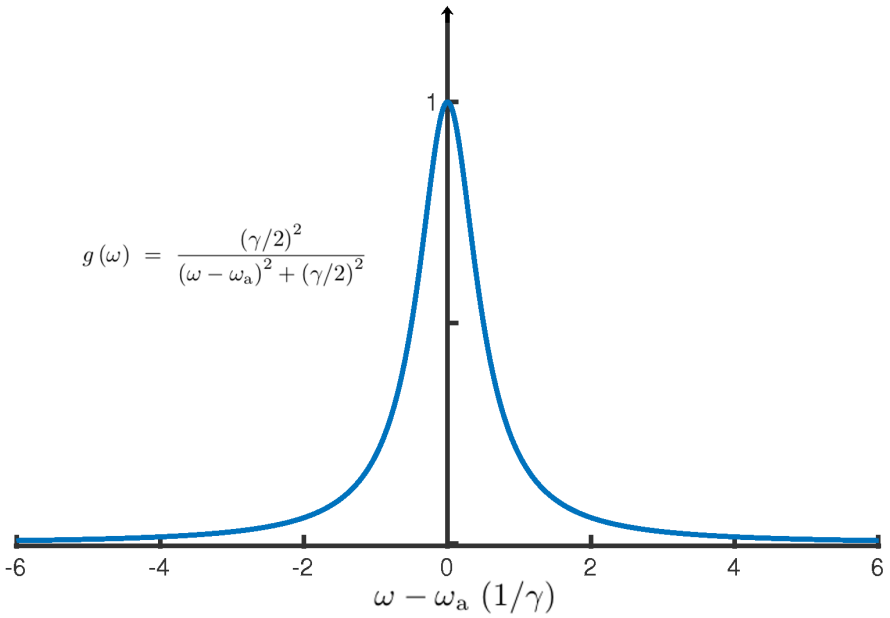

Figure 2.2: Lorenztian line shape of Eq. (2.181).

As we can see from Fig. 2.2, the strongest absorption happens when the light frequency is resonant with the atomic transition. The amplitude and bandwidth of the absorption is given by the decoherence rate γ.

Eq. (2.180) describes the absorption for a single atom. In order to see how the light is affected by the whole medium, we substitute Eq. (2.180) into the evolution of the magnitude of the electric field in Eq. (2.170):

$$\frac{\partial \mathcal{E}(x,\tau)}{\partial x} = \mu_0 n \mu \omega c \frac{\Omega}{\gamma} g(\omega) N. \tag{2.185}$$

Here, we continue to assume a plane wave with the carrier frequency $\omega_0 = \omega$ such that ϕ is constant and does not experience any times and space evolution. Recalling that $\Omega = \mu\mathcal{E}$, the evolution equation of the light field becomes

$$\frac{\partial \mathcal{E}(x,\tau)}{\partial x} = \frac{n\mu^2\omega}{\varepsilon_0 c\gamma} g(\omega) N\mathcal{E} = \frac{1}{2} n\sigma_{\mathrm{eg}}(\omega) N\mathcal{E}, \tag{2.186}$$

where $\mu_0\varepsilon_0 = 1/c^2$ has been used. $\sigma_{\mathrm{eg}}(\omega)$ is the frequency-dependent stimulated emission cross Section defined by

$$\sigma_{\mathrm{eg}}(\omega) = \frac{2\mu^2\omega}{\varepsilon_0 c\gamma} g(\omega). \tag{2.187}$$

From Eq. (B.20), one has the relationship between the dipole moment and the Einstein

A coefficient for a two-level system as

$$\mu^2 = \frac{3\pi\varepsilon_0\hbar c^3}{\omega_{\rm a}^3}A_{\rm eg}. \tag{2.188}$$

Therefore, the stimulated-emission cross section can be written as

$$\sigma_{\rm eg}(\omega) = \frac{6\pi c^2}{\omega_{\rm a}^2}\frac{\omega}{\omega_{\rm a}}\frac{A_{\rm eg}}{\gamma}g(\omega). \tag{2.189}$$

In the resonant case, one has $g(\omega) = g(\omega_{\rm a}) = 1$. The stimulated emission cross Section becomes

$$\sigma_{\rm eg}(\omega_{\rm a}) = \frac{6\pi c^2}{\omega_{\rm a}^2}\frac{A_{\rm eg}}{\gamma}. \tag{2.190}$$

If there is only spontaneous decay, $\gamma = A_{\rm eg}$ and

$$\sigma_{\rm eg}(\omega_{\rm a}) = \frac{6\pi c^2}{\omega_{\rm a}^2} = \frac{3\lambda_{\rm a}^2}{2\pi}. \tag{2.191}$$

This means that the cross Section nearly equals the size of the photons [114], as defined by it's wavelength.

Furthermore, we can also describe the propagation of the light field in terms of the photon flux passing through the atomic medium. This is done with the following definitions of the intensity and photon flux:

$$\mathcal{I} = \frac{c\varepsilon_0}{2}\mathbf{E}^2 = \frac{c\varepsilon_0}{2}\mathcal{E}^2, \tag{2.192}$$

$$\mathcal{J} = \frac{\mathcal{I}}{\hbar\omega}. \tag{2.193}$$

With these relations, one can derive the evolution equation of the photon flux as

$$\frac{\partial\mathcal{J}}{\partial x} = \frac{c\varepsilon_0}{2\hbar\omega}\frac{\partial\mathcal{E}^2}{\partial x} = \frac{c\varepsilon_0}{2\hbar\omega}2\mathcal{E}\frac{\partial\mathcal{E}}{\partial x} = n\sigma_{\rm eg}N\mathcal{J}. \tag{2.194}$$

As the multiplication nN represents the number density of population inversion, it is from Eq. (2.194) that one reveals the physical meaning of $\sigma_{\rm eg}$ as the cross Section of stimulated emission.

Besides, we can also obtain the evolution of the population inversion as

$$\begin{aligned}
\dot{N} &= -2\Omega b - \gamma(N+1) \\
&= -2\frac{\Omega^2}{\gamma}g(\omega)N - \Gamma(N+1) \\
&= -2\frac{\mu^2}{\hbar^2\gamma}\mathcal{E}^2 g(\omega)N - \Gamma(N+1) \\
&= -2\frac{\mu^2}{\hbar^2\gamma}\frac{2\hbar\omega}{c\varepsilon_0}g(\omega)\mathcal{J}N - \Gamma(N+1) \\
&= -2\sigma_{\rm eg}(\omega)\mathcal{J}N - \Gamma(N+1).
\end{aligned} \tag{2.195}$$

By combining Eq. (2.194) and Eq. (2.195), one obtains the *rate-equation description* of the light-matter interaction:

$$\frac{\partial \mathcal{J}(x,\tau)}{\partial x} = n\sigma_{\mathrm{eg}}(\omega) N \mathcal{J}(x,\tau), \tag{2.196}$$

$$\frac{\partial N(x,\tau)}{\partial \tau} = -2\sigma_{\mathrm{eg}}(\omega) \mathcal{J}(x,\tau) N - \Gamma(N+1). \tag{2.197}$$

Here, n is the atomic density, $\sigma_{\mathrm{eg}}(\omega)$ is the stimulated photon emission cross Section with ω the carrier frequency of the light field and $N = \rho_{\mathrm{ee}} - \rho_{\mathrm{gg}}$ is the population inversion. Γ is the decay rate of the excited state. The factor of 2 in the stimulated process on the right hand of Eq. (2.197) represents that a depopulation in the excited state ρ_{ee} is always accompanied by an increase in population ρ_{gg} in the ground state by the same amount, resulting in a change in the population difference by two times of that amount.

For a steady state where N is constant, one can solve Eq. (2.186) and Eq. (2.196) to get the evolution of electric field and the photon flux as

$$\mathcal{E}(x,\tau) = \mathcal{E}(0,\tau) e^{\frac{1}{2}Gx}, \tag{2.198}$$

$$\mathcal{J}(x,\tau) = \mathcal{J}(0,\tau) e^{Gx}, \tag{2.199}$$

with

$$G = n\sigma_{\mathrm{eg}}(\omega) N \tag{2.200}$$

being the gain/attenuation coefficient.

2.5 Summary

Starting with Maxwell's equations and density matrix theory, we obtain two sets of equations that can be used to describe the amplification of a laser in a gain medium. One is given by the elaborate Maxwell–Bloch equations in Eqs. (2.151-2.157) based on density matrix theory; the other is given by the simpler rate equations, Eq. (2.196) and Eq. (2.197), which have been widely used in the laser community. Our calculations show that the latter approach is only accurate for atomic systems in a steady state, or in other words, for the case where the changes in the populations of the atomic state are negligible during the presence of the laser field. Otherwise, one needs to use the Maxwell–Bloch equations.

For the transient lasing considered in this thesis, the populations are underlying fast pumping and decay processes. Therefore, the Maxwell–Bloch equations are used in Chapters 5–7 to fully describe the establishment and propagation of the laser field.

Chapter 3

Multipole transitions

As we realized, a narrower laser bandwidth can be achieved by choosing a transition beyond electric-dipole transitions in the lasing ions. Therefore, in this Chapter, we generalize the density-matrix theory with the usually considered electric-dipole transitions to multipole transitions. We start with the Dirac equation and derive the general interaction Hamiltonian between plane-wave light and matter. The multipole expansion of the plane wave in spherical harmonics results in a series of multipole-transition terms. We will first derive the multipole expansion of the light-matter interaction Hamiltonian, based on Walther Johnson's book on *Atomic structure theory* [115], and obtain the multipole moment for each transition. After that we generalize the density-matrix theory for any multipole transitions. A direct method to get the coupling strength, or multipole moment, in the interaction Hamiltonian needs atomic structure calculations. Considering that there are already existing atomic codes that can be adopted to obtain the energies, rates and oscillator strengths for a given atomic transition, we express the multipole moment, Einstein A coefficient and interaction Hamiltonian in terms of the oscillator strength. With such relations, the light-atom coupling strength can be represented with realistic atomic parameters.

3.1 The Dirac equation

To consider radiative transitions, the spin angular momentum should also be included consistently in the theory. In Schrödinger equation there is no spin information and the spin effect has to be introduced by hand. However, the Dirac equation includes the spin automatically and the coupling between spin and orbit angular momentum is also included therein. Also, for the highly charged ions considered in this work, realistic effects are important. Thus, in this Chapter, we will start with Dirac equation.

Similarly to the Schrödinger equation, the time-dependent Dirac equation for a single electron is given as [115]

$$i\hbar\frac{\partial}{\partial t}\Psi(\mathbf{r},t) \quad = \quad H\Psi(\mathbf{r},t). \tag{3.1}$$

The difference is in the definition of the Hamiltonian and the wave function. Firstly, the Hamiltonian for Dirac equation is defined through

$$H \quad = \quad c\boldsymbol{\alpha}\cdot\boldsymbol{p}+\beta mc^2+V(r), \tag{3.2}$$

with c being the speed of light and $\boldsymbol{\alpha}$ and β are the 4×4 Dirac matrices:

$$\boldsymbol{\alpha} \quad = \quad \begin{bmatrix} 0 & \boldsymbol{\sigma} \\ \boldsymbol{\sigma} & 0 \end{bmatrix}, \beta = \begin{bmatrix} 1_{2\times 2} & 0 \\ 0 & -1_{2\times 2} \end{bmatrix}. \tag{3.3}$$

The vector matrix $\boldsymbol{\sigma} = (\sigma_x, \sigma_y, \sigma_z)$ is constructed from the 2×2 Pauli matrices

$$\sigma_x = \begin{bmatrix} 0 & 1 \\ 1 & 0 \end{bmatrix}, \sigma_y = \begin{bmatrix} 0 & -i \\ i & 0 \end{bmatrix}, \sigma_z = \begin{bmatrix} 1 & 0 \\ 0 & -1 \end{bmatrix}. \tag{3.4}$$

As discussed before in Sec. 2.2, when an external field is involved, the momentum $\boldsymbol{p}$ should be replaced by $\boldsymbol{p} - q\mathbf{A}(\mathbf{r}, t)$, with $\mathbf{A}(\mathbf{r}, t)$ being the vector potential. This yields the interaction Hamiltonian between the bound electron and the external field

$$H_{\mathrm{I}} = ce\boldsymbol{\alpha} \cdot \mathbf{A}(\mathbf{r}, t), \tag{3.5}$$

where $q = -e$ for an electron was used. For a plane wave $\mathbf{A}(\mathbf{r}, t) = \boldsymbol{\mathcal{A}} e^{i(\mathbf{k}\cdot\mathbf{r} - \omega t)} + h.c.$, one has the expressions for the electric and magnetic field as [108]

$$\begin{aligned} \mathbf{E}(\mathbf{r}, t) &= -\nabla\phi(\mathbf{r}, t) - \frac{\partial}{\partial t}\mathbf{A}(\mathbf{r}, t), \\ \mathbf{B}(\mathbf{r}, t) &= -\nabla \times \mathbf{A}(\mathbf{r}, t), \end{aligned}$$

where ϕ is the scalar potential. For the gauge $\nabla\phi(\mathbf{r}, t) = 0$, one has the amplitude of both fields

$$\begin{aligned} \boldsymbol{\mathcal{E}} &= i\omega\boldsymbol{\mathcal{A}} = i\omega\mathcal{A}\hat{\epsilon}, \\ \boldsymbol{\mathcal{B}} &= i\mathbf{k} \times \boldsymbol{\mathcal{A}} = ik\mathcal{A}[\hat{k} \times \hat{\epsilon}], \end{aligned}$$

with

$$\begin{aligned} \mathcal{E} &= i\omega\mathcal{A}, \\ \mathcal{B} &= ik\mathcal{A}, \end{aligned}$$

and

$$\boldsymbol{\mathcal{A}} = \frac{1}{i\omega}\boldsymbol{\mathcal{E}} = \frac{1}{ik}\hat{k} \times \boldsymbol{\mathcal{B}}.$$

Therefore, the Hamiltonian can be written in terms of electric or magnetic fields as

$$\begin{aligned} H_{\mathrm{I}} &= \frac{ce}{i\omega}\boldsymbol{\alpha} \cdot \boldsymbol{\mathcal{E}} e^{i(\mathbf{k}\cdot\mathbf{r} - \omega t)} + h.c. \\ &= \frac{ce\mathcal{E}}{i\omega}\boldsymbol{\alpha} \cdot \hat{\epsilon} e^{i(\mathbf{k}\cdot\mathbf{r} - \omega t)} + h.c. \\ &= -\boldsymbol{d} \cdot \boldsymbol{\mathcal{E}} e^{-i\omega t} + h.c., \end{aligned}$$

or

$$\begin{aligned} H_{\mathrm{I}} &= \frac{ce}{ik}\boldsymbol{\alpha} \cdot [\hat{k} \times \boldsymbol{\mathcal{B}}] e^{i(\mathbf{k}\cdot\mathbf{r} - \omega t)} + h.c. \\ &= \frac{ce\mathcal{B}}{ik}\boldsymbol{\alpha} \cdot \hat{\epsilon} e^{i(\mathbf{k}\cdot\mathbf{r} - \omega t)} + h.c. \\ &= -\boldsymbol{m} \cdot \boldsymbol{\mathcal{B}} e^{-i\omega t} + h.c.. \end{aligned}$$

The effective electric and magnetic momenta are defined according to

$$\boldsymbol{d} = -\frac{ce}{i\omega}\left(\boldsymbol{\alpha}\cdot\hat{\epsilon}\right)e^{i\mathbf{k}\cdot\mathbf{r}}\hat{\epsilon}^{*}, \tag{3.6}$$

$$\boldsymbol{m} = -\frac{ce}{ik}\left(\boldsymbol{\alpha}\cdot\hat{\epsilon}\right)e^{i\mathbf{k}\cdot\mathbf{r}}[\hat{k}\times\hat{\epsilon}^{*}]. \tag{3.7}$$

Note that $|\boldsymbol{d}| = |\boldsymbol{m}|/c$. As we can see, at this stage, there is no difference between electric- and magnetic-multipole interactions. After the multipole expansion, one can obtain monopole, dipole and quadrupole contributions to the effective momenta. The dimensions of $\boldsymbol{d}$ and $\boldsymbol{m}$ are

$$[\boldsymbol{d}] = \left[\frac{ce}{i\omega}\right] = \left[\frac{e}{k}\right] = [er]\,, \tag{3.8}$$

$$[\boldsymbol{m}] = \left[\frac{ce}{ik}\right] = [ecr] = [e\hbar]\,, \tag{3.9}$$

Indicating that they represent effective 'dipole' moments.

In density-matrix theory, one needs to know the matrix form of the interaction Hamiltonian. According to Eq. (2.94), each element of the Hamiltonian can be written as

$$[H_{\mathrm{I}}]_{ba} \equiv \langle b|\, H_{\mathrm{I}}\,|a\rangle = \frac{ec\mathcal{E}}{i\omega}\int \mathrm{d}\mathbf{r}\psi_b^{\dagger}\left(\boldsymbol{\alpha}\cdot\hat{\epsilon}e^{i(\mathbf{k}\cdot\mathbf{r}-\omega t)} + h.c.\right)\psi_a. \tag{3.10}$$

In principle, one could calculate this integral directly and obtain each matrix element of the Hamiltonian. However, in the following, we will show how these terms can be calculated from the Einstein A coefficient and oscillator strength that can be obtained from ab atomic database or code. The first step of such an approach is to recognize the relation between $[H_{\mathrm{I}}]_{ba}$ and the dimensionless transition amplitude T_{ab}. In first-order time-dependent perturbation theory (Appx. A.3), the matrix element T_{ab} for a wave polarized in $\hat{\epsilon}_\nu$ is

$$T_{ab}(\hat{k},\nu) = \int \mathrm{d}\mathbf{r}\psi_b^{\dagger}\boldsymbol{\alpha}\cdot\hat{\epsilon}_\nu e^{i\mathbf{k}\cdot\mathbf{r}}\psi_a. \tag{3.11}$$

Therefore, the interaction Hamiltonian can be written as

$$[H_{\mathrm{I}}]_{ba} = \frac{ec\mathcal{E}}{i\omega}T_{ab}(\hat{k},\nu)e^{-i\omega t} + h.c. = d\cdot\mathcal{E} + h.c., \tag{3.12}$$

with the scalar effective 'dipole' moment given as

$$d = \frac{ec}{i\omega}T_{ab}(\hat{k},\nu). \tag{3.13}$$

Using the relation between the Einstein A coefficient and the transition amplitude

$$A_{ba} = \frac{\alpha}{2\pi}\omega\int \mathrm{d}\Omega_k \sum_{\nu}\left|T_{ba}(\hat{k},\nu)\right|^2 = 6\alpha\omega\left|T_{ba}(\hat{k},\nu)\right|^2, \tag{3.14}$$

one obtains the effective 'dipole' moment as

$$d^2 = \frac{3e^2c^2}{4\alpha\omega^3}A_{ba}. \tag{3.15}$$

Here, Eq. (3.15) is a general relation between the 'dipole' moment and the Einstein A coefficient. Later we will show that, for all multipole transitions, there is always an effective 'dipole' moment as defined in Eq. (3.13) related to the multipole transition.

3.2 Multipole transition amplitude

The multipole transition series originate from the multipole expansion of the vector light field in the basis of vector spherical harmonics. To proceeds, we define a new field

$$\mathbf{A}(\mathbf{r},\omega) = \hat{\epsilon}e^{i\mathbf{k}\cdot\mathbf{r}},$$

which is just a normalized vector potential of a plane-wave light field. Expanding this function in the basis of vector spherical harmonics (see Appx. E), in velocity gauge, one obtains [115]

$$\mathbf{A}(\mathbf{r},\omega) = 4\pi \sum_{JM\lambda} i^{J-\lambda} \left(\boldsymbol{Y}_{JM}^{(\lambda)*}(\hat{k})\cdot\hat{\epsilon}\right) \boldsymbol{a}_{JM}^{(\lambda)}(\mathbf{r}), \tag{3.16}$$

with the multipole potential $\boldsymbol{a}_{JM}^{(\lambda)}(\mathbf{r})$ given by

$$\boldsymbol{a}_{JM}^{(0)}(\mathbf{r}) = j_J(kr)\boldsymbol{Y}_{JM}^{(0)}(\hat{r}), \tag{3.17}$$

$$\boldsymbol{a}_{JM}^{(1)}(\mathbf{r}) = \left[j'_J(kr) + \frac{j_J(kr)}{kr}\right]\boldsymbol{Y}_{JM}^{(1)}(\hat{r}) + \sqrt{J(J+1)}\frac{j_J(kr)}{kr}\boldsymbol{Y}_{JM}^{(-1)}(\hat{r}). \tag{3.18}$$

Here, J is the total angular momentum and M is the magnetic quantum number of the transition. The definition of the spherical Bessel functions $j_J(kr)$ and the vector spherical harmonics $\boldsymbol{Y}_{JM}^{(\lambda)}(\hat{r})$ can be found in Appx. E and in reference [115]. Especially, $\lambda = 0$ corresponds to magnetic multipole potentials and $\lambda = 1$ corresponds to electric multipole potentials. All information on the polarization $\hat{\epsilon}$ and propagation direction $\hat{k}$ is included in the expansion coefficients $\boldsymbol{Y}_{JM}^{(\lambda)*}(\hat{k})\cdot\hat{\epsilon}$. The strength $\mathcal{A}$ of the field is normalized in the definition of $\mathbf{A}(\mathbf{r},\omega)$.

Based on the multipole expansion of the field, the transition amplitude from state $|a\rangle$ to state $|b\rangle$ defined in Eq. (3.11) can be expanded into a series of multipole transition amplitudes as

$$T_{ba}(\hat{k},\nu) = 4\pi \sum_{JM\lambda} i^{J-\lambda} \left(\boldsymbol{Y}_{JM}^{(\lambda)*}(\hat{k})\cdot\hat{\epsilon}_\nu\right) \left[T_{JM}^{(\lambda)}\right]_{ba}, \tag{3.19}$$

with the multipole transition amplitude being

$$\left[T_{JM}^{(\lambda)}\right]_{ba} = \int \mathrm{d}\mathbf{r}\psi_b^\dagger \boldsymbol{\alpha}\cdot\boldsymbol{a}_{JM}^{(\lambda)}(\mathbf{r})\psi_a. \tag{3.20}$$

For spontaneous emission from an excited state to the ground state, the photon can be emitted to any direction and polarization. In order to obtain the total transition probability, one needs to sum the transition probability over all the propagation directions $\hat{k}$ and polarizations $\hat{\epsilon}_\nu$. This results in the total transition probability (Einstein A coefficient) as

$$A_{ba} = \frac{\alpha}{2\pi}\omega\left|T_{ba}\right|^2, \tag{3.21}$$

with

$$|T_{ba}|^2 = \left| \sum_{\hat{k},\nu} T_{ba}(\hat{k},\nu) e^{i\varphi(\hat{k},\nu)} \right|^2 .$$

The extra phase factor $\varphi(\hat{k},\nu)$ characterizing the phase of a wave for a given $\hat{k}$ and ϵ_ν. Physically, they stem from the vector potential through

$$\mathbf{A}(\mathbf{r},\omega) = \int \mathrm{d}\Omega_k \sum_\nu \mathcal{A}(\hat{k},\nu)\hat{\epsilon}_\nu e^{i\mathbf{k}\cdot\mathbf{r}+i\varphi(\hat{k},\nu)}.$$

If we assume that the photons emitted into different directions and polarizations are incoherent with each other, we obtain

$$\left\langle |T_{ba}|^2 \right\rangle = \sum_{\hat{k},\nu} \left| T_{ba}(\hat{k},\nu) \right|^2 = \int \mathrm{d}\Omega_k \sum_\nu \left| T_{ba}(\hat{k},\nu) \right|^2 ,$$

with the term for a given $\hat{k}$ and $\hat{\epsilon}$ being

$$\begin{aligned} & \left| T_{ba}(\hat{k},\nu) \right|^2 \\ = \; & 16\pi^2 \sum_{J'M'\lambda'} i^{-J'+\lambda'} \left(\boldsymbol{Y}^{(\lambda)}_{J'M'}(\hat{k}) \cdot \hat{\epsilon}^*_\nu \right) \left[T^{(\lambda')}_{J'M'} \right]^*_{ba} \sum_{JM\lambda} i^{J-\lambda} \left(\boldsymbol{Y}^{(\lambda)*}_{JM}(\hat{k}) \cdot \hat{\epsilon}_\nu \right) \left[T^{(\lambda)}_{JM} \right]_{ba} . \end{aligned}$$

In the above equation, the effects of integration and summation only show up in the two coefficients of the multipole expansion

$$\left(\boldsymbol{Y}^{(\lambda)}_{J'M'}(\hat{k}') \cdot \hat{\epsilon}^*_{\nu'} \right) \left(\boldsymbol{Y}^{(\lambda)*}_{JM}(\hat{k}) \cdot \hat{\epsilon}_\nu \right),$$

which can be easily calculated. Firstly, the summation over $\hat{\epsilon}_\nu$ gives

$$\sum_\nu \left(\boldsymbol{Y}^{(\lambda)}_{J'M'}(\hat{k}) \cdot \hat{\epsilon}^*_\nu \right) \left(\boldsymbol{Y}^{(\lambda)*}_{JM}(\hat{k}) \cdot \hat{\epsilon}_\nu \right) = \left(\boldsymbol{Y}^{(\lambda)}_{J'M'}(\hat{k}) \cdot \boldsymbol{Y}^{(\lambda)*}_{JM}(\hat{k}) \right).$$

Then integration over all the propagation directions leads to the orthogonality relation

$$\int \mathrm{d}\Omega_k \left(\boldsymbol{Y}^{(\lambda)}_{J'M'}(\hat{k}) \cdot \boldsymbol{Y}^{(\lambda)*}_{JM}(\hat{k}) \right) = \delta_{J'J}\delta_{M'M}\delta_{\lambda'\lambda},$$

expressed in with the Kronecker δ symbols. Therefore, one obtains

$$\left| T_{ba}(\hat{k},\nu) \right|^2 = 16\pi^2 \sum_{JM\lambda} \left| \left[T^{(\lambda)}_{JM} \right]_{ba} \right|^2 , \tag{3.22}$$

which gives the total transition probability as

$$A_{ba} = \frac{\alpha}{2\pi}\omega \left\langle |T_{ba}|^2 \right\rangle = 8\pi\alpha\omega \sum_{JM\lambda} \left| \left[T^{(\lambda)}_{JM} \right]_{ba} \right|^2 . \tag{3.23}$$

This is an incoherent summation over all the possible multipole transitions. Selection rules based on angular momentum conservation laws are included in the multipole transition momenta $\left[T^{(\lambda)}_{JM} \right]_{ba}$. From Eqs. (3.17,3.18,3.20) and the orthogonality relation in

spherical harmonics, only one J and λ remains, and all the other terms vanish. Therefore, the Einstein A coefficient is only characterized by a specific J-pole λ-transition

$$A_{ba} = \left[A_J^{(\lambda)}\right]_{ba} = 8\pi\alpha\omega \sum_M \left|\left[T_{JM}^{(\lambda)}\right]_{ba}\right|^2. \tag{3.24}$$

From Eq. (E.56), we also know the relation between the Einstein A coefficient and the reduced oscillator strength

$$\left[A_J^{(\lambda)}\right]_{ba} = -\frac{2\alpha\hbar\omega^2}{mc^2}\left[\bar{f}_J^{(\lambda)}\right]_{ba}. \tag{3.25}$$

3.3 The Hamiltonian of multipole transitions

For a light field, the vector potential can be written in terms of a carrier frequency ω_0 and envelope $\mathcal{A}$:

$$\mathbf{A}^{(+)}(\mathbf{x},t) = \frac{1}{2}\boldsymbol{\mathcal{A}}(\mathbf{x},t)\, e^{i(\mathbf{k}_0\cdot\mathbf{x}-\omega_0 t)} = \frac{1}{2}\boldsymbol{\mathcal{A}}(\mathbf{x}_0+\mathbf{r},t)\, e^{i(\mathbf{k}_0\cdot\mathbf{x}_0-\omega_0 t)} e^{i\mathbf{k}_0\cdot\mathbf{r}}. \tag{3.26}$$

The coordinate $\mathbf{x} = \mathbf{x}_0 + \mathbf{r}$ is separated into the coordinate of the nucleus $\mathbf{x}_0$ and the coordinate of the electron $\mathbf{r}$. If the envelopes vary slowly in the range of the atomic size, one can approximate $\boldsymbol{\mathcal{A}}(\mathbf{x}_0+\mathbf{r},t) \approx \boldsymbol{\mathcal{A}}(\mathbf{x}_0,t)$. This leads to

$$\mathbf{A}^{(+)}(\mathbf{x},t) \approx \mathbf{A}^{(+)}(\mathbf{x}_0,t)\, e^{i\mathbf{k}_0\cdot\mathbf{r}} = \frac{1}{2}\boldsymbol{\mathcal{A}}(\mathbf{x}_0,t)\, e^{i(\mathbf{k}_0\cdot\mathbf{x}_0-\omega_0 t)} e^{i\mathbf{k}_0\cdot\mathbf{r}}. \tag{3.27}$$

With $\mathbf{x}_0$ being a parameter, the electric field has the form

$$\mathbf{E}^{(+)}(\mathbf{x},t) \approx \mathbf{E}^{(+)}(\mathbf{x}_0,t)\, e^{i\mathbf{k}_0\cdot\mathbf{r}} = \frac{1}{2}\boldsymbol{\mathcal{E}}(\mathbf{x}_0,t)\, e^{i(\mathbf{k}_0\cdot\mathbf{x}_0-\omega_0 t)} e^{i\mathbf{k}_0\cdot\mathbf{r}}, \tag{3.28}$$

where $\boldsymbol{\mathcal{E}}(\mathbf{x}_0,t) = i\omega_0\boldsymbol{\mathcal{A}}(\mathbf{x}_0,t)$ is the envelope of the electric field. Here, it is a complex function because the phase function is absorbed into $\boldsymbol{\mathcal{E}}(\mathbf{x}_0,t)$. The Hamiltonian in Eq. (3.6) is replaced by

$$H_{\mathrm{I}} = -\boldsymbol{d}\cdot\boldsymbol{\mathcal{E}}(\mathbf{x}_0,t)\, e^{i(\mathbf{k}_0\cdot\mathbf{x}_0-\omega_0 t)} + h.c.,$$

with the effective 'dipole' moment $\boldsymbol{d}$ defined by Eq. (3.6).

Based on discussions in Appx. E.2.2, the effective moment can be expanded in terms of multipole momenta

$$\boldsymbol{d} = \sum_{JM\lambda} \boldsymbol{d}_{JM}^{(\lambda)}, \tag{3.29}$$

with

$$\begin{aligned}\boldsymbol{d}_{JM}^{(\lambda)} &= -\frac{ce\hat{\epsilon}^*}{i\omega}\left(4\pi i^{J-\lambda}\left(\boldsymbol{Y}_{JM}^{(\lambda)*}(\hat{k})\cdot\hat{\epsilon}\right)\sqrt{\frac{(2J+1)(J+1)}{4\pi J}}\frac{k^J}{(2J+1)!!}q_{JM}^{(\lambda)}(\mathbf{r})\right)\\ &= -\frac{ce\hat{\epsilon}^*}{i\omega}\left(4\pi i^{J-\lambda}\left(\boldsymbol{Y}_{JM}^{(\lambda)*}(\hat{k})\cdot\hat{\epsilon}\right)\sqrt{\frac{(2J+1)(J+1)}{4\pi J}}t_{JM}^{(\lambda)}(\mathbf{r})\right),\end{aligned} \tag{3.30}$$

with $q^{(\lambda)}_{JM}(\mathbf{r})$ being the electric and magnetic J-pole-moment operator for $\lambda = 1$ and $\lambda = 0$, respectively. $t^{(\lambda)}_{JM}(\mathbf{r})$ is the corresponding J-pole-transition operator. Therefore, the Hamiltonian can be expanded in terms of multipole transitions Hamiltonian as

$$H_{\rm I} = \sum_{JM\lambda} d^{(\lambda)}_{JM} \cdot \mathcal{E}\left(\mathbf{x}_0, t\right) e^{i(\mathbf{k}_0\cdot\mathbf{x}_0 - \omega_0 t)} + h.c. = \sum_{JM\lambda} \left[H^{(\lambda)}_{JM}\right]_{\rm I}, \tag{3.31}$$

with the multipole transitions Hamiltonian given by

$$\left[H^{(\lambda)}_{JM}\right]_{\rm I} = d^{(\lambda)}_{JM} \cdot \mathcal{E}\left(\mathbf{x}_0, t\right) e^{i(\mathbf{k}_0\cdot\mathbf{x}_0 - \omega_0 t)} + h.c. \tag{3.32}$$

In matrix form, each element of the Hamiltonian is

$$\left[H^{(\lambda)}_{JM}\right]_{{\rm I}ba} = \langle\psi_b| d^{(\lambda)}_{JM} |\psi_a\rangle \cdot \mathcal{E}\left(\mathbf{x}_0, t\right) e^{i(\mathbf{k}_0\cdot\mathbf{x}_0 - \omega_0 t)} + h.c.. \tag{3.33}$$

As we discussed before, for given eigenstates $|\psi_a\rangle$ and $|\psi_b\rangle$, there is only one nonzero multipole transition and all the other terms vanish. Substituting the relation between multipole transition operator and its corresponding oscillator strength from E.52, the amplitude of the effective multipole moment $\mu^{(\lambda)}_{JM}$ between the two states is given as

$$\mu^{(\lambda)}_{JM} = \left|\langle\psi_b| d^{(\lambda)}_{JM} |\psi_a\rangle\right| = \frac{4\pi c e}{\omega} \left|\boldsymbol{Y}^{(\lambda)*}_{JM}(\hat{k})\cdot\hat{\epsilon}\right| \sqrt{\frac{\hbar\omega_{ba}}{4\pi m c^2}\left[f^{(\lambda)}_{JM}\right]_{ab}}. \tag{3.34}$$

Therefore, we obtain the new form of the matrix element of the interaction Hamiltonian as

$$\left[H^{(\lambda)}_{JM}\right]_{{\rm I}ba} = \mu^{(\lambda)}_{JM}\mathcal{E} e^{i(\mathbf{k}_0\cdot\mathbf{x}_0 - \omega_0 t + \phi_0)} + h.c., \tag{3.35}$$

with the term ϕ_0 being defined according to

$$\langle\psi_b| d^{(\lambda)}_{JM} |\psi_a\rangle = \mu^{(\lambda)}_{JM} e^{i\phi_0}. \tag{3.36}$$

By defining the multipole Rabi frequency

$$\Omega = \mu^{(\lambda)}_{JM}\mathcal{E}, \tag{3.37}$$

the Hamiltonian is represented in the same form of what we obtained for electric-dipole transition in Sec. (2.3). Because the oscillator strength can be obtained from e.g. the GRASP atomic structure code, the above form gives the direct calculations of the coupling strength for given multipole transitions.

3.4 Multipole wave propagation

There have been many discussions on Maxwell's equations including quadrupole terms [116–120]. However, all of them are based on Cartesian coordinates which makes the discussions difficult to be generalized to higher multipole radiation cases. Here we will show how they can be simplified in the basis of multipole potentials.

As introduced in Sec. 2.1, Maxwell's equations in a medium without free charges and

currents are given as [108]

$$\nabla \cdot \mathbf{D} = 0, \tag{3.38}$$
$$\nabla \cdot \mathbf{B} = 0, \tag{3.39}$$
$$\nabla \times \mathbf{E} = -\frac{\partial \mathbf{B}}{\partial t}, \tag{3.40}$$
$$\nabla \times \mathbf{H} = \mu_0 \frac{\partial \mathbf{D}}{\partial t}, \tag{3.41}$$

where the displacement field $\mathbf{D}$ and the magnetizing field $\mathbf{H}$ are defined through

$$\mathbf{D} = \varepsilon_0 \mathbf{E} + \mathbf{P}, \tag{3.42}$$
$$\mathbf{H} = \frac{1}{\mu_0}\mathbf{B} - \mathbf{M}. \tag{3.43}$$

Usually, the polarization field $\mathbf{P}$ and magnetization field $\mathbf{M}$ are defined through the electric-dipole moment and the magnetic-dipole moment

$$\mathbf{P} = N \langle e\mathbf{r} \rangle, \tag{3.44}$$
$$\mathbf{M} = N \left\langle \frac{e}{m} (\mathbf{L} + \mathbf{2S}) \right\rangle. \tag{3.45}$$

When multipole radiation is considered, one can generalized the field $\mathbf{P}$ to an effective multipole polarization field

$$\mathbf{P}^{(\lambda)}_{\mathbf{JM}} = N \left\langle \boldsymbol{d}^{(\lambda)}_{JM} \right\rangle. \tag{3.46}$$

In this way, the Maxwell-Bloch equation would be of the same form as derived in Sec. 2.4 and Appx. D.

We start tart with the wave propagation equation from Eq. (2.27)

$$\nabla^2 \mathbf{E}(\mathbf{x}_0, t) - \frac{1}{c^2} \frac{\partial^2 \mathbf{E}(\mathbf{x}_0, t)}{\partial t^2} = \mu_0 \frac{\partial^2 \mathbf{P}(\mathbf{x}_0, t)}{\partial t^2}, \tag{3.47}$$

and

$$\mathbf{E}^{(+)}(\mathbf{x}_0, t) = \frac{1}{2} \boldsymbol{\mathcal{E}}(\mathbf{x}_0, t)\, e^{i(\mathbf{k}_0 \cdot \mathbf{x}_0 - \omega_0 t)}, \tag{3.48}$$
$$\mathbf{P}^{(+)}(\mathbf{x}_0, t) = \frac{1}{2} \boldsymbol{\mathcal{P}}(\mathbf{x}_0, t)\, e^{i(\mathbf{k}_0 \cdot \mathbf{x}_0 - \omega_0 t)}, \tag{3.49}$$

with $\mathcal{E}$ and $\mathcal{P}$ being the amplitude of the envelope of electric field and polarization field, respectively. The Laplace operator ∇^2 now is acting with respect to $\mathbf{x}_0$. In Chapter 2, the wave propagation of $\mathcal{E}$ is accounted for in terms of amplitude and phase functions separately. However, from Appx. D, one also obtains the wave propagation equation of the complex field:

$$\frac{\partial \mathcal{E}}{\partial t} + c \frac{\partial \mathcal{E}}{\partial x_0} = \frac{i \mu_0 \omega_0 c^2}{2} \boldsymbol{\mathcal{P}} \cdot \hat{\epsilon}^*. \tag{3.50}$$

As the Hamiltonian in Eq. (3.35) represents the same form as the Hamiltonian of the electric-dipole transitions discussed in Chapter 2 and Appx. D, the corresponding

Maxwell–Bloch equations used their can be directly applied to the case of multipole transitions.

In terms of the complex light field discussed in Appx. D, one obtains the Maxwell–Bloch equations for multipole transitions as:

$$\dot{\rho}_{\rm gg} = \frac{i}{2}\left(\Omega\rho_{\rm ge} - \Omega^*\rho_{\rm eg}\right) + \Gamma\rho_{\rm ee}, \tag{3.51}$$

$$\dot{\rho}_{\rm ge} = i\frac{\Omega^*}{2}\left(\rho_{\rm gg} - \rho_{\rm ee}\right) - i\Delta\rho_{\rm ge} - \frac{\gamma}{2}\rho_{\rm ge}, \tag{3.52}$$

$$\dot{\rho}_{\rm eg} = i\frac{\Omega}{2}\left(\rho_{\rm ee} - \rho_{\rm gg}\right) + i\Delta\rho_{\rm eg} - \frac{\gamma}{2}\rho_{\rm eg}, \tag{3.53}$$

$$\dot{\rho}_{\rm ee} = \frac{i}{2}\left(\Omega^*\rho_{\rm eg} - \Omega\rho_{\rm ge}\right) - \Gamma\rho_{\rm ee}. \tag{3.54}$$

with

$$\Omega = \mu_{JM}^{(\lambda)}\mathcal{E}, \quad \Delta = \omega_0 - \omega_{\rm a} \quad \text{and} \quad \gamma = \Gamma + \beta, \tag{3.55}$$

and they are coupled to the light propagation equation

$$\frac{\partial\mathcal{E}}{\partial t} + c\frac{\partial\mathcal{E}}{\partial x} = -i\mu_0 n\mu\omega_0 c\rho_{\rm eg}. \tag{3.56}$$

These equations are extensively used in Chapters 5–7.

Compared to the Maxwell–Bloch equations given by Eqs. (2.151–2.157) where the amplitude and phase of the light field is treated separately, Eqs. (3.51–3.56) are equations with a complex light field and the singularity problems in the numerical simulation is removed. Therefore, the equations represented here are extensively used in the numerical and analytical discussion of lasing processes in Chapters 5–7.

3.5 Summary

In this Chapter, we generalized the Maxwell–Bloch theory to include multipole transitions. The multipole moment and the Rabi frequency are written in a form which allows their direct evaluations by the help of existing computer codes or transitions. As we show later, lasing transitions with higher multipole rates lead to a narrower bandwidth in the X-ray lasing.

Chapter 4

Spectral broadening

The gain medium of our lasing scheme is based on highly charged ions in a hot dense plasma in which fast collisions occur (see also Appendix F), resulting in a broadening of the lasing transition [121–126]. Therefore, in this Chapter, different spectral broadening effects e.g. the Doppler broadening, electron-ion impact broadening and ion-ion Stark broadening arising in the plasma are considered. The Doppler broadening is presented in Sec. 4.1 by assuming a Maxwell–Boltzmann distribution of the ions' kinetic energy. Then, the formula for the electron impact broadening in the presence of a Coulomb scattering potential is derived in Sec. 4.2. After that, the formula for the ionic Stark broadening of the transition in He-like ions is discussed. The evaluation of these formulas requires detailed calculations of atomic structures. However, we show how these formulas can be approximately calculated with Einstein A coefficients and oscillator strengths from an atomic code.

4.1 Doppler broadening

For an atom moving with velocity u, the corresponding Doppler shift of frequency ν_0 is given as [125, 126]

$$\delta\nu = \frac{u}{c}\nu_0. \tag{4.1}$$

Therefore, the the frequency seen by the atom is

$$\nu = \left(1 - \frac{u}{c}\right)\nu_0. \tag{4.2}$$

For gases with Maxwell-Boltzmann velocity distribution, different atoms get different Doppler shift. The corresponding distribution of the shift is just given by the Maxwell–Boltzmann distribution of the gas

$$\phi(\nu) = \frac{2\sqrt{\ln 2}}{\sqrt{\pi}\Delta\nu_D}\exp\left\{-\left(\frac{2\sqrt{\ln 2}}{\Delta\nu_D}(\nu-\nu_0)\right)^2\right\}, \tag{4.3}$$

which is also a Gaussian distribution with the FWHM given as

$$\Delta\nu_D = 2\sqrt{\frac{2k_{\mathrm{B}}T_{\mathrm{i}}\ln 2}{m_{\mathrm{i}}c^2}}\nu_0, \tag{4.4}$$

with $k_{\mathrm{B}} = 1.38\times10^{-23}\ \mathrm{m^2\cdot kg\cdot s^{-2}\cdot K^{-1}}$ the Boltzmann's constant, T_{i} the temperature of the ion gas and m_{i} the mass of the atom. Introducing the mass number $M_{\mathrm{i}} = m_{\mathrm{i}}/m_{\mathrm{p}}$,

with $m_{\rm p} = 1.673 \times 10^{-27}$ kg, the Doppler broadening can be rewritten in a form

$$\frac{\Delta\nu_D}{\nu_0} = 7.689 \times 10^{-5}\sqrt{T_{\rm i}[\text{eV}]/M_{\rm i}}. \tag{4.5}$$

Here, the temperature is in units of eV, with 1 eV equivalent to 11594 K. The relative broadening $\frac{\Delta\nu_D}{\nu_0}$ is proportional to the square of temperature, and inversely proportional to the mass of the atom.

For Ne^{8+} with $M_{\rm i} = 20$, the relative Doppler broadening under temperature $T_{\rm i} = 0.042$ eV gives

$$\frac{\Delta\nu_D}{\nu_0} = 3.523 \times 10^{-6}. \tag{4.6}$$

In the case of x-ray lasing with $h\nu_0 = 920$ eV, the Doppler broadening in the unit of meV is given as

$$h\Delta\nu_D = 3.24 \text{ meV} . \tag{4.7}$$

4.2 Electron–impact broadening

In hot plasmas, the collisions between electron–ion and ion–ion modify the wave function of the bound electron states in the ions. When the collisions are much faster compared to the time scale Δt we are interested about, the ion undergoes large number of collisions with electrons or ions. Therefore, the average modifications of the wave functions of the bound electrons results in an effective Hamiltonian given by Eq. (F.68):

$$\mathcal{H} = i\hbar\sum_i f_i(S_i - 1), \tag{4.8}$$

with f_i the collision frequency and S_i the scattering matrix of the i-th type of collisions. For a low-temperature dense plasma, as discussed in this thesis, the ions move much slower compared the electrons such that the ion-ion collisions are inefficient. Thus, the spectral broadening by neighboring ions are accounted by a quasi Stark field discussed in Sec. 4.3. Nevertheless, the procedure for the calculation of both electron–ion and ion–ion impact broadenings are the same. In the following, we will first derive the general formula for the impact broadening of collisions with a charge particle. After that, we will only focus on the results for the case of electron-impact broadening.

The collisions lead to energy shifts and spectral broadenings of the ionic transitions

$$\frac{1}{i\hbar}\mathcal{H} = w + id. \tag{4.9}$$

To calculate the values of the shift and broadening of a specific transition for a ion under collisions with other charged particles (electrons or ions), in the following, we will call the ion we are interested in as the emitter and call the other charged particles colliding with the ion as the perturbers. Then the total interaction experienced by the emitter is given by

$$U = \sum_i U_i, \tag{4.10}$$

with U_i the interaction between the emitter and the i-th perturber given by

$$U_i = \frac{(Z+1)Z_i e^2}{4\pi\varepsilon_0 R_i} - \frac{Z_i e^2}{4\pi\varepsilon_0 \left|\boldsymbol{r}-\boldsymbol{R}_i\right|}. \tag{4.11}$$

Here, Z is the charge number of the emitter, Z_i is the charge number of the i-th perturber. $\boldsymbol{R}_i$ is the displacement of the i-th perturber with respect to the nuclei of the emitter, and $\boldsymbol{r}$ is the displacement of the electron in the emitter. For $R_i \gg r$, one has

$$\begin{aligned}
\frac{Z_i e^2}{4\pi\varepsilon_0 \left|\boldsymbol{r}-\boldsymbol{R}_i\right|} &= \frac{Z_i e^2}{4\pi\varepsilon_0 \sqrt{R_i^2 + r^2 - 2\boldsymbol{r}\cdot\boldsymbol{R}_i}} \\
&\approx \frac{Z_i e^2}{4\pi\varepsilon_0 \sqrt{R_i^2 - 2\boldsymbol{r}\cdot\boldsymbol{R}_i}} \\
&= \frac{Z_i e^2}{4\pi\varepsilon_0 R_i} \frac{1}{\sqrt{1 - 2\frac{\boldsymbol{r}\cdot\boldsymbol{R}_i}{R_i^2}}} \\
&\approx \frac{Z_i e^2}{4\pi\varepsilon_0 R_i} \left(1 - \frac{\boldsymbol{r}\cdot\boldsymbol{R}_i}{R_i^2} + \frac{3}{2}\left(\frac{\boldsymbol{r}\cdot\boldsymbol{R}_i}{R_i^2}\right)^2 + ...\right).
\end{aligned} \tag{4.12}$$

Thus, the i-th interaction Hamiltonian can be approximated as

$$U_i \approx \frac{Z Z_i e^2}{4\pi\varepsilon_0 R_i} + \frac{Z_i e^2}{4\pi\varepsilon_0 R_i^3}\boldsymbol{r}\cdot\boldsymbol{R}_i - \frac{3Z_i e^2}{8\pi\varepsilon_0 R_i^5}\left(\boldsymbol{r}\cdot\boldsymbol{R}_i\right)^2. \tag{4.13}$$

The first term refers to the Coulomb interaction between the two particles, the second term refers to the dipole interaction that describe the potential energy of and charged perturber in the field of the emitter's electron-nuclei dipole. The third term refers to quadrupole interaction which is prominent only when the perturber is very close to the emitter. Surely, Coulomb interaction is much stronger than the dipole and quadrupole interactions when $R_i \gg r$. However, such Coulomb term has no dependence on the bound electrons in the emitter, it only acts as a global phase shift for all the eigenstates, thus affecting the trajectories of the perturbers during the collisions. Besides, the quadrupole term is also small compared to dipole term when $R_i \gg r$, we will also neglect such effect in the following. Therefore, the interaction Hamiltonian giving rise to phase shift, thus broadening can be approximately accounted for as [121, 122, 125, 126]

$$U_i \approx \frac{Z_i e^2}{4\pi\varepsilon_0 R_i^3}\boldsymbol{r}\cdot\boldsymbol{R}_i. \tag{4.14}$$

With this interaction Hamiltonian, the scattering matrix can be written as (Appx. F.6)

$$\begin{aligned}
S_i - 1 &= \frac{1}{i\hbar}\int_{-\infty}^{\infty} \mathrm{d}t U_i(t) + \left(\frac{1}{i\hbar}\right)^2 \int_{-\infty}^{\infty}\mathrm{d}t_1 \int_{-\infty}^{t_1}\mathrm{d}t_2 U_i(t_1)U_i(t_2) \\
&\quad + \left(\frac{1}{i\hbar}\right)^3 \int_{-\infty}^{\infty}\mathrm{d}t_1 \int_{-\infty}^{t_1}\mathrm{d}t_2 \int_{-\infty}^{t_2}\mathrm{d}t_3 U_i(t_1)U_i(t_2)U_i(t_3) + ...
\end{aligned} \tag{4.15}$$

4.2.1 Classical trajectory

In order to calculate the integrals in Eq. (4.15), one needs to know the expressions of $U_i(t)$. The quest for $U_i(t)$ is equivalent to the quest for the trajectory $\boldsymbol{R}_i(t)$ of the i-th perturber [122, 125, 127]. From Eq. (4.13), the trajectory is mainly determined by the first term describing the Coulomb interaction. Therefore, the equation of motion for $\boldsymbol{R}_i(t)$ is given by

$$\mu_i \frac{\mathrm{d}^2 \boldsymbol{R}_i}{\mathrm{d}t^2} = \frac{Z Z_i e^2}{4\pi\varepsilon_0 R_i^3} \boldsymbol{R}_i, \tag{4.16}$$

with μ_i the reduced mass of the two collision particles. Solution of such equation is

$$R_i(t) = \frac{R_0}{\epsilon \cos\theta(t) + 1} \quad \text{for} \quad Z Z_i < 0, \tag{4.17}$$

$$R_i(t) = \frac{R_0}{\epsilon \cos\theta(t) - 1} \quad \text{for} \quad Z Z_i > 0, \tag{4.18}$$

with

$$R_0 = \frac{4\pi\varepsilon_0 b_i^2 v_i^2}{|Z Z_i| e^2} \tag{4.19}$$

being the closest distance the perturber can approach to the emitter. Because the perturber comes with a finite velocity and energy, one would expect $\epsilon > 1$ and the orbit to be a hyperbola curve with the form

$$\frac{x^2}{a_i^2} - \frac{y^2}{b_i^2} = 1. \tag{4.20}$$

However, as shown in the following, we do not have to perform the trajectory integral along the hyperbola curves [122]. By making use of the relation

$$\frac{\mathrm{d}\boldsymbol{R}_i}{\mathrm{d}t} = \boldsymbol{v}_i, \tag{4.21}$$

one obtains

$$\mu_i \dot{\boldsymbol{v}}_i = \frac{Z Z_i e^2}{4\pi\varepsilon_0 R_i^3} \boldsymbol{R}_i. \tag{4.22}$$

Therefore, the dipole interaction Hamiltonian can be rewritten as

$$U_i \approx \frac{Z_i e^2}{4\pi\varepsilon_0 R_i^3} \boldsymbol{r} \cdot \boldsymbol{R}_i = \frac{1}{i\hbar} \frac{\mu_i}{Z} \boldsymbol{r} \cdot \dot{\boldsymbol{v}}_i \tag{4.23}$$

This means that

$$\begin{aligned} \frac{1}{i\hbar} \int_{-\infty}^{\infty} \mathrm{d}t U_i(t) &= \frac{\mu_i}{i\hbar Z} \boldsymbol{r} \cdot [\boldsymbol{v}_i(\infty) - \boldsymbol{v}_i(-\infty)] \\ &= \frac{1}{i\hbar Z} \boldsymbol{r} \cdot \Delta \boldsymbol{p}_i \end{aligned} \tag{4.24}$$

with $\Delta \boldsymbol{p}_i = \mu_i \left[\boldsymbol{v}_i(\infty) - \boldsymbol{v}_i(-\infty)\right]$ the momentum transfer during the collision (Appx. F.4). Then the S-matrix is given as

$$\begin{aligned} S_i - 1 &= \frac{1}{i\hbar Z}\boldsymbol{r}\cdot\Delta\boldsymbol{p}_i + \frac{1}{2}\left(\frac{1}{i\hbar Z}\boldsymbol{r}\cdot\Delta\boldsymbol{p}_i\right)^2 + ... \\ &= \frac{\boldsymbol{r}\cdot\Delta\boldsymbol{p}_i}{i\hbar Z} - \frac{1}{2\hbar^2 Z^2}\left(\boldsymbol{r}\cdot\Delta\boldsymbol{p}_i\right)^2 + ... \end{aligned} \tag{4.25}$$

We can see that the first-order term is nonzero only for off-diagonal matrix elements with electric dipole transition. The second-order term is finite for all the possible matrix elements.

Considering thermal effects without any drifting velocity, the average of $\Delta\boldsymbol{p}_i$ gives zero value in the first order term of the S-matrix. Therefore, if one only keeps the lowest nonvanishing term, we have

$$S_i - 1 = -\frac{1}{2\hbar^2 Z^2}\left(\boldsymbol{r}\cdot\Delta\boldsymbol{p}_i\right)^2. \tag{4.26}$$

What we should emphasize is that $\boldsymbol{R}_i$, $\boldsymbol{v}_i$ and $\boldsymbol{p}_i$ are vector parameters describing the perturbers. On the other hand, $\boldsymbol{r}$ is a matrix vector represent the electrons in the emitter. Thus, $\boldsymbol{r}$ commutes with $\boldsymbol{p}_i$.

4.2.2 Thermal effects

Firstly, the quadratic term can be rewritten as

$$\left(\boldsymbol{r}\cdot\Delta\boldsymbol{p}_i\right)^2 = \left(r_x\Delta p_{ix} + r_y\Delta p_{iy} + r_z\Delta p_{iz}\right)^2. \tag{4.27}$$

All the terms like $p_{ix}p_{iy}$, $p_{ix}p_{iz}$ and $p_{iy}p_{iz}$ in Eq. (4.27) will vanish after thermal average. Thus

$$\begin{aligned} \left\langle\left(\boldsymbol{r}\cdot\Delta\boldsymbol{p}_i\right)^2\right\rangle &= r_x^2\left\langle\Delta p_{ix}^2\right\rangle + r_y^2\left\langle\Delta p_{iy}^2\right\rangle + r_z^2\left\langle\Delta p_{iz}^2\right\rangle \\ &= \frac{1}{3}\left\langle\Delta p_i^2\right\rangle\left(r_x^2 + r_y^2 + r_z^2\right) \\ &= \frac{1}{3}\left\langle\Delta p_i^2\right\rangle\boldsymbol{r}\boldsymbol{r}. \end{aligned} \tag{4.28}$$

One should keep in mind that $r_x^2+r_y^2+r_z^2 \neq r^2$. This is because each r_x, r_y, r_z corresponds to an operator

$$\begin{aligned} r_x &= \sum_{ij} x_{ij}\left|i\right\rangle\left\langle j\right|, \\ r_y &= \sum_{ij} y_{ij}\left|i\right\rangle\left\langle j\right|, \\ r_z &= \sum_{ij} z_{ij}\left|i\right\rangle\left\langle j\right|, \end{aligned}$$

and

$$\left\langle i\right|\boldsymbol{r}\boldsymbol{r}\left|j\right\rangle = \sum_k \left\langle i\right|\boldsymbol{r}\left|k\right\rangle\left\langle k\right|\boldsymbol{r}\left|j\right\rangle. \tag{4.29}$$

From Appx. F.4, the change in momentum for $\boldsymbol{v}_i(-\infty) = v_i\hat{\boldsymbol{z}}$ is

$$\Delta\boldsymbol{p}_i = \mu_i\Delta\boldsymbol{v}_i = \mu_i v_i\left(\sin\theta\cos\phi\hat{\boldsymbol{x}} + \sin\theta\sin\phi\hat{\boldsymbol{y}} + (\cos\theta - 1)\hat{\boldsymbol{z}}\right). \tag{4.30}$$

This means

$$(\Delta p_i)^2 = 4\mu_i^2 v_i^2 \sin^2\frac{\theta}{2}, \tag{4.31}$$

and

$$S_i(\boldsymbol{v}_i) - 1 = -\frac{1}{6\hbar^2 Z^2}\left\langle\Delta p_i^2\right\rangle \boldsymbol{r}\boldsymbol{r} = -\frac{2\mu_i^2 v_i^2}{3\hbar^2 Z^2}\sin^2\frac{\theta}{2}\boldsymbol{r}\boldsymbol{r}. \tag{4.32}$$

The collision frequency for a given velocity is given as

$$f_i(\boldsymbol{v}_i) = N v_i \sigma_i(v_i) F(\boldsymbol{v}_i), \tag{4.33}$$

with N the density of the perturbers and $F(\boldsymbol{v}_i)$ the velocity distribution function. $\sigma_i(v_i) = \frac{b_\perp^2}{4\sin^4\frac{\theta}{2}}$ is the differential cross section given in Eq. (F.15) with

$$b_\perp = \frac{ZZ_i e^2}{4\pi\varepsilon_0\mu_i v_i^2}. \tag{4.34}$$

Therefore, the effective Hamiltonian can be calculated as

$$\begin{aligned}
\mathcal{H} &= i\hbar\sum_i f_i(S_i - 1) \\
&= i\hbar N\int v_i F(\boldsymbol{v}_i)\mathrm{d}\boldsymbol{v}_i \int 2\pi\sin\theta\mathrm{d}\theta\sigma_i(S_i - 1) \\
&= i\hbar N\int v_i F(\boldsymbol{v}_i)\mathrm{d}\boldsymbol{v}_i \times \int 4\pi\sin\frac{\theta}{2}\cos\frac{\theta}{2}\mathrm{d}\theta\frac{b_\perp^2}{4\sin^4\frac{\theta}{2}}\left\{-\frac{2\mu_i^2 v_i^2\sin^2\frac{\theta}{2}}{3\hbar^2 Z^2}\right\}\boldsymbol{r}\boldsymbol{r} \\
&= -i\frac{4\pi\mu_i^2}{3\hbar Z^2}N\int F(\boldsymbol{v}_i)v_i^3\mathrm{d}\boldsymbol{v}_i\int \mathrm{d}\,\sin\frac{\theta}{2}\frac{b_\perp^2}{\sin\frac{\theta}{2}}\boldsymbol{r}\boldsymbol{r} \\
&= -i\frac{4\pi\mu_i^2}{3\hbar Z^2}N\int F(\boldsymbol{v}_i)v_i^3\mathrm{d}\boldsymbol{v}_i\int\frac{\mathrm{d}\,\sin\frac{\theta}{2}}{\sin\frac{\theta}{2}}\left[\frac{ZZ_i e^2}{4\pi\varepsilon_0\mu_i v_i^2}\right]^2\boldsymbol{r}\boldsymbol{r} \\
&= -i\frac{4\pi Z_i^2 e^4\boldsymbol{r}\boldsymbol{r}}{3(4\pi\varepsilon_0)^2\hbar}N\ln\Lambda\int F(\boldsymbol{v}_i)\frac{1}{v_i}\mathrm{d}\boldsymbol{v}_i \\
&= -i\frac{4\pi Z_i^2 e^4\boldsymbol{r}\boldsymbol{r}}{3(4\pi\varepsilon_0)^2\hbar}\left(\frac{1}{v_i}\right)_{\mathrm{av}}N\ln\Lambda.
\end{aligned} \tag{4.35}$$

Here, $\ln\Lambda = \int\frac{\mathrm{d}\,\sin\frac{\theta}{2}}{\sin\frac{\theta}{2}} \approx \ln\frac{\lambda_\mathrm{D}}{b_\perp}$ is the Coulomb logarithm. λ_D is the Debye length of the plasma. For electrons, one has

$$\lambda_\mathrm{D} = \sqrt{\frac{\varepsilon_0 k_\mathrm{B} T_\mathrm{e}}{N_\mathrm{e} e^2}} = 7.44\sqrt{\frac{T_\mathrm{e}[\mathrm{eV}]}{N_\mathrm{e}[\mathrm{cm}^{-3}]}}. \tag{4.36}$$

Furthermore, with $\boldsymbol{r}$ in units of Bohr radius $a_0 = \frac{4\pi\varepsilon_0\hbar^2}{Zm_\mathrm{e}e^2}$ in the emitter, one has the

effective Hamiltonian as

$$\mathcal{H} = -i\frac{4\pi Z_i^2\hbar^3 N\ln\Lambda}{3\bar{v}_i Z^2 m_\mathrm{e}^2}\boldsymbol{rr}, \tag{4.37}$$

where we have taken the relation

$$\left(\frac{1}{v_i}\right)_\mathrm{av} = \sqrt{\frac{2\mu_i}{\pi k_\mathrm{B}T}} = \frac{4}{\pi}\frac{1}{\bar{v}_i}. \tag{4.38}$$

The corresponding shift and broadening operator can be calculated through

$$\phi = \frac{1}{i\hbar}\mathcal{H} = -\frac{16Z_i^2\hbar^2 N\ln\Lambda}{3\bar{v}_i Z^2 m_\mathrm{e}^2}\boldsymbol{rr}, \tag{4.39}$$

or

$$\phi = -\frac{16}{3\bar{v}_i}N\left(\frac{Z_i\hbar}{Zm_\mathrm{e}}\right)^2\ln\Lambda\times\boldsymbol{rr}. \tag{4.40}$$

With $\bar{v}_i = \sqrt{\frac{8k_\mathrm{B}T}{\pi\mu_i}}$, one has

$$\phi = -\frac{8}{3}\sqrt{\frac{\pi\mu_i}{2k_\mathrm{B}T}}N\left(\frac{Z_i\hbar}{Zm_\mathrm{e}}\right)^2\ln\Lambda\times\boldsymbol{rr}. \tag{4.41}$$

For electron impact scattering, $Z_i = -1$ and the reduced mass $\mu_i = m_\mathrm{e}$, one obtains

$$\begin{aligned}\phi &= -\frac{8}{3}\sqrt{\frac{\pi m_\mathrm{e}}{2k_\mathrm{B}T}}N_\mathrm{e}\left(\frac{\hbar}{Zm_\mathrm{e}}\right)^2\ln\Lambda\times\boldsymbol{rr}\\ &= -1.66\times10^{-9}\frac{N_\mathrm{e}[\mathrm{cm}^{-3}]}{\sqrt{T[\mathrm{eV}]}}\frac{1}{Z^2}\ln\Lambda\times\boldsymbol{rr}\\ &\approx -0.83\times10^{-9}\frac{N_\mathrm{i}[\mathrm{cm}^{-3}]}{\sqrt{T[\mathrm{eV}]}}\ln\Lambda\times\boldsymbol{rr}\end{aligned} \tag{4.42}$$

From this formula, the electron-ion impact broadening is proportional to the ion density, but inversely proportional to the electron temperature.

For further calculations, one needs to know the value of $\boldsymbol{rr}$. In the following, we will show how this can be calculated from oscillator strengths. Starting with Eq. (4.35), one defines

$$\mathcal{H} = \beta\boldsymbol{rr}, \tag{4.43}$$

with

$$\beta = -i\frac{4\pi Z_i^2 e^4}{3(4\pi\varepsilon_0)^2\hbar}\left(\frac{1}{v_i}\right)_\mathrm{av}N\ln\Lambda. \tag{4.44}$$

Now, $\boldsymbol{r}$ is again in SI units. As an example, we calculate the diagonal elements of the effective Hamiltonian

$$\mathcal{H}_{nn} = \beta\langle n|\,\boldsymbol{rr}\,|n\rangle = \beta\sum_k\langle n|\,\boldsymbol{r}\,|k\rangle\langle k|\,\boldsymbol{r}\,|n\rangle = \frac{\beta}{e^2}\sum_k\mu_{nk}^2, \tag{4.45}$$

where $\mu_{nk} = e\,|\langle n|\,\boldsymbol{r}\,|k\rangle|$ is the dipole moment between state $|n\rangle$ and $|k\rangle$. From Eq. (B.18), we will have

$$\mathcal{H}_{nn} = \beta\frac{3\hbar^2}{2m_\mathrm{e}}\frac{g_n}{T_N}\sum_k\frac{\bar{f}_{nk}}{\hbar\omega_{kn}} = \beta\frac{3\hbar^2}{2m_\mathrm{e}}\frac{g_n}{T_N}\sum_k\frac{\bar{f}_{nk}}{E_k - E_n}. \tag{4.46}$$

With $\bar{f}_{nk}$ and $\hbar\omega_{kn}$ can be calculated from graspa, the value of $\mathcal{H}_{nn}$ can be obtained.

4.3 Ion-ion Stark broadening

In a low temperature dense plasma, the ions move slowly that, for the time scale we are interested, they can be treated as static. Therefore, the interaction between the emitter the the neighboring ions can be accounted for by the Stark effect [122, 128, 129]. In the following, we will first introduce the atomic calculations of the Stark effects. By introducing the random distance between the emitter and neighbor ions, one obtains a distribution of the Stark shift over different coordinate, resulting in an inhomogeneous spectral broadening.

4.3.1 Stark effect

For an atom in an external static electric field, the potential energy for the atom sitting at $\boldsymbol{R}$ is [122, 125]

$$V_\mathrm{int} = eV(\boldsymbol{R}) + \sum_i eV(\boldsymbol{R}+\boldsymbol{r}_i), \tag{4.47}$$

with $V(\boldsymbol{R})$ the potential energy of the nuclei and $V(\boldsymbol{R}+\boldsymbol{r}_i)$ the potential energy for the i-th bound-electron in the atom. For a given atom, the value of $V(\boldsymbol{R})$ is constant and can be set to zero. Furthermore, if the external electric field changes little within the size of the atom (thus within $\boldsymbol{r}_i$), one has

$$V_\mathrm{int} = \sum_i eV(\boldsymbol{R}+\boldsymbol{r}_i) = \sum_i e\,(-\nabla V)\,\boldsymbol{r}_i = \sum_i \boldsymbol{F}\boldsymbol{d}_i, \tag{4.48}$$

with $\boldsymbol{F} = -\nabla V$ the electric field strength at $\boldsymbol{R}$ and $\boldsymbol{d}_i = e\boldsymbol{r}_i$ the electric dipole moment of the i-th electron. Define the total dipole moment of the atom as

$$\boldsymbol{D} = \sum_i \boldsymbol{d}_i, \tag{4.49}$$

we have

$$V_\mathrm{int} = \boldsymbol{F}\cdot\boldsymbol{D}. \tag{4.50}$$

First order – Perturbation theory gives the first-order energy correction due to V_int as

$$E_n^{(1)} = \langle n|\,V_\mathrm{int}\,|n\rangle = \boldsymbol{F}\cdot\langle n|\,\boldsymbol{D}\,|n\rangle\,. \tag{4.51}$$

Usually, $\langle n|\,\boldsymbol{D}\,|n\rangle = 0$ because $\boldsymbol{D}$ has odd parity.

First-order Stark effect exists only for degenerate systems that can be coupled by electric dipole interactions. As an example, we take $n = 2$, there would be states $|200\rangle$

for angular momentum $l = 0$, and $|20-1\rangle$, $|200\rangle$, $|201\rangle$ for angular momentum $l = 1$. If energy for all the four states are degenerate, such as H-like ions [122], then coupling between $|200\rangle$ and the other three states would give the first-order Stark corrections

$$E_n^{(1)} = D_n F, \tag{4.52}$$

with $D_n = |\langle s|\, \boldsymbol{D}\, |p\rangle|$ the absolute value of the dipole moment that can be calculated from the oscillator strength. By approximation, one has

$$D_n \approx \frac{n^2}{Z} e a_0 = \frac{4\pi\varepsilon_0 \hbar^2}{m_\mathrm{e} e Z} n^2. \tag{4.53}$$

Second order – For nondegenerate state, the first-order energy correction vanishes and one needs to go to the second order perturbation where

$$E_n^{(2)} = \sum_{k\neq n} \frac{\langle n|\, V_\mathrm{int}\, |k\rangle \langle k|\, V_\mathrm{int}\, |n\rangle}{E_n - E_k} = -\frac{1}{2} \sum_{i,j=x,y,z} F_i \alpha_{n;ij} F_j, \tag{4.54}$$

with the polarizability tensor α_{ij} defined as

$$\alpha_{n;ij} = -2 \sum_{k\neq n} \frac{\langle n|\, D_i\, |k\rangle \langle k|\, D_j\, |n\rangle}{E_n - E_k}, \tag{4.55}$$

and

$$\boldsymbol{D} = D_x \hat{\boldsymbol{x}} + D_y \hat{\boldsymbol{y}} + D_z \hat{\boldsymbol{z}}. \tag{4.56}$$

When the hyperfine structure in the atom is negligible, the polarizability tensor is isotropic [128, 129], therefore,

$$\alpha_{n;ij} = \delta_{ij} \alpha_n. \tag{4.57}$$

So, the second-order Stark effect gives an energy correction of

$$E_n^{(2)} = -\frac{1}{2} \alpha_n F^2, \tag{4.58}$$

with

$$\alpha_n = -2 \sum_i \sum_{k\neq n} \frac{\langle n|\, D_i\, |k\rangle \langle k|\, D_i\, |n\rangle}{E_n - E_k} = -2 \sum_{k\neq n} \frac{D_{nk}^2}{E_n - E_k}, \tag{4.59}$$

and

$$D_{nk}^2 = |\langle n|\, \boldsymbol{D}\, |k\rangle|^2 . \tag{4.60}$$

Oscillator strength – To calculate the value for the two coefficients corresponding to linear and quadratic Stark effects, one makes use of the relation between oscillator strength and electric dipole moment in Eq. (B.18)

$$D_{nk}^2 = \frac{3\hbar^2 e^2}{2 m_\mathrm{e}} \frac{g_n}{T_N} \frac{\bar{f}_{nk}}{E_k - E_n}. \tag{4.61}$$

Then we have

$$\alpha_n = \frac{3\hbar^2 e^2}{m_\mathrm{e}} \sum_{k\neq n} \frac{g_n}{T_N} \frac{\bar{f}_{nk}}{(E_n - E_k)^2} \tag{4.62}$$

4.3.2 Quasi-static-field broadening by ions

In the plasma, ions move much slower that electrons such that one can treat the ions almost static. Then the emitters will have Stark shift by the Coulomb field of the nearby ions. The distance between ions is randomly distributed, leading to a random Stark shift. This will cause an extra broadening of the emission line.

In perturbation theory, the energy shift for transition between $|i\rangle$ and $|j\rangle$ follows

$$\Delta\nu_{ij}(F) = C_{ij}F^m, \tag{4.63}$$

with $m = 1$ the linear Stark effect and $m = 2$ the quadratic Stark effect. The strength of the electric field can be approximated as $F \approx \frac{1}{4\pi\varepsilon_0} Z_\mathrm{p} e/R^2$, which is valid if there is only one perturber nearby and all the other perturbers are far away. Quasi-static approximation holds if the perturbers move sufficiently slow that the characteristic frequency v/R is much smaller compared to the Stark shift frequency [122, 125]

$$v/R \ll \Delta\nu_{ij}(F). \tag{4.64}$$

With the expression for F, one has

$$\frac{1}{R} = \left(\frac{\Delta\nu_{ij}(F)}{C_{ij} Z_\mathrm{p} e}\right)^{\frac{1}{2n}}, \tag{4.65}$$

This gives the criterion for quasi-static approximation

$$\Delta\nu_{ij}(F) \gg \left(\frac{v^2}{Z_\mathrm{p} e}\right)^{\frac{n}{2n-1}} \left(\frac{1}{C_{ij}}\right)^{\frac{1}{2n-1}}. \tag{4.66}$$

4.3.2.1 Linear Stark broadening

For first order, $n = 1$, the corresponding averaged Stark coefficient given in reference [125] is

$$\bar{C}_{ij}(F) \approx \frac{3\hbar}{2m_\mathrm{e} eZ} \left(n_i^2 - n_j^2\right) \tag{4.67}$$

with n_i and n_j the principle quantum number of the initial and final states. It is similar to our former calculation of first order Stark effect

$$\bar{C}_{ij}(F) \approx \frac{1}{2\pi\hbar}(D_{n_i} - D_{n_j}). \tag{4.68}$$

where the prefactor $\frac{1}{2\pi\hbar}$ comes from $E = h\nu$. Taking $v^2 \approx \frac{3k_\mathrm{B}T}{\mu}$, one has

$$\Delta\nu_{ij} \gg \frac{2Zm_\mathrm{e}k_\mathrm{B}T}{\hbar Z_\mathrm{p}\mu\left(n_i^2 - n_j^2\right)}, \tag{4.69}$$

where μ is the reduced mass of the emitter-perturber pair.

To calculate the mean Stark shift, one can approximate the mean field strength as [125, 130]

$$\bar{F} \approx \frac{1}{4\pi\varepsilon_0} 8 Z_\mathrm{p} e N^{\frac{2}{3}} = \frac{2 Z_\mathrm{p} e}{4\pi\varepsilon_0} N^{\frac{2}{3}}. \tag{4.70}$$

Calculation of the above mean field strength has also included the cases where two or more perturbers are presented at the same time. With such field strength, the *linear Stark broadening* can be approximated by

$$\nu_{ij} \quad = \quad \frac{12 Z_\mathrm{p} \hbar}{Z m_\mathrm{e}} \left(n_i^2 - n_j^2 \right) N^{\frac{2}{3}}. \tag{4.71}$$

Relation in Eq. (4.69) gives the lower density limit of quasi static approximation

$$N \quad \gtrsim \quad \left(\frac{k_\mathrm{B} T}{6\mu} \right)^{\frac{3}{2}} \left(\frac{Z m_\mathrm{e}}{Z_\mathrm{p} \hbar} \right)^3 \left(\frac{1}{n_i^2 - n_j^2} \right)^3. \tag{4.72}$$

For x-ray lasing with $n_i = 2$, $n_j = 1$, $Z = Z_\mathrm{p} = 8$, $\mu = \frac{1}{2} m_\mathrm{Ne}$ and $T = 10^4$ K, one has the lower limit as

$$N \quad \gtrsim \quad 5.44^{10} T^{\frac{3}{2}} = 5.44 \times 10^{16} \mathrm{m}^{-3}. \tag{4.73}$$

For our x-ray lasing with ion density $N = 10^{24}$ m^{-3}, a quasi-static treatment of ions is therefore sufficient.

Besides, the collision between electron-ions gives $Z = 8$, $Z_\mathrm{p} = 1$, $\mu = m_\mathrm{e}$, this gives the lower limit for a quasi-static treatment of electrons as

$$N_\mathrm{e} \quad \gtrsim \quad 5.44 \times 10^{16} \left(\frac{m_\mathrm{Ne}}{m_\mathrm{e}} \right)^{\frac{3}{2}} * Z^3 = 6.91 \times 10^{25} \mathrm{m}^{-3}.$$

This means that, for ion density $N = 10^{24}$ m^{-3}, the electron density would be approximately $N_\mathrm{e} = 8 \times 10^{24}$ m^{-3}, which is quite close to the lower density limit for electrons.

The quasi-static broadening from nearby ions can be approximated through

$$\nu_{ij} \quad = \quad \frac{12 \times 8 \times 1.05 \times 10^{-34}}{8 \times 9.11 \times 10^{-31}} (2^2 - 1^2) N^{\frac{2}{3}} = 3.57 \times 10^{-3} N^{\frac{2}{3}}$$

For $N = 10^{24}$ m^{-3}, one has

$$\nu_{ij} \quad = \quad 3.57 \times 10^{13} \text{ s}^{-1} \tag{4.74}$$

with the corresponding broadening of

$$\Delta\omega_\mathrm{s} \quad = \quad h\nu_{ij} = 148.2 \text{ meV} \tag{4.75}$$

4.3.2.2 Quadratic Stark broadening

For second order, one has

$$\bar{C}_{ij} \quad \approx \quad -\frac{1}{4\pi\hbar} \alpha_n,$$

$$\overline{(F^2)} \approx \bar{F}^2 \approx \frac{64Z_{\rm p}^2e^2N^{\frac{4}{3}}}{(4\pi\varepsilon_0)^2}.$$

This results in the formula for *Quadratic Stark broadening* as:

$$\begin{aligned}\nu_{ij} &= \bar{C}_{ij}\overline{(F^2)} \\ &= \frac{1}{4\pi\hbar}\frac{3\hbar^2e^2}{m_{\rm e}}\sum_{k\neq n}\frac{g_n}{T_N}\frac{\bar{f}_{nk}}{(E_n-E_k)^2}\frac{64Z_{\rm p}^2e^2N^{\frac{4}{3}}}{(4\pi\varepsilon_0)^2} \\ &= \frac{3}{\pi^3}\frac{\hbar e^4Z_{\rm p}^2}{m_{\rm e}\varepsilon_0^2}N^{\frac{4}{3}}\sum_{k\neq n}\frac{g_n}{T_N}\frac{f_{kn}}{(E_n-E_k)^2}. \end{aligned} \quad (4.76)$$

If we take the energy E_n in units of eV, we have the another form of the *Quadratic Stark broadening*:

$$\nu_{ij} = \frac{3}{\pi^3}\frac{\hbar e^2}{m_{\rm e}\varepsilon_0^2}Z_{\rm p}^2N^{\frac{4}{3}}\sum_{k\neq n}\frac{g_k}{g_n}\frac{\bar{f}_{nk}}{(E_n-E_k)^2}. \quad (4.77)$$

The prefactor has a value of

$$\frac{3}{\pi^3}\frac{\hbar e^2}{m_{\rm e}\varepsilon_0^2} = 3.47\times10^{-21}.$$

The oscillator strength f_{kn} and energies E_n, E_k can be calculated from GRASP atomic code.

To give an estimation, we find that the energy difference between 1s2s and 1s2p in He-like ions can be approximated by $E_n - E_k \sim Z$ eV, thus $(E_n - E_k)^2 \sim Z^2$ in the second-order Stark broadening. Because $\bar{f}_{nk} \sim 1$,

$$Z_{\rm p}^2\sum_{k\neq n}\frac{g_n}{T_N}\frac{\bar{f}_{nk}}{(E_n-E_k)^2} \approx 1.$$

So the shifted frequency is about

$$\nu_{ij} = 3.47\times10^{-21}N^{\frac{4}{3}}.$$

For $N = 10^{24}$ m^{-3}, this gives a second-order Stark broadening of

$$\begin{aligned}\nu_{ij} &= 3.47\times10^{11}\ {\rm s}^{-1}, \\ h\nu_{ij} &= 1.44\ {\rm meV}.\end{aligned}$$

4.4 Summary

In summary, the spectral broadening effects in plasma including Doppler broadening $\Delta\nu_D$, electron-ion impact broadening ϕ and ion-ion quasi-static Stark broadening ν_{ij} have been considered. In total, they have the following forms:

$$\text{Doppler broadening: } \frac{\Delta\nu_D}{\nu_0} = 7.689\times10^{-5}\sqrt{T_{\rm i}[{\rm eV}]/M_{\rm i}},$$

electron impact broadening: $\phi = -0.83 \times 10^{-9} \frac{N_{\mathrm{i}}[\mathrm{cm}^{-3}]}{\sqrt{T[\mathrm{eV}]}} \ln\Lambda \times \boldsymbol{rr}$,

ion Stark broadening, first-order: $\nu_{ij} = \frac{12\hbar}{m_{\mathrm{e}}} \left(n_i^2 - n_j^2\right) N^{\frac{2}{3}}$,

ion Stark broadening, second-order: $\nu_{ij} = \frac{3}{\pi^3} \frac{\hbar e^2}{m_{\mathrm{e}} \varepsilon_0^2} Z_{\mathrm{p}}^2 N^{\frac{4}{3}} \sum_{k \neq n} \frac{g_k}{g_n} \frac{\bar{f}_{nk}}{(E_n - E_k)^2}$,

with the following scaling laws on the temperature and density of the plasma:

$$\Delta\nu_D \sim \sqrt{TZ^3}, \tag{4.78}$$

$$\phi \sim \frac{1}{\sqrt{T}} N_{\mathrm{ion}}, \tag{4.79}$$

$$\nu_{ij} \sim N^{\frac{2}{3}} \quad \text{first-order}, \tag{4.80}$$

$$\nu_{ij} \sim N^{\frac{4}{3}} \quad \text{second-order}. \tag{4.81}$$

The formulas derived here are used in order to calculate the broadening effect in our lasing scheme put forward in Chapter 5.

Chapter 5

Narrow-band hard-X-ray lasing with highly charged ions

Since the advent of X-ray free-electron lasers (XFELs), considerable efforts have been devoted to achieve X-ray pulses with better temporal coherence [30, 31, 52, 98–102]. Here, we put forward a scheme to generate fully coherent X-ray lasers (XRLs) based on population inversion in highly charged ions (HCIs), created by fast inner-shell photoionization using XFEL pulses in a laser-produced plasma. Numerical simulations presented in this Chapter show that one can obtain high-intensity, femtosecond X-ray pulses of relative bandwidths $\Delta\omega/\omega = 10^{-5} - 10^{-7}$ by orders of magnitude narrower than in XFEL pulses for wavelengths down to the sub-ångström regime. Such XRLs may be applicable in the study of X-ray quantum optics [75–78] and metrology [79], investigating nonlinear interactions between X-rays and matter [80, 81], or in high-precision spectroscopy studies in laboratory astrophysics [82]. Parts of this Chapter have been presented in reference [74].

5.1 Lasing scheme based on HCIs

The photoionization-pumped atomic laser we put forward is illustrated in Fig. 5.1, where the Li-like HCIs are initially prepared in a $1s^2 2l$ ($l = s, p$) state in a laser-produced plasma [106]. A SASE XFEL pulse tuned above the K-edge of the ions first removes a K-shell electron from the Li-like ions, creating He-like ions in the $1s2l$ excited states. Subsequent decay to the $1s^2$ ground state leads to emission of X-ray photons via four possible Kα transitions: one magnetic-dipole ($M1$) transition from the $^3S_1$ state, two electric-dipole ($E1$) transitions from the $^3P_1$ or $^1P_1$ states, and one magnetic-quadrupole ($M2$) transition from the $^3P_2$ state. The population inversion in the He-like ions resulting from this photoionization-pumping scheme leads to amplification of the emitted X-rays, i.e., to inner-shell X-ray lasing.

Former soft X-ray lasers based on outer-shell transitions have demonstrated line focusing to generate laser-produced plasma with a length up to 9 cm [13, 16, 131]. Therefore, experimental realization could be achieved. The laser intensity to reach such conditions can be estimated through the formula [132, 133]

$$T_\mathrm{e} \approx 3.6 \times I_{16}\lambda_\mu^2 \ (\mathrm{keV}) \tag{5.1}$$

with T_e being the electron temperature in units of keV, I_{16} the laser intensity normalized to 1×10^{16} W cm^{-2}, λ_μ the laser wavelength in unit of μm. The highest temperature needed is 25 keV in the case of Xe plasma, corresponding to a laser intensity around 6.9×10^{16} W cm^{-2}. Assuming a line focusing geometry of 10 μm$\times$1 cm (10^{-4} cm^2 in focusing area), the total power needed for such an experiment can be estimated as 10^{-4} cm^2 $\times$ 6.9×10^{16} W cm^{-2} = 6.9 TW.

The total energy needed to generate such a plasma can be estimated from the total kinetic energy of the electrons plus the average binding energy of the electrons in a neutral atom

$$W \approx (T_\mathrm{e} + 0.5W_0)N_\mathrm{e}SL \tag{5.2}$$

with W_0 the ionization threshold of the $1s^2 2s$ configuration in Li-like ions. N_e is the electron density, S and L are the cross section and length of the plasma, respectively. For lasing with e.g. a Xe plasma, the values we assume are $S = 1\ \mu\mathrm{m}^2$, $L = 8$ mm and $N_\mathrm{e} \approx 52 \times N_i = 52 \times 2.7 \times 10^{21}\ \mathrm{cm}^{-3}$. This gives the total number of electrons in the plasma being approximately

$$N_\mathrm{e}SL = 52 \times 2.7 \times 10^{21} \times 10^{-8} \times 0.8 = 1.12 \times 10^{15}. \tag{5.3}$$

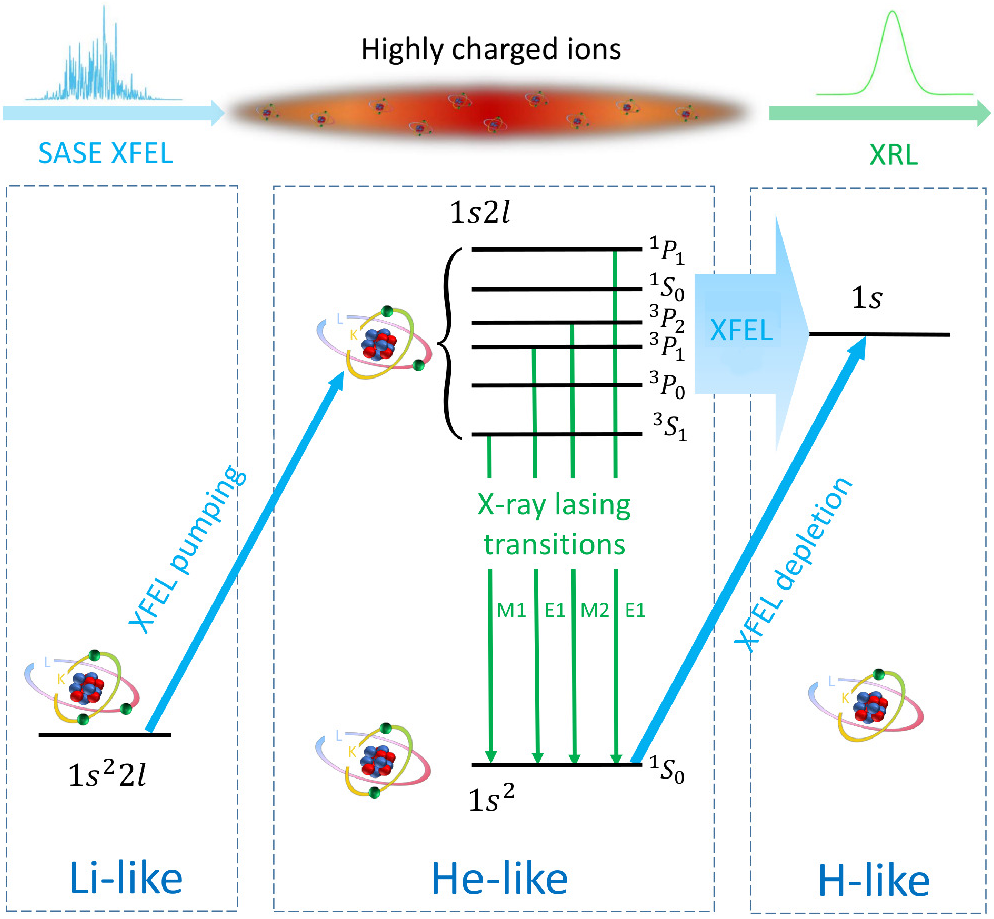

Figure 5.1: Scheme of the lasing process. An upper lasing state $1s2l$ of He-like ions is pumped through K-shell photoionization of Li-like ions initially in a $1s^2 2l$ state by an XFEL pulse tuned above the K-edge of the He-like ions (blue arrow left). Lasing takes place through one of the four possible transitions from an upper lasing state $1s2l$ to the lower lasing state $1s^2$ (green arrows). The state $1s^2$ is depleted through further K-shell photoionization by the same XFEL pulse (blue arrow right). L-shell photoionization of the upper lasing states is represented by the thick blue arrow. The order of the $1s2l$ states may vary for different elements.

Considering that $W_0 = 9$ keV, the total energy needed is

$$W \approx (25 + 4.5) \times 10^3 \times 1.6 \times 10^{-19} \times 1.12 \times 10^{15} = 5.3 \text{ J}. \tag{5.4}$$

Assuming an absorption rate of the laser pulse by the plasma being 10% [134], this corresponds to a laser output energy of 53 J which can be achieved at currently existing high power laser facilities [135]. With the power 6.9 TW estimated before, the duration of the pulse to deliver such energy is around 7.7 ps. Besides, the simulation of the sequential ionization of Xe in Fig. 5.2 indicates that Li-Like Xe can be generated in 5 ps. Compare this duration with the pulse duration, one can expect that there is significant fraction of Li-like ions.

Two factors determine which transition of the ion will lase. Firstly, population inversion is needed to have stimulated emission. Typical XFEL facilities, with peak photon fluxes of 10^{33} – 10^{35} cm^{-2} s^{-1} [35, 62], yield an inverse ionization rate of a few femtoseconds, such that XFEL pulses can effectively photoionize all the Li-like ions. Transitions with upper-state lifetimes longer than 1 fs are necessary to ensure sufficient population inversion between the $1s2l$ and $1s^2$ state. Furthermore, the finite lifetime of the plasma $\tau_p \sim 10$ ps [136] also influences the lasing process. Sufficient amplification of X-ray radiation will take place only from transitions whose decay is slower than XFEL pumping, but faster than plasma expansion.

5.2 Theoretical description

Suitable XRL transitions in He-like ions are shown in Table 5.1. A full description of the lasing process should account for all the $1s2l$ ($l = s, p$) states in He-like ions. However, the lifetimes of these states differ from each other by orders of magnitude. When only

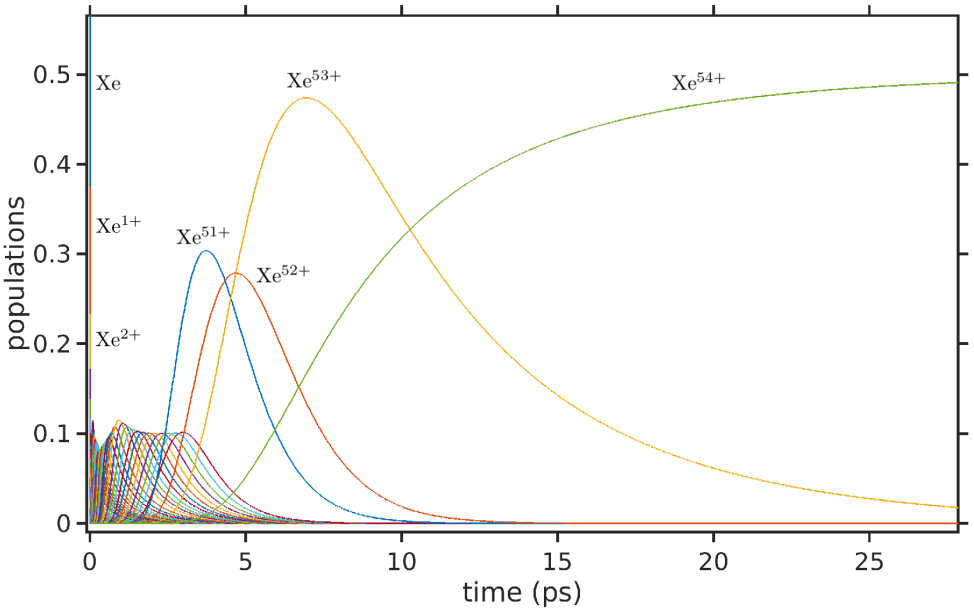

Figure 5.2: Sequential ionization of Xe. Collisional ionization of Xe is calculated in the simulation, with the ionization rate obtained from FLYCHK simulations [106]. He- and Li-like highly charged states are dominant after 3 ps.

one of the four Kα transitions in the He-like ions satisfies the lasing requirements, a two-level description of the ions is sufficient.

For light ions, Ne^{8+} for example, the $E1$ transition with a decay rate of 9.24×10^{12} s^{-1} from the $^1P_1$ state will develop lasing. The other transitions have decay times much larger than the plasma expansion time, and their contribution is negligible compared to the $^1P_1$ state, such that they can be neglected. For heavy ions like Xe^{52+}, however, since the two $E1$ transition rates scale as $\sim Z^4$ (Z being the atomic number), they correspond to 3.05×10^{15} s^{-1} for $^3P_1$ and 6.82×10^{15} s^{-1} for $^1P_1$, respectively, which are too large to enable population inversion with available XFEL pulses. On the other hand, the decay rates of the $M1$ transition from the $^3S_1$ state and the $M2$ transition from the $^3P_2$ state are 3.7×10^{11} s^{-1} and 2.56×10^{12} s^{-1}, respectively, which are sufficient for lasing to take place before the expansion of the plasma. However, the $M1$ transition from the $^3S_1$ state is dominated by large Stark broadening effects, such that the amplification of photons emitted from this transition is much slower than for those emitted in the $M2$ transition. Within the characteristic length L_c for the $M2$ transition, the presence of the $^3S_1$ state can hence be neglected. Similar arguments are applicable to Kr^{34+}.

For Ar^{16+}, there are two transitions that may lase simultaneously, as listed in Table 5.1. However, the lifetimes τ of these states differ from each other by a factor of 63. The XFEL photon flux can be tuned properly to exclude one of them from lasing. For instance, in order to obtain lasing from the $^3P_1 \rightarrow {}^1S_0$ transition, a mean peak flux of 2.29×10^{33} cm^{-2} s^{-1} for the XFEL pulses is applied. This generates an upper state pumping rate and a lower-state depletion rate which are 32 and 58 times larger than the decay rate of the $^3P_1$ upper state, respectively, resulting in population inversion of the transition. At the same time, for this value of the peak flux, the pumping rate of the $^1P_1$ upper state is only 0.26 times the decay rate of the $^1P_1$ state, too small to obtain population inversion in the $^1P_1 \rightarrow {}^1S_0$ transition. Thereby, lasing will only take place from the $^3P_1$ state. A sufficient amplification of the X-ray photons emitted from the $^1P_1$ state needs higher XFEL peak fluxes and higher ion densities. When such conditions are met, e.g., for the parameters shown in Table 5.1, lasing from the $^1P_1 \rightarrow {}^1S_0$ transition takes place. Saturation will be reached much sooner than for the $^3P_1 \rightarrow {}^1S_0$ transition, such that the $^3P_1$ state can be neglected.

With the Maxwell–Bloch equations in Eqs. (3.51–3.56), one can construct the equations of motion describing the lasing processes put forward in this here. Assuming XFEL pulses propagating along the $\hat{x}$ direction, the evolution of the X-ray laser field in the slowly varying envelope approximation is given by [103, 104]

$$\frac{\partial\mathcal{A}(x,t)}{\partial t}+c\frac{\partial\mathcal{A}(x,t)}{\partial x}=i\frac{\mu_0\omega_0c^2}{2}\mathcal{F}(x,t), \tag{5.5}$$

where $\mathcal{A}(x,t)$ is either the electric field $\mathcal{E}(x,t)$ or the magnetic field $\mathcal{B}(x,t)$, depending on the specific transition. μ_0 is the vacuum permeability and c is the vacuum speed of light. $\mathcal{F}(x,t)$ corresponds to the polarization field induced by $\mathcal{E}(x,t)$ for $E1$ transitions, or the magnetization field and magnetic-quadrupole field induced by $\mathcal{B}(x,t)$ for $M1$ transitions and $M2$ transitions, respectively.

For a given lasing transition, we assume all Li-like ions are pumped into the corresponding upper lasing state of such transition by the XFEL pulse. Using $|\mathrm{e}\rangle$ and $|\mathrm{g}\rangle$ to represent the upper lasing state and the lower lasing state, respectively, the dynamics of the He-like ions are described by the Bloch equations of the density matrix

$$\dot{\rho}_{\mathrm{ee}}(x,t) \;=\; -\mathrm{Im}[\Omega(x,t)(x,t)\rho_{\mathrm{eg}}(x,t)]+\sigma_0 j_{\mathrm{xfel}}(x,t)\rho_{00}(x,t) \tag{5.6}$$

$$\begin{aligned} & -\sigma_{\rm e} j_{\rm xfel}(x,t)\rho_{\rm ee}(x,t) - \Gamma\rho_{\rm ee}(x,t), \\ \dot{\rho}_{\rm eg}(x,t) &= \frac{-i}{2}\Omega(x,t)(\rho_{\rm ee}(x,t) - \rho_{\rm gg}(x,t)) \\ & -\frac{\gamma}{2}\rho_{\rm eg}(x,t) + S(x,t), \end{aligned} \tag{5.7}$$

$$\begin{aligned} \dot{\rho}_{\rm gg}(x,t) &= {\rm Im}[\Omega(x,t)\rho_{\rm eg}(x,t)] - \sigma_{\rm g} j_{\rm xfel}(x,t)\rho_{\rm gg}(x,t) \\ & +\Gamma\rho_{\rm ee}(x,t). \end{aligned} \tag{5.8}$$

The carrier frequency ω_0 is chosen to be resonant with the lasing transition. $\rho_{\rm ee}$ and $\rho_{\rm gg}$ are the populations of $|{\rm e}\rangle$ and $|{\rm g}\rangle$, and the off-diagonal term $\rho_{\rm eg}$ represents the coherence between the two lasing states. $\Omega(x,t) = \wp\mathcal{E}(x,t)/\hbar$ for an $E1$ transition (or $\Omega(x,t) = m\mathcal{B}(x,t)/\hbar$ for an $M1$ transition, and $\Omega(x,t) = k_0 q_{yx}\mathcal{B}(x,t)/\hbar$ for an $M2$ transition [137]) is the time- and space-dependent Rabi frequency, with $\wp$ the electric-dipole moment, m the magnetic-dipole moment, and q_{yx} the yx-component of the magnetic-quadrupole tensor. XFEL pumping of the $|{\rm e}\rangle$ state from Li-like ions is accounted for through the second term in the right-hand side of Eq. (6.2), with ρ_{00} being the population of Li-like ions, $j_{\rm xfel}$ the photon flux of the XFEL pump pulse, and σ_0 the K-shell photoionization cross section of the pump process ($1s^2 2l \rightarrow 1s2l$). The XFEL pulse also depletes the $|{\rm e}\rangle$ and $|{\rm g}\rangle$ states, as modeled by the third term on the right-hand side of Eq. (6.2) and the second term on the right-hand side of Eq. (6.3), respectively, with $\sigma_{\rm e}$ and $\sigma_{\rm g}$ being the corresponding photoionization cross sections. In Eqs. (6.2) and (6.3), $\Gamma\rho_{\rm ee}(x,t)$ describes spontaneous emission at rate Γ. In Eq. (6.3), the parameter

$$\gamma = \Gamma + \Delta\omega_{\rm e\text{-}i} + (\sigma_{\rm e} + \sigma_{\rm g}) j_{\rm xfel}(x,t) \tag{5.9}$$

models the three contributions to the decay of the off-diagonal elements: Γ is the decoherence originating from spontaneous photon emission; the second term $\Delta\omega_{\rm e\text{-}i}$ accounts for the broadening from electron–ion collisions [138]; and the final term describes the contribution from depletion of the total population of He-like ions. $S(x,t)$ in Eq. (6.3) is a Gaussian white-noise term added phenomenologically, which satisfies $\langle S^*(x,t)S(z,t')\rangle = F(z,t_1)\delta(t-t')$. For $E1$ transitions, one has [103]

$$F(x,t) = \frac{\varepsilon_0\hbar\omega_0}{N_{\rm i}\wp^2}\frac{d}{8\pi L}\frac{\gamma^2}{\omega_0^2}\Gamma\rho_{\rm ee}(x,t), \tag{5.10}$$

where ε_0 is the vacuum permitivity and $N_{\rm i}$ stands for the density of the ions in the plasma. $d = 0.4$ μm is the radius of the XFEL spot on the plasma and L is the length of the plasma.

The coupling between the Maxwell equations and the Bloch equations is given through the induced fields $\mathcal{P} = -2N_{\rm i}\wp\rho_{\rm eg}$, $\mathcal{M} = -2N_{\rm i}m\rho_{\rm eg}$ and $\mathcal{Q} = -2N_{\rm i}q\rho_{\rm eg}$ for $E1$, $M1$, and $M2$ transitions, respectively. Absorption of the XFEL pulse by the ions is included through the rate equations

$$\frac{\partial j_{\rm xfel}}{\partial z} = -\sum_{\rm k}\sigma_{\rm k}\rho_{\rm kk}N_{\rm i}j_{\rm xfel}, \tag{5.11}$$

where k={0, e, g} represents the three different states.

5.3 Numerical simulations

Simulations for each transition have been conducted by solving the Maxwell–Bloch equations [103, 104] numerically in retarded-time coordinates for 1,000 different realizations of SASE XFEL pulses. For most of the ions displayed in Table 5.1, only one of the four transitions in Fig. 5.1 satisfies the requirements for lasing described above, such that a two-level description of the He-like ions is applicable. For Ar^{16+} ions, there are two transitions which may lase simultaneously. Thus, the XFEL peak flux is tuned properly to ensure that only one of them lases. Values of the initial populations of the states in Li- and He-like ions are computed with the FLYCHK method [106]. XFEL frequencies and photon fluxes are then fixed such that K-shell photoionization of the $1s^2 2l$ and $1s^2$ states ensures population inversion in the He-like ions. Except for the transition from Kr^{34+} $^3P_2$, which needs more than 10 cm to reach saturated intensity, all the other transitions are predicted to generate high-intensity X-ray pulses within 1 cm with small bandwidths. For $E1$ transitions in Ne^{8+} and Ar^{16+}, a significant improvement of $\Delta\omega/\omega$ is obtained compared to SASE XFEL pulses [35] and XRLs with neutral atoms [30, 31]. When going to heavier Kr^{34+} and Xe^{52+} ions, the $M2$ transitions provide an even more significant reduction of the bandwidth, with $\Delta\omega/\omega_0$ being 3.7×10^{-7} and 1.5×10^{-6}, respectively. The resulting 13- and 30-keV lasers feature similar bandwidths as the untested XFELO scheme [102], with intensities of $\sim 10^{18}$ W cm^{-2}. The relative bandwidths are by 2 to 3 orders of magnitude narrower than the value predicted for future seeded-XFEL sources at analogous hard-X-ray wavelengths around 0.41 – 0.95 Å [35].

To understand the properties of our XRLs and how they develop in the plasma, simulation results for the $^3P_1 \rightarrow {}^1S_0$ transition in Ar^{16+} are shown in Figs. 5.6–5.12 for the corresponding parameters listed in Table 5.1. We use a partial-coherence method [93] to simulate 124-fs-long SASE XFEL pulses with a spectral width of 1.55 eV and a peak photon flux of 2.29×10^{33} cm^{-2} s^{-1}. This results in a peak pumping rate of 6.04×10^{13} s^{-1} for the upper lasing state, and a depletion rate of 5.63×10^{13} s^{-1} for the lower lasing state. They are 32 and 58 times larger than the spontaneous-emission rate of the $^3P_1$ state, ensuring population inversion.

5.3.1 Initial conditions

Values of the initial populations of the states in Li- and He-like ions are computed with the FLYCHK code [106]

$$\rho_{00}(x, t = 0) = \rho_{\text{Li-like}}, \tag{5.12}$$

$$\rho_{\text{ee}}(x, t = 0) = 0, \tag{5.13}$$

$$\rho_{\text{gg}}(x, t = 0) = \rho_{\text{He-like}}, \tag{5.14}$$

where $\rho_{\text{Li-like}}$ and $\rho_{\text{He-like}}$ are the fractions of Li-like ions ($1s^2 2l$ state) and He-like ions ($1s^2$ state) shown in Fig. 5.3. The initial population of the $1s2l$ upper lasing states in He-like ions is found to be negligible. Thus, most of the He-like ions are in the lower lasing state and no population inversion exists before XFEL-pulse pumping sets in. Since the decay of the upper lasing state in He-like ions is much slower than the K-shell photoionization rate, after the Li-like ions are pumped to a $1s2l$ state, this decays on a time scale much longer than the inverse of the K-shell photoionization rate. Population inversion develops after the lower lasing state ($1s^2$) of the He-like ions has been depleted by the XFEL pulse. In the simulation, only evolutions of the He-like ions are described by density-matrix theory. The evolution of the populations of the other charge states is

Table 5.1: Results for selected X-ray lasing transitions for different elements. Radiative parameters like transition energy ω_0, natural linewidth Γ and upper-state lifetime τ are obtained from the GRASP code [105]. The XFEL photon energy ω_{xfel}, tuned above the K-shell ionization threshold of the $1s^2$ state, and the mean peak flux (ph. stands for photons), used in the 1,000 realizations of the SASE XFEL pulses, are fixed to ensure population inversion and the applicability of the two-level approximation. Electron temperature T_{e} and ion density N_{i} ($n_0 = 10^{20}$ cm^{-3}) are chosen to enable a significant fraction of Li-like ions in the plasma [106] (see Fig. 5.3). The broadening effects, with Doppler broadening $\Delta\omega_{\text{D}}$, electron–ion impact broadening $\Delta\omega_{\text{e-i}}$, and ion–ion Stark broadening $\Delta\omega_{\text{i-i}}$, are calculated for given T_{e} and N_{i} based on Maxwell–Boltzmann distributions [125], with ion temperature $T_{\text{i}} = 487$ K. The characteristic length L_{c} is the optimal length defined in Fig. 5.12. The XRL intensity I_{c} as well as the relative bandwidth $\Delta\omega/\omega_0$ at this length are obtained by averaging over 1,000 simulations, with the uncertainties arising from the random XFEL pulse profiles. The upper and lower bounds are the values at the 10th and 90th percentiles of the corresponding distributions (as shown in Figs. 5.12d,f for $\text{Ar}^{16+}\ {}^3P_1$).

Radiative parameters				XFEL		Plasma conditions					Simulation results		
Upper state $1s2l$	ω_0 (keV)	Γ (meV)	τ (ps)	ω_{xfel} (keV)	peak flux (ph./cm^2/s)	T_{e} (keV)	N_{i} (n_0)	$\Delta\omega_{\text{D}}$ (meV)	$\Delta\omega_{\text{e-i}}$ (meV)	$\Delta\omega_{\text{i-i}}$ (meV)	L_{c} (mm)	I_{c} (W/cm^2)	$\Delta\omega/\omega_0$
$\text{Ne}^{8+}\ {}^1P_1$	0.920	6.08	0.10	1.197	1.10×10^{34}	0.035	0.02	3.23	0.08	0.06	2.8	$4.5^{+9.3}_{-4.4} \times 10^{12}$	$7.8^{+4.3}_{-2.7} \times 10^{-5}$
$\text{Ar}^{16+}\ {}^3P_1$	3.120	1.16	0.57	4.124	2.29×10^{33}	0.25	0.25	7.80	1.38	9.81	3.3	$5.0^{+3.8}_{-4.0} \times 10^{14}$	$7.8^{+1.9}_{-2.1} \times 10^{-6}$
$\text{Ar}^{16+}\ {}^1P_1$	3.137	72.2	0.009	4.124	1.98×10^{35}	0.25	2.48	7.83	0.29	25.22	0.35	$1.5^{+1.4}_{-0.8} \times 10^{16}$	$4.7^{+2.0}_{-1.7} \times 10^{-5}$
$\text{Kr}^{34+}\ {}^3P_2$	13.087	0.07	9.46	17.316	1.87×10^{34}	6.20	0.50	22.58	0.45	2.76	289	$4.3^{+7.6}_{-4.2} \times 10^{16}$	$3.7^{+1.6}_{-1.1} \times 10^{-7}$
$\text{Xe}^{52+}\ {}^3P_2$	30.589	1.91	0.34	40.304	7.45×10^{34}	25.00	27.0	42.16	7.60	126	8.5	$4.7^{+6.9}_{-4.5} \times 10^{18}$	$1.5^{+0.6}_{-0.5} \times 10^{-6}$

modeled through rate equations.

Generation of the highly charged ions involves many complex processes. However, experiments [139–141] shown that under given electron temperature and density, the plasma will mainly consists of ions in highly charged states. In reference [139], experiments at LULI2000 facility generated Kr and Xe plasmas with most of the ions being Kr^{25+} to Kr^{27+} and Xe^{26+} to Xe^{31+}, respectively. Other experiments [140] with Nb and Ta at LULI2000 facility in 2015 produced plasmas with a mean charge state of $\langle Z \rangle = 30$ and $\langle Z \rangle = 44$, respectively. The main feature of these experiments is the laser intensity which is around 10^{14} W cm^{-2} (1.5 ns). This has prevented the laser to generate even higher charged states. By adopting a higher laser intensity (5×10^{18} W cm^{-2}, 700 fs), in 2017, He- and H-like sulfur ions were obtained in a plasma generated by Orion laser facility at AWE, UK [141]. All these measurements are coincident with atomic simulations based on collisional-radiative atomic kinetics models like Averroes [142] and FLYCHK [106]. Therefore, one can use these atomic models to predict the plasma properties.

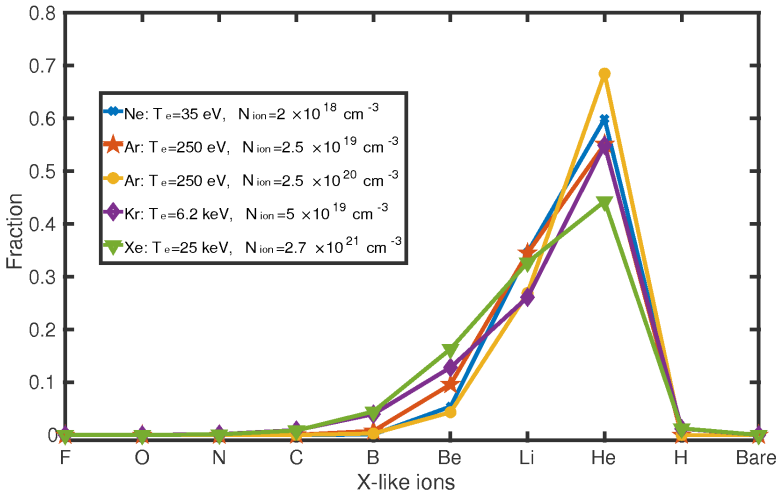

Figure 5.3: Charge-state distributions for different elements and simulation parameters.

Table 5.2: Charge state distributions for Ar. The fractions of different ions under given electron temperatures assuming an ion density $N_i = 2.5 \times 10^{19}\text{cm}^{-3}$.

Charge number	50 (eV)	100 (eV)	150 (eV)	200 (eV)	250 (eV)	300 (eV)	350 (eV)	400 (eV)
0	1.28E-20	1.07E-30	7.47E-37	6.03E-41	4.05E-44	1.45E-46	1.65E-48	4.19E-50
1	2.84E-17	6.87E-27	8.41E-33	7.47E-37	9.15E-40	4.17E-42	5.80E-44	1.76E-45
2	3.61E-14	2.97E-23	7.06E-29	1.21E-32	1.48E-35	8.64E-38	1.48E-39	5.35E-41
3	3.62E-11	1.15E-19	4.96E-25	1.06E-28	1.82E-31	1.36E-33	2.87E-35	1.42E-36
4	1.58E-08	2.25E-16	2.00E-21	7.02E-25	1.69E-27	1.64E-29	4.25E-31	2.61E-32
5	3.22E-06	2.66E-13	5.25E-18	3.07E-21	1.02E-23	1.27E-25	4.04E-27	2.47E-28
6	3.14E-04	1.71E-10	7.58E-15	5.89E-18	2.64E-20	4.25E-22	1.67E-23	1.21E-24
7	1.04E-02	3.44E-08	3.27E-12	4.14E-15	2.66E-17	5.72E-19	2.85E-20	2.55E-21
8	1.26E-01	8.49E-06	3.01E-09	8.18E-12	8.79E-14	2.76E-15	1.84E-16	2.09E-17
9	4.93E-01	6.23E-04	8.66E-07	5.21E-09	9.57E-11	4.44E-12	4.01E-13	5.80E-14
10	3.38E-01	1.60E-02	8.31E-05	1.11E-06	3.53E-08	2.44E-09	3.02E-10	5.61E-11
11	3.14E-02	1.58E-01	2.99E-03	8.68E-05	4.74E-06	4.90E-07	8.30E-08	1.99E-08
12	2.37E-04	4.47E-01	4.48E-02	2.96E-03	2.78E-04	4.29E-05	9.93E-06	3.08E-06
13	1.89E-07	3.23E-01	2.59E-01	4.54E-02	7.68E-03	1.79E-03	5.65E-04	2.25E-04
14	1.49E-11	5.48E-02	5.04E-01	2.83E-01	9.51E-02	3.51E-02	1.56E-02	8.13E-03
15	3.09E-17	9.33E-04	1.70E-01	4.20E-01	3.44E-01	2.31E-01	1.58E-01	1.15E-01
16	1.54E-23	4.60E-06	1.97E-02	2.48E-01	5.53E-01	7.32E-01	8.26E-01	8.77E-01
17	1.75E-59	6.31E-24	3.20E-14	4.65E-10	7.36E-08	1.71E-06	1.51E-05	7.67E-05
18	4.30E-71	3.94E-44	7.70E-28	2.42E-20	4.05E-16	2.19E-13	1.89E-11	5.38E-10

Our FLYCHK simulations have provided the experimental conditions, e.g. temperatures and densities, needed to generate highly charged ions in the plasma. For each element considered, one can obtain the distributions of the charged states (Table 5.2) as well as the electronic configurations (Table 5.3) in the plasma. Such charged states and electronic-configuration distributions, acting as the initial conditions, are the input of our subsequent simulations with Maxwell–Bloch equations. However, as we can see from the figure, only a few charge states dominate the populations and the others are negligible. For each charge state, more than 96.4% of the populations are in their ground state configurations, with the populations in the other configurations up to three orders of magnitude smaller. Though they may contribute to the background emission, these excited configurations can be omitted in the simulations because of their low density.

Table 5.3: Electronic-configuration distribution for Ar. The density for different electronic configurations are listed in the case of a total ion density $N_i = 2.5 \times 10^{19}\text{cm}^{-3}$ with electron temperature $T_e = 250$ eV. The red color refers to the excited electrons in the corresponding charge state. The electron number stands for the number of bound electrons in given ionization stage; the level number for each ionization stage is counted from the corresponding ground state configurations; the level name represents the superconfiguration defined in reference [106]; the configuration for singly and doubly excited state are for a principal quantum number up to 10 is accounted.

Electron number	level number	level name	energy (eV)	degeneracy	configuration	maximum shell, n	density
1	1	hy1	0.0000	2	1 0 0 0 0 0 0 0 0 0	1	1.01E+04
2	1	he1s	0.0000	1	2 0 0 0 0 0 0 0 0 0	1	1.38E+19
2	2	he2st	3104.2000	3	1 1 0 0 0 0 0 0 0 0	2	3.18E+11
2	3	he2ss	3124.6001	1	1 1 0 0 0 0 0 0 0 0	2	1.11E+11
2	4	he2pt	3123.6001	9	1 1 0 0 0 0 0 0 0 0	2	7.88E+11
2	5	he2ps	3139.6001	3	1 1 0 0 0 0 0 0 0 0	2	5.83E+09
2	6	he3ps	3683.6491	36	1 0 1 0 0 0 0 0 0 0	3	1.49E+10
2	7	he4ps	3874.6790	64	1 0 0 1 0 0 0 0 0 0	4	5.85E+09
2	8	he5ps	3963.2015	100	1 0 0 0 1 0 0 0 0 0	5	3.21E+09
2	9	he6ps	4011.2937	144	1 0 0 0 0 1 0 0 0 0	6	3.50E+09
2	10	he7ps	4040.1938	196	1 0 0 0 0 0 1 0 0 0	7	4.02E+09
2	11	he8ps	4055.3251	256	1 0 0 0 0 0 0 1 0 0	8	4.82E+09
2	12	he9ps	4068.8349	324	1 0 0 0 0 0 0 0 1 0	9	5.71E+09
2	13	he10ps	4078.4984	400	1 0 0 0 0 0 0 0 0 1	10	6.74E+09
2	14	he11ps	4085.6482	484	1 0 0 0 0 0 0 0 0 0	11	7.92E+09
2	15	he12ps	4091.0864	576	1 0 0 0 0 0 0 0 0 0	12	9.22E+09
2	16	he13ps	4095.3185	676	1 0 0 0 0 0 0 0 0 0	13	1.06E+10
2	17	he14ps	4098.6765	784	1 0 0 0 0 0 0 0 0 0	14	1.22E+10
3	1	li2s	0.0000	2	2 1 0 0 0 0 0 0 0 0	2	2.31E+18
3	2	li2p	33.9817	6	2 1 0 0 0 0 0 0 0 0	2	5.98E+18
3	3	li3s	517.8149	2	2 0 1 0 0 0 0 0 0 0	3	1.27E+16
3	4	li3p	527.1846	6	2 0 1 0 0 0 0 0 0 0	3	2.99E+16
3	5	li3d	531.0147	10	2 0 1 0 0 0 0 0 0 0	3	3.85E+16
3	6	li4s	695.0732	2	2 0 0 1 0 0 0 0 0 0	4	1.85E+15
3	7	li4p	698.9396	6	2 0 0 1 0 0 0 0 0 0	4	5.33E+15
3	8	li4d	700.5104	10	2 0 0 1 0 0 0 0 0 0	4	8.51E+15
3	9	li4f	700.6742	14	2 0 0 1 0 0 0 0 0 0	4	1.20E+16
3	10	li5s	776.1229	2	2 0 0 0 1 0 0 0 0 0	5	9.42E+14
3	11	li5p	778.1493	6	2 0 0 0 1 0 0 0 0 0	5	2.80E+15
3	12	li5d	778.9801	10	2 0 0 0 1 0 0 0 0 0	5	4.64E+15
3	13	li5f	779.0683	14	2 0 0 0 1 0 0 0 0 0	5	6.53E+15
3	14	li5g	779.0942	18	2 0 0 0 1 0 0 0 0 0	5	8.46E+15
3	15	li6	821.6196	72	2 0 0 0 0 1 0 0 0 0	6	2.46E+16
3	16	li7	847.3138	98	2 0 0 0 0 0 1 0 0 0	7	2.89E+16
3	17	li8	863.9893	128	2 0 0 0 0 0 0 1 0 0	8	3.47E+16
3	18	li9	875.4214	162	2 0 0 0 0 0 0 0 1 0	9	4.17E+16
3	19	li10	883.5982	200	2 0 0 0 0 0 0 0 0 1	10	4.98E+16
3	20	op	3084.6816	4	1 2 0 0 0 0 0 0 0 0	2	1.44E+11
3	21	qr	3114.3101	6	1 2 0 0 0 0 0 0 0 0	2	1.45E+10
3	22	st	3123.7200	6	1 2 0 0 0 0 0 0 0 0	2	1.63E+11
3	23	jkl	3138.1516	14	1 2 0 0 0 0 0 0 0 0	2	3.19E+11
3	24	abcd	3144.3916	12	1 2 0 0 0 0 0 0 0 0	2	1.73E+10
3	25	mn	3161.6416	4	1 2 0 0 0 0 0 0 0 0	2	4.29E+10

Charge state and electronic configurations with significant populations (> 0.001), have been taken into account in our numerical simulations. Because the X-ray lasing only

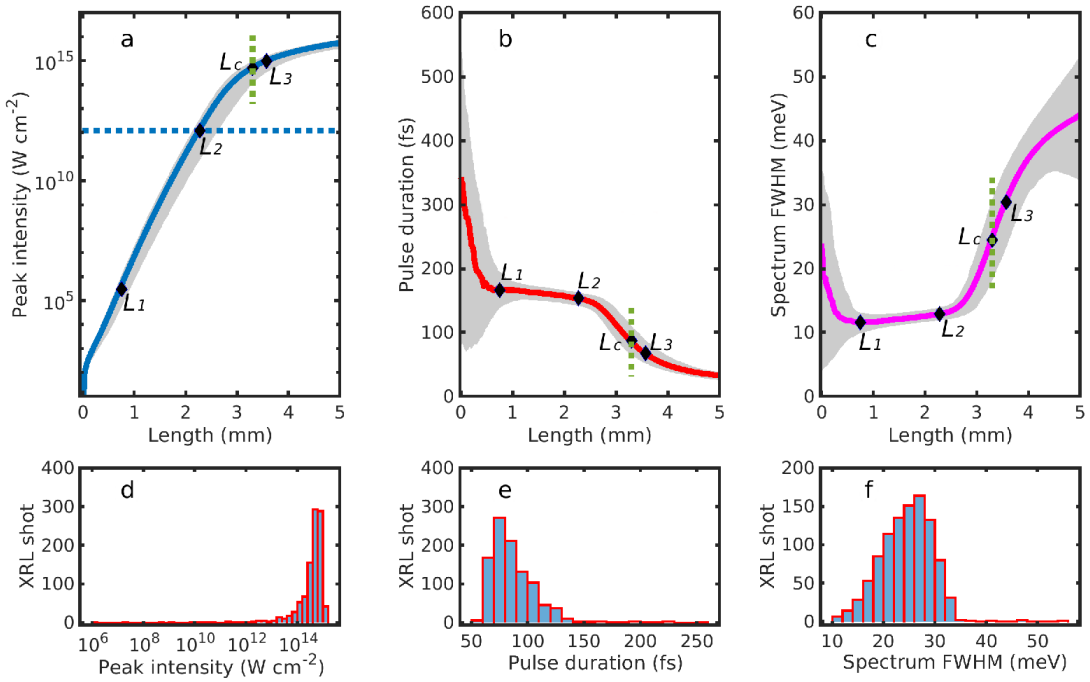

Figure 5.4: Evolution of the XRLs over 1,000 simulations (for the Ar^{16+} $^3P_1$ transitions). **a-c**, Peak intensity, pulse duration and spectral full width at half maximum (FWHM) for the X-ray laser. The solid lines display results averaged over 1,000 simulations. The dotted line in (**a**) indicates the saturation intensity $I_s = 1.18 \times 10^{12}$ W cm^{-2}. L_1, L_2 and L_3 mark the lengths for the XRL pulse to reach transform-limited profile, saturation intensity and Rabi flopping, respectively. L_c refers to the characteristic length that optimizes the intensity and bandwidth of the XRL pulses. Here, it is defined as the length at which the slope of the solid line in (**a**) is 1/3 of the slope at L_2. The gray areas in (**a-c**) indicate the distribution areas of the results over 1,000 simulations. At a given length, the bottom and top edges of the areas indicate the 10th and 90th percentiles of the distributions, respectively. **d-f**, Distributions of the peak intensity, pulse duration and spectral FWHM at L_c along the green dotted lines in (**a-c**). In (**d**), there are 15 simulations whose peak intensities locate in the unsaturated region $10^6 \sim 10^{12}$ W cm^{-2}, indicating that 1.5% of the SASE XFEL pulses cannot provide enough pumping. More details can be found in Fig. 5.5.

happens in the He-like ions, only such ions have been described by a density matrix through the Bloch equations. Evolutions of the other ions are described by rate equations. Besides, the three broadening effects are also calculated under the presence of different charge states in the plasma.

5.3.2 Averaged results

Average results over 1,000 SASE-pulse realizations are shown in Figs. 5.12a-c. The peak intensity of the XRL, shown by the solid line in Fig. 5.12a, increases exponentially during the initial propagation stage, then displays a saturation behavior. The dotted line indicates the saturation intensity

$$I_s = \hbar\Gamma\omega_0^3/6\pi c^2 \tag{5.15}$$

at which the stimulated-emission rate equals the spontaneous-emission rate. This is also the intensity from which the amplification begins to slow down. The evolution of

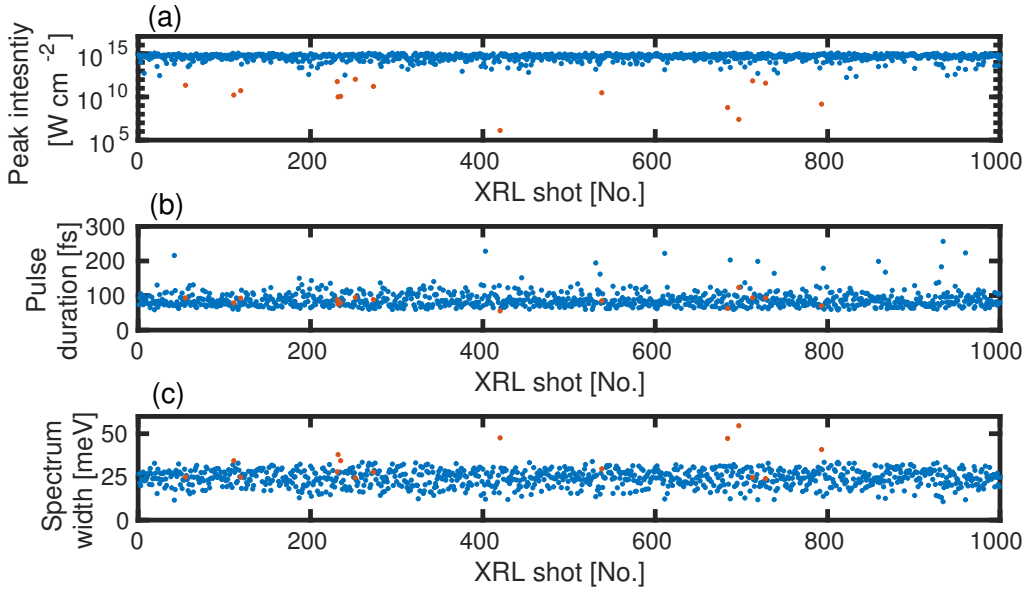

Figure 5.5: Distributions of the XRLs at L_c over 1,000 simulations (Ar^{16+} $^3P_1$). **a-c**, Peak intensity, pulse duration and spectral full width at half maximum (FWHM) for the X-ray laser. Blue dots correspond to the simulation shots whose intensities at L_c is higher than the saturation intensity. Red dots represents the ones with intensities lower than the saturation intensity.

the pulse duration and the spectral width are shown by the solid lines in Figs. 5.12b,c. At $L = 0$, only spontaneous emission takes place: the 342-fs average pulse duration is mainly determined by the lifetime of the $^3P_1$ state (Fig. 5.12b), whereas the 23.5-meV intrinsic spectral width before propagation (Fig. 5.12c) is mostly due to the sum of the natural linewidth Γ and the three broadening effects shown in Table 5.1.

5.3.3 Individual results

During its propagation in the medium, gain narrowing and saturation rebroadening will also contribute to the final bandwidth. This can be observed by inspecting the four distinct propagation regions separated by L_1, L_2 and L_3 in Figs. 5.12a-c, which can also be followed in Figs. 5.6a,b for a single simulation. Up to $L_1 = 0.75$ mm, both the pulse duration and spectral FWHM decrease severely. The laser intensity and spectrum in this region for a single simulation are spiky and noisy, as the ions irradiate randomly in time and space (Figs. 5.6a,b). When the spontaneously emitted signal propagates and stimulated emission sets in, it selectively amplifies the frequencies around ω_0 such that the XRL pulse approaches a fully coherent transform-limited profile at L_1 [104], with a bandwidth smaller than the intrinsic width. Thereafter, a gradual broadening of the spectrum is observed in the region L_1L_2. The broadening increases abruptly from $L_2 = 2.3$ mm, where the saturation intensity has been reached and the stimulated-emission rate exceeds the spontaneous-emission rate. This is accompanied by a substantial slowing down of the amplification of the intensity and a significant decrease of the pulse duration in the region between L_2 and L_3 (Figs. 5.12a,b). Further propagation of the XRL pulse after $L_3 = 3.5$ mm is characterized by the onset of Rabi flopping (Fig. 5.6a) which is reflected by a splitting in the XRL spectrum (Fig. 5.6b).

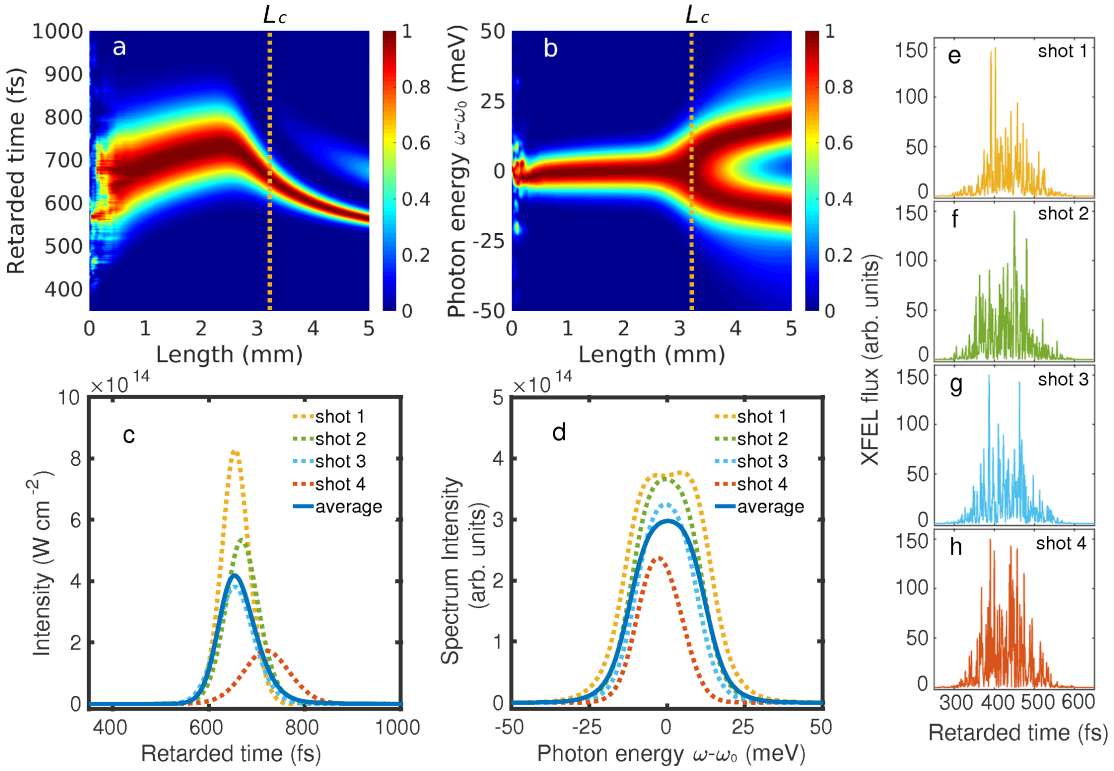

Figure 5.6: Evolution of the normalized XRL intensity and spectrum (Ar^{16+} $^3P_1$, single simulation). **a**, Intensity shown as a function of retarded time and propagation length. **b**, Power spectrum displayed as a function of photon energy and propagation length. For a given length, the intensity and spectrum are normalized to the maximum value of the corresponding profiles at that length. The vertical dotted lines indicate the characteristic length L_c shown in Fig. 5.12. For lengths larger than L_c, the strength of the second peak in (**a**) appearing around retarded times of ~ 700 fs has been multiplied by a factor of 5 for better visibility. **c**,**d**, XRL pulse profile and spectrum at L_c. The yellow dotted lines correspond to the results from the simulation in (**a**,**b**). Three other simulation results (green, blue and red dotted lines) at L_c are also included for comparison, with the solid lines corresponding to the results averaged over 1,000 simulations. **e**-**h**, SASE XFEL pulses used in the four simulations in (**c**,**d**). Differences in amplitudes and positions of the peak intensities in (**c**,**d**) are the result of shot-to-shot random profiles of the SASE XFEL pulses. XRL intensity and spectrum as a function of propagation length for the XFEL pulses in (**f**-**h**), and averaged over 1,000 simulations, can be found in the Figs. 5.7–5.9 and Fig. 5.10, respectively. In (**c**,**d**), the blue solid lines are obtained by averaging XRL pulse shapes and spectra as a function of retarded time and frequency, respectively. The peak intensity of the averaged XRL pulse shape in (**c**), therefore, differs from the averaged value of the XRL peak intensity displayed in Fig. 5.12a and Table 5.1, because the position of the intensity peak varies from shot to shot.

This effect is much stronger and more marked than for previous XFEL-pumped transient lasers with neutral atoms [104] due to the absence of Auger decay [93]. At the same time, the gain of the laser intensity in this region is strongly suppressed.

The optimal choice for a coherent XRL pulse is located in the third region L_2L_3, where saturation has already been reached while the bandwidth is still narrow. By choosing the medium length to be $L_c = 3.3$ mm, as shown in Fig. 5.12, one will obtain an approximately 87-fs-long XRL pulse with an average peak intensity of $I_c = 5.0 \times 10^{14}$ W cm^{-2} ($\sim$80% fluctuations) and an average bandwidth of $\Delta\omega = 24.5$ meV ($\sim$30% fluctuations) as shown in Table 5.1. This gives $\Delta\omega/\omega_0 = 7.8 \times 10^{-6}$ for a total of 6.5×10^8 coherent

photons, with a peak brilliance of 1.4×10^{31} photons/s/mm^2/mrad^2/0.1%bandwidth.

5.4 Other individual simulations

Simulation results of the intensity profile and spectrum as a function of propagation length for shots 2–4 in Figs. 5.6, as well as the intensity profile and spectrum averaged over 1,000 simulations, are displayed in Figs. 5.7–5.9 and Fig. 5.10, respectively. Shot-to-shot differences are a consequence of the random SASE-XFEL-pulse profiles used, shown in Figs. 5.6e-f.

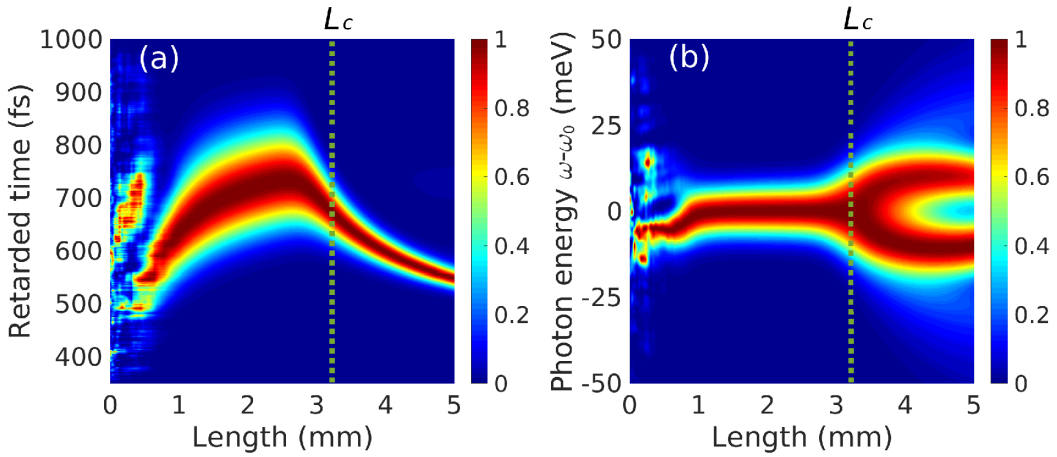

Figure 5.7: Evolution of the normalized X-ray laser intensity and spectrum (shot 2). Results for SASE-pulse shot 2 in Fig. 5.6f; green dotted lines in Figs. 5.6c,d. **a**, Intensity shown as a function of retarded time and propagation length. **b**, Power spectrum displayed as a function of photon energy and propagation length. For a given length, the intensity and spectrum are normalized to the maximum value of the corresponding profiles at such length. The vertical dotted lines indicate the characteristic length L_c defined in Figs. 5.12. The decrease in the XRL bandwidth at the end of the medium is a result of XFEL absorption.

5.4.1 XFEL parameters

Using the radiative parameters displayed in Table 5.1, and the corresponding K-shell and L-shell photoionization cross sections shown in Table 5.4, the XFEL parameters are fixed such that the requirements for lasing described in Sec. 5.2 are satisfied, and significant population inversion can be obtained. In particular, the XFEL photon energies $\omega_{\rm xfel}$ listed in Table 5.1 are tuned above the K-edge of the He-like ions, in order to ensure depletion of the initial population in the lower lasing state of He-like ions. For the elements considered, this photon energy is also above the K-edge of the corresponding Li-like ions. Photoionization of Li-like ions to a $1s2l$ excited state in He-like ions then ensures population inversion of the considered lasing transition. Most of the XFEL bandwidths listed in Table 5.4 are chosen taking into account realistic parameters at XFEL facilities in operation or under construction. Only for the case of Kr^{34+} and Xe^{52+}, the smallest values of the XFEL coherence times, thus the largest values of the XFEL bandwidths, used in the simulations are limited by the time steps ($\delta t = 0.0001\tau = 0.95$ fs for Kr^{34+} and $\delta t = 0.001\tau = 0.34$ fs for Xe^{52+}) employed in our numerical calculations of the Maxwell–Bloch equations. However, simulation runs with smaller time steps, thus

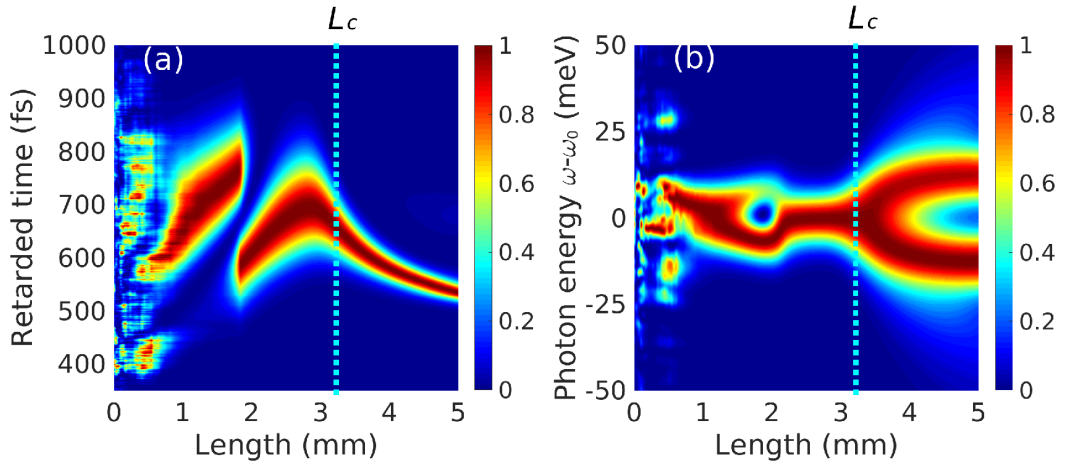

Figure 5.8: Same as Fig. 5.7 for shot 3. Results for SASE-pulse shot 3 in Fig. 5.6g; blue dotted lines in Figs. 5.6c,d. The exotic structures in both intensity and spectrum around $L = 2$ mm originate from XFEL photoionization of the upper lasing state. The decay of this state is different during and after the XFEL pulse. This renders it possible that two peaks develop and propagate before saturation.

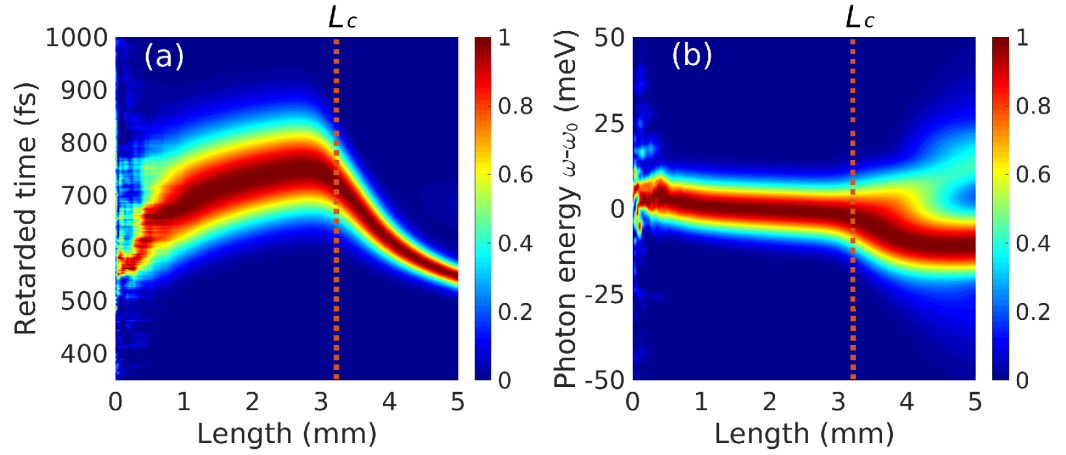

Figure 5.9: Same as Fig. 5.7 for shot 4. Results for SASE-pulse shot 4 in Fig. 5.6h; red dotted lines in Figs. 5.6c,d. A slight shift of the peak of the spectrum from ω_0 is here apparent.

larger XFEL bandwidths, provide results which are not significantly different. This is because photoionization pumping is determined by the XFEL flux and is not significantly influenced by the properties of the XFEL spectrum [104]. Therefore, when we compare the bandwidth of the XRLs and XFEL pulses in the main text, we refer to the realistic bandwidth measured at XFEL facilities and not to the values used in this table.

5.5 Line broadening in plasma

In the following, we explain in detail the role of the presence of Doppler, collisional and Stark broadening effects discussed in 4, as they are also comparable to the relatively

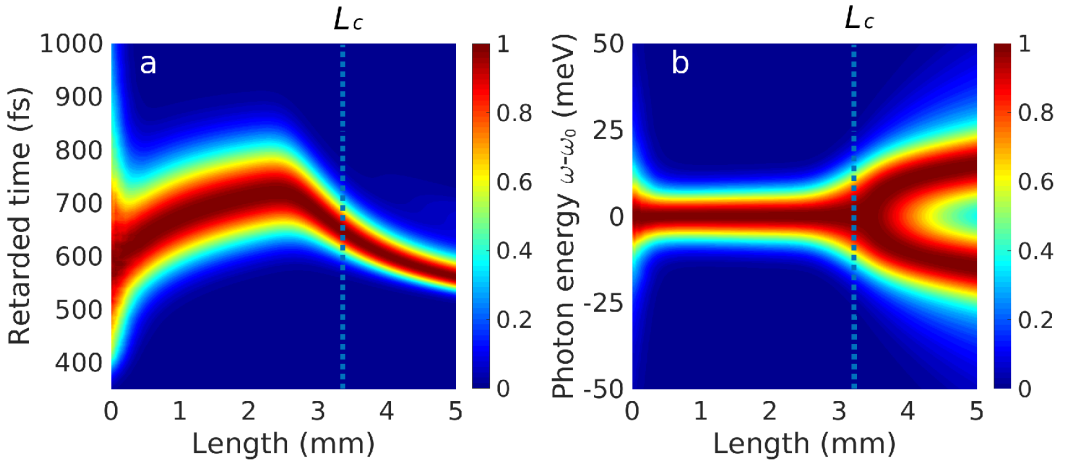

Figure 5.10: Evolution of the normalized X-ray laser intensity and spectrum averaged over 1,000 realizations of SASE XFEL pulses. Intensity and spectra evaluated at the characteristic length L_c are exhibited by the solid lines in Figs. 5.6c,d. The chaotic features for small propagation lengths, which are shown for single simulations in Figs. 5.6a,b and in Figs. 5.7–5.9 above, become smooth here.

Table 5.4: Extended XFEL parameters. K-shell ionization cross section σ_0 and σ_g, together with the L-shell ionization cross section σ_e, are calculated from the LANL Atomic Physics Codes [143] (kb $= 10^{-21}$ cm^2). SASE XFEL parameters such as pulse duration, bandwidth and total photons inserted into the medium are simulated with a partial-coherence method [93]. The number of photons absorbed during the lasing process is obtained from our numerical solutions of Eqs. (6.2 – 5.11).

XFEL ionization cross section				XFEL parameters			
Upper state $1s2l$	σ_0 (kb)	σ_e (kb)	σ_g (kb)	duration (fs)	bandwidth (eV)	photons inserted	photons absorbed
$Ne^{8+}\ ^1P_1$	39.1	1.6	151.2	21.3	6.25	2.4×10^{12}	6.3×10^{9}
$Ar^{16+}\ ^3P_1$	24.6	0.48	44.6	124	1.55	2.9×10^{12}	1.0×10^{12}
$Ar^{16+}\ ^1P_1$	12.4	0.47	44.6	2.0	74	3.8×10^{12}	2.7×10^{10}
$Kr^{34+}\ ^3P_2$	6.24	0.12	10.9	202	0.57	3.9×10^{13}	2.0×10^{13}
$Xe^{52+}\ ^3P_2$	2.66	0.06	5.31	72.5	1.96	5.6×10^{13}	3.6×10^{13}

small natural linewidth. As shown in Table 5.1, the Doppler broadening

$$\Delta\omega_D = \sqrt{\frac{8\ln 2 k_B T_i}{m_i c^2}}\omega_0, \tag{5.16}$$

with k_B being the Boltzmann constant, T_i the ion temperature and m_i the mass of the He-like ions, is not significant for light ions, but it becomes dominant for heavy ions like Kr^{34+} and Xe^{52+}.

The electron-impact broadening is given by [138]

$$\Delta\omega_{e\text{-}i} = -\frac{16}{3\bar{v}_e}\frac{N_e\hbar^2}{Z_i^2 m_e^2}\ln\Lambda\ \langle \boldsymbol{rr}\rangle\,, \tag{5.17}$$

with $\bar{v}_e = \sqrt{8k_B T_e/\pi m_e}$ being the average thermal velocity of the electrons in the plasma and N_e the electron density, and Z_i the charge number of the ions. T_e and m_e are the

electron temperature and electron mass, respectively. $\ln\Lambda \sim 10$ is the Coulomb logarithm and $\boldsymbol{rr}$ is a tensor with $\boldsymbol{r}$ being the dipole operator of the bound electrons in the ions. This broadening is significant only for light ions such as Ne^{8+} and Ar^{16+} with lower electron temperatures, but becomes negligible compared to $\Delta\omega_D$ for heavy ions and higher electron temperatures.

The quadratic Stark broadening from ion–ion interaction is calculated through [125]

$$\Delta\omega_{i\text{-}i} = \alpha\overline{F^2}, \tag{5.18}$$

with

$$\alpha = -\frac{1}{4\pi\hbar}\sum_{k\neq j}\wp_{jk}^2/(eE_{kj}^2), \tag{5.19}$$

$$\overline{F^2} = 4Z_p^2e^2N_i^{\frac{4}{3}}/(\pi\varepsilon_0)^2, \tag{5.20}$$

where α is the quadratic Stark coefficient which would be different for each transition, and $\overline{F^2}$ is the mean-square electric-field strength generated by nearby perturbing ions with charge number Z_p. $\wp_{jk}$ and E_{jk} are the electric-dipole moment and energy difference between the states $|j\rangle$ and $|k\rangle$, respectively. $\Delta\omega_{i\text{-}i}$, in general, is negligible for ion density $N_i < 10^{19}$ cm^{-3}, but becomes large for dense ion gases.

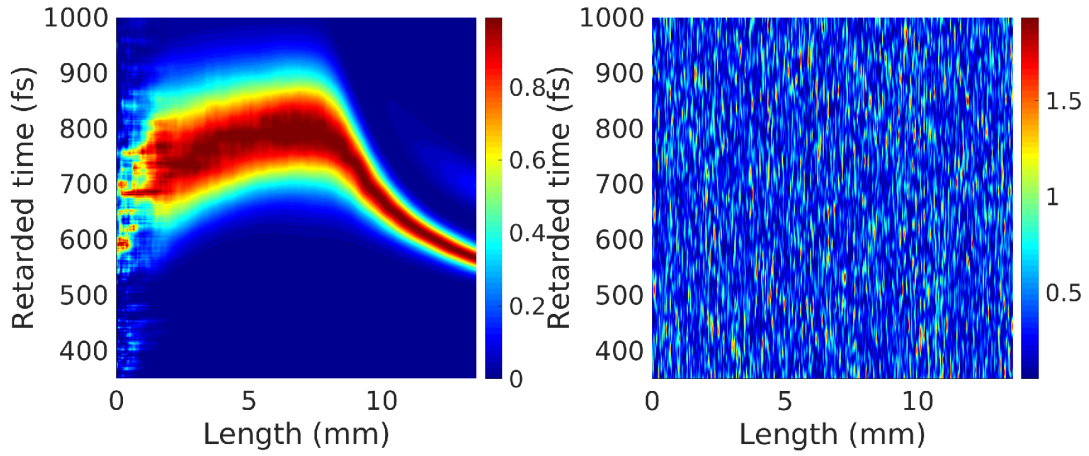

Figure 5.11: XRL intensity evolution in an inhomogeneous plasma. **a,** normalized XRL intensity. **b,** normalized plasma density (or temperature). For a given length, the intensity in (**a**) is normalized to the maximum value of the corresponding profiles at that length. In (**b**), with the mean values being 1, the density and temperature are normalized to $n_0 = 2.5 \times 10^{19}$ cm^{-3} and $T_e = 250$ eV, respectively.

In general, the natural broadening and electron–ion impact broadening are homogeneous for each ion, yielding a Lorentzian spectrum. The Doppler broadening and ion–ion Stark broadening, on the other hand, are inhomogeneous for different ions, and result in a Gaussian spectrum. For systems involving both homogeneous and inhomogeneous broadenings, as it is the case here, the real spectrum has a Voigt lineshape given by the convolution of the Lorentzian and Gaussian profiles, with a FWHM $\Delta\omega_V$ approximately

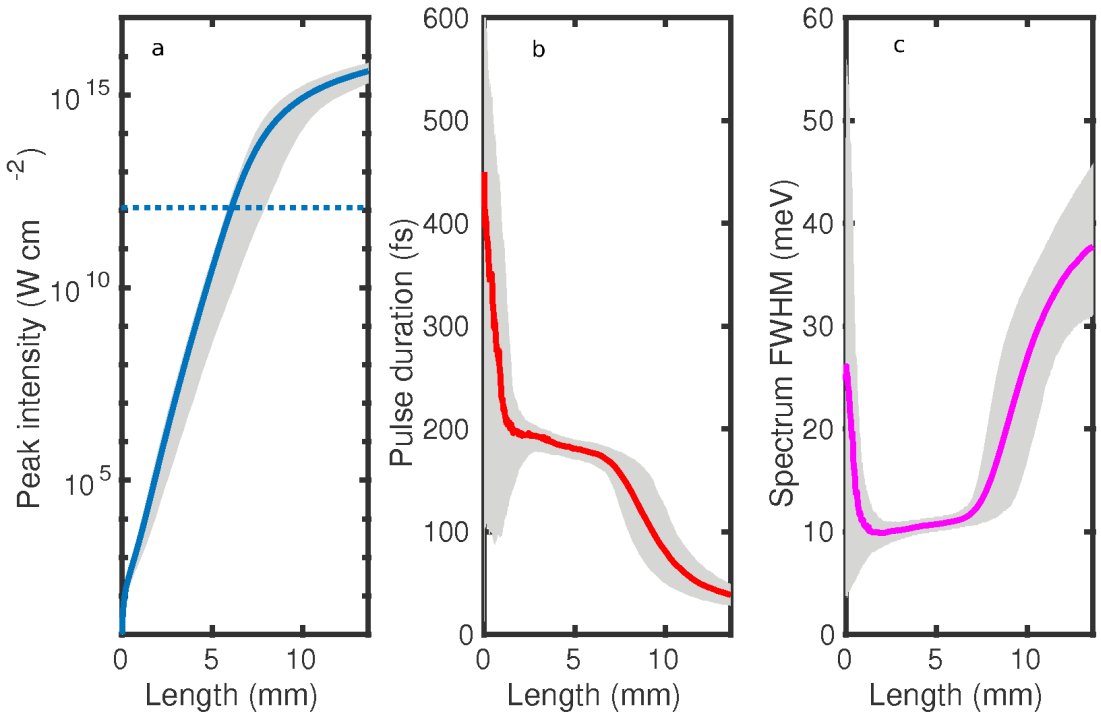

Figure 5.12: Evolution of the XRLs in an inhomogeneous plasma with averaging over 1,000 simulations (Ar^{16+} $^3P_1$). **a-c**, Peak intensity, pulse duration and spectral full width at half maximum (FWHM) for the X-ray laser.

given by [144]

$$\Delta\omega_{\mathrm{V}} \quad = \quad 0.5364\Delta\omega_{\mathrm{L}} + \sqrt{0.2166\Delta\omega_{\mathrm{L}}^2 + \Delta\omega_{\mathrm{G}}^2}. \tag{5.21}$$

Here, $\Delta\omega_{\mathrm{L}} = \Gamma + \Delta\omega_{\text{e-i}}$ is the FWHM of the Lorentzian function, and $\Delta\omega_{\mathrm{G}} = \Delta\omega_{\mathrm{D}} + \Delta\omega_{\text{i-i}}$ is the FWHM of the Gaussian function.

Numerical simulations of the lasing process accounting for the inhomogeneous broadening should take into account the distributions of the thermal velocity as well as the Stark shift of the ions, which renders the simulations time consuming. However, Eq. (5.21) shows that

$$\Delta\omega_{\mathrm{V}} \sim \Delta\omega_{\mathrm{L}} + \Delta\omega_{\mathrm{G}} = \Gamma + \Delta\omega_{\text{e-i}} + \Delta\omega_{\mathrm{D}} + \Delta\omega_{\text{i-i}} \tag{5.22}$$

For the sake of simplicity, we can approximate the parameter in Eq. (5.9) as

$$\gamma = \Gamma + \Delta\omega_{\text{e-i}} + \Delta\omega_{\mathrm{D}} + \Delta\omega_{\text{i-i}} + (\sigma_{\mathrm{e}} + \sigma_{\mathrm{g}})j_{\mathrm{xfel}}(x,t). \tag{5.23}$$

With this approximation, the distribution of the ions over different thermal velocities and Stark shifts is automatically included in the Maxwell–Bloch equations. This simplification may lead to a maximum of 25% overestimate of the bandwidth compared to the Voigt bandwidth $\Delta\omega_{\mathrm{V}}$ in the simulations. However, this will not change our conclusions in the main text.

5.6 Plasma inhomogeneities

For the above simulations, we assumed that the plasma is homogeneous in space and time. Considering that the plasma may undergo fluctuations in both temperature and density, simulations including these inhomogeneous effects should also be included to verify whether the narrow-band lasing still holds.

Our new simulations considering fluctuations in the plasma density and temperature, show in Fig. 5.11, yield the same conclusions. We assume the same behavior in density and temperature fluctuations, see Fig. 5.11.b. The only difference is that, large density fluctuations may need a longer plasma length, but the spectral width does not change significantly.

5.7 Summary

In this Chapter, combining the theoretical results of the previous Chapters, we put forward a scheme to obtain high-intensity X-ray lasers with bandwidths up to three orders of magnitude narrower compared to the value predicted for seeded-XFEL sources in the hard-X-ray regime [35]. The gain medium consists of highly charged ions generated in laser-produced plasma. To show that our scheme can work with current experimental capabilities, we perform numerical simulations with realistic systems for elements such as Ne, Ar, Kr and Xe. As shown in Sec. 5.1, the plasma needed for lasing can be generated by existing picosecond optical lasers with an intensity around 10^{17} W cm^{-2}. Depending on the elements used, the electron temperatures in the plasmas are in the range of 35 eV to 25 keV with the ion densities varying between $2\times10^{18}-2.7\times10^{21}$ cm^{-3}. A high-intensity X-ray laser can be obtained after a 1-cm-long exponential amplification in a laser-produced plasma (see Table 5.1). For lasing based on Ne^{8+} and Ar^{14+}, the $E1$ transitions are sufficient to develop X-ray pulses with saturation intensity. The wavelength of the XRL is around 1.4 nm (920 eV) and 0.4 nm (3137 eV) for Ne^{8+} and Ar^{14+}, respectively, with a relative bandwidth around 10^{-5}. However, for heavier elements, the $M2$ transition at a wavelength of 0.95 Å (13.1 keV) and 0.42 Å (30.6 keV) for Kr^{34+} and Xe^{52+} has been employed, respectively, resulting in a relative bandwidth of around 3×10^{-7} and 1.5×10^{-6}, respectively.

Chapter 6

Analytical solutions to the Maxwell–Bloch equations

In Chapter 5, numerical simulations are performed based on the Maxwell–Bloch equations introduced in Sec. 3.4. Though, exact solutions to these equations are not available, they can be solved under certain approximations. In this Chapter, we show that for transient lasing discussed in Chapter 5, the analytical result on the spectrum and pulse shape can be approximately calculated when the laser intensity is below the saturation intensity.

6.1 Formal solutions to the Maxwell–Bloch equations

Assume the atoms are prepared in the excited state through instantaneous pumping. The corresponding Bloch equations for the density matrix elements are given as

$$\dot{\rho}_{\mathrm{ee}}(x,t) = -\mathrm{Im}[\frac{\wp\mathcal{E}(x,t)}{\hbar}\rho_{\mathrm{eg}}(x,t)] - \Gamma\rho_{\mathrm{ee}}(x,t), \tag{6.1}$$

$$\dot{\rho}_{\mathrm{eg}}(x,t) = \frac{i}{2}\frac{\wp\mathcal{E}(x,t)}{\hbar}(\rho_{\mathrm{ee}}(x,t) - \rho_{\mathrm{gg}}(x,t)) - \frac{\gamma}{2}\rho_{\mathrm{eg}}(x,t) + S(x,t), \tag{6.2}$$

$$\dot{\rho}_{\mathrm{gg}}(x,t) = \mathrm{Im}[\frac{\wp\mathcal{E}(x,t)}{\hbar}\rho_{\mathrm{eg}}(x,t)] + \Gamma\rho_{\mathrm{ee}}(x,t). \tag{6.3}$$

Here, $\wp$ is the electric dipole moment, Γ is the spontaneous emission rate and γ is the decoherence of the off-diagonal element. $\mathcal{E}(x,t)$ is the envelope of the electric field satisfying the following propagation equation

$$\frac{\partial\mathcal{E}(x,t)}{\partial t} + c\frac{\partial\mathcal{E}(x,t)}{\partial x} = i\frac{\mu_0\omega_0c^2}{2}\mathcal{P}(x,t). \tag{6.4}$$

where $\mathcal{P}(x,t) = -2N\wp\rho_{\mathrm{eg}}(x,t)$ refers to the macroscopic polarization field induced by the interaction between the atoms and light field.

Solving these partial differential equations are challenging. In the following, we transform to the retarded-time coordinate, where the form of the Bloch equations remains unchanged, while the propagation of the light field is replaced by

$$\frac{\partial\mathcal{E}(x,t)}{\partial x} = i\frac{\mu_0\omega_0c}{2}\mathcal{P}(x,t) = -i\mu_0\omega_0cN\wp\rho_{\mathrm{eg}}(x,t). \tag{6.5}$$

From now on, in this Chapter, t represents the retarded time. Now we find that the evolution equation of the electric field becomes an ordinary differential equation. It is

possible to perform a formal integral yielding

$$\mathcal{E}(x,t) = -i\mu_0\omega_0 cN\wp\int_0^x \rho_{\mathrm{eg}}(x',t)dx', \tag{6.6}$$

where we have assumed $\mathcal{E}(0,t) = 0$ as the boundary condition for the light field. This formal solution indicates that, in the retarded-time coordinate, the amplitude of the light field at a given position x is just a result of accumulation of all the emissions in the direction of $\boldsymbol{x}$ between $0 \sim x$. By introducing the population inversion

$$\mathcal{D}(x,t) \;=\; \rho_{\mathrm{ee}}(x,t) - \rho_{\mathrm{gg}}(x,t), \tag{6.7}$$

one can rewrite the evolution of the off-diagonal element in Eq. (6.3) as

$$\dot{\rho}_{\mathrm{eg}}(x,t) \;=\; \frac{i}{2}\frac{\wp\mathcal{E}(x,t)}{\hbar}\mathcal{D}(x,t) - \frac{\gamma}{2}\rho_{\mathrm{eg}}(x,t) + S(x,t). \tag{6.8}$$

Substituting Eq. (6.6) into the above equation results in

$$\dot{\rho}_{\mathrm{eg}}(x,t) \;=\; \frac{\mu_0\omega_0 cN\wp^2}{2\hbar}\mathcal{D}(x,t)\int_0^x \rho_{\mathrm{eg}}(x',t)dx' - \frac{\gamma}{2}\rho_{\mathrm{eg}}(x,t) + S(x,t). \tag{6.9}$$

The evolution of the $\rho_{\mathrm{eg}}(x,t)$ is governed by a integral-differential equation, which cannot be solved exactly. Therefore, we will show how this can be solved approximately based on some model simplifications.

The complexity in Eq. (6.9) comes from two aspects. One is the integral $\int_0^x \rho_{\mathrm{eg}}(x',t)dx'$ over space, the other is the population inversion $\mathcal{D}(x,t)$ which depends on another differential equation

$$\dot{\mathcal{D}}(x,t) \;=\; -2\mathrm{Im}\left[\frac{\wp\mathcal{E}(x,t)}{\hbar}\rho_{\mathrm{eg}}(x,t)\right] - \Gamma\left(\mathcal{D}(x,t)+1\right). \tag{6.10}$$

Thus, our model simplification will mainly address these two terms.

6.2 Small-signal assumption

Eq. (6.10) shows that the evolution of the population inversion $\mathcal{D}(x,t)$ depends on two processes: the stimulated emission/absorption from the first term, and the spontaneous decay from the second term. The first simplification that we perform for $\mathcal{D}(x,t)$ is to restrict our considerations to the small-signal regime. In this regime, the light field is weak enough so that the stimulated processes can be omitted because they are much slower than the spontaneous decay

$$\dot{\mathcal{D}}(x,t) \;\approx\; -\Gamma\left(\mathcal{D}(x,t)+1\right). \tag{6.11}$$

Assuming all the atoms are in their excited states at the retarded time $t = 0$, $\mathcal{D}(x,0) = 1$, the solution to this equation is simply given as

$$\mathcal{D}(x,t) \;=\; 2e^{-\Gamma t} - 1. \tag{6.12}$$

With this assumption, the two coupled differential equations, Eq. (6.9) and Eq. (6.10), are reduced to Eq. (6.9) only, with the population inversion $\mathcal{D}(x,t)$ being a well-defined

function.

6.3 Exponential-amplification assumption

We can see that Eq. (6.9) is still a integral-differential equation even in the small-signal regime. To proceed analytically, it has to be simplified. For this purpose, we notice that when a weak light beam propagates through a medium with population inversion, the stimulated emission will lead to an exponential amplification of the intensity of the light beam. Similar features have also been obtained in Chapter 5, where the numerical simulations of the Maxwell–Bloch equations predict the exponential amplification of $\mathcal{E}(x,t)$, as shown in Fig. 5.12a. Motivated by this, we assume that $\mathcal{E}(x,t)$ is a solution of

$$\frac{\partial \mathcal{E}(x,t)}{\partial x} = \mathcal{G}(x)\mathcal{E}(x,t). \tag{6.13}$$

$\mathcal{G}(x)$ is the effective gain coefficient that may depend on x. By comparing it with Eq. (6.5), one can deduce the relation between the light field and the off-diagonal element

$$\mathcal{E}(x,t) \approx -i\frac{\mu_0\omega_0 c N \wp}{\mathcal{G}(x)}\rho_{\mathrm{eg}}(x,t). \tag{6.14}$$

This result can be directly substituted into Eq. (6.8) to obtain a differential equation which is simpler than Eq. (6.9)

$$\dot{\rho}_{\mathrm{eg}}(x,t) = \mathcal{B}(x)\mathcal{D}(x,t)\rho_{\mathrm{eg}}(x,t) - \frac{\gamma}{2}\rho_{\mathrm{eg}}(x,t) + S(x,t), \tag{6.15}$$

with the coefficient

$$\mathcal{B}(x) = \frac{\mu_0\omega_0 c N \wp^2}{2\hbar\mathcal{G}(x)} \tag{6.16}$$

being inversely proportional to the effective gain coefficient. On the other hand, comparison between Eq. (6.14) and Eq. (6.6) indicates

$$\int_0^x \rho_{\mathrm{eg}}(x',t)dx' \approx \mathcal{A}(x)\rho_{\mathrm{eg}}(x,t), \tag{6.17}$$

with the coefficient

$$\mathcal{A}(x) = \frac{1}{\mathcal{G}(x)} \tag{6.18}$$

being a function that only depends on x.

Both of the above two approaches leads to the simplified equation Eq. (6.15) for $\rho_{\mathrm{eg}}(x,t)$ with a formal solution given as

$$\rho_{\mathrm{eg}}(x,t) = \int_{-\infty}^{t} dt' \left[e^{\int_{t'}^{t}\left[\mathcal{B}(x)\mathcal{D}(x,t'')-\frac{\gamma}{2}\right]dt''} S(x,t') \right]. \tag{6.19}$$

Because this formula only depends on the retarded time t, in the following, we only

consider the solutions at given medium length x, and drop the x-dependent relation,

$$\rho_{\mathrm{eg}}(t) = \int_{-\infty}^{t} dt' \left[e^{\int_{t'}^{t} [\mathcal{B}\mathcal{D}(t'') - \frac{\gamma}{2}] dt''} S(t') \rho_{\mathrm{ee}}(t') \right]. \tag{6.20}$$

We notice that, the Gaussian noise term $S(t')$ modeling spontaneous emission is multiplied by the population of the excited state. Eq. (6.20) can be substituted back into Eq. (6.14) to obtain the light field as

$$\mathcal{E}(x,t) = -i \frac{\mu_0 \omega_0 c N \wp}{\mathcal{G}(x)} \int_{-\infty}^{t} dt' \left[e^{\int_{t'}^{t} [\mathcal{B}\mathcal{D}(t'') - \frac{\gamma}{2}] dt''} S(t') \rho_{\mathrm{ee}}(t') \right]. \tag{6.21}$$

One should keep in mind that the evolution equation in Eq. (6.13) only holds in the regime where exponential amplification exists. This means that it is only correct in the small-signal regime far from saturation. In the saturated regime, this approximation breaks down and one needs to solve Eq. (6.9) directly.

In the following, we consider two cases of population dynamics, instantaneous pumping and transient pumping, to see how the light field may look like.

6.4 Instantaneous pumping

For instantaneous pumping, we consider the case where a δ-function-like pump pulse excites all the atoms into the excited state. In the small-signal regime, this means

$$\rho_{\mathrm{ee}}(t) = \begin{cases} 0, & t < 0, \\ e^{-\Gamma t}, & t \geq 0, \end{cases}$$

and

$$\mathcal{D}(t) = \begin{cases} 0, & t < 0, \\ 2e^{-\Gamma t} - 1, & t \geq 0. \end{cases}$$

Substituting these results into Eq. (6.20), we obtain

$$\rho_{\mathrm{eg}}(t) = \int_{0}^{t} dt' \left[e^{\int_{t'}^{t} [\mathcal{B}\mathcal{D}(t'') - \frac{\gamma}{2}] dt''} S(t') e^{-\Gamma t'} \right]. \tag{6.22}$$

The inner integral over t'' is calculated as

$$\begin{aligned} \int_{t'}^{t} \left[\mathcal{B}\mathcal{D}(t'') - \frac{\gamma}{2} \right] dt'' &= \int_{t'}^{t} \left[\mathcal{B} \left(2e^{-\Gamma t''} - 1 \right) - \frac{\gamma}{2} \right] dt'' \\ &= \int_{t'}^{t} \left[2\mathcal{B} e^{-\Gamma t''} - \mathcal{B} - \frac{\gamma}{2} \right] dt'' \\ &= -\frac{2\mathcal{B}}{\Gamma} \left(e^{-\Gamma t} - e^{-\Gamma t'} \right) - \left(\mathcal{B} + \frac{\gamma}{2} \right) (t - t'). \end{aligned} \tag{6.23}$$

Thus,

$$\rho_{\mathrm{eg}}(t) = \int_{0}^{t} dt' \left[e^{-\frac{2\mathcal{B}}{\Gamma} \left(e^{-\Gamma t} - e^{-\Gamma t'} \right) - \left(\mathcal{B} + \frac{\gamma}{2} \right)(t - t')} S(t') e^{-\Gamma t'} \right]. \tag{6.24}$$

Setting $\Gamma = 1$, one gets

$$\begin{aligned}\rho_{\rm eg}(t) &= \int_0^t dt' \left[e^{-2\mathcal{B}\left(e^{-t}-e^{-t'}\right)-\left(\mathcal{B}+\frac{\gamma}{2}\right)(t-t')} S(t') e^{-t'} \right] \\ &= e^{-2\mathcal{B}e^{-t}-\left(\mathcal{B}+\frac{\gamma}{2}\right)t} \int_0^t dt' \left[e^{2\mathcal{B}e^{-t'}+\left(\mathcal{B}+\frac{\gamma}{2}-1\right)t'} S(t') \right] \\ &= e^{-g_1(t)} \int_0^t dt' \left[e^{g_0(t')} S(t') \right], \end{aligned} \tag{6.25}$$

with

$$g_0(t) = 2\mathcal{B}e^{-t} + \left(\mathcal{B}+\frac{\gamma}{2}-1\right)t, \tag{6.26}$$

$$g_1(t) = 2\mathcal{B}e^{-t} + \left(\mathcal{B}+\frac{\gamma}{2}\right)t. \tag{6.27}$$

6.4.1 Spontaneous-emission regime

For $t \ll 1/\left(\mathcal{B}+\frac{\gamma}{2}\right)$, the following also holds:

$$t' \ll 1/\left(\mathcal{B}+\frac{\gamma}{2}\right) < 1, \tag{6.28}$$

and

$$\begin{aligned} e^{-2\mathcal{B}e^{-t}-\left(\mathcal{B}+\frac{\gamma}{2}\right)t} &\approx e^{-2\mathcal{B}}, \\ \int_0^t dt' \left[e^{2\mathcal{B}e^{-t'}+\left(\mathcal{B}+\frac{\gamma}{2}-1\right)t'} S(t') \right] &\approx \int_0^t dt' \left[e^{2\mathcal{B}} S(t') \right]. \end{aligned}$$

Furthermore,

$$\rho_{\rm eg}(t) = \int_0^t dt' S(t') \tag{6.29}$$

gives a random walk behavior for $t \ll 1$. As t is the retard time, the random walk represents the spontaneous emission behavior at the very beginning.

6.4.2 Long-time regime

For $t \gg 1$, one first has the approximate expression for the prefactor

$$e^{-2\mathcal{B}e^{-t}-\left(\mathcal{B}+\frac{\gamma}{2}\right)t} \approx e^{-\left(\mathcal{B}+\frac{\gamma}{2}\right)t} \ll 1.$$

The integral, on the other hand, can be divided into three parts:

$$\int_0^t dt' = \int_0^\delta dt' + \int_\delta^{t-\delta} dt' + \int_{t-\delta}^t dt'.$$

Firstly,

$$\int_0^\delta dt' \left[e^{2\mathcal{B}e^{-t'}+\left(\mathcal{B}+\frac{\gamma}{2}-1\right)t'} S(t') \right] \approx \int_0^t dt' \left[e^{2\mathcal{B}} S(t') \right] = e^{2\mathcal{B}} \int_0^t dt' S(t').$$

Multiplied with the prefactor, one obtains a negligible contribution. Secondly,

$$\int_{\delta}^{t-\delta} dt' \left[e^{2\mathcal{B}e^{-t'}+(\mathcal{B}+\frac{\gamma}{2}-1)t'} S(t') \right] \leq e^{2\mathcal{B}} \int_{\delta}^{t-\delta} dt' \left[e^{(\mathcal{B}+\frac{\gamma}{2}-1)t'} S(t') \right],$$

multiplied with the prefactor, one has

$$\begin{aligned} e^{-(\mathcal{B}+\frac{\gamma}{2})t} \int_{\delta}^{t-\delta_1} dt' \left[e^{2\mathcal{B}e^{-t'}+(\mathcal{B}+\frac{\gamma}{2}-1)t'} S(t') \right] &\leq e^{2\mathcal{B}} \int_{\delta}^{t-\delta_1} dt' \left[e^{-(\mathcal{B}+\frac{\gamma}{2})(t-t')} e^{-t'} S(t') \right] \\ &\leq e^{2\mathcal{B}} \int_{\delta}^{t-\delta_1} dt' \left[e^{-(\mathcal{B}+\frac{\gamma}{2})\delta_1} e^{-t'} S(t') \right] \\ &\approx 0 \text{ for } \delta_1 \geq 2. \end{aligned}$$

Lastly, the third integral can be obtained through

$$\begin{aligned} e^{-(\mathcal{B}+\frac{\gamma}{2})t} \int_{t-\delta_1}^{t} dt' \left[e^{2\mathcal{B}e^{-t'}+(\mathcal{B}+\frac{\gamma}{2}-1)t'} S(t') \right] &\approx \int_{t-\delta_1}^{t} dt' \left[e^{-(\mathcal{B}+\frac{\gamma}{2})(t-t')} e^{-t'} S(t') \right] \\ &\leq \int_{t-\delta_1}^{t} dt' \left[e^{-t'} S(t') \right] \\ &\approx 0 \text{ for } \delta_1 \gg 1. \end{aligned}$$

Thus, all together, we know that

$$\rho_{\mathrm{eg}}(t) = 0 \text{ for } t \gg 1. \tag{6.30}$$

6.4.3 Stimulated-emission regime: approximate analytical results

For $t \sim 1$, we now approximate the exponent in the integral

$$g_0(t) = 2\mathcal{B}e^{-t} + \left(\mathcal{B} + \frac{\gamma}{2} - 1 \right) t, \tag{6.31}$$

by a parabolic function

$$f_0(t) = a_0 \left(t - b_0 \right)^2 + c_0. \tag{6.32}$$

The coefficient of the parabolic function can be obtained by assuming that, on the one hand, $g_0(0) = f_0(0)$; on the other hand, the minima of the two functions $g_0(t)$ and $f_0(t)$ overlap at $t_{\min}$, Therefore,

$$b_0 = t_{\min}, \tag{6.33}$$

$$c_0 = g_0(t_{\min}), \tag{6.34}$$

$$a_0 b_0^2 + c_0 = 2\mathcal{B}. \tag{6.35}$$

Firstly, $t_{\min}$ can be found from $g'(t_{\min}) = 0$. One has

$$-2\mathcal{B}e^{-t} + \left(\mathcal{B} + \frac{\gamma}{2} - 1 \right) = 0. \tag{6.36}$$

This equation gives

$$t_{\min} = \ln\left[\frac{2\mathcal{B}}{\mathcal{B}+\frac{\gamma}{2}-1}\right] < 1. \tag{6.37}$$

Then one can calculate the minimum of $g_0(t_{\min})$ through

$$\begin{aligned} g_0(t_{\min}) &= 2\mathcal{B}e^{-t_{\min}} + \left(\mathcal{B}+\frac{\gamma}{2}-1\right)t_{\min} \\ &= 2\mathcal{B}e^{-\ln\left[\frac{2\mathcal{B}}{\mathcal{B}+\frac{\gamma}{2}-1}\right]} + \left(\mathcal{B}+\frac{\gamma}{2}-1\right)\ln\left[\frac{2\mathcal{B}}{\mathcal{B}+\frac{\gamma}{2}-1}\right] \\ &= 2\mathcal{B}\frac{\mathcal{B}+\frac{\gamma}{2}-1}{2\mathcal{B}} + \left(\mathcal{B}+\frac{\gamma}{2}-1\right)\ln\left[\frac{2\mathcal{B}}{\mathcal{B}+\frac{\gamma}{2}-1}\right] \\ &= \left(\mathcal{B}+\frac{\gamma}{2}-1\right)\left(1+\ln\left[\frac{2\mathcal{B}}{\mathcal{B}+\frac{\gamma}{2}-1}\right]\right) \\ &< 2\left(\mathcal{B}+\frac{\gamma}{2}-1\right). \end{aligned} \tag{6.38}$$

Therefore, we have the equaling for b_0 and c_0:

$$b_0 = \ln\left[\frac{2\mathcal{B}}{\mathcal{B}+\frac{\gamma}{2}-1}\right], \tag{6.39}$$

$$c_0 = \left(\mathcal{B}+\frac{\gamma}{2}-1\right)\left(1+\ln\left[\frac{2\mathcal{B}}{\mathcal{B}+\frac{\gamma}{2}-1}\right]\right), \tag{6.40}$$

and

$$a_0 = \frac{2\mathcal{B}-c_0}{b_0^2}. \tag{6.41}$$

Because $0 < b_0 < 1$, and

$$\left(\mathcal{B}+\frac{\gamma}{2}-1\right) < c_0 < 2\left(\mathcal{B}+\frac{\gamma}{2}-1\right),$$

it also holds:

$$a_0 = \frac{2\mathcal{B}-c_0}{b_0^2} > 2\mathcal{B}-c_0 > \mathcal{B}-\frac{\gamma}{2}+1.$$

Thus, the value of $\rho_{\rm eg}(t)$ for $t \sim 1$ can be approximated by

$$\rho_{\rm eg}(t) = e^{-g_1(t)}\int_0^t dt'\left[e^{g_0(t')}S(t')\right] \approx e^{-g_1(t)}\int_0^t dt'\left[e^{f_0(t')}S(t')\right]. \tag{6.42}$$

To have a better understanding of the behavior of these functions, we may first drop the Gaussian noise term $S(t)$. The integral can be approximated by

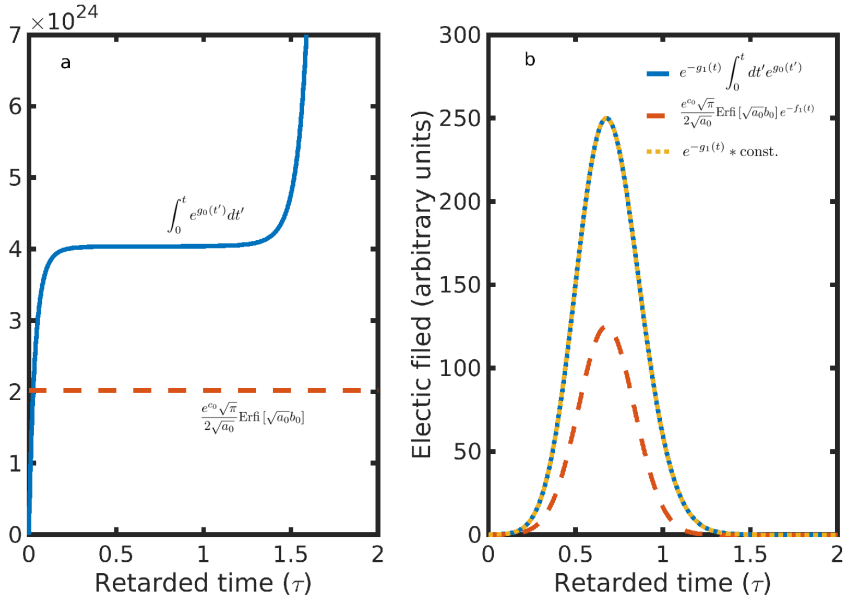

Figure 6.1: Light pulse without noise. a, the integral in Eq. (6.43). **b,** electric field strength of the light field. In (**a**), the accurate value of the integral (blue solid line) shows a step-like platform with an approximate behavior of an imaginary error function. The red dashed line represents our approximated value of the integral. In (**b**), the accurate pulse shape (blue solid line) overlaps with the function $e^{-g_1(t)}$ (yellow dotted line), indicating that the profile of the pulse is determined by $e^{-g_1(t)}$. The approximate result (red dashed line) from Eq. (6.46) has also been shown. $\mathcal{B} = 30, \gamma = 1$.

$$\begin{aligned}
\int_0^t e^{g_0(t')}dt' &\approx \int_0^t e^{f_0(t')}dt' \\
&= \int_0^t e^{a_0(t'-b_0)^2+c_0}dt' \\
&= \frac{e^{c_0}\sqrt{\pi}\mathrm{Erfi}\left[\sqrt{a_0}(t'-b_0)\right]}{2\sqrt{a_0}}\Bigg|_0^t \\
&= \frac{e^{c_0}\sqrt{\pi}}{2\sqrt{a_0}}\left(\mathrm{Erfi}\left[\sqrt{a_0}(t-b_0)\right] - \mathrm{Erfi}\left[\sqrt{a_0}(-b_0)\right]\right) \\
&= \frac{e^{c_0}\sqrt{\pi}}{2\sqrt{a_0}}\left(\mathrm{Erfi}\left[\sqrt{a_0}(t-b_0)\right] + \mathrm{Erfi}\left[\sqrt{a_0}b_0\right]\right). \qquad (6.43)
\end{aligned}$$

Then the integral has a behavior similar to an imaginary error function (Fig. 6.1a). The off-diagonal element can be approximated as

$$\rho_{\mathrm{eg}}(t) \approx e^{-g_1(t)}\frac{e^{c_0}\sqrt{\pi}}{2\sqrt{a_0}}\left(\mathrm{Erfi}\left[\sqrt{a_0}(t-b_0)\right] + \mathrm{Erfi}\left[\sqrt{a_0}b_0\right]\right). \qquad (6.44)$$

In the region of interest, one can approximate

$$\left(\mathrm{Erfi}\left[\sqrt{a_0}(t-b_0)\right] + \mathrm{Erfi}\left[\sqrt{a_0}b_0\right]\right) \approx \mathrm{Erfi}\left[\sqrt{a_0}b_0\right],$$

and the final result for the off-diagonal element is given as

$$\rho_{\rm eg}(t) \approx \frac{e^{c_0}\sqrt{\pi}}{2\sqrt{a_0}}\,{\rm Erfi}\left[\sqrt{a_0}b_0\right]e^{-g_1(t)}. \tag{6.45}$$

At the same time, the light field is given by

$$\mathcal{E}(x,t) = -i\frac{\mu_0\omega_0 cN\wp}{\mathcal{G}(x)}\frac{e^{c_0}\sqrt{\pi}}{2\sqrt{a_0}}\,{\rm Erfi}\left[\sqrt{a_0}b_0\right]e^{-g_1(t)}. \tag{6.46}$$

In Fig. 6.1b, we plot the electric field by numerical integration of Eq. (6.25), exhibited by the blue solid line. While the approximate result (red dashed line) from Eq. (6.46) gives a similar pulse profile with a relatively smaller peak value, by setting the peak value of the red dashed line to be the same as the blue solid line, the two curves (yellow dotted line) overlap with each other. This indicates that, by using Eq. (6.31) instead of (6.30) to model the function $g_0(t)$, one can find the pulse shape and spectrum given by

$$\mathcal{E}(x,t) = Ce^{-g_1(t)} = Ce^{-2\mathcal{B}e^{-t}-\left(\mathcal{B}+\frac{\gamma}{2}\right)t}, \tag{6.47}$$

and its Fourier transform (where C is a constant) well reproduce the numerical solution of Eq. (6.25).

Furthermore, the function $g_1(t)$ can also be approximated by a parabolic function

$$f_1(t) = a_1\left(t-b_1\right)^2 + c_1, \tag{6.48}$$

with the coefficients given as

$$b_1 = \ln\left[\frac{2\mathcal{B}}{\mathcal{B}+\frac{\gamma}{2}}\right], \tag{6.49}$$

$$c_1 = \left(\mathcal{B}+\frac{\gamma}{2}\right)\left(1+\ln\left[\frac{2\mathcal{B}}{\mathcal{B}+\frac{\gamma}{2}}\right]\right), \tag{6.50}$$

$$a_1 = \frac{2\mathcal{B}-c_1}{b_1^2}. \tag{6.51}$$

Again, we know that

$$\begin{aligned} b_1 &< \ln 2 < 1, \\ \mathcal{B}+\frac{\gamma}{2} &< c_1 < 2\mathcal{B}+\gamma, \\ a_1 &> \mathcal{B}-\frac{\gamma}{2}. \end{aligned}$$

This approximation of $g_1(t)$ indicates that the final pulse shape resembles a Gaussian function given by $e^{-f_1(t)}$, which is apparent from Fig. 6.1b. The FWHM pulse duration, therefore, can be calculated from the following relation:

$$a_1\left(t_h-b_1\right)^2 + c_1 = c_1 + \ln 2. \tag{6.52}$$

This gives

$$t_h = b_1 \pm \sqrt{\frac{\ln 2}{a_1}}, \tag{6.53}$$

and the pulse duration

$$\Delta t = 2\sqrt{\frac{\ln 2}{a_1}}. \tag{6.54}$$

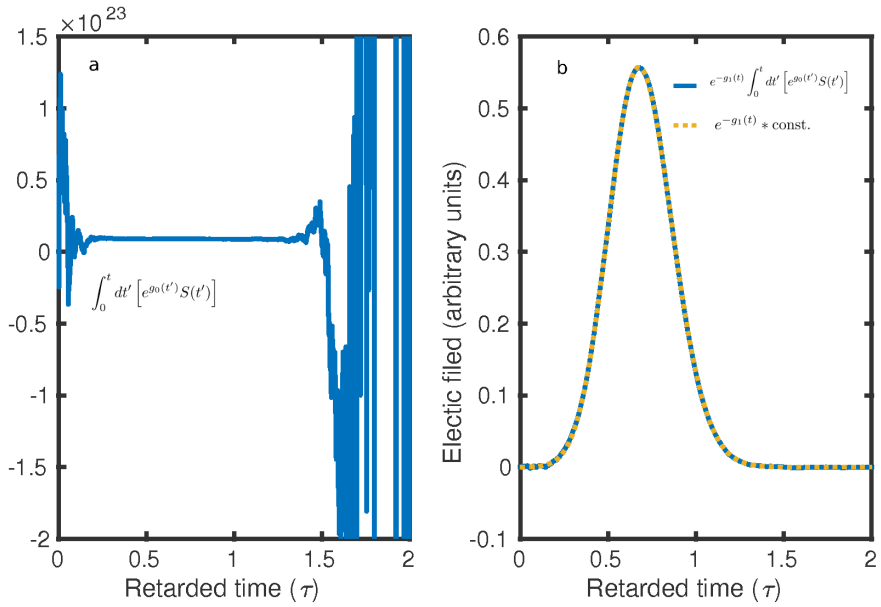

Figure 6.2: Light pulse with noise. a, the integral in Eq. (6.25). **b,** electric field strength of the light field. In (**a**), the accurate value of the integral (blue solid line) shows a step-like platform for times between (0.2,1.3) with a similar behavior as in Fig. 6.1. In (**b**), the accurate pulse shape (blue solid line) overlaps with the function $e^{-g_1(t)}$ (yellow dotted line), indicating that the profile of the pulse is determined by $e^{-g_1(t)}$. Here, $\mathcal{B} = 30, \gamma = 1$.

When the noise term $S(t)$ is included, one obtains the same conclusion for the pulse profile. As depicted in Fig. 6.2a, the presence of a noise term leads to fast oscillations at the front and tail of the integral in Eq. (6.25). However, for the time between (0.2,1.3), there is still a platform similar to Fig. 6.1a. Therefore, the profile of the light pulse is again determined by the Gaussian-like function $e^{-g_1(t)}$.

The existence of $S(t)$ leads to fluctuations in the peak value for different realizations of the noise. Its average value can be found through the correlations

$$\begin{aligned}
\langle \rho_{\rm eg}(t)\rho_{\rm eg}(t_1)\rangle &= e^{-g_1(t)}e^{-g_1(t_1)}\int_0^t dt' \int_0^{t_1} dt_1' \left[e^{f_0(t')}e^{f_0(t_1')}\langle S(t')S(t_1')\rangle\right] \\
&= e^{-g_1(t)}e^{-g_1(t_1)}\int_0^t dt' \int_0^{t_1} dt_1' \left[e^{f_0(t')}e^{f_0(t_1')}F\delta(t'-t_1')\right] \\
&= Fe^{-g_1(t)}e^{-g_1(t_1)}\int_0^{\min(t,t_1)} dt' e^{2f_0(t')}.
\end{aligned} \tag{6.55}$$

Therefore,

$$\begin{aligned}\left\langle \rho_{\rm eg}^2(t)\right\rangle &= Fe^{-2g_1(t)}\int_0^t dt' e^{2f_0(t')}\\ &= F\frac{e^{2c_0}\sqrt{\pi}}{2\sqrt{2a_0}}\mathrm{Erfi}\left[\sqrt{2a_0}b_0\right]e^{-2g_1(t)},\end{aligned} \tag{6.56}$$

and

$$\left\langle |\mathcal{E}_s(x,t)|^2\right\rangle = \left(\frac{\mu_0\omega_0 cN\wp}{\mathcal{G}(x)}\right)^2 F\frac{e^{2c_0}\sqrt{\pi}}{2\sqrt{2a_0}}\mathrm{Erfi}\left[\sqrt{2a_0}b_0\right]e^{-2g_1(t)}. \tag{6.57}$$

The ratio between the light intensity with and without the noise term is calculated as

$$\frac{\left\langle |\mathcal{E}_s(x,t)|^2\right\rangle}{|\mathcal{E}(x,t)|^2} = F\frac{\sqrt{2a_0}}{\sqrt{\pi}}\frac{\mathrm{Erfi}\left[\sqrt{2a_0}b_0\right]}{\mathrm{Erfi}\left[\sqrt{a_0}b_0\right]}. \tag{6.58}$$

6.5 Transient pumping

Similarly to what we derived above, and considering that the excited state is pumped from another initial state (assuming $\Gamma = 1$), the Bloch equations are

$$\dot\rho_{00}(t) = -w\rho_{00}(t), \tag{6.59}$$
$$\dot\rho_{\rm ee}(t) = -\rho_{\rm ee}(t) + w\rho_{00}(t), \tag{6.60}$$
$$\dot\rho_{\rm gg}(t) = \rho_{\rm ee}(t). \tag{6.61}$$

With all the ions initially in the $|0\rangle$ state at $t = 0$, one can solve the equations to give

$$\rho_{00}(t) = e^{-wt}, \tag{6.62}$$
$$\rho_{\rm ee}(t) = \frac{w}{w-1}\left(e^{-t} - e^{-wt}\right), \tag{6.63}$$
$$\rho_{\rm gg}(t) = \frac{1}{w-1}\left(e^{-wt} - we^{-t} + (w-1)\right). \tag{6.64}$$

Correspondingly, one obtains the time-dependent population inversion given as

$$\mathcal{D}(t) = \frac{1}{w-1}\left(2we^{-t} - (w-1) - (w+1)e^{-wt}\right). \tag{6.65}$$

For $w \gg 1$, this population inversion reduces to the case of instantaneous pumping of $|\mathrm{e}\rangle$:

$$\mathcal{D}(t) = \frac{1}{w-1}\left(2we^{-t} - (w-1)\right) \approx 2e^{-t} - 1,$$

as derived in the former sections. Therefore, the formal integral of the off-diagonal element has the form

$$\begin{aligned}\rho_{\rm eg}(t) &= \int_{-\infty}^t dt'\left[e^{\int_{t'}^t\left[\mathcal{B}\mathcal{D}(t'')-\frac{\gamma}{2}\right]dt''}S(t')\rho_{\rm eg}(t')\right].\\ &= \int_0^t dt'\left[e^{\int_{t'}^t\left[\mathcal{B}\mathcal{D}(t'')-\frac{\gamma}{2}\right]dt''}S(t')\rho_{\rm eg}(t')\right].\end{aligned}$$

The inner integral over t'' is calculated as

$$\begin{aligned}
\int_{t'}^{t}\left[\mathcal{B}\mathcal{D}(t'')-\frac{\gamma}{2}\right]dt'' &= \int_{t'}^{t}\left[\mathcal{B}\frac{1}{w-1}\left(2we^{-t}-(w-1)-(w+1)e^{-wt}\right)-\frac{\gamma}{2}\right]dt'' \\
&= \int_{t'}^{t}\left[\frac{\mathcal{B}}{w-1}\left(2we^{-t}-(w+1)e^{-wt}\right)-\mathcal{B}-\frac{\gamma}{2}\right]dt'' \\
&= -\frac{\mathcal{B}}{w-1}\left(2we^{-t}-2we^{-t'}-\frac{w+1}{w}\left(e^{-wt}-e^{-wt'}\right)\right) \\
&\quad -\left(\mathcal{B}+\frac{\gamma}{2}\right)(t-t') \\
&= -\frac{2w\mathcal{B}}{w-1}\left(e^{-t}-e^{-t'}-\frac{w+1}{2w^2}\left(e^{-wt}-e^{-wt'}\right)\right) \\
&\quad -\left(\mathcal{B}+\frac{\gamma}{2}\right)(t-t').
\end{aligned}$$

Thus, one obtains

$$\begin{aligned}
\rho_{\mathrm{eg}}(t) &= e^{-\frac{2w\mathcal{B}}{w-1}\left(e^{-t}-\frac{w+1}{2w^2}e^{-wt}\right)-\left(\mathcal{B}+\frac{\gamma}{2}\right)t} \\
&\quad \times\int_0^t dt'\left[e^{\frac{2w\mathcal{B}}{w-1}\left(e^{-t'}-\frac{w+1}{2w^2}e^{-wt'}\right)+\left(\mathcal{B}+\frac{\gamma}{2}\right)t'}S(t')\frac{w}{w-1}\left(e^{-t'}-e^{-wt'}\right)\right].
\end{aligned}$$

In other way, this can be written as

$$\rho_{\mathrm{eg}}(t) = \frac{w}{w-1}e^{-g_1(t)}\left\{\int_0^t dt' e^{g_2(t')}S(t')-\int_0^t dt' e^{g_3(t')}S(t')\right\}, \tag{6.66}$$

with

$$\begin{aligned}
g_1(t) &= \frac{2w\mathcal{B}}{w-1}\left(e^{-t}-\frac{w+1}{2w^2}e^{-wt}\right)+\left(\mathcal{B}+\frac{\gamma}{2}\right)t, \\
g_2(t) &= \frac{2w\mathcal{B}}{w-1}\left(e^{-t}-\frac{w+1}{2w^2}e^{-wt}\right)+\left(\mathcal{B}+\frac{\gamma}{2}-1\right)t, \\
g_3(t) &= \frac{2w\mathcal{B}}{w-1}\left(e^{-t}-\frac{w+1}{2w^2}e^{-wt}\right)+\left(\mathcal{B}+\frac{\gamma}{2}-w\right)t.
\end{aligned}$$

Also in this case, we approximate these functions with parabolic functions, which leads to an approximate solution of the integral (see Fig. 6.3). In particular, the two functions $g_2(t)$ and $g_3(t)$ only influence the peak value of the final pulse. The profile of the pulse is a Gaussian-like function determined by $g_1(t)$.

To generalize our conclusions, we introduce a function $G(t)$ which satisfies

$$\frac{\mathrm{d}}{\mathrm{d}t}G(t) = \mathcal{B}\mathcal{D}(t)-\frac{\gamma}{2}t. \tag{6.67}$$

With this function, the formal solution in Eq. (6.20) can be rewritten as

$$\rho_{\mathrm{eg}}(t) = \int_{-\infty}^{t}dt'\left[e^{G(t)-G(t')}S(t')\rho_{\mathrm{ee}}(t')\right] = e^{G(t)}\int_{-\infty}^{t}dt'\left[e^{-G(t')}S(t')\rho_{\mathrm{ee}}(t')\right].$$

The integral usually has a behavior similar to a shifted imaginary error function with a

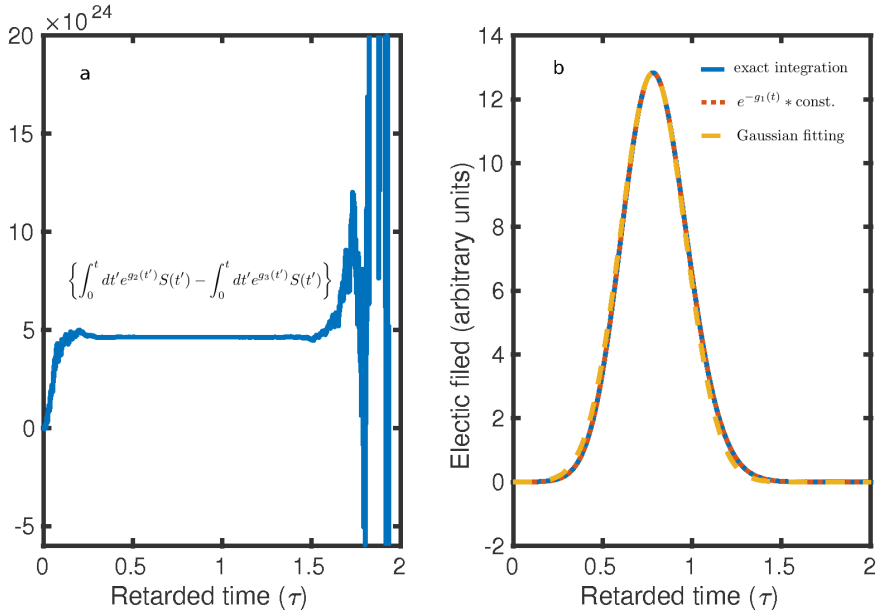

Figure 6.3: Light pulse under transient pumping. a, the integral in Eq. (6.66). **b,** electric field strength of the light field. In (**a**), the accurate value of the integral (blue solid line) shows a step-like platform for times between (0.2,1.5) with a similar behavior as in Fig. 6.1. In (**b**), the accurate pulse shape (blue solid line) overlaps with the function $e^{-g_1(t)}$ (red dotted line) and the Gaussian fitting curve (yellow dashed line). Here, $\mathcal{B} = 30, \gamma = 1, w = 2$.

plateau that can be approximated by a constant. Then one obtains

$$\mathcal{E}(x,t) \quad = \quad Ce^{G(t)} = Ce^{\int_0^t dt'(\mathcal{B}\mathcal{D}(t') - \frac{\gamma}{2}t')}. \tag{6.68}$$

As long as we know the population inversion and $\mathcal{B}$, the pulse profile and spectrum can be deduced from the above function.

The analytical solution of the laser field given in Eq. (6.68) represents a Gaussian-like function, as shown in Fig. 6.3b. Compared to the Gaussian XRL pulses we obtained in Fig. 5.6c with numerical simulations, they show a good agreement. The physics still missing in our analytical solution is the intensity. In Eq. (6.68), it shows up as an integration constant. Nevertheless, with the analytical solution, one can estimate the conditions needed to obtain coherent X-ray laser pulses. As shown in Fig. 6.4, a smooth coherent pulse is obtained only if $\mathcal{B} > \gamma$ holds.

6.6 Duration of population inversion

Eq. (6.68) gives a general solution to transient lasing under given population inversion. In this Section, we discuss how population inversion is generated in different pumping schemes.

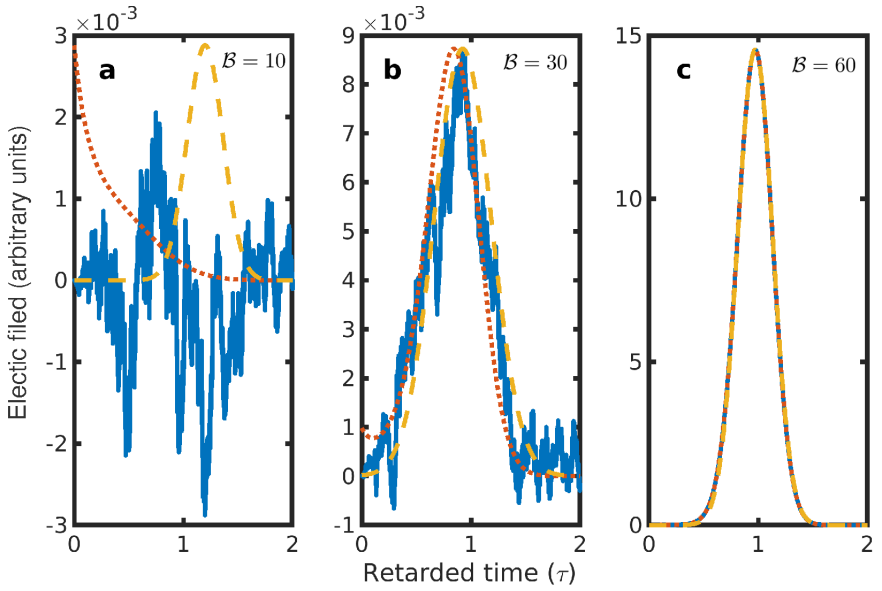

Figure 6.4: Light pulse under transient pumping: different gain. a, $\mathcal{B} = 10$. **b,** $\mathcal{B} = 30$. **c,** $\mathcal{B} = 60$. The legends of each line are the same as in Fig. 6.3b. A smooth light pulse develops only when the gain parameter $\mathcal{B}$ is much larger than the decoherence rate γ. For all the three figures, $\gamma = 10, w = 2$.

6.6.1 Slow ground-state depletion

If the decay of the ground state is negligible, the population inversion for transient pumping is given by Eq. (6.65):

$$\mathcal{D}(t) \quad = \quad \frac{1}{w-1}\left(2we^{-t} - (w-1) - (w+1)e^{-wt}\right). \tag{6.69}$$

In general, $\mathcal{D}(x,0) = 0$ at the beginning, then it becomes positive for a short time duration, after which it decreases and stays in a negative value. Here, in this Section, we calculate the time duration of the positive population inversion, in the limit of fast and slow pumping. This can be found by solving $\mathcal{D}(t) = 0$. We know already the first solution is at $t = 0$. Then the task remaining is to find the second solution.

6.6.1.1 Fast pumping: $w \gg 1$ regime

When the pumping rate is much larger than the decay rate of the upper state, it corresponds to instantaneous pumping:

$$\mathcal{D}(t) \quad \approx \quad 2e^{-t} - 1 \qquad \text{for } t > 0. \tag{6.70}$$

Then, $\mathcal{D}(t) = 0$ gives $t = \ln 2$. This also means that

$$\Delta t = \ln 2 < 1.$$

6.6.1.2 Slow pumping: $w \ll 1$ regime

When the pumping rate is much smaller than the decay rate of the upper state,

$$\rho_{\rm ee}(t) \approx we^{-wt} \qquad \text{for } 1 \ll t \ll 1/w. \tag{6.71}$$

The "lifetime" of the upper state $|{\rm e}\rangle$ is increased to the time $\sim 1/w \gg 1$. The population inversion is

$$\begin{aligned} \mathcal{D}(t) &= \frac{1}{w-1}\left(2we^{-t} - (w-1) - (w+1)e^{-wt}\right) \\ &\approx -2we^{-t} + (w-1) + (w+1)e^{-wt} \\ &= -2ws + (w-1) + (w+1)s^w, \end{aligned} \tag{6.72}$$

where $s = e^{-t}$. Considering the expansion

$$s^w \approx 1 + ({\rm ln}s)w + \frac{1}{2}({\rm ln}s)^2w^2 + ...,$$

one has

$$\begin{aligned} \mathcal{D}(t) &= -2ws + (w-1) + (w+1)s^w \\ &\approx -2ws + (w-1) + (w+1)(1 + w{\rm ln}s) \\ &= -2ws + 2w + w{\rm ln}s \\ &= w(-2e^{-t} + 2 - t), \end{aligned} \tag{6.73}$$

and then $\mathcal{D}(t) = 0$ means $-2e^{-t} + 2 - t = 0$. Defining

$$k(t) = 2 - t - 2e^{-t}, \tag{6.74}$$

we know that $k(1) = 1 - \frac{2}{e} > 0$ and $k(2) = -\frac{2}{e^2} < 0$. The solution for $\mathcal{D}(t) = 0$ is located in the region of $1 < t < 2$, which means that the duration for population inversion satisfies

$$1 < \Delta t < 2.$$

The magnitude of the population inversion is also in the range of w, which can be calculated from the peak value of $\mathcal{D}(t)$, or $k(t)$:

$$k'(t) = -1 + 2e^{-t} = 0,$$

yielding $t_p = {\rm ln}2$. Then

$$k(t_p) = 2 - {\rm ln}2 - 2e^{-{\rm ln}2} = 1 - {\rm ln}2, \tag{6.75}$$

and

$$\mathcal{D}(t) = w(1 - {\rm ln}2). \tag{6.76}$$

All together, this means that the duration of the population inversion exists for any values of the pumping rate. The time scale of the population inversion is on the same scale of the lifetime of the upper state. However, the magnitude of the population

inversion is negligibly small for small pumping rates (in the same order as the pumping rate), see Fig. 6.5.

6.6.2 Fast ground-state depletion

When the decay rate of the ground state is much faster than the pumping rate, atoms decayed to the ground state will be immediately depleted. In this case, one can always take $\rho_{\mathrm{gg}}(t) = 0$ and the population inversion is just determined by the population in the excited state:

$$\mathcal{D}(t) = \rho_{\mathrm{ee}}(t) \quad = \quad \frac{w}{w-1}\left(e^{-t} - e^{-wt}\right). \tag{6.77}$$

The behavior of $\mathcal{D}(t)$ for different pumping rates in Fig. 6.6a show a pulse-like inversion. Similarly to the former Section, the peak of $\mathcal{D}(t)$ can be calculated as

$$t_p \quad = \quad \frac{\ln w}{w-1}. \tag{6.78}$$

Details of the dependence of $\mathcal{D}(t_p)$, and the FWHM duration of positive inversion Δt can be found in Fig. 6.6b. Compared to Fig. 6.5, the FWHM duration for positive population inversion is not limited anymore, and it increases exponentially for small pumping rates. However, the peak value of the inversion is still proportional to w.

6.7 Summary

For lasing based on transient population inversion, we solved the Maxwell–Bloch equations analytically in the small-signal regime, in the assumption of exponential amplification of the electric field. This allows one to introduce a gain function. The profile of the light pulse is universally characterized by a Gaussian-like profile, with its duration and spectral width determined by the gain coefficient and decoherence rate. In order to

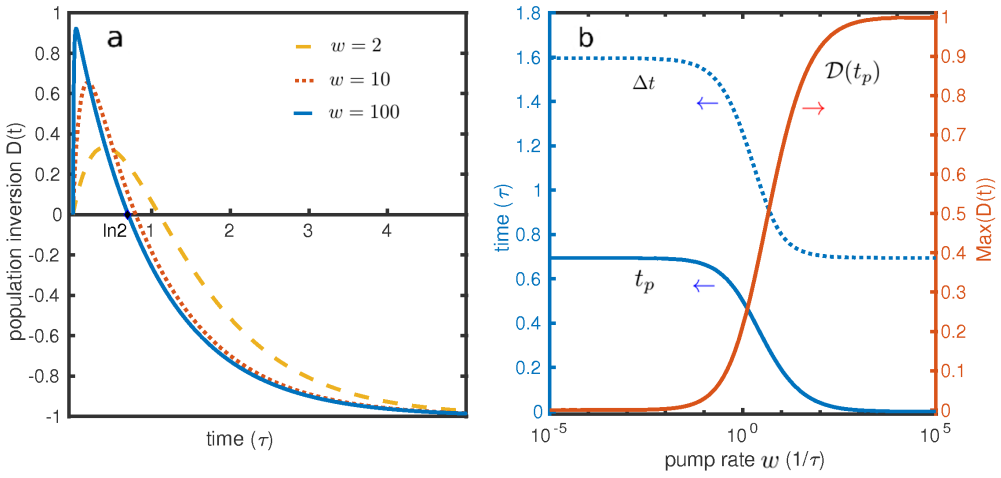

Figure 6.5: Population inversion for different pumping rates. a, time evolution of population inversion for a pumping rate $w = 2$ (yellow dashed line), $w = 10$ (red dotted line) and $w = 100$ (blue solid line). **b,** the value (red solid line) and position (blue solid line) of peak population inversion, as well as the duration (blue dotted line) for positive population inversion.

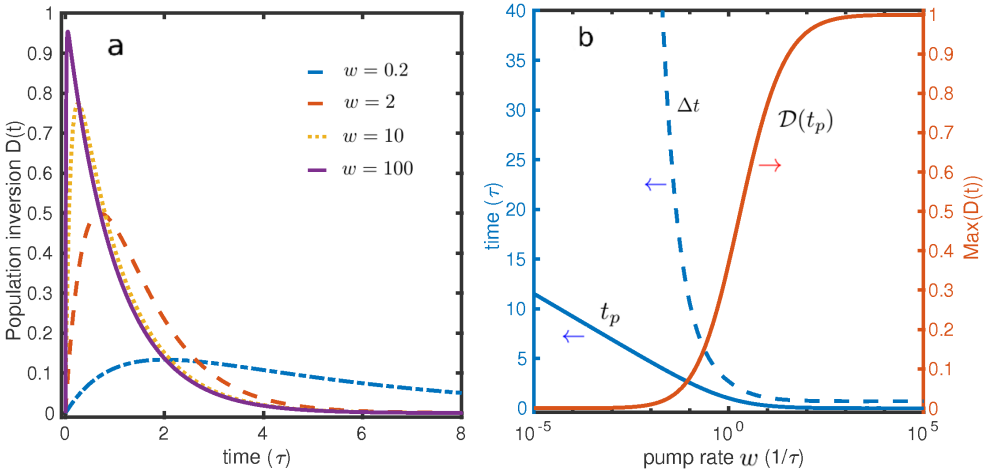

Figure 6.6: Population inversion for different pumping rates under fast ground-state depletion. a, time evolution of population inversion for a pumping rate $w = 0.2$ (blue dash-dotted line), $w = 2$ (red dashed line), $w = 10$ (yellow dotted line) and $w = 100$ (purple solid line). **b,** the value (red solid line) and position (blue solid line) of peak population inversion, as well as the FWHM duration (blue dotted line) for positive population inversion.

have a coherent laser pulse, the gain should be much larger than the decoherence rate. Besides, we also find that, when the lasing element is pumped from another element, independent of the pump rate, there always exists population inversion in the lasing element for times within the lifetime.

Chapter 7

Seeding in transient X-ray laser

In Chapters 5 and 6, we considered X-ray lasing seeded by spontaneously emitted photons. Numerical and analytical solutions of the Maxwell–Bloch equations under transient XFEL pumping were solved in the time domain, giving an X-ray laser with a smooth Gaussian-like profile. Nevertheless, the numerical results indicate shot-to-shot fluctuations in the intensity, pulse duration and spectral width of the output laser. These fluctuations mainly originate from two stochastic processes: one is the random behavior of the SASE XFEL pump pulse, the other is the noisy spontaneous-emission seeding. In this Chapter, we study a lasing process seeded by a weak external X-ray radiation from either HHG sources or XFEL sources.

Through a step-function-like XFEL pump pulse, one obtains a transient population inversion in the medium. Compared to the case of constant population inversion where the atom responds linearly to the light field which renders the corresponding equations easily solvable, light propagation in a transient medium will be more complex. The coupling between different frequencies leads to a different mechanism of spectral evolution in the medium. Here we consider a simple seeding spectrum, a monochromatic light, to show how such a transient effect may modify the input spectrum.

7.1 Light propagation equations

The accurate wave propagation equations in time and frequency domain are given as

$$\frac{\partial^2 \mathrm{E}(z,t)}{\partial z^2} - \frac{1}{c^2}\frac{\partial^2 \mathrm{E}(z,t)}{\partial t^2} = \mu_0 \frac{\partial^2 \mathrm{P}(z,t)}{\partial t^2}, \tag{7.1}$$

$$\frac{\partial^2 \hat{\mathrm{E}}(z,\omega)}{\partial z^2} + \frac{\omega^2}{c^2}\hat{\mathrm{E}}(z,\omega) = -\mu_0\omega^2 \hat{\mathrm{P}}(z,\omega), \tag{7.2}$$

respectively. In the slowly varying envelope approximation, the evolution of the envelope functions is described by

$$\frac{\partial \mathcal{E}(z,t)}{\partial z} + \frac{1}{c}\frac{\partial \mathcal{E}(z,t)}{\partial t} = -i\frac{\mu_0\omega_0 c}{2}\mathcal{P}(z,t), \tag{7.3}$$

$$\frac{\partial \hat{\mathcal{E}}(z,\tilde{\omega})}{\partial z} + \frac{i\tilde{\omega}}{c}\hat{\mathcal{E}}(z,\tilde{\omega}) = -i\frac{\mu_0\omega_0 c}{2}\hat{\mathcal{P}}(z,\tilde{\omega}), \tag{7.4}$$

with $\tilde{\omega} = \omega - \omega_0$, and the envelope functions defined as

$$\mathrm{E}(z,t) = \mathcal{E}(z,t)e^{i\omega_0 t - ik_0 z}, \quad \hat{\mathrm{E}}(z,\omega) = \hat{\mathcal{E}}(z,\tilde{\omega})e^{-ik_0 z}, \tag{7.5}$$

$$\mathrm{P}(z,t) = \mathcal{P}(z,t)e^{i\omega_0 t - ik_0 z}, \quad \hat{\mathrm{P}}(z,\omega) = \hat{\mathcal{P}}(z,\tilde{\omega})e^{-ik_0 z}. \tag{7.6}$$

7.2 Polarization in a transient medium

The dynamics for the off-diagonal element ρ_{eg} of the density matrix is

$$\dot{\rho}_{\mathrm{eg}} = \frac{i\wp\mathcal{E}(t)}{2\hbar}D(t) + \left(i\Delta - \frac{\gamma}{2}\right)\rho_{\mathrm{eg}}(t), \tag{7.7}$$

with $D(t) = \rho_{\mathrm{ee}} - \rho_{\mathrm{gg}}$ being the population inversion, $\Delta = \omega_0 - \omega_a$ the detuning between the atom and the carrier frequency, and γ being the decoherence. Assuming $\rho_{\mathrm{eg}}(0) = 0$, the formal solution of Eq. (7.7) gives

$$\rho_{\mathrm{eg}}(t) = \int_0^t e^{\left(i\Delta - \frac{\gamma}{2}\right)(t-t')}\frac{i\wp\mathcal{E}(t')}{2}D(t')\mathrm{d}t'. \tag{7.8}$$

Considering the relation between the polarization envelope and the off-diagonal element

$$\mathcal{P} = -2n_{\mathrm{a}}\wp\rho_{\mathrm{eg}}, \tag{7.9}$$

one can have the corresponding formal solution for the polarization envelope

$$\begin{aligned}\mathcal{P}(t) &= -2n_{\mathrm{a}}\wp\int_0^t e^{\left(i\Delta - \frac{\gamma}{2}\right)(t-t')}\frac{i\wp\mathcal{E}(t')}{2\hbar}D(t')\mathrm{d}t' \\ &= \varepsilon_0\int_0^t \chi(t-t')\mathcal{E}(t')D(t')\mathrm{d}t'.\end{aligned} \tag{7.10}$$

Here, the susceptibility is defined according to

$$\chi(t-t') = \begin{cases} -\frac{in_{\mathrm{a}}\wp^2}{\varepsilon_0\hbar}e^{\left(i\Delta - \frac{\gamma}{2}\right)(t-t')}, & t \geq t', \\ 0, & t < t'; \end{cases} \tag{7.11}$$

or

$$\chi(t) = \begin{cases} -\frac{in_{\mathrm{a}}\wp^2}{\varepsilon_0\hbar}e^{\left(i\Delta - \frac{\gamma}{2}\right)t}, & t \geq 0, \\ 0, & t < 0. \end{cases} \tag{7.12}$$

Eq. (7.10) reveals that, because of the finite-time response given by $\chi(t-t')$, the polarization at time t is a weighted sum of all the history experienced by the medium during $t' \leq t$. To continue, the integral in Eq. (7.10) can be extended to $\pm\infty$ based on two arguments: Firstly, if the light field or the polarization appears only after $t = 0$, then $\mathcal{E}(t) = 0$ and $D(t) = 0$ for $t < 0$, and one can extend the integral to $-\infty$,

$$\mathcal{P}(t) = \varepsilon_0\int_{-\infty}^t \chi(t-t')\mathcal{E}(t')D(t')\mathrm{d}t'.$$

Secondly, due to causality, $\chi(t-t') = 0$ for $t' > t$ as defined above, the upper limit of the integral can be extended to ∞ to have

$$\mathcal{P}(t) = \varepsilon_0\int_{-\infty}^{\infty} \chi(t-t')\mathcal{E}(t')D(t')\mathrm{d}t'. \tag{7.13}$$

Though Eq. (7.10) is intuitive for understanding the underlying physics of the origin of polarization, the new formal solution in Eq. (7.13) is more convenient for frequency analysis.

Defining a new function

$$\mathcal{Y}(t) \;=\; \mathcal{E}(t)D(t), \tag{7.14}$$

the integral becomes

$$\mathcal{P}(t) \;=\; \varepsilon_0 \int_{-\infty}^{\infty} \chi(t-t')\mathcal{Y}(t')\mathrm{d}t'. \tag{7.15}$$

One can immediately recognize that the polarization $\mathcal{P}(t)$ is a convolution of the susceptibility $\chi(t)$ and the new function $\mathcal{Y}(t)$. In frequency domain, this gives

$$\hat{\mathcal{P}}(\tilde{\omega}) \;=\; \varepsilon_0 \hat{\chi}(\tilde{\omega})\hat{\mathcal{Y}}(\tilde{\omega}), \tag{7.16}$$

with

$$\begin{aligned}
\hat{\chi}(\tilde{\omega}) &= \frac{1}{\sqrt{2\pi}} \int_{-\infty}^{\infty} \chi(t) e^{-i\tilde{\omega}t}\mathrm{d}t \\
&= -\frac{1}{\sqrt{2\pi}} \int_{0}^{\infty} \frac{i n_\mathrm{a} \wp^2}{\varepsilon_0 \hbar} e^{\left(i\Delta - \frac{\gamma}{2}\right)t} e^{-i\tilde{\omega}t}\mathrm{d}t \\
&= -\frac{i n_\mathrm{a} \wp^2}{\sqrt{2\pi}\varepsilon_0 \hbar} \frac{1}{i(\Delta-\tilde{\omega}) - \frac{\gamma}{2}} \left. e^{\left(i(\Delta-\tilde{\omega}) - \frac{\gamma}{2}\right)t} \right|_0^\infty \\
&= \frac{i n_\mathrm{a} \wp^2}{\sqrt{2\pi}\varepsilon_0 \hbar} \frac{1}{i(\Delta-\tilde{\omega}) - \frac{\gamma}{2}} \\
&= \frac{n_\mathrm{a} \wp^2}{\sqrt{2\pi}\varepsilon_0 \hbar} \frac{(\Delta-\tilde{\omega}) - i\frac{\gamma}{2}}{(\Delta+\tilde{\omega})^2 + \left(\frac{\gamma}{2}\right)^2},
\end{aligned} \tag{7.17}$$

and

$$\begin{aligned}
\hat{\mathcal{Y}}(\tilde{\omega}) &= \int_{-\infty}^{\infty} \hat{\mathcal{E}}(\tilde{\omega}-\tilde{\omega}')\hat{D}(\tilde{\omega}')\mathrm{d}\tilde{\omega}' \\
&= \int_{-\infty}^{\infty} \hat{D}(\tilde{\omega}-\tilde{\omega}')\hat{\mathcal{E}}(\tilde{\omega}')\mathrm{d}\tilde{\omega}'.
\end{aligned} \tag{7.18}$$

This means that, in the frequency domain, the polarization for each frequency component is given by

$$\hat{\mathcal{P}}(\tilde{\omega}) \;=\; \varepsilon_0 \hat{\chi}(\tilde{\omega}) \int_{-\infty}^{\infty} \hat{D}(\tilde{\omega}-\tilde{\omega}')\hat{\mathcal{E}}(\tilde{\omega}')\mathrm{d}\tilde{\omega}', \tag{7.19}$$

or

$$\hat{\mathcal{P}}(\tilde{\omega}) \;=\; \varepsilon_0 \hat{\chi}(\tilde{\omega}) \int_{-\infty}^{\infty} \hat{D}(\tilde{\omega}')\hat{\mathcal{E}}(\tilde{\omega}-\tilde{\omega}')\mathrm{d}\tilde{\omega}'. \tag{7.20}$$

When the atoms are in a steady state, the population inversion varies slowly compared

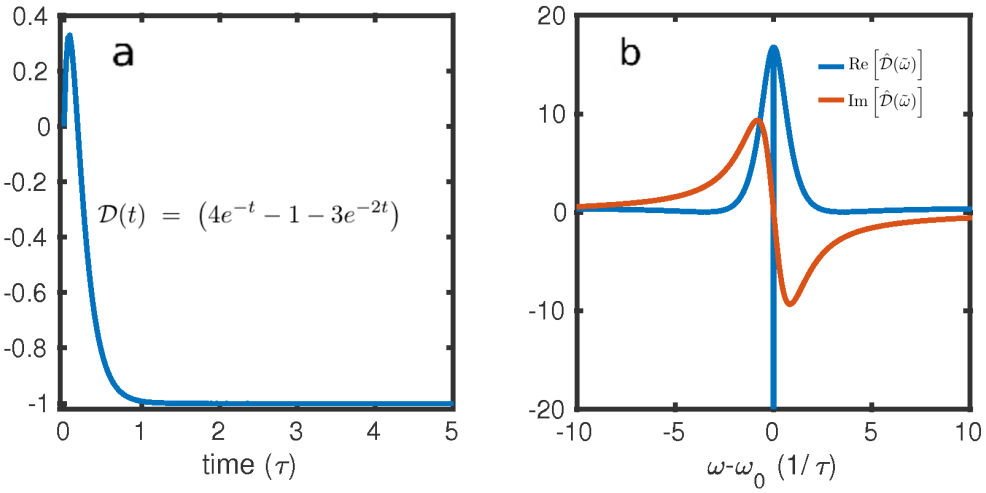

Figure 7.1: Spectrum of population inversion $\hat{\mathcal{D}}(\tilde{\omega})$. a, $\mathcal{D}(t)$ in Eq. (6.69) for $w = 2$. **b,** Fourier transform of the corresponding $\mathcal{D}(t)$ in (**a**): real part (blue line) and imaginary part (red line). There is a δ-function component in the spectrum because $\mathcal{D}(t) = -1$ for large t.

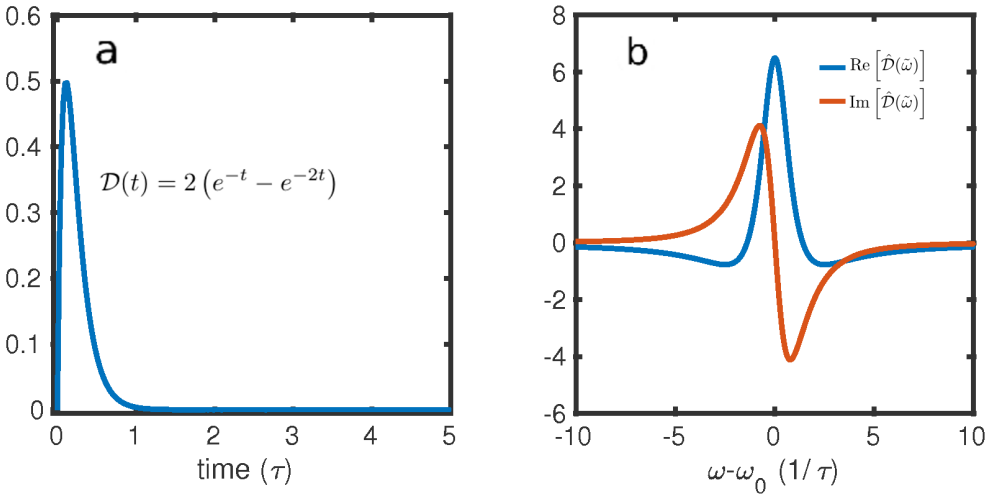

Figure 7.2: Spectrum of population inversion $\hat{\mathcal{D}}(\tilde{\omega})$. a, $\mathcal{D}(t)$ in Eq. (6.77) for $w = 2$. **b,** Fourier transform of the corresponding $\mathcal{D}(t)$ in (**a**): real part (blue line) and imaginary part (red line).

to the envelope of the light field. One can take $D(t) = const.$ such that $\hat{D}(\tilde{\omega}')$ can be treated as a delta function. One will obtain the linear polarization relation

$$\hat{\mathcal{P}}(\tilde{\omega}) \quad = \quad \varepsilon_0 \hat{\chi}(\tilde{\omega}) \hat{\mathcal{E}}(\tilde{\omega}) \tag{7.21}$$

discussed in Appx. G. For a given input frequency $\tilde{\omega}$, the polarization responds to this input frequency only. However, for a time-dependent population inversion, each frequency component of the polarization depends on all the other frequency components of the input electric field. When we consider the propagation of the light pulse in such a transient medium, the spectrum of the light field will change as it propagates. This would make the spectrum of the polarization field change accordingly. In the other extreme case where the time scale of the population inversion is much smaller than the duration of the light pulse, $D(t)$ becomes a δ-like function with the $\hat{D}(\tilde{\omega})$ being much

broader than the input spectrum $\hat{\mathcal{E}}(\tilde{\omega})$. Then one can take $\hat{D}(\tilde{\omega}') = \hat{D}(\tilde{\omega})$ and

$$\hat{\mathcal{P}}(\tilde{\omega}) = \varepsilon_0 \hat{\chi}(\tilde{\omega}) \hat{D}(\tilde{\omega}) \int_{-\infty}^{\infty} \hat{\mathcal{E}}(\tilde{\omega} - \tilde{\omega}') \mathrm{d}\tilde{\omega}' = \text{const.} * \varepsilon_0 \hat{\chi}(\tilde{\omega}) \hat{D}(\tilde{\omega}). \tag{7.22}$$

In this case, the spectrum of the polarization field is determined by the susceptibility $\hat{\chi}(\tilde{\omega})$ and by the population inversion. Only the power of the light field is added to the polarization field. On the other hand, when $\hat{D}(\tilde{\omega})$ is broad, the input spectrum can be taken as a delta function, and one will also arrive to Eq. (7.22)).

We should also keep in mind that the population inversion and susceptibility are not always independent from each other. In reality, the duration of $D(t)$ is always longer than the duration of the susceptibility $\chi(t)$. This is because the decoherence rate should always be larger than the decay rate of the population, thus the decoherence time is shorter than the lifetime of the atoms. In turn, the spectrum of $\hat{\chi}(\tilde{\omega})$ will always be broader than $\hat{D}(\tilde{\omega})$.

Similarly to the envelope function, the full polarization field can be calculated through

$$\begin{aligned} \mathrm{P}(t) &= e^{i\omega_0 t} \varepsilon_0 \int_{-\infty}^{\infty} \chi(t - t') \mathcal{E}(t') D(t') \mathrm{d}t' \\ &= \varepsilon_0 \int_{-\infty}^{\infty} \chi(t - t') e^{i\omega_0 (t - t')} \mathcal{E}(t') e^{i\omega_0 t'} D(t') \mathrm{d}t' \\ &= \varepsilon_0 \int_{-\infty}^{\infty} \mathrm{X}(t - t') \mathrm{E}(t') D(t') \mathrm{d}t' \\ &= \varepsilon_0 \int_{-\infty}^{\infty} \mathrm{X}(t - t') \mathrm{Y}(t') \mathrm{d}t'. \end{aligned} \tag{7.23}$$

The new susceptibility function is defined by

$$\mathrm{X}(t - t') = \chi(t - t') e^{i\omega_0 (t - t')} = \begin{cases} \frac{i n_\mathrm{a} \wp^2}{\varepsilon_0 \hbar} e^{-\left(i\omega_\mathrm{a} + \frac{\gamma}{2}\right)(t - t')}, & t \geq t', \\ 0, & t < t'; \end{cases} \tag{7.24}$$

and

$$\hat{\mathrm{X}}(\omega) = \hat{\chi}(\omega - \omega_0) = \frac{n_\mathrm{a} \wp^2}{\sqrt{2\pi} \varepsilon_0 \hbar} \frac{(\omega - \omega_\mathrm{a}) + i\frac{\gamma}{2}}{(\omega - \omega_\mathrm{a})^2 + \left(\frac{\gamma}{2}\right)^2}. \tag{7.25}$$

$Y(t)$ is defined as

$$Y(t) = \mathrm{E}(t) D(t) = \mathcal{Y}(t) e^{i\omega_0 t}. \tag{7.26}$$

Therefore, the polarization in the time and frequency domain can be written as

$$\mathrm{P}(t) = \varepsilon_0 \int_{-\infty}^{\infty} \mathrm{X}(t-t')\mathrm{E}(t')D(t')\mathrm{d}t', \tag{7.27}$$

and

$$\hat{\mathrm{P}}(\omega) = \varepsilon_0 \hat{\mathrm{X}}(\omega) \int_{-\infty}^{\infty} \hat{D}(\omega-\omega')\hat{\mathrm{E}}(\omega')\mathrm{d}\omega', \tag{7.28}$$

or

$$\hat{\mathrm{P}}(\omega) = \varepsilon_0 \hat{\mathrm{X}}(\omega) \int_{-\infty}^{\infty} \hat{D}(\omega')\hat{\mathrm{E}}(\omega-\omega')\mathrm{d}\omega'. \tag{7.29}$$

7.3 Monochromatic seeding

First, for monochromatic input light with spectrum and envelope being

$$\hat{\mathrm{E}}(z,\omega) = \mathrm{E}(z)e^{-ik_{\mathrm{in}}z}\delta(\omega-\omega_{\mathrm{in}}), \quad \hat{\mathcal{E}}(z,\tilde{\omega}) = \mathcal{E}(z)e^{-i\tilde{k}_{\mathrm{in}}z}\delta(\tilde{\omega}-\tilde{\omega}_{\mathrm{in}}), \tag{7.30}$$

$$\mathrm{E}(z,t) = \mathrm{E}(z)e^{-ik_{\mathrm{in}}z}e^{i\omega_{\mathrm{in}}t}, \quad \mathcal{E}(z,t) = \mathcal{E}(z)e^{-i\tilde{k}_{\mathrm{in}}z}e^{i\tilde{\omega}_{\mathrm{in}}t}, \tag{7.31}$$

the polarization spectrum and envelope are given as

$$\hat{\mathcal{P}}(z,\tilde{\omega}) = \varepsilon_0 \mathcal{E}(z)\hat{\chi}(\tilde{\omega})\hat{D}(\tilde{\omega}-\tilde{\omega}_{\mathrm{in}})e^{-i\tilde{k}_{\mathrm{in}}z}, \tag{7.32}$$

$$\mathcal{P}(z,t) = \varepsilon_0 \mathcal{E}(z)e^{-i\tilde{k}_{\mathrm{in}}z} \int_{-\infty}^{\infty} \chi(t-t')D(t')e^{i\tilde{\omega}_{\mathrm{in}}t'}\mathrm{d}t', \tag{7.33}$$

or

$$\hat{\mathrm{P}}(z,\omega) = \varepsilon_0 \mathrm{E}(z)\hat{\mathrm{X}}(\omega)\hat{D}(\omega-\omega_{\mathrm{in}})e^{-ik_{\mathrm{in}}z}, \tag{7.34}$$

$$\mathrm{P}(z,t) = \varepsilon_0 \mathrm{E}(z)e^{-ik_{\mathrm{in}}z} \int_{-\infty}^{\infty} \mathrm{X}(t-t')D(t')e^{i\omega_{\mathrm{in}}t'}\mathrm{d}t'. \tag{7.35}$$

For monochromatic light, Eq. (7.19) and Eq. (7.28) have been reduced to simpler forms shown in Eq. (7.33) and Eq. (7.35). In Eq. (7.19) and Eq. (7.28), we have coupling between all the frequency components. However, for the case of monochromatic seeding, there is a coupling between the input frequency and the other frequencies only. This simplification makes an analytical treatment possible.

7.3.1 Medium in steady state

As mentioned before, if the atoms are in a steady state where the populations are constant, $\hat{D}(\tilde{\omega}) = D\delta(\tilde{\omega})$, and one gets

$$\hat{\mathcal{P}}(z,\tilde{\omega}) = \varepsilon_0 \mathcal{E}(z)D\hat{\chi}(\tilde{\omega})\delta(\tilde{\omega}-\tilde{\omega}_{\mathrm{in}})e^{-i\tilde{k}_{\mathrm{in}}z} = \varepsilon_0 D\hat{\chi}(\tilde{\omega})\hat{\mathcal{E}}(z,\tilde{\omega}), \tag{7.36}$$

or

$$\hat{\mathcal{P}}(z,\tilde{\omega}) = \begin{cases} \varepsilon_0 D\hat{\chi}(\tilde{\omega})\hat{\mathcal{E}}(z,\tilde{\omega}), & \tilde{\omega} = \tilde{\omega}_{\mathrm{in}}, \\ 0, & \text{otherwise.} \end{cases} \tag{7.37}$$

In the time domain, this means that the polarization envelope is independent of t

$$\begin{aligned}\mathcal{P}(z,t) &= \varepsilon_0 D\mathcal{E}(z)e^{-i\tilde{k}_{\rm in}z}\int_{-\infty}^{\infty}\chi(t-t')e^{i\tilde{\omega}_{\rm in}t'}\mathrm{d}t' \\ &= \varepsilon_0 D\mathcal{E}(z)e^{-i\tilde{k}_{\rm in}z}e^{i\tilde{\omega}_{\rm in}t}\int_{-\infty}^{\infty}\chi(t-t')e^{-i\tilde{\omega}_{\rm in}(t-t')}\mathrm{d}t' \\ &= \varepsilon_0 D\mathcal{E}(z)\hat{\chi}(\tilde{\omega}_{\rm in})e^{-i\tilde{k}_{\rm in}z}e^{i\tilde{\omega}_{\rm in}t} \\ &= \varepsilon_0 D\hat{\chi}(\tilde{\omega}_{\rm in})\mathcal{E}(z,t). \end{aligned} \tag{7.38}$$

Therefore, the full polarization field is given by

$$\mathrm{P}(z,t) = \varepsilon_0 D\hat{\mathrm{X}}(\omega_{\rm in})\mathrm{E}(z,t), \tag{7.39}$$

$$\hat{\mathrm{P}}(z,\omega) = \begin{cases}\varepsilon_0 D\hat{\mathrm{X}}(\omega_{\rm in})\hat{\mathrm{E}}(z,\omega_{\rm in}), & \omega=\omega_{\rm in},\\ 0, & \text{otherwise.}\end{cases} \tag{7.40}$$

Similarly to Eq. (7.21), the polarization only has a frequency component which is the same as the input frequency, $\omega_{\rm in}=\omega_0+\tilde{\omega}_{\rm in}$. The other frequencies are not present.

The propagation equation for the light with frequency $\tilde{\omega}_{\rm in}$ is given as

$$\frac{\partial^2\hat{\mathrm{E}}(z,\omega_{\rm in})}{\partial z^2}+\frac{\omega_{\rm in}^2}{c^2}\hat{\mathrm{E}}(z,\omega_{\rm in}) = -\frac{\omega_{\rm in}^2}{c^2}D\hat{\mathrm{X}}(\omega_{\rm in})\hat{\mathrm{E}}(z,\omega_{\rm in}), \tag{7.41}$$

$$\frac{\partial\hat{\mathcal{E}}(z,\tilde{\omega}_{\rm in})}{\partial z}+\frac{i\tilde{\omega}_{\rm in}}{c}\hat{\mathcal{E}}(z,\tilde{\omega}_{\rm in}) = -i\frac{\omega_0}{2c}D\hat{\chi}(\tilde{\omega}_{\rm in})\hat{\mathcal{E}}(z,\tilde{\omega}_{\rm in}), \tag{7.42}$$

where we used the relation $\mu_0\varepsilon_0=1/c^2$. With $\hat{\mathrm{X}}(\omega_{\rm in})=\hat{\chi}(\tilde{\omega}_{\rm in})$, the solutions are given by

$$\hat{\mathrm{E}}(z,\omega_{\rm in}) = \hat{\mathrm{E}}(0,\omega_{\rm in})e^{-ik_{\rm in}\sqrt{1+D\hat{\mathrm{X}}(\omega_{\rm in})}} = \hat{\mathrm{E}}(0,\omega_{\rm in})e^{-ik_{\rm in}\sqrt{1+D\hat{\chi}(\tilde{\omega}_{\rm in})}z}, \tag{7.43}$$

$$\hat{\mathcal{E}}(z,\tilde{\omega}_{\rm in}) = \hat{\mathcal{E}}(0,\tilde{\omega}_{\rm in})e^{-\frac{i}{c}\left[\tilde{\omega}_{\rm in}+\frac{1}{2}D\hat{\chi}(\tilde{\omega}_{\rm in})\omega_0\right]z}. \tag{7.44}$$

These results are presented more in depth in our discussions in Appx. G.

7.3.2 Transient population inversion

In the following, we restrict our discussions in the small-gain regime by assuming that the amplitude of the seeding field does change during the interaction with the transient medium. Such conditions are generally satisfied when the propagation length is shorter than a critical length given below.

We know that for transient population inversion, there are other frequencies generated by the polarization field $\hat{\mathcal{P}}(\tilde{\omega})$. The amplitude of these frequencies are $\hat{\mathcal{E}}(0,\tilde{\omega})=0$ at the beginning. After propagation through the medium, such frequencies will start showing up according to the equation

$$\frac{\partial^2\hat{\mathrm{E}}(z,\omega)}{\partial z^2}+\frac{\omega^2}{c^2}\hat{\mathrm{E}}(z,\omega) = -\frac{\omega^2}{c^2}\mathrm{E}(z)\hat{\mathrm{X}}(\omega)\hat{D}(\omega-\omega_{\rm in})e^{-ik_{\rm in}z}, \tag{7.45}$$

$$\frac{\partial\hat{\mathcal{E}}(z,\tilde{\omega})}{\partial z}+\frac{i\tilde{\omega}}{c}\hat{\mathcal{E}}(z,\tilde{\omega}) = -i\frac{\omega_0}{2c}\mathcal{E}(z)\hat{\chi}(\tilde{\omega})\hat{D}(\tilde{\omega}-\tilde{\omega}_{\rm in})e^{-i\tilde{k}_{\rm in}z}. \tag{7.46}$$

After some time of propagation, the spectrum will no longer be δ-function-like anymore,

and one has to include the contributions from frequencies other than the input frequency. The light field in time domain is also changed so that $\mathcal{E}_0(z,t)$ is no longer constant. There will be a bump propagating with the transient inversion pulse (pumping XFEL pulse). Then, all the frequencies will interweave with each other and one needs to solve the general propagation equation

$$\frac{\partial^2 \hat{\mathrm{E}}(z,\omega)}{\partial z^2} + \frac{\omega^2}{c^2}\hat{\mathrm{E}}(z,\omega) = -\frac{\omega^2}{c^2}\hat{\mathrm{X}}(\omega)\int_{-\infty}^{\infty}\hat{D}(\omega-\omega')\hat{\mathrm{E}}(z,\omega')\mathrm{d}\omega', \tag{7.47}$$

$$\frac{\partial \hat{\mathcal{E}}(z,\tilde{\omega})}{\partial z} + \frac{i\tilde{\omega}}{c}\hat{\mathcal{E}}(z,\tilde{\omega}) = -i\frac{\omega_0}{2c}\hat{\chi}(\tilde{\omega})\int_{-\infty}^{\infty}\hat{D}(\tilde{\omega}-\tilde{\omega}')\hat{\mathcal{E}}(z,\tilde{\omega}')\mathrm{d}\tilde{\omega}'. \tag{7.48}$$

We study this for a small susceptibility $|\hat{\chi}(\tilde{\omega})| \ll 1$, the amplitudes of the generated frequencies will be much smaller compared to the input field, $|\hat{\mathcal{E}}(z,\tilde{\omega})| \ll |\mathcal{E}(z)|$ for $\tilde{\omega} \neq \tilde{\omega}_{\mathrm{in}}$. We therefore assume a monochromatic frequency with a δ-function-like spectrum

$$\hat{\mathcal{E}}(z,\tilde{\omega}) = \mathcal{E}(z)e^{-i\tilde{k}z}\delta(\tilde{\omega}-\tilde{\omega}_{\mathrm{in}}) \tag{7.49}$$

On the left-hand side of Eq. (7.46), one has

$$\begin{aligned}
&\frac{\partial \hat{\mathcal{E}}(z,\tilde{\omega})}{\partial z} + \frac{i\tilde{\omega}}{c}\hat{\mathcal{E}}(z,\tilde{\omega}) \\
=\ &\left[\frac{\partial \mathcal{E}(z)}{\partial z} - i\tilde{k}\mathcal{E}(z)\right]e^{-i\tilde{k}z}\delta(\tilde{\omega}-\tilde{\omega}_{\mathrm{in}}) + \frac{i\tilde{\omega}}{c}\mathcal{E}(z)e^{-i\tilde{k}z}\delta(\tilde{\omega}-\tilde{\omega}_{\mathrm{in}}) \\
=\ &\frac{\partial \mathcal{E}(z)}{\partial z}e^{-i\tilde{k}z}\delta(\tilde{\omega}-\tilde{\omega}_{\mathrm{in}}) = \frac{\partial \mathcal{E}(z)}{\partial z}e^{-i\tilde{k}_{\mathrm{in}}z}\delta(\tilde{\omega}-\tilde{\omega}_{\mathrm{in}}).
\end{aligned} \tag{7.50}$$

This means that Eq. (7.46) yields

$$\frac{\partial \mathcal{E}(z)}{\partial z}\delta(\tilde{\omega}-\tilde{\omega}_{\mathrm{in}}) = -i\frac{\omega_0}{2c}\mathcal{E}(z)\hat{\chi}(\tilde{\omega})\hat{D}(\tilde{\omega}-\tilde{\omega}_{\mathrm{in}}). \tag{7.51}$$

Integrate over $\tilde{\omega}$ on both sides of Eq. (7.51) gives

$$\frac{\partial \mathcal{E}(z)}{\partial z} = -i\frac{\omega_0}{2c}\mathcal{E}(z)\int_{-\infty}^{\infty}d\tilde{\omega}\hat{\chi}(\tilde{\omega})\hat{D}(\tilde{\omega}-\tilde{\omega}_{\mathrm{in}}). \tag{7.52}$$

If $\hat{D}(\tilde{\omega}-\tilde{\omega}_{\mathrm{in}})$ is a delta function, one recovers Eq. (7.38) for the evolution of $\mathcal{E}(z)$ under constant population inversion. In Eq. (7.38), only the frequency component $\hat{\chi}(\tilde{\omega})$ contributes to the light evolution. However, for the transient population inversion in Eq. (7.52), all frequency components of the susceptibility will contribute to the evolution of the light field. Defining

$$W(\tilde{\omega}_{\mathrm{in}}) = \int_{-\infty}^{\infty}d\tilde{\omega}\hat{\chi}(\tilde{\omega})\hat{D}(\tilde{\omega}-\tilde{\omega}_{\mathrm{in}}), \tag{7.53}$$

one obtains a simpler form

$$\frac{\partial \mathcal{E}(z)}{\partial z} = -i\frac{\omega_0}{2c}W(\tilde{\omega}_{\mathrm{in}})\mathcal{E}(z), \tag{7.54}$$

with the solution given by

$$\mathcal{E}(z) \quad = \quad \mathcal{E}(0)e^{-i\frac{\omega_0}{2c}W(\tilde{\omega}_{\rm in})z}. \tag{7.55}$$

As long as the monochromatic approximation still holds, the spectrum of the light field is given by

$$\hat{\rm E}(z,\omega) \quad = \quad \mathcal{E}(0)e^{-i\frac{\omega_0}{2c}W(\tilde{\omega}_{\rm in})z}e^{-ik_{\rm in}z}\delta(\omega-\omega_{\rm in}). \tag{7.56}$$

Accordingly, the light field in time domain is given by

$${\rm E}(z,t) \quad = \quad {\rm E}(0)e^{-i\frac{\omega_0}{2c}W(\tilde{\omega}_{\rm in})z}e^{i\omega_{\rm in}t-ik_{\rm in}z}, \tag{7.57}$$

where we have taken ${\rm E}(0)=\mathcal{E}(0)$. For the monochromatic approximation to hold, one should ensure

$$\left|{\rm Re}[i\frac{\omega_0}{2c}W(\tilde{\omega}_{\rm in})z]\right| = \left|{\rm Im}[\frac{1}{2}W(\tilde{\omega}_{\rm in})k_0 z]\right| \ll 1. \tag{7.58}$$

This gives an estimate of the critical length for monochromatic approximation to be valid,

$$z_{\rm c} \quad \approx \quad \frac{0.2}{|{\rm Im}[W(\tilde{\omega}_{\rm in})]|\,k_0}. \tag{7.59}$$

With this definition, $z_{\rm c}$ corresponds to the propagation distance after which the amplitude of the input frequency has been changed by a fraction of 10%.

In the time domain, transient population inversion leads to a transient amplification of the input field. As a result, there would be a peak bumped out of the uniform light field. When $z \ll z_{\rm c}$, the peak is not significant and the light field can be treated as a uniform field described by a plane wave. However, when z approaches $z_{\rm c}$, the peak becomes strong compared to the uniform field. Therefore, the plane-wave description should be replaced by a pulse description.

In the following, we consider how the other frequency components are evolving in the monochromatic approximation. This can be examined through the formal solution of Eq. (7.46):

$$\begin{aligned}\hat{\mathcal{E}}(z,\tilde{\omega}) \quad &= \quad \int_0^z e^{-i\frac{\tilde{\omega}}{c}(z-z')}\left(-i\frac{\omega_0}{2c}\hat{\chi}(\tilde{\omega})\hat{D}(\tilde{\omega}-\tilde{\omega}_{\rm in})\mathcal{E}(z')e^{-i\tilde{k}_{\rm in}z'}\right){\rm d}z' \\ &= \quad -i\frac{\omega_0}{2c}\hat{\chi}(\tilde{\omega})\hat{D}(\tilde{\omega}-\tilde{\omega}_{\rm in})e^{-i\frac{\tilde{\omega}}{c}z}\int_0^z \mathcal{E}(z')e^{i\left(\frac{\tilde{\omega}}{c}-\tilde{k}_{\rm in}\right)z'}{\rm d}z'.\end{aligned} \tag{7.60}$$

For slowly varying envelope approximation to be valid, one usually needs $\frac{\tilde{\omega}}{c} \approx \tilde{k}_{\rm in}$. Moreover, $\mathcal{E}(z')=\hat{\mathcal{E}}(0)$ is sufficient for $z \ll z_{\rm c}$. The above result can be simplified to be

$$\hat{\mathcal{E}}(z,\tilde{\omega}) \quad = \quad -i\frac{\omega_0}{2c}\hat{\chi}(\tilde{\omega})\hat{D}(\tilde{\omega}-\tilde{\omega}_{\rm in})e^{-i\frac{\tilde{\omega}}{c}z}\mathcal{E}(0)z. \tag{7.61}$$

This indicates that the amplitudes of these frequency components increase linearly with

z. Therefore, the full spectrum amplitude for $z \ll z_{\mathrm{c}}$ is given by

$$|\hat{\mathcal{E}}(z,\tilde{\omega})| = \begin{cases} \mathcal{E}(0), & \tilde{\omega} = \tilde{\omega}_{\mathrm{in}}, \\ \mathcal{E}(0)\frac{\omega_0}{2c}\left|\hat{\chi}(\tilde{\omega})\hat{D}(\tilde{\omega}-\tilde{\omega}_{\mathrm{in}})\right| z, & \text{otherwise.} \end{cases} \tag{7.62}$$

7.4 Summary

In this Chapter, the transient laser seeded by an external radiation field is analyzed in the small-gain regime in frequency domain. We were able to point out a new stimulated-emission process: when a single frequency radiation interacts with an excited atom, the spectrum of the radiation emitted via stimulated emission, instead of being a δ-function, possesses a broadband profile in frequency space.

Chapter 8

Summary and outlook

Summary

In this thesis, we put forward a scheme to generate fully coherent lasers in the hard-X-ray regime with a relative bandwidth of approximately $\Delta\omega/\omega = 10^{-5} \sim 10^{-7}$. The gain medium consists of highly charged ions generated in a laser-produced plasma. Population inversion between the $1s2l$ and the $1s^2$ states is achieved by fast K-shell photoionization of Li-like ions. Therefore, stimulated emission from the long-lived $1s2l$ excited state gives rise to lasing. Compared to former X-ray sources, the laser generated in our scheme has advantages as it features a better temporal coherence and narrower bandwidth. Together with their high brightness, our X-ray lasers will open up a new regime of coherent control of ionic and nuclear states in X-ray quantum optics, enable the investigation of nonlinear interactions between X-rays and matter and improve high-precision spectroscopic studies in laboratory astrophysics.

To show that our scheme can work with current experimental capabilities, we perform numerical simulations in Chapter 5 with realistic systems for elements such as Ne, Ar, Kr and Xe. The equations of motions, or Maxwell–Bloch equations, used in the simulations, are developed in Chapter 2 for electric-dipole interactions, and then generalized to multipole transitions in Chapter 3. Formulas to calculate spectral broadening effects such as Doppler broadening, electron-impact broadening and ion Stark broadening in the hot dense plasma medium are derived in Chapter 4. The Doppler broadening, scaling as $\Delta\omega_{\rm D}/\omega \sim \sqrt{T_{\rm i}}$, becomes significant when the ion temperature $T_{\rm i}$ is high. The electron-impact broadening, scaling as $\Delta\omega_{\rm e\text{-}i} \sim N_{\rm e}/\sqrt{T_{\rm e}}$, only depends on the temperature and density of the electrons. This broadening will be significant for cold dense plasmas. The quadratic Stark broadening is induced by the Coulomb field of neighboring ions. Therefore, it scales as $\Delta\omega_{\rm i\text{-}i} \sim N_{\rm i}^{4/3}$, which is severe for large ion densities. As shown in Sec. 5.1, the plasma needed for lasing can be generated by existing picosecond optical lasers with an intensity around 10^{17} W cm^{-2}. Depending on the elements used, the electron temperatures in the plasmas are in the range of 35 eV to 25 keV with the ion densities varying between $2 \times 10^{18} - 2.7 \times 10^{21}$ cm^{-3}. The ions are assumed to stay at room temperatures, for the time scale when a laser is developed, because they are too heavy to be thermalized by the hot electrons.

For each lasing transition, we perform 1000 simulations with different realizations of the chaotic XFEL pulses, which show that a high-intensity X-ray laser can be obtained after a 1-cm-long exponential amplification in a laser-produced plasma (see Table 5.1). For lasing based on Ne^{8+} and Ar^{14+} ions, the $E1$ transitions are sufficient to develop X-ray pulses reaching the saturation intensity. The wavelength is around 1.4 nm (920 eV) and 0.4 nm (3137 eV) for Ne^{8+} and Ar^{14+}, respectively, with a relative bandwidth around 10^{-5}. However, for heavier elements, the $E1$ transition rates scale as $\sim Z^4$, becoming too fast to achieve sufficient population inversion for the laser to develop. Instead, the $M2$ transition at a wavelength of 0.95 Å (13.1 keV) and 0.42 Å (30.6 keV)

for Kr^{34+} and Xe^{52+} were employed, respectively, resulting in a relative bandwidth of around 3×10^{-7} and 1.5×10^{-6}, respectively. These bandwidths are up to three orders of magnitude narrower than the bandwidth of X-ray pulses generated at state-of-art X-ray sources [35].

Evolution of a single-shot XRL pulse, as shown in Figs. 5.6–5.9, is found to be noisy for short propagation lengths. This random feature is smoothed out during laser amplification, resulting in a smooth Gaussian profile at intermediate propagation lengths. The spectral widths are much smaller than the sum of all the broadenings in this region, indicating a gain-narrowing phenomenon before the saturation rebroadening sets in. Though the intensity, pulse duration and spectral width of single XRL pulses undergo fluctuations from shot to shot, their stabilities are still much better than the pulses from XFELs.

Furthermore, the analytical solutions to the Maxwell–Bloch equations are discussed in Chapters 2, 6 and 7 for particular approximations and assumptions. These solutions provide a useful insight into light-matter interaction, and help in interpreting our numerical results at intermediate propagation lengths. In Sec. 2.4, we consider the case where the atoms are in a steady state. For such cases, the widely used rate equations are rederived. Our analysis indicates that the rate-equation approach often used by the laser community for continuous lasers is insufficient to fully describe transient lasers. In Chapter 6, the Maxwell–Bloch equations are solved in the time domain for the case of small signals where the laser field is far below the saturation intensity. The solution of the laser pulse resembles a Gaussian-like function which is in agreement with numerical simulation results in Chapter 5. The duration of the pulse, thus the bandwidth of the spectrum, is mainly determined by the gain coefficient, providing a theoretical explanation of the gain-narrowing effect we observed in our numerical simulations.

Lastly, when the Maxwell–Bloch equations are considered in frequency space in Chapter 7, we were able to point out a new stimulated-emission regime: when single frequency radiation interacts with an excited atom, the spectrum of the radiation emitted via stimulated emission, instead of being a δ-function, possesses a broadband profile in frequency space.

Outlook

Based on the results obtained in this thesis, several new ideas can be addressed in the future. Firstly, it would be interesting to extend our considerations of X-ray lasing to other elements, which can produce X-ray lasers in a different wavelength range. In particular, going to elements heavier than Xe can be considered to obtain X-ray lasers at even shorter wavelengths. As the $E1$ transition rate scales as $\sim Z^4$, the inner-shell XRLs based on neutral atoms can hardly generate population inversions pumped by XFEL pulses. However, the XRLs from He-like ions can always find a transition beyond the $E1$ transitions that features a much lower decay rate. Besides the $M1$ and $M2$ transitions discussed in this thesis, $E2$ transitions may be employed for X-ray lasing from elements heavier than Xe.

Besides that, our density-matrix theory considered in Chapter 2 is based on the two-level approximation, where only one of the four main transitions is considered. Including more transitions may be needed to study more complex systems or regimes where a two-level approximation cannot be applied. Similarly to other atom-based lasers, the wavelengths of our XRLs are discrete. In the future, three-wave interactions by synchronizing optical/XUV lasers with XFEL pulses could be investigated to tune the frequencies in

a broad range.

Secondly, a different lasing scheme can also be considered to generate hard-X-ray pulses using relativistically accelerated ions pumped by a counterpropagating optical or XFEL lasers. As the highest photon energy of current XFEL pulses is only around 30 keV, this renders the pumping of XRL transitions even with Xe challenging. However, this problem could be solved with highly relativistic ions generated in conventional or laser-based accelerators. If an ion moves at a speed close to the velocity of light with a Lorentz factor of $\gamma = E/m_{\mathrm{i}}c^2$, and collides with a photon propagating in the opposite direction, due to the relativistic Doppler effect, the energy of the photon seen by the ion will be increased by a factor of γ. This scheme can effectively push the XFEL photon energy to the ionization threshold of an element even as heavy as uranium. When the lifetime of the excited state is longer than the time needed for the pumping pulse to propagate through the ion beam, population inversion is created at every coordinate of the ion beam. Subsequent spontaneous emission from the excited state leads to lasing in both forward and backward directions. In particular, the photon energy from the laser in the forward direction of the ion beam will be increased by a factor of γ, resulting in wavelengths shorter than 0.12 Å ($\sim$ 100 keV).

Moreover, a more elaborate simulation of the generation of He-like ions in a laser-produced plasma can be considered in the future. In the thesis, we considered sequential collisional ionizations to estimate the time needed for the production of He-like ions. Other processes like collisional excitation, photoionization, photoexcitation and field-induced tunneling ionization are also involved in the generation of plasma. Simulations involving all these processes would be beneficial not only for the XRL lasing, but also for the general understanding of laser-plasma interactions.

Furthermore, in Appx. G, the light propagation theory is generalized to the case of media with significant nonlinear dispersion. Although such a case has been extensively studied in nonlinear optics, generalization of the concepts to light interacting with a resonant medium may lead to new phenomena. As a first step, we find an upper limit of the atomic density for the slowly varying envelope approximation to be valid in describing resonant light-matter interactions. When the nonlinear light propagation effects are considered in a dense medium, the slowly varying envelope approximation breaks down. The interplay between nonlinear dispersion and strong absorption/amplification may lead to the development of novel light sources.

The analytical solution to the Maxwell–Bloch equations discussed in Chapter 6 provides results consistent with the numerical simulations. Applications of the results in designing and optimizing transient lasers is still missing and will be included in our upcoming manuscripts. The seeded-XRL scheme proposed in Chapter 7 is solved only in the small-gain regime. In the future, solutions in the high-gain regime will be considered.

The theory describing light-matter interaction through multipole transitions have been developed in Chapter 3. Graham and Raab [145] found that the electric octopole and the magnetic quadrupole effects are important to explain linear birefringence in cubic crystals. Therefore, applications of our theory to systems other than the X-ray lasing system described in this thesis will be considered.

Appendices

Appendix A

Perturbation theory

Though the dipole approximation has been implemented, the Schrödinger equation with Hamiltonian given in Eq. (2.87) is still not exactly solvable, and so an approximative method such perturbation theory has to be adopted [110]. In the following, we will first introduce time-independent perturbation theory for nondegenerate cases, then extend it to the time-dependent case.

A.1 Bare Hamiltonian and Hilbert space

As we discussed in Sec. 2.2, the full Hamiltonian can be divided into two parts, one is the Hamiltonian

$$H_0 = H_{\mathrm{A}} + H_{\mathrm{EM}} \tag{A.1}$$

describing a bare atom and the free field which is exactly solvable, the other is the Hamiltonian H_{I} representing the interaction between the atom and light field, given by Eq. (2.85). When the light can be treated as a classical field, one can drop the free electromagnetic energy H_{EM} from the bare Hamiltonian.

In principle, there is no exact solution to this problem. Nevertheless, one can still gain many important insights into this problem under some approximations. As a first step, we define the Hilbert space based on the complete eigenvectors of the bare Hamiltonian. Then all the wave functions and operators (including the interaction Hamiltonian) can be represented by the basis of the Hilbert space. This procedure is important because it provides us the mathematical foundations for further approximations to be introduced.

The Schrödinger equation of an atom free of any external field is given by

$$i\hbar\frac{\partial\Psi_0\left(\mathbf{r}_0,\mathbf{r},t\right)}{\partial t} = \left[\frac{\mathbf{p}^2}{2m}+V\left(\mathbf{r}\right)\right]\Psi_0\left(\mathbf{r}_0,\mathbf{r},t\right), \tag{A.2}$$

as defined earlier in Sec. 2.2. After separation of variables, one arrives at the stationary Schrödinger equation

$$\left[\frac{\mathbf{p}^2}{2m}+V\left(\mathbf{r}\right)\right]\left|\psi^{(0)}_{nlm}\right\rangle = E^{(0)}_{nlm}\left|\psi^{(0)}_{nlm}\right\rangle, \tag{A.3}$$

where we assume the atom is a hydrogen-like system so that quantum numbers n, l, m fully classify the complete eigenbasis. For many-electron systems, the procedures are similar but with different notations of the orthonormal basis.

Solving this stationary Schrödinger equation one obtains the eigenvectors which define the Hilbert space of the quantum system. Any wave function can be expanded in this

eigenbasis as a vector

$$\left|\Psi^{(0)}\right\rangle = \sum_{k=\{nlm\}} c_k^{(0)} \left|\psi_k^{(0)}\right\rangle . \tag{A.4}$$

The operator $\hat{F}$ is represented in a matrix form

$$\hat{F} = \sum_{ij} F_{ij} \left|\psi_i^{(0)}\right\rangle \left\langle\psi_j^{(0)}\right| , \tag{A.5}$$

with the elements given by

$$F_{ij} = \left\langle\psi_i^{(0)}\right| \hat{F} \left|\psi_j^{(0)}\right\rangle . \tag{A.6}$$

The dynamics of the wave function of this system are then just described by time-dependent coefficients for each eigenvector.

When interaction with an extra field is involved, it is Hamiltonian can also be expressed in a matrix form:

$$H_{\mathrm{I}} = \sum_{ij} H_{ij}^1 \left|\psi_i^{(0)}\right\rangle \left\langle\psi_j^{(0)}\right| . \tag{A.7}$$

The Schrödinger equation can be expressed in a matrix form as well:

$$i\hbar \frac{\partial}{\partial t} \left|\Psi\left(\mathbf{r}_0, \mathbf{r}, t\right)\right\rangle = \left[H_0 + H_{\mathrm{I}}\right] \left|\Psi\left(\mathbf{r}_0, \mathbf{r}, t\right)\right\rangle , \tag{A.8}$$

with

$$\left|\Psi\left(\mathbf{r}_0, \mathbf{r}, t\right)\right\rangle = \sum_{k=\{nlm\}} c_k(t) \left|\psi_k^{(0)}\right\rangle . \tag{A.9}$$

Due to the infinite number of eigenvectors, the matrix-form Schrödinger equation is actually an infinite set of coupled linear equations. An exact solution of this system is not possible. Thus one needs to make approximations based on the problem at hand [110].

For instance, one can truncate the number of levels involved if H_{I} only has significant couplings between a finite number of eigenstates. As a result, one obtains a finite-dimensional matrix, thus a finite number of coupled linear equations. The simplest cases would be e.g. the two-level, three-level or four-level approximation, which are discussed in Sec. 2.3. This simplified problem can be either solved numerically (with exact diagonalization method), or analytically. The accuracy of this method is limited by the truncation of levels.

Another way to gain insight in the coupled equations is based on perturbation series [110]. This approach is available when the interaction Hamiltonian is perturbatively small, such that the magnitude of each coefficient $c_k(t)$ only deviates negligibly from $c_k^{(0)}$.

For the interaction between light and atoms, as an example, if the frequency of the light is tuned far from the atomic resonance, it will have a negligible influence on the atomic state. Therefore, perturbation theory is applicable. When the light is close to resonance, singularities show up in perturbation series. One needs to use the two-level approximation instead of the perturbation approach to solve the problem. If the

strength of the light field is low, stimulated emission/absorption would be much smaller compared to the decay of the atoms. In such case, a rate-equation description is sufficient to describe the two-level system. However, when the field becomes strong enough, Rabi flopping will show up and the populations of the eigenstates will undergo fast changes. In this situation, a density-matrix theory [111] should be used for the two-level system. Until now, the light field is still perturbative compared to the static electric field of the atomic nuclei. Rabi oscillation in the populations is only a result of resonance (or in full quantum theory, a result of degenerate-state perturbation). When the light intensity becomes ultra-strong so that tunneling ionization becomes possible, both perturbative and level-truncation approaches fail to describe the problem, and some other ideas need to be introduced.

A.2 Time-independent perturbation theory

Supposing the coupling energy between the atom and light is small compared to the bare atomic Hamiltonian [110].,

$$H_{\mathrm{I}} \ll H_0, \tag{A.10}$$

one can first solve the Schrödinger equation of the bare atomic state with H_0, and treat H_{I} as a perturbation. When the later is involved, the stationary Schrödinger equation has the form

$$\left[\frac{\mathbf{p}^2}{2m} + V(\mathbf{r}) + H_{\mathrm{I}}\right] |\psi_{nlm}\rangle . \quad = \quad E_{nlm} |\psi_{nlm}\rangle \tag{A.11}$$

Because the equation is not analytically solvable, we do not know the exact form of the eigenvectors $|\psi_{nlm}\rangle$ and eigenenergies E_{nlm}. For perturbative H_{I}, $|\psi_{nlm}\rangle$ and E_{nlm} only deviate to a small extent from $\left|\psi^{(0)}_{nlm}\right\rangle$ and $E^{(0)}_{nlm}$. Therefore, they can be expanded as

$$E_{nlm} = E^{(0)}_{nlm} + E^{(1)}_{nlm} + E^{(2}_{nlm} + ..., \tag{A.12}$$

$$|\psi_{nlm}\rangle = \left|\psi^{(0)}_{nlm}\right\rangle + \left|\psi^{(1)}_{nlm}\right\rangle + \left|\psi^{(2)}_{nlm}\right\rangle + ..., \tag{A.13}$$

with $E^{(1)}_{nlm}$ and $E^{(2)}_{nlm}$ being the first- and second-order corrections to the eigenenergy, respectively. $\left|\psi^{(1)}_{nlm}\right\rangle$ and $\left|\psi^{(2)}_{nlm}\right\rangle$ are the first- and second-order corrections to the eigenvector, respectively. For each order, the eigenvectors are orthonormal to each other:

$$\left\langle \psi^{(\mathrm{i})}_{nlm} \middle| \psi^{(\mathrm{j})}_{nlm} \right\rangle = \delta_{ij}. \tag{A.14}$$

The Schrödinger equation becomes

$$\begin{aligned} & (H_0 + H_{\mathrm{I}}) \left(\left|\psi^{(0)}_{nlm}\right\rangle + \left|\psi^{(1)}_{nlm}\right\rangle + \left|\psi^{(2)}_{nlm}\right\rangle + ... \right) \\ = & \left(E^{(0)}_{nlm} + E^{(1)}_{nlm} + E^{(2}_{nlm} + ... \right) \left(\left|\psi^{(0)}_{nlm}\right\rangle + \left|\psi^{(1)}_{nlm}\right\rangle + \left|\psi^{(2)}_{nlm}\right\rangle + ... \right). \end{aligned} \tag{A.15}$$

Accordingly, one obtains the sequential equations

$$H_0 \left|\psi^{(0)}_{nlm}\right\rangle = E^{(0)}_{nlm} \left|\psi^{(0)}_{nlm}\right\rangle,$$

$$
\begin{aligned}
H_0\left|\psi_{nlm}^{(1)}\right\rangle + H_{\rm I}\left|\psi_{nlm}^{(0)}\right\rangle &= E_{nlm}^{(0)}\left|\psi_{nlm}^{(1)}\right\rangle + E_{nlm}^{(1)}\left|\psi_{nlm}^{(0)}\right\rangle, \\
H_0\left|\psi_{nlm}^{(2)}\right\rangle + H_{\rm I}\left|\psi_{nlm}^{(1)}\right\rangle &= E_{nlm}^{(0)}\left|\psi_{nlm}^{(2)}\right\rangle + E_{nlm}^{(1)}\left|\psi_{nlm}^{(1)}\right\rangle + E_{nlm}^{(2)}\left|\psi_{nlm}^{(0)}\right\rangle, \\
&\cdots
\end{aligned}
$$

which can be solved iteratively.

Firstly, one can multiply the second equation by $\left\langle\psi_{n'l'm'}^{(0)}\right|$ to give

$$
\left\langle\psi_{n'l'm'}^{(0)}\right| H_0\left|\psi_{nlm}^{(1)}\right\rangle + \left\langle\psi_{n'l'm'}^{(0)}\right| H_{\rm I}\left|\psi_{nlm}^{(0)}\right\rangle = \left\langle\psi_{n'l'm'}^{(0)}\right| E_{nlm}^{(0)}\left|\psi_{nlm}^{(1)}\right\rangle + \left\langle\psi_{n'l'm'}^{(0)}\right| E_{nlm}^{(1)}\left|\psi_{nlm}^{(0)}\right\rangle.
$$

With $\left\langle\psi_{n'l'm'}^{(0)}\right| H_0 = \left\langle\psi_{n'l'm'}^{(0)}\right| E_{n'l'm'}^{(0)}$, we have

$$
\left\langle\psi_{n'l'm'}^{(0)}\right| E_{n'l'm'}^{(0)}\left|\psi_{nlm}^{(1)}\right\rangle + \left\langle\psi_{n'l'm'}^{(0)}\right| H_{\rm I}\left|\psi_{nlm}^{(0)}\right\rangle = \left\langle\psi_{n'l'm'}^{(0)}\right| E_{nlm}^{(0)}\left|\psi_{nlm}^{(1)}\right\rangle + \left\langle\psi_{n'l'm'}^{(0)}\right| E_{nlm}^{(1)}\left|\psi_{nlm}^{(0)}\right\rangle.
$$

For $n'=n, l'=l, m'=m$, one obtains the first-order correction of the eigenenergy

$$
E_{nlm}^{(1)} = \left\langle\psi_{nlm}^{(0)}\right| H_{\rm I}\left|\psi_{nlm}^{(0)}\right\rangle.
$$

For the other quantum numbers, one obtains the first-order correction of the eigenvector

$$
\left\langle\psi_{n'l'm'}^{(0)}\right|\left.\psi_{nlm}^{(1)}\right\rangle = \frac{\left\langle\psi_{n'l'm'}^{(0)}\right| H_{\rm I}\left|\psi_{nlm}^{(0)}\right\rangle}{E_{nlm}^{(0)} - E_{n'l'm'}^{(0)}},
$$

or

$$
\left|\psi_{nlm}^{(1)}\right\rangle = \sum_{\{n'l'm'\}} \frac{\left\langle\psi_{n'l'm'}^{(0)}\right| H_{\rm I}\left|\psi_{nlm}^{(0)}\right\rangle}{E_{nlm}^{(0)} - E_{n'l'm'}^{(0)}}\left|\psi_{n'l'm'}^{(0)}\right\rangle.
$$

Usually, $E_{nlm}^{(1)}=0$ for certain cases, then one needs to go to second-order corrections of the eigenenergy by solving the third equation:

$$
\begin{aligned}
&\left\langle\psi_{n'l'm'}^{(0)}\right| H_0\left|\psi_{nlm}^{(2)}\right\rangle + \left\langle\psi_{n'l'm'}^{(0)}\right| H_{\rm I}\left|\psi_{nlm}^{(1)}\right\rangle \\
= &\left\langle\psi_{n'l'm'}^{(0)}\right| E_{nlm}^{(0)}\left|\psi_{nlm}^{(2)}\right\rangle + \left\langle\psi_{n'l'm'}^{(0)}\right| E_{nlm}^{(1)}\left|\psi_{nlm}^{(1)}\right\rangle + \left\langle\psi_{n'l'm'}^{(0)}\right| E_{nlm}^{(2)}\left|\psi_{nlm}^{(0)}\right\rangle.
\end{aligned}
$$

For $n'=n, l'=l, m'=m$, one obtains the second-order correction of the eigenenergy

$$
E_{nlm}^{(2)} = \left\langle\psi_{nlm}^{(0)}\right| H_{\rm I}\left|\psi_{nlm}^{(1)}\right\rangle = \sum_{\{n'l'm'\}} \frac{\left|\left\langle\psi_{n'l'm'}^{(0)}\right| H_{\rm I}\left|\psi_{nlm}^{(0)}\right\rangle\right|^2}{E_{nlm}^{(0)} - E_{n'l'm'}^{(0)}}.
$$

One may notice that levels lower than $\left|\psi_{nlm}^{(0)}\right\rangle$ give positive contributions to the second-order correction; levels higher than $\left|\psi_{nlm}^{(0)}\right\rangle$ give negative contributions. As a results, the ground state always becomes lower due to a perturbation.

A.3 Time-dependent perturbation theory

When the perturbative Hamiltonian is time dependent, the Schrödinger equation reads [110].

$$i\hbar\frac{\partial\Psi\left(\mathbf{r},t\right)}{\partial t} = \left[\frac{\mathbf{p}^2}{2m}+V\left(\mathbf{r}\right)+H_{\mathrm{I}}(t)\right]\Psi\left(\mathbf{r},t\right), \tag{A.16}$$

or

$$i\hbar\frac{\partial\Psi\left(\mathbf{r},t\right)}{\partial t} = \left[H_0+H_{\mathrm{I}}(t)\right]\Psi\left(\mathbf{r},t\right). \tag{A.17}$$

To proceed, one needs to adapt the interaction picture where the bare Hamiltonian H_0 is eliminated

$$i\hbar\frac{\partial\Psi_{\mathrm{I}}\left(\mathbf{r},t\right)}{\partial t} = H_{\mathrm{I}}(t)\Psi_{\mathrm{I}}\left(\mathbf{r},t\right), \tag{A.18}$$

with

$$\Psi_{\mathrm{I}}\left(\mathbf{r},t\right) = e^{-\frac{1}{i\hbar}H_0 t}\Psi\left(\mathbf{r},t\right), \tag{A.19}$$

and

$$H^{\mathrm{I}}\left(t\right) = e^{-\frac{1}{i\hbar}H_0 t}H_{\mathrm{I}}(t)e^{\frac{1}{i\hbar}H_0 t}. \tag{A.20}$$

The formal solution of this equation is given by directly integrating the equation over time

$$\Psi_{\mathrm{I}}\left(\mathbf{r},t\right) = \Psi_{\mathrm{I}}\left(\mathbf{r},0\right)+\frac{1}{i\hbar}\int_0^t H_{\mathrm{I}}(t_1)\Psi_{\mathrm{I}}\left(\mathbf{r},t_1\right)\mathrm{d}t_1. \tag{A.21}$$

This integral equation is still not solvable because we do not know $\Psi_{\mathrm{I}}\left(\mathbf{r},t_1\right)$ yet. To tackle this problem, one can substitute $\Psi_{\mathrm{I}}\left(\mathbf{r},t_1\right)$ iteratively into the formal integral to get a series of integrals

$$\begin{aligned}\Psi_{\mathrm{I}}\left(\mathbf{r},t\right) &= \Psi_{\mathrm{I}}\left(\mathbf{r},0\right)+\frac{1}{i\hbar}\int_0^t H^{\mathrm{I}}(t_1)\left\{\Psi_{\mathrm{I}}\left(\mathbf{r},0\right)+\frac{1}{i\hbar}\int_0^{t_1}H^{\mathrm{I}}(t_2)\Psi_{\mathrm{I}}\left(\mathbf{r},t_2\right)\mathrm{d}t_2\right\}\mathrm{d}t_1\\ &= \Psi_{\mathrm{I}}\left(\mathbf{r},0\right)+\frac{1}{i\hbar}\int_0^t \mathrm{d}t_1 H^{\mathrm{I}}(t_1)\Psi_{\mathrm{I}}\left(\mathbf{r},0\right)\\ &\quad+\left(\frac{1}{i\hbar}\right)^2\int_0^t\mathrm{d}t_1\int_0^{t_1}\mathrm{d}t_2 H^{\mathrm{I}}(t_1)H^{\mathrm{I}}(t_2)\Psi_{\mathrm{I}}\left(\mathbf{r},t_2\right)\end{aligned}$$

Continuing the iteration, one obtains

$$\begin{aligned}\Psi_{\mathrm{I}}\left(\mathbf{r},t\right) &= \Psi_{\mathrm{I}}\left(\mathbf{r},0\right)+\frac{1}{i\hbar}\int_0^t \mathrm{d}t_1 H^{\mathrm{I}}(t_1)\Psi_{\mathrm{I}}\left(\mathbf{r},0\right)\\ &\quad+\left(\frac{1}{i\hbar}\right)^2\int_0^t\mathrm{d}t_1\int_0^{t_1}\mathrm{d}t_2 H^{\mathrm{I}}(t_1)H^{\mathrm{I}}(t_2)\Psi_{\mathrm{I}}\left(\mathbf{r},0\right)\\ &\quad+\left(\frac{1}{i\hbar}\right)^3\int_0^t\mathrm{d}t_1\int_0^{t_1}\mathrm{d}t_2\int_0^{t_2}\mathrm{d}t_3 H^{\mathrm{I}}(t_1)H^{\mathrm{I}}(t_2)H^{\mathrm{I}}(t_3)\Psi_{\mathrm{I}}\left(\mathbf{r},0\right)\\ &\quad+\ldots\end{aligned}$$

$$
\begin{aligned}
&= \Psi_{\mathrm{I}}(\mathbf{r},0)+\sum_{k=1}^{\infty}\left(\frac{1}{i\hbar}\right)^{k}\int_0^t \mathrm{d}t_1\int_0^{t_1}\mathrm{d}t_2...\int_0^{t_{n-1}}\mathrm{d}t_n H^{\mathrm{I}}(t_1)H^{\mathrm{I}}(t_2)...H^{\mathrm{I}}(t_n)\Psi_{\mathrm{I}}(\mathbf{r},0)\\
&= \Psi(\mathbf{r},0)+\sum_{k=1}^{\infty}\left(\frac{1}{i\hbar}\right)^{k}\int_0^t \mathrm{d}t_1\int_0^{t_1}\mathrm{d}t_2...\int_0^{t_{n-1}}\mathrm{d}t_n H^{\mathrm{I}}(t_1)H^{\mathrm{I}}(t_2)...H^{\mathrm{I}}(t_n)\Psi(\mathbf{r},0)\,.
\end{aligned}
$$

In the last step, we have used the relation

$$
\Psi_{\mathrm{I}}(\mathbf{r},0) = e^{-\frac{1}{i\hbar}H_0 0}\Psi(\mathbf{r},t=0)=\Psi(\mathbf{r},0)\,, \tag{A.22}
$$

which means the wave function of the initial state is the same in the Schrödinger picture and in the interaction picture. Until now, the result for $\Psi_{\mathrm{I}}(\mathbf{r},t)$ is accurate without any approximation. However, the solution is represented by an infinity of terms, each corresponding to a perturbation of a given order. For each term, we know the expression of the interaction Hamiltonian $H^{\mathrm{I}}(t_n)$ and the initial wave function $\Psi_{\mathrm{I}}(\mathbf{r},0)$, and so one can calculate the perturbation series to any accuracy by stopping at a given order. As an example, first-order perturbation thereby gives

$$
\Psi_{\mathrm{I}}(\mathbf{r},t) \approx \Psi(\mathbf{r},0)+\frac{1}{i\hbar}\int_0^t \mathrm{d}t_1 H^{\mathrm{I}}(t_1)\Psi(\mathbf{r},0)\,. \tag{A.23}
$$

For some cases e.g. scattering problems, we are only interested in the final state of the system far after the scattering. Therefore, the equation above can be rewritten as

$$
\begin{aligned}
&\Psi_{\mathrm{I}}(\mathbf{r},\infty)\\
&= \Psi(\mathbf{r},-\infty)+\sum_{k=1}^{\infty}\left(\frac{1}{i\hbar}\right)^{k}\int_{-\infty}^{\infty} \mathrm{d}t_1\int_{-\infty}^{t_1}\mathrm{d}t_2...\int_{-\infty}^{t_{n-1}}\mathrm{d}t_n H^{\mathrm{I}}(t_1)H^{\mathrm{I}}(t_2)...H^{\mathrm{I}}(t_n)\Psi(\mathbf{r},-\infty)\,,
\end{aligned}
$$

which gives the definition of the scattering operator

$$
\Psi_{\mathrm{I}}(\mathbf{r},\infty) = S\Psi(\mathbf{r},-\infty)\,,
$$

with

$$
S = I+\sum_{k=1}^{\infty}S^{(k)},
$$

and

$$
S^{(k)} = \left(\frac{1}{i\hbar}\right)^{k}\int_{-\infty}^{\infty} \mathrm{d}t_1\int_{-\infty}^{t_1}\mathrm{d}t_2...\int_{-\infty}^{t_{n-1}}\mathrm{d}t_n H^{\mathrm{I}}(t_1)H^{\mathrm{I}}(t_2)...H^{\mathrm{I}}(t_n).
$$

The first-order scattering gives

$$
S \approx I+\frac{1}{i\hbar}\int_{-\infty}^{\infty}\mathrm{d}t H^{\mathrm{I}}(t), \tag{A.24}
$$

with the scattering amplitude from an initial state $|i\rangle$ to a final state $|f\rangle$ given as

$$
S_{fi}^{(1)} = \frac{1}{i\hbar}\int_{-\infty}^{\infty}\mathrm{d}t\,\langle f_{\mathrm{I}}|\,H^{\mathrm{I}}(t)\,|i_{\mathrm{I}}\rangle = frac1i\hbar\int_{-\infty}^{\infty}\mathrm{d}t\,\langle f_{\mathrm{I}}|\,H^{\mathrm{I}}(t)\,|i\rangle\,. \tag{A.25}
$$

As we are only interested in the amplitude, one can drop the extra phase term in $\langle f_{\mathrm{I}}| =$

$e^{\frac{1}{i\hbar}H_0 * \infty} \langle f|$. This gives a new definition of the scattering amplitude as:

$$\begin{aligned} S_{fi}^{(1)} &= \frac{1}{i\hbar}\int_{-\infty}^{\infty} \mathrm{d}t \, \langle f| \, H^{\mathrm{I}}(t) \, |i\rangle \\ &= \frac{1}{i\hbar}\int_{-\infty}^{\infty} \mathrm{d}t \, \langle f| \, e^{-\frac{1}{i\hbar}H_0 t} H_{\mathrm{I}}(t) e^{\frac{1}{i\hbar}H_0 t} \, |i\rangle \\ &= \frac{1}{i\hbar}\int_{-\infty}^{\infty} \mathrm{d}t \, \langle f| \, e^{-iE_{if}t/\hbar} H_{\mathrm{I}}(t) \, |i\rangle \, , \end{aligned} \tag{A.26}$$

with $E_{if} = E_i - E_f$.

As an example, for interaction $H_{\mathrm{I}}(t) = H_{\mathrm{I}}(\omega)e^{-i\omega t} + h.c.$, one has

$$\begin{aligned} S_{fi}^{(1)} &= \frac{1}{i\hbar}\int_{-\infty}^{\infty} \mathrm{d}t \, \langle f| \, e^{-\frac{1}{i\hbar}E_f t} H_{\mathrm{I}}(t) e^{\frac{1}{i\hbar}E_i t} \, |i\rangle \\ &= \frac{1}{i\hbar}\int_{-\infty}^{\infty} \mathrm{d}t \, \langle f| \, e^{-i\omega_{if}t} \left(H_{\mathrm{I}}(\omega)e^{-i\omega t} + h.c. \right) |i\rangle \\ &= \frac{1}{i\hbar}\int_{-\infty}^{\infty} \mathrm{d}t \, \langle f| \left(H_{\mathrm{I}}(\omega)e^{-i(E_{if}+\hbar\omega)t/\hbar} + H_{\mathrm{I}}^{\dagger}(\omega)e^{-i(E_{if}-\hbar\omega)t/\hbar} \right) |i\rangle \\ &= -2\pi i \, \langle f| \left(H_{\mathrm{I}}(\omega)\delta(E_{if}+\hbar\omega) + H_{\mathrm{I}}^{\dagger}(\omega)\delta(E_{if}-\hbar\omega) \right) |i\rangle \\ &= -2\pi i \delta(E_{if}+\hbar\omega) \, \langle f| \, H_{\mathrm{I}}(\omega) \, |i\rangle - 2\pi i \delta(E_{if}-\hbar\omega) \, \langle f| \, H_{\mathrm{I}}^{\dagger}(\omega) \, |i\rangle \, . \end{aligned} \tag{A.27}$$

Based on these results, one can define the transition amplitude

$$T_{fi} = \begin{cases} \langle f| \, H_{\mathrm{I}}(\omega) \, |i\rangle \, , & \text{for } E_i < E_f, \text{ excitation} \, , \\ \langle f| \, H_{\mathrm{I}}^{\dagger}(\omega) \, |i\rangle \, , & \text{for } E_i > E_f, \text{ emission} \, . \end{cases} \tag{A.28}$$

Appendix B

More on density matrix theory

B.1 Atomic calculation of Rabi frequencies

As defined in Sec. 2.3.1, all the parameters in the *rotating-phase picture* are real functions. The coupling strength between the atoms and electromagnetic field is given as

$$\begin{aligned}\Omega(\mathbf{x},t) &= \left| e\langle \mathrm{e}|\,\mathbf{r}\,|\mathrm{g}\rangle\,\boldsymbol{\mathcal{E}}(\mathbf{x},t)\right| \\ &= \left| e\langle \mathrm{e}|\,\mathbf{r}\,|\mathrm{g}\rangle\,\hat{\epsilon}\right|\mathcal{E}(\mathbf{x},t) \\ &= \left| e\langle \mathrm{e}|\,\mathbf{r}\cdot\hat{\epsilon}\,|\mathrm{g}\rangle\right|\mathcal{E}(\mathbf{x},t), \end{aligned} \tag{B.1}$$

with $\mathcal{E}(\mathbf{x},t)$ the scalar amplitude of the electromagnetic wave and $\hat{\epsilon}$ its polarization vector. Assuming that the light propagates along $\hat{x}$ direction, the polarization of the light can be

$$\hat{\epsilon} = \cos\alpha\hat{y} + \sin\alpha\hat{z}, \text{for linear polarization,} \tag{B.2}$$

or

$$\hat{\epsilon}_{\pm} = \frac{1}{\sqrt{2}}\left(\hat{y} \pm \mathrm{i}\hat{z}\right), \text{for circular polarization.} \tag{B.3}$$

Here, based on the example of the hydrogen atom, we will shown how the value of $\langle \mathrm{e}|\,\mathbf{r}\cdot\hat{\epsilon}\,|\mathrm{g}\rangle$ can be calculated.

To start with, we should realize that, as long as the main axis ($\hat{z}$) is fixed, the magnitude and direction of $\langle \mathrm{e}|\,\mathbf{r}\,|\mathrm{g}\rangle$ are fixed quantities for a given atom with specific states $|\mathrm{g}\rangle$ and $|\mathrm{e}\rangle$:

$$\langle \mathrm{e}|\,\mathbf{r}\,|\mathrm{g}\rangle = \langle \mathrm{e}|\,x\,|\mathrm{g}\rangle\,\hat{x} + \langle \mathrm{e}|\,y\,|\mathrm{g}\rangle\,\hat{y} + \langle \mathrm{e}|\,z\,|\mathrm{g}\rangle\,\hat{z}. \tag{B.4}$$

The dipole moment, $\langle \boldsymbol{d}\rangle = \mathrm{Re}\left[\rho_{\mathrm{ge}}\langle \mathrm{e}|\,\mathbf{r}\,|\mathrm{g}\rangle\right]$, may change during the interaction with the radiation field. The value $\langle \mathrm{e}|\,\mathbf{r}\,|\mathrm{g}\rangle$, however, is always a constant vector as long as the two energy levels are given.

As an example, we assume the ground state is $|\mathrm{g}\rangle = \psi_{100}$ and the excited state is $|\mathrm{e}\rangle = \psi_{210}$ using the indices nlm with the hydrogen-atom quantum numbers. With the length normalized to the Bohr radius a_0, we have

$$\begin{aligned}\langle \mathrm{e}|\,x\,|\mathrm{g}\rangle &= \int_0^{\infty} dr \int_0^{\pi} d\theta \int_0^{2\pi} d\varphi \left(r^2\sin\theta\right)\left(\frac{1}{4\sqrt{2\pi}}e^{-r/2}r\cos\theta\right)\left(r\sin\theta\cos\varphi\right)\left(\frac{1}{\sqrt{\pi}}e^{-r}\right) = 0, \\ \langle \mathrm{e}|\,y\,|\mathrm{g}\rangle &= \int_0^{\infty} dr \int_0^{\pi} d\theta \int_0^{2\pi} d\varphi \left(r^2\sin\theta\right)\left(\frac{1}{4\sqrt{2\pi}}e^{-r/2}r\cos\theta\right)\left(r\sin\theta\sin\varphi\right)\left(\frac{1}{\sqrt{\pi}}e^{-r}\right) = 0, \end{aligned}$$

Table B.1: Coupling factors $\langle \mathrm{e}|\,\mathbf{r}\,|\mathrm{g}\rangle\cdot\hat{\epsilon}$ between hydrogen a atom and light for different atomic excited states, different light propagation and polarization directions. We assume the atoms are polarized along the $\hat{z}$ direction e.g. by applying a magnetic field $\boldsymbol{B} = B_z\hat{z}$. The ground state of the hydrogen atom is $|\psi_{100}\rangle$.

Propagation direction	Polarization: $\hat{\epsilon}$	Excited states $\langle \mathrm{e}|\,\mathbf{r}\,|\mathrm{g}\rangle$ /0.744936		
		$\lvert\psi_{211}\rangle$, $m=+1$	$\lvert\psi_{210}\rangle$, $m=0$	$\lvert\psi_{21-1}\rangle$, $m=-1$
		$\frac{1}{\sqrt{2}}(\hat{x}+i\hat{y})$	$\hat{z}$	$\frac{1}{\sqrt{2}}(\hat{x}-i\hat{y})$
along $\hat{x}$	$\hat{z}$	0	1	0
	$\hat{y}$	$\frac{1}{\sqrt{2}}i$	0	$-\frac{1}{\sqrt{2}}i$
	$\frac{1}{\sqrt{2}}(\hat{y}+i\hat{z})$	$\frac{1}{2}i$	$\frac{1}{\sqrt{2}}i$	$-\frac{1}{2}i$
	$\frac{1}{\sqrt{2}}(\hat{y}-i\hat{z})$	$\frac{1}{2}i$	$-\frac{1}{\sqrt{2}}i$	$-\frac{1}{2}i$
along $\hat{y}$	$\hat{z}$	0	1	0
	$\hat{x}$	$\frac{1}{\sqrt{2}}i$	0	$\frac{1}{\sqrt{2}}i$
	$\frac{1}{\sqrt{2}}(\hat{z}+i\hat{x})$	$\frac{1}{2}i$	$\frac{1}{\sqrt{2}}i$	$\frac{1}{2}i$
	$\frac{1}{\sqrt{2}}(\hat{z}-i\hat{x})$	$-\frac{1}{2}i$	$\frac{1}{\sqrt{2}}i$	$-\frac{1}{2}i$
along $\hat{z}$	$\hat{x}$	$\frac{1}{\sqrt{2}}$	0	$\frac{1}{\sqrt{2}}$
	$\hat{y}$	$\frac{1}{\sqrt{2}}i$	0	$-\frac{1}{\sqrt{2}}i$
	$\frac{1}{\sqrt{2}}(\hat{x}+i\hat{y})$	0	0	1
	$\frac{1}{\sqrt{2}}(\hat{x}-i\hat{y})$	1	0	0

$$\langle \mathrm{e}|\,z\,|\mathrm{g}\rangle = \int_0^\infty dr\int_0^\pi d\theta\int_0^{2\pi} d\varphi\left(r^2\sin\theta\right)\left(\frac{1}{4\sqrt{2\pi}}e^{-r/2}r\cos\theta\right)(r\cos\theta)\left(\frac{1}{\sqrt{\pi}}e^{-r}\right) = 0.744936,$$

where we have used the transformation

$$x = r\sin\theta\cos\varphi, \tag{B.5}$$
$$y = r\sin\theta\sin\varphi, \tag{B.6}$$
$$z = r\cos\theta. \tag{B.7}$$

Similarly, if the excited state is $|\mathrm{e}\rangle = \psi_{211}$, then

$$\langle \mathrm{e}|\,x\,|\mathrm{g}\rangle = \int_0^\infty dr\int_0^\pi d\theta\int_0^{2\pi} d\varphi\left(r^2\sin\theta\right)\left(\frac{1}{8\sqrt{\pi}}e^{-r/2}r\sin\theta e^{i\phi}\right)^*(r\sin\theta\cos\varphi)\left(\frac{1}{\sqrt{\pi}}e^{-r}\right) = 0.526749+0i,$$
$$\langle \mathrm{e}|\,y\,|\mathrm{g}\rangle = \int_0^\infty dr\int_0^\pi d\theta\int_0^{2\pi} d\varphi\left(r^2\sin\theta\right)\left(\frac{1}{8\sqrt{\pi}}e^{-r/2}r\sin\theta e^{i\phi}\right)^*(r\sin\theta\sin\varphi)\left(\frac{1}{\sqrt{\pi}}e^{-r}\right) = 0-0.526749i,$$
$$\langle \mathrm{e}|\,z\,|\mathrm{g}\rangle = \int_0^\infty dr\int_0^\pi d\theta\int_0^{2\pi} d\varphi\left(r^2\sin\theta\right)\left(\frac{1}{8\sqrt{\pi}}e^{-r/2}r\sin\theta e^{i\phi}\right)^*(r\cos\theta)\left(\frac{1}{\sqrt{\pi}}e^{-r}\right) = 0+0i.$$

And, if the excited state is $|\mathrm{e}\rangle = \psi_{21-1}$, one has

$$\langle \mathrm{e}|\,x\,|\mathrm{g}\rangle = \int_0^\infty dr\int_0^\pi d\theta\int_0^{2\pi} d\varphi\left(r^2\sin\theta\right)\left(\frac{1}{8\sqrt{\pi}}e^{-r/2}r\sin\theta e^{-i\phi}\right)^*(r\sin\theta\cos\varphi)\left(\frac{1}{\sqrt{\pi}}e^{-r}\right) = 0.526749+0i,$$
$$\langle \mathrm{e}|\,y\,|\mathrm{g}\rangle = \int_0^\infty dr\int_0^\pi d\theta\int_0^{2\pi} d\varphi\left(r^2\sin\theta\right)\left(\frac{1}{8\sqrt{\pi}}e^{-r/2}r\sin\theta e^{-i\phi}\right)^*(r\sin\theta\sin\varphi)\left(\frac{1}{\sqrt{\pi}}e^{-r}\right) = 0+0.526749i,$$
$$\langle \mathrm{e}|\,z\,|\mathrm{g}\rangle = \int_0^\infty dr\int_0^\pi d\theta\int_0^{2\pi} d\varphi\left(r^2\sin\theta\right)\left(\frac{1}{8\sqrt{\pi}}e^{-r/2}r\sin\theta e^{-i\phi}\right)^*(r\cos\theta)\left(\frac{1}{\sqrt{\pi}}e^{-r}\right) = 0+0i.$$

In total, the dipole vectors for three different electric-dipole transitions are

$$\begin{aligned}
\langle \mathrm{e}|\,\mathbf{r}\,|\mathrm{g}\rangle &= 0.744936\hat{z}, && \text{for } m=0,\\
\langle \mathrm{e}|\,\mathbf{r}\,|\mathrm{g}\rangle &= 0.526749\hat{x} - i0.526749\hat{y}, && \text{for } m=+1,\\
\langle \mathrm{e}|\,\mathbf{r}\,|\mathrm{g}\rangle &= 0.526749\hat{x} + i0.526749\hat{y}, && \text{for } m=-1.
\end{aligned}$$

We also note that, for all the excited states, one has

$$|\langle \mathrm{e}|\,\mathbf{r}\,|\mathrm{g}\rangle| \neq \langle \mathrm{e}|\,r\,|\mathrm{g}\rangle\,, \tag{B.8}$$

where $|\langle \mathrm{e}|\,\mathbf{r}\,|\mathrm{g}\rangle| = 0.744936$, but $\langle \mathrm{e}|\,r\,|\mathrm{g}\rangle = 0$.

The coupling between the dipole and the light field under different propagation and polarization directions are given in table B.1. One can see that the value of the coupling factors $\langle \mathrm{e}|\,\mathbf{r}\,|\mathrm{g}\rangle \cdot \hat{\epsilon}$ is not simply decided by the selection rules according the the polarizations. It can be positive, negative or even a complex number. This is why we introduce a phase term ϕ_0 when defining the Rabi frequency in Eqs. (2.113–2.117). Therefore, $\langle \mathrm{e}|\,\mathbf{r}\,|\mathrm{g}\rangle \cdot \hat{\epsilon} \neq \langle \mathrm{e}|\,\mathbf{r}\,|\mathrm{g}\rangle \cdot \hat{\epsilon}^*$.

Another conclusion from this calculation is that $\mu = |\langle \mathrm{e}|\,\mathbf{r}\,|\mathrm{g}\rangle|$ is independent of M_z. This is because when the principle quantum number and the angular momentum quantum number are given, the different magnetic substates will only contribute a phase factor to the wave functions. Therefore, they do not modify the amplitude of the dipole moment.

B.2 Atomic calculation of electric-dipole momenta

After the direct calculation of the electric-dipole moment described in Appx. B.1, in this section, we discuss two other methods to calculate it. The first method starts from Einstein A coefficient which can be calculated by using e.g. the GRASP package (for $E1$, $M1$, $E2$ and $M2$ transitions) [105]; the other method starts from the oscillator strength which can be obtained through either the GRASP package or from the Los Alamos Atomic Physics Codes (only for $E1$ transitions) [143].

In a transition from an excited state $|a\rangle$ to a lower state $|b\rangle$, the spontaneous emission probability per second is given as

$$w_{ab}^{\mathrm{sp}} = \frac{4\alpha}{3}\frac{\omega^3}{c^2}\big|\,\langle a|\,\mathbf{r}\,|b\rangle\,\big|^2. \tag{B.9}$$

The corresponding oscillator strength is defined through [115]

$$f_{ab} = \frac{2m_{\mathrm{e}}\omega_{ba}}{3\hbar}\big|\,\langle a|\,\mathbf{r}\,|b\rangle\,\big|^2. \tag{B.10}$$

For degenerate levels such as atoms without a Zeeman splitting, the spontaneous emission probability is obtained by summing over all the allowed transitions between the magnetic substates of the excited and final state, and averaging over the excited state. This gives the Einstein A coefficient of spontaneous emission:

$$A_{ab} = \sum_{i,j}\frac{1}{g_a}w_{a_jb_i}^{\mathrm{sp}} = \sum_{i,j}\frac{4\alpha}{3}\frac{\omega^3}{c^2}\frac{1}{g_a}\big|\,\langle a_i|\,\mathbf{r}\,|b_j\rangle\,\big|^2 = \frac{4\alpha}{3}\frac{\omega^3}{c^2e^2}\frac{1}{g_a}\sum_{i,j}\mu_{ij}^2, \tag{B.11}$$

with g_a being the magnetic sublevel degeneracy of the excited state and

$$\mu_{ij} = e\big|\,\langle a_i|\,\mathbf{r}\,|b_j\rangle\,\big|. \tag{B.12}$$

The oscillator strength for a degenerate system is defined as a reduced oscillator strength

$$\bar{f}_{ab} = \sum_{i,j} \frac{1}{g_a} f_{a_j b_i} = \sum_{i,j} \frac{2m_e\omega_{b_i a_j}}{3\hbar} \frac{1}{g_a} |\langle a_j| \mathbf{r} |b_i\rangle|^2 = \frac{2m_e\omega_{ba}}{3\hbar e^2} \frac{1}{g_a} \sum_{i,j} \mu_{ji}^2, \quad \text{(B.13)}$$

which is obtained again by summing over all the allowed transitions between the magnetic substates of the excited and final states, and then averaging over the excited state. From Eq. (B.10) and Eq. (B.13), one can notice that

$$f_{ab} = -f_{ba}, \quad \text{(B.14)}$$

$$\bar{f}_{ab} = -\frac{g_b}{g_a} \bar{f}_{ba}. \quad \text{(B.15)}$$

Due to $\omega_{a_i b_j} = \omega$ and $\mu_{ij} = \mu_{ji}$, a comparison of Eq. (B.11) and Eq. (B.13) gives the relationship between the Einstein A coefficient and the reduced oscillator strength:

$$A_{ab} = -\frac{2\alpha\hbar\omega^2}{m_e c^2} \bar{f}_{ab} = \frac{2\alpha\hbar\omega^2}{m_e c^2} \frac{g_b}{g_a} \bar{f}_{ba} = \frac{\omega^2 e^2}{2\pi\epsilon_0 m_e c^3} \frac{g_b}{g_a} \bar{f}_{ba}. \quad \text{(B.16)}$$

As we know from Appx. B.1, the $\mu_{ij} = \mu$ are independent of the magnetic substates when l_a and l_b are given. This results in the following relations:

$$A_{ab} = \frac{4\alpha}{3} \frac{\omega^3}{c^2 e^2} \frac{T_N}{g_a} \mu^2, \quad \text{(B.17)}$$

$$\bar{f}_{ab} = \frac{2m_e\omega_{ba}}{3\hbar e^2} \frac{T_N}{g_a} \mu^2, \quad \text{(B.18)}$$

with T_N being the number of all allowed transitions between the initial and final states. Besides, $\mu_{ij} = \mu$ also indicates that the oscillator strength and transition probability are the same for transitions between different magnetic substates. Therefore, one has the following relation between the reduced oscillator strength and the oscillator strength:

$$\bar{f}_{ab} = \frac{T_N}{g_a} f_{ab}. \quad \text{(B.19)}$$

Then, one can obtain the light electric dipole moment from the Einstein A coefficient as

$$\mu^2 = \frac{3}{4\alpha} \frac{c^2 e^2}{\omega^3} \frac{g_a}{T_N} A_{ab} = \frac{3\pi\varepsilon_0\hbar c^3}{\omega^3} \frac{g_a}{T_N} A_{ab} = \frac{3\pi\varepsilon_0\hbar^4 c^3}{(\hbar\omega)^3} \frac{g_a}{T_N} A_{ab}, \quad \text{(B.20)}$$

or

$$\begin{aligned} \mu^2 &= \frac{3 \times 3.14 \times 8.85 \times 10^{-12} \times 1.05^4 \times 10^{-34\times4} \times 3^3 \times 10^{8\times3}}{(1.6 \times 10^{-19})^3 (\hbar\omega)^3} \times \frac{g_a}{T_N} A_{ab} \\ &= \frac{83.367 \times 10^{-12} \times 1.22 \times 10^{-136} \times 27 \times 10^{24}}{4.096 \times 10^{-54} (\hbar\omega)^3} \times \frac{g_a}{T_N} A_{ab} \\ &= 670.4 \times 10^{-82} \frac{1}{(\hbar\omega)^3} \times \frac{g_a}{T_N} A_{ab}, \end{aligned}$$

with $\hbar\omega$ given in units of eV.

For the transition $1s2p\ ^1P_1 \longrightarrow 1s^2\ ^1S_0$ in Ne^{8+}, one has $g_a = T_N = 3$. With the

parameters $\hbar\omega = 920$ eV and $A_{ab} = 9 \times 10^{12}$ obtained from a GRASP calculation, one can calculate the electric-dipole moment as

$$\mu^2 = 670.4 \times 10^{-82} \times \frac{1}{920^3} \times \frac{3}{3} \times 9 \times 10^{12} = 77.488 \times 10^{-62}\ \mathrm{C}^2 \cdot \mathrm{m}^2.$$

So, we have

$$\mu = 8.8 \times 10^{-31} \mathrm{C} \cdot \mathrm{m} = 0.104\ ea_0,$$

with $ea_0 = 8.48 \times 10^{-30} \mathrm{C} \cdot \mathrm{m}$.

On the other hand, the electric dipole can also be calculated from the oscillator strength

$$f = \frac{2}{3} \frac{m_\mathrm{e}\omega}{\hbar} \left| \langle \mathrm{e} | \mathbf{r} | \mathrm{g} \rangle \right|^2 = \frac{2}{3} \frac{m_\mathrm{e}\omega}{\hbar e^2} \mu^2. \tag{B.21}$$

So that

$$\begin{aligned} \mu^2 &= \frac{3}{2} \frac{\hbar e^2}{m_\mathrm{e}\omega} \frac{g_b}{T_N} f = \frac{3}{2} \frac{\hbar \lambda e^2}{m_\mathrm{e} 2\pi c} \frac{g_b}{T_N} f \\ &= 1.5 \times \frac{1.05 \times 10^{-34} \times 1.6^2 \times 10^{-38}}{9.11 \times 10^{-31} \times 6.28 \times 3 \times 10^8} \times \frac{g_b}{T_N} \times (\lambda_0 \times 10^{-10}) \times (f_0 \times 10^{-1}) \\ &= 2.35 \times 10^{-62} \times \frac{g_b}{T_N} (\lambda_0 \times f_0). \end{aligned}$$

For our transition $1s2p\ ^1P_1 \longrightarrow 1s^2\ ^1S_0$ in Ne^{8+}, the wavelength and the oscillator strength can also be obtained from the Los Alamos Atomic Physics Code as $\lambda = 13.45$ Å and $f = 0.76228$. Because there is only one possible ground state, $g_b = 1$, and the number of transitions are $T_N = 3$:

$$\mu^2 = 2.35 \times 10^{-62} \times \frac{1}{3} \times (13.45 \times 7.6228) = 0.803 \times 10^{-60}\ \mathrm{C}^2 \cdot \mathrm{m}^2,$$

which gives

$$\mu = 0.896 \times 10^{-30} \mathrm{C} \cdot \mathrm{m} = 0.106\ ea_0.$$

One can see that the electric-dipole momenta calculated from different codes and approaches are approximately equal to each other.

B.3 Lindblad Hamiltonian

In Eq. (2.133), the coupling of the two-level system with the reservoir is given by the Lindblad form [112]

$$\dot{\rho} = L(\rho) = \frac{\Gamma}{2} \left(2\sigma^- \rho \sigma^+ - \sigma^+ \sigma^- \rho - \rho \sigma^+ \sigma^- \right), \tag{B.22}$$

with the operators

$$\sigma^+ = |\mathrm{e}\rangle \langle \mathrm{g}|, \tag{B.23}$$

$$\sigma^- = |\mathrm{g}\rangle \langle \mathrm{e}|. \tag{B.24}$$

ρ and Γ is the density matrix and decay rate defined in Sec. 2.3, respectively. One should notice that the right-hand side of the Lindblad form does not change under any unitary transformation U_i. Take the first term for example

$$U_\mathrm{i}\sigma^-\rho\sigma^+U_\mathrm{i}^\dagger = U_\mathrm{i}\sigma^-U_\mathrm{i}^\dagger U_\mathrm{i}\rho U_\mathrm{i}^\dagger U_\mathrm{i}\sigma^+U_\mathrm{i}^\dagger = \sigma_\mathrm{i}^-\rho_\mathrm{i}\sigma_\mathrm{i}^+, \tag{B.25}$$

with the new excitation and deexcitation operators defined as

$$\sigma_\mathrm{i}^+ = U_\mathrm{i}\sigma^+U_\mathrm{i}^\dagger = U_\mathrm{i}\left|\mathrm{e}\right\rangle\left\langle\mathrm{g}\right|U_\mathrm{i}^\dagger = \left|e_\mathrm{i}\right\rangle\left\langle g_\mathrm{i}\right|, \tag{B.26}$$

$$\sigma_\mathrm{i}^- = U_\mathrm{i}\sigma^-U_\mathrm{i}^\dagger = U_\mathrm{i}\left|\mathrm{g}\right\rangle\left\langle\mathrm{e}\right|U_\mathrm{i}^\dagger = \left|g_\mathrm{i}\right\rangle\left\langle e_\mathrm{i}\right|. \tag{B.27}$$

Here, $|g_\mathrm{i}\rangle$ and $|e_\mathrm{i}\rangle$ are the new eigenstates in after the unitary transformation. Therefore, no matter which picture we are working in, one could always use the same Lindblad form to describe the decay process and include it directly to the von Neumann equation.

In the matrix form, the three terms can be reformulated as

$$\begin{aligned}\sigma^-\rho\sigma^+ &= \begin{bmatrix}0&1\\0&0\end{bmatrix}\begin{bmatrix}\rho_\mathrm{gg}&\rho_\mathrm{ge}\\\rho_\mathrm{eg}&\rho_\mathrm{ee}\end{bmatrix}\begin{bmatrix}0&0\\1&0\end{bmatrix}\\ &= \begin{bmatrix}\rho_\mathrm{eg}&\rho_\mathrm{ee}\\0&0\end{bmatrix}\begin{bmatrix}0&0\\1&0\end{bmatrix}\\ &= \begin{bmatrix}\rho_\mathrm{ee}&0\\0&0\end{bmatrix},\end{aligned} \tag{B.28}$$

$$\begin{aligned}\sigma^+\sigma^-\rho &= \left|\mathrm{e}\right\rangle\left\langle\mathrm{e}\right|\rho\\ &= \begin{bmatrix}0&0\\0&1\end{bmatrix}\begin{bmatrix}\rho_\mathrm{gg}&\rho_\mathrm{ge}\\\rho_\mathrm{eg}&\rho_\mathrm{ee}\end{bmatrix}\\ &= \begin{bmatrix}0&0\\\rho_\mathrm{eg}&\rho_\mathrm{ee}\end{bmatrix},\end{aligned} \tag{B.29}$$

$$\begin{aligned}\rho\sigma^+\sigma^- &= \rho\left|\mathrm{e}\right\rangle\left\langle\mathrm{e}\right|\\ &= \begin{bmatrix}\rho_\mathrm{gg}&\rho_\mathrm{ge}\\\rho_\mathrm{eg}&\rho_\mathrm{ee}\end{bmatrix}\begin{bmatrix}0&0\\0&1\end{bmatrix}\\ &= \begin{bmatrix}0&\rho_\mathrm{ge}\\0&\rho_\mathrm{ee}\end{bmatrix}.\end{aligned} \tag{B.30}$$

Adding them together, one obtains the matrix form of the Lindblad Hamiltonian:

$$\dot\rho = \Gamma\begin{bmatrix}\rho_\mathrm{ee}&-\frac{1}{2}\rho_\mathrm{ge}\\-\frac{1}{2}\rho_\mathrm{eg}&-\rho_\mathrm{ee}\end{bmatrix}. \tag{B.31}$$

Appendix C

Schrödinger picture, interaction picture and rotating-phase picture

The dynamics of any quantum system can be studied in different equivalent pictures. Each of these pictures has their own advantages. In the following, We introduce three pictures that are used in our thesis, namely the Schrödinger picture, the interaction picture and the rotating-phase picture.

Considering a two-level system interacting with an electric field of the form

$$\mathbf{E}\left(\mathbf{x},t\right)=\frac{1}{2}\left(\boldsymbol{\mathcal{E}}_{\mathrm{m}}\left(\mathbf{x},t\right)e^{-i\omega_0 t}+\boldsymbol{\mathcal{E}}_{\mathrm{m}}^{*}\left(\mathbf{x},t\right)e^{i\omega_0 t}\right), \tag{C.1}$$

with $\boldsymbol{\mathcal{E}}_{\mathrm{m}}\left(\mathbf{x},t\right)$ given by Eq. (2.102), the Hamiltonian is given as

$$H=H_0+H_{\mathrm{I}}, \tag{C.2}$$

with

$$H_0=\left[\begin{array}{cc}0 & 0\\ 0 & \omega_{\mathrm{a}}\end{array}\right], \tag{C.3}$$

and

$$H_{\mathrm{I}} \;=\; e\mathbf{r}\cdot\mathbf{E}\left(\mathbf{x},t\right)=\frac{e\mathbf{r}}{2}\left(\boldsymbol{\mathcal{E}}_{\mathrm{m}}\left(\mathbf{x},t\right)e^{-i\omega_0 t}+\boldsymbol{\mathcal{E}}_{\mathrm{m}}^{*}\left(\mathbf{x},t\right)e^{i\omega_0 t}\right). \tag{C.4}$$

C.1 Schrödinger picture

In the Schrödinger picture, the wave function of the atomic state of a two-level system has the form

$$\left|\psi(t)\right\rangle=c_{\mathrm{g}}(t)\left|\mathrm{g}\right\rangle+c_{\mathrm{e}}(t)\left|\mathrm{e}\right\rangle. \tag{C.5}$$

The corresponding density matrix is defined as [107]

$$\rho=\left|\psi\right\rangle\left\langle\psi\right|=\left[\begin{array}{cc}c_{\mathrm{g}}c_{\mathrm{g}}^{*} & c_{\mathrm{g}}c_{\mathrm{e}}^{*}\\ c_{\mathrm{e}}c_{\mathrm{g}}^{*} & c_{\mathrm{e}}c_{\mathrm{e}}^{*}\end{array}\right]=\left[\begin{array}{cc}\rho_{\mathrm{gg}} & \rho_{\mathrm{ge}}\\ \rho_{\mathrm{eg}} & \rho_{\mathrm{ee}}\end{array}\right]. \tag{C.6}$$

According to the Schrödinger equation, one can derive the equation of motion for the density matrix:

$$\dot{\rho} \;=\; \frac{d}{dt}\left|\psi\right\rangle\left\langle\psi\right|+h.c.=\frac{1}{i}H\left|\psi\right\rangle\left\langle\psi\right|-\frac{1}{i}\left|\psi\right\rangle\left\langle\psi\right|H=\frac{1}{i}\left[H,\rho\right], \tag{C.7}$$

which means

$$\dot{\rho} = i\left[\rho, H\right] = i\left[\rho, H_0 + H_\mathrm{I}\right]. \tag{C.8}$$

Here, Eq. (C.8) is called the von Neumann equation, which is the starting point for studying the dynamics of a quantum system in density matrix theory. Because we do not consider any spatial variations for the atomic system we are interested in, the partial derivative with respect to time is changed to be the total derivative.

One of the advantages of density matrix theory is that the global phase of the quantum system is eliminated from the theory. For a given atomic wave function

$$|\psi(0)\rangle = \frac{1}{\sqrt{2}} e^{i\beta}\left[|\mathrm{g}\rangle + e^{i\beta_0}|\mathrm{e}\rangle\right], \tag{C.9}$$

the phase β would never enter the density matrix element and one can just neglect it. In other words, the global phase of the atom has no effect on the dynamics of the atomic state. Therefore, one can drop it without changing the physics. Only the phase difference β_0 between $|\mathrm{e}\rangle$ and $|\mathrm{g}\rangle$ will enter the density matrix and hence affect the evolution of the density matrix elements. Supposing all the atoms are staying in their ground state at $t = 0$, even though their phase may be different between each other, in the language of the density matrix, they are indistinguishable particles. These arguments give us the idea to prepare an ensemble of atoms in a state with the same initial conditions for density-matrix.

C.2 Interaction picture

The wave function $\left|\psi^\mathrm{I}\right\rangle$ in the interaction picture is obtained by the following unitary transformation of the wave function $|\psi\rangle$ in the Schrödinger picture [107],

$$U_0 = e^{iH_0 t} = \begin{bmatrix} 1 & 0 \\ 0 & e^{i\omega_\mathrm{a} t} \end{bmatrix}, \tag{C.10}$$

which gives

$$\left|\psi^\mathrm{I}\right\rangle = U_0|\psi\rangle = \begin{bmatrix} 1 & 0 \\ 0 & e^{i\omega_\mathrm{a} t} \end{bmatrix} \begin{bmatrix} c_\mathrm{g} \\ c_\mathrm{e} \end{bmatrix} = \begin{bmatrix} c_\mathrm{g} \\ c_\mathrm{e} e^{i\omega_\mathrm{a} t} \end{bmatrix}. \tag{C.11}$$

Therefore, one can express $\left|\psi^\mathrm{I}\right\rangle$ in the basis of Schrödinger picture as

$$\left|\psi^\mathrm{I}\right\rangle = C_\mathrm{g}|\mathrm{g}\rangle + C_\mathrm{e}|\mathrm{e}\rangle, \tag{C.12}$$

with the relations of the coefficients given as

$$C_\mathrm{g} = c_\mathrm{g}, \tag{C.13}$$

$$C_\mathrm{e} = c_\mathrm{e} e^{i\omega_\mathrm{a} t}. \tag{C.14}$$

Accordingly, the corresponding density matrix in the interaction picture reads

$$\rho^{\mathrm{I}} = \left|\psi^{\mathrm{I}}\right\rangle \left\langle\psi^{\mathrm{I}}\right| = \left[\begin{array}{cc} C_{\mathrm{g}}C_{\mathrm{g}}^{*} & C_{\mathrm{g}}C_{\mathrm{e}}^{*} \\ C_{\mathrm{e}}C_{\mathrm{g}}^{*} & C_{\mathrm{e}}C_{\mathrm{e}}^{*} \end{array}\right] = \left[\begin{array}{cc} \rho_{\mathrm{gg}}^{\mathrm{I}} & \rho_{\mathrm{ge}}^{\mathrm{I}} \\ \rho_{\mathrm{eg}}^{\mathrm{I}} & \rho_{\mathrm{ee}}^{\mathrm{I}} \end{array}\right]. \tag{C.15}$$

This density matrix can also be written in the basis of Schrödinger picture as

$$\rho^{\mathrm{I}} = \left[\begin{array}{cc} \rho_{\mathrm{gg}}^{\mathrm{I}} & \rho_{\mathrm{ge}}^{\mathrm{I}} \\ \rho_{\mathrm{eg}}^{\mathrm{I}} & \rho_{\mathrm{ee}}^{\mathrm{I}} \end{array}\right] = \left[\begin{array}{cc} \rho_{\mathrm{gg}} & \rho_{\mathrm{ge}}e^{-i\omega_{\mathrm{a}}t} \\ \rho_{\mathrm{eg}}e^{i\omega_{\mathrm{a}}t} & \rho_{\mathrm{ee}} \end{array}\right]. \tag{C.16}$$

One can see that the off-diagonal elements in the interaction picture can be regarded as the envelope function of the off-diagonal elements in Schrödinger picture:

$$\rho_{\mathrm{ge}}^{\mathrm{I}} = \rho_{\mathrm{ge}}e^{-i\omega_{\mathrm{a}}t} = \tilde{\rho}_{\mathrm{ge}}, \tag{C.17}$$

$$\rho_{\mathrm{eg}}^{\mathrm{I}} = \rho_{\mathrm{eg}}e^{i\omega_{\mathrm{a}}t} = \tilde{\rho}_{\mathrm{eg}}. \tag{C.18}$$

The same results can also be obtained by an equivalent form $\rho^{\mathrm{I}} = U_0\rho U_0^{\dagger}$ due to

$$\rho^{\mathrm{I}} = U_0\rho U_0^{\dagger} = U_0\left|\psi\right\rangle\left\langle\psi\right|U_0^{\dagger} = \left|\psi^{\mathrm{I}}\right\rangle\left\langle\psi^{\mathrm{I}}\right|. \tag{C.19}$$

The time-evolution of the density matrix is given as

$$\frac{\partial\rho^{\mathrm{I}}}{\partial t} = \frac{\partial\left(U_0\rho U_0^{\dagger}\right)}{\partial t} = \frac{\partial U_0}{\partial t}\rho U_0^{\dagger} + U_0\frac{\partial\rho}{\partial t}U_0^{\dagger} + U_0\rho\frac{\partial U_0^{\dagger}}{\partial t}. \tag{C.20}$$

With

$$\frac{\partial U_0}{\partial t} = \frac{\partial}{\partial t}e^{iH_0t} = iH_0e^{iH_0t} = iH_0U_0, \tag{C.21}$$

$$\frac{\partial U_0^{\dagger}}{\partial t} = \frac{\partial}{\partial t}e^{-iH_0t} = -iH_0e^{-iH_0t} = -iH_0U_0^{\dagger}, \tag{C.22}$$

we obtain

$$\frac{\partial U_0}{\partial t}\rho U_0^{\dagger} + U_0\rho\frac{\partial U_0^{\dagger}}{\partial t} = iH_0U_0\rho U_0^{\dagger} - iU_0\rho U_0^{\dagger}H_0 = iH_0\rho^{\mathrm{I}} - i\rho^{\mathrm{I}}H_0 = i[H_0, \rho^{\mathrm{I}}].$$

Furthermore,

$$U_0\frac{\partial\rho}{\partial t}U_0^{\dagger} = U_0\left(i\left[\rho, H_0 + H_{\mathrm{I}}\right]\right)U_0^{\dagger} = U_0\left(i\left[\rho, H_0\right]\right)U_0^{\dagger} + U_0\left(i\left[\rho, H_{\mathrm{I}}\right]\right)U_0^{\dagger}. \tag{C.23}$$

With

$$\begin{aligned} U_0\left(i\left[\rho, H_0\right]\right)U_0^{\dagger} &= i\left(U_0\rho H_0U_0^{\dagger} - U_0H_0\rho U_0^{\dagger}\right) \\ &= i\left(U_0\rho U_0^{\dagger}H_0 - H_0U_0\rho U_0^{\dagger}\right) \\ &= i\left(\rho^{\mathrm{I}}H_0 - H_0\rho^{\mathrm{I}}\right) \\ &= i\left[\rho^{\mathrm{I}}, H_0\right], \end{aligned} \tag{C.24}$$

and

$$\begin{aligned} U_0 \left(i \left[\rho, H_{\mathrm{I}} \right] \right) U_0^\dagger &= i \left(U_0 \rho H_{\mathrm{I}} U_0^\dagger - U_0 H_{\mathrm{I}} \rho U_0^\dagger \right) \\ &= i \left(U_0 \rho U_0^\dagger U_0 H_{\mathrm{I}} U_0^\dagger - U_0 H_{\mathrm{I}} U_0^\dagger U_0 \rho U_0^\dagger \right) \\ &= i \left(\rho^{\mathrm{I}} H^{\mathrm{I}} - H^{\mathrm{I}} \rho^{\mathrm{I}} \right) \\ &= i \left[\rho^{\mathrm{I}}, H^{\mathrm{I}} \right], \end{aligned} \tag{C.25}$$

we obtain

$$U_0 \frac{\partial \rho}{\partial t} U_0^\dagger = i \left[\rho^{\mathrm{I}}, H_0 \right] + i \left[\rho^{\mathrm{I}}, H^{\mathrm{I}} \right]. \tag{C.26}$$

All together, this yields the von Neumann equation in the interaction picture:

$$\dot{\rho} = i \left[\rho^{\mathrm{I}}, H^{\mathrm{I}} \right], \tag{C.27}$$

with the Hamiltonian in the interaction picture being (see Eq. (2.120))

$$H^{\mathrm{I}} = U_0 H_{\mathrm{I}} U_0^\dagger = \frac{\Omega \left(\mathbf{x}, t \right)}{2} \begin{bmatrix} 0 & e^{-i\theta(\mathbf{x},t)} \\ e^{i\theta(\mathbf{x},t)} & 0 \end{bmatrix}, \tag{C.28}$$

and

$$\theta \left(\mathbf{x}, t \right) = \mathbf{k} \cdot \mathbf{x} - \Delta t + \phi \left(\mathbf{x}, t \right) + \phi_0. \tag{C.29}$$

C.3 Rotating-phase picture

In order to deal with the phase term in the interaction picture, one could go to the rotating-phase picture through the unitary transformation

$$U_\theta = \begin{bmatrix} 1 & 0 \\ 0 & e^{-i\theta(\mathbf{x},t)} \end{bmatrix}. \tag{C.30}$$

Under this transformation, the wave function is

$$\left| \psi^{\mathrm{M}} \right\rangle = U_\theta \left| \psi^{\mathrm{I}} \right\rangle = \begin{bmatrix} 1 & 0 \\ 0 & e^{-i\theta} \end{bmatrix} \begin{bmatrix} C_{\mathrm{g}} \\ C_{\mathrm{e}} \end{bmatrix} = \begin{bmatrix} C_{\mathrm{g}} \\ C_{\mathrm{e}} e^{-i\theta} \end{bmatrix}. \tag{C.31}$$

Then we get the relations between the coefficients in the rotating-phase picture, the interaction picture and the Schrödinger picture as

$$C'_{\mathrm{g}} = C_{\mathrm{g}} = c_{\mathrm{g}}, \tag{C.32}$$

$$C'_{\mathrm{e}} = C_{\mathrm{e}} e^{-i\theta} = c_{\mathrm{e}} e^{i\omega_{\mathrm{a}} t - i\theta}. \tag{C.33}$$

Similarly to the former transformation, the density matrix is replaced by

$$\rho^{\mathrm{M}} = U_\theta \rho^{\mathrm{I}} U_\theta^\dagger = \begin{bmatrix} \rho^{\mathrm{I}}_{\mathrm{gg}} & \rho^{\mathrm{I}}_{\mathrm{ge}} e^{i\theta} \\ \rho^{\mathrm{I}}_{\mathrm{eg}} e^{-i\theta} & \rho^{\mathrm{I}}_{\mathrm{ee}} \end{bmatrix}. \tag{C.34}$$

Therefore, one can have the following relations for the density matrix elements in these three pictures:

$$\rho^{\mathrm{M}}_{\mathrm{ge}} = \rho^{\mathrm{I}}_{\mathrm{ge}} e^{i\theta} = \rho_{\mathrm{ge}} e^{-i\omega_{\mathrm{a}} t + i\theta}, \tag{C.35}$$
$$\rho^{\mathrm{M}}_{\mathrm{eg}} = \rho^{\mathrm{I}}_{\mathrm{eg}} e^{-i\theta} = \rho_{\mathrm{eg}} e^{i\omega_{\mathrm{a}} t - i\theta}, \tag{C.36}$$
$$\rho^{\mathrm{M}}_{\mathrm{gg}} = \rho^{\mathrm{I}}_{\mathrm{gg}} = \rho_{\mathrm{gg}}, \tag{C.37}$$
$$\rho^{\mathrm{M}}_{\mathrm{ee}} = \rho^{\mathrm{I}}_{\mathrm{ee}} = \rho_{\mathrm{ee}}. \tag{C.38}$$

The evolution of the density matrix ρ^{M} in this new picture can be derived as

$$\frac{\partial \rho^{\mathrm{M}}}{\partial t} = \frac{\partial \left(U_\theta \rho^{\mathrm{I}} U_\theta^\dagger \right)}{\partial t} = \frac{\partial U_\theta}{\partial t} \rho^{\mathrm{I}} U_\theta^\dagger + U_\theta \frac{\partial \rho^{\mathrm{I}}}{\partial t} U_\theta^\dagger + U_\theta \rho^{\mathrm{I}} \frac{\partial U_\theta^\dagger}{\partial t}. \tag{C.39}$$

The three terms on the right hand side can be calculated as follows:

$$\begin{aligned} \frac{\partial U_\theta}{\partial t} \rho^{\mathrm{I}} U_\theta^\dagger &= \begin{bmatrix} 0 & 0 \\ 0 & -i\frac{\partial \theta}{\partial t} e^{-i\theta} \end{bmatrix} \begin{bmatrix} \rho^{\mathrm{I}}_{\mathrm{gg}} & \rho^{\mathrm{I}}_{\mathrm{ge}} \\ \rho^{\mathrm{I}}_{\mathrm{eg}} & \rho^{\mathrm{I}}_{\mathrm{ee}} \end{bmatrix} \begin{bmatrix} 1 & 0 \\ 0 & e^{i\theta} \end{bmatrix} \\ &= \begin{bmatrix} 0 & 0 \\ -i\frac{\partial \theta}{\partial t} e^{-i\theta} \rho^{\mathrm{I}}_{\mathrm{eg}} & -i\frac{\partial \theta}{\partial t} e^{-i\theta} \rho^{\mathrm{I}}_{\mathrm{ee}} \end{bmatrix} \begin{bmatrix} 1 & 0 \\ 0 & e^{i\theta} \end{bmatrix} \\ &= \begin{bmatrix} 0 & 0 \\ -i\frac{\partial \theta}{\partial t} e^{-i\theta} \rho^{\mathrm{I}}_{\mathrm{eg}} & -i\frac{\partial \theta}{\partial t} \rho^{\mathrm{I}}_{\mathrm{ee}} \end{bmatrix} \\ &= -i \begin{bmatrix} 0 & 0 \\ \frac{\partial \theta}{\partial t} \rho^{\mathrm{M}}_{\mathrm{eg}} & \frac{\partial \theta}{\partial t} \rho^{\mathrm{M}}_{\mathrm{ee}} \end{bmatrix}, \end{aligned} \tag{C.40}$$

and

$$\begin{aligned} U_\theta \rho^{\mathrm{I}} \frac{\partial U_\theta^\dagger}{\partial t} &= \begin{bmatrix} 1 & 0 \\ 0 & e^{-i\theta} \end{bmatrix} \begin{bmatrix} \rho^{\mathrm{I}}_{\mathrm{gg}} & \rho^{\mathrm{I}}_{\mathrm{ge}} \\ \rho^{\mathrm{I}}_{\mathrm{eg}} & \rho^{\mathrm{I}}_{\mathrm{ee}} \end{bmatrix} \begin{bmatrix} 0 & 0 \\ 0 & i\frac{\partial \theta}{\partial t} e^{i\theta} \end{bmatrix} \\ &= \begin{bmatrix} 1 & 0 \\ 0 & e^{-i\theta} \end{bmatrix} \begin{bmatrix} 0 & i\frac{\partial \theta}{\partial t} e^{-i\theta} \rho^{\mathrm{I}}_{\mathrm{ge}} \\ 0 & i\frac{\partial \theta}{\partial t} e^{i\theta} \rho^{\mathrm{I}}_{\mathrm{ee}} \end{bmatrix} \\ &= \begin{bmatrix} 0 & i\frac{\partial \theta}{\partial t} e^{i\theta} \rho^{\mathrm{I}}_{\mathrm{ge}} \\ 0 & i\frac{\partial \theta}{\partial t} \rho^{\mathrm{I}}_{\mathrm{ee}} \end{bmatrix} \\ &= i \begin{bmatrix} 0 & \frac{\partial \theta}{\partial t} \rho^{\mathrm{M}}_{\mathrm{ge}} \\ 0 & \frac{\partial \theta}{\partial t} \rho^{\mathrm{M}}_{\mathrm{ee}} \end{bmatrix}, \end{aligned} \tag{C.41}$$

furthermore,

$$\begin{aligned} U_\theta \frac{\partial \rho^{\mathrm{I}}}{\partial t} U_\theta^\dagger &= U_\theta \left(i \left[\rho^{\mathrm{I}}, H^{\mathrm{I}} \right] \right) U_\theta^\dagger \\ &= i \left(U_\theta \rho^{\mathrm{I}} H^{\mathrm{I}} U_\theta^\dagger - U_\theta H^{\mathrm{I}} \rho^{\mathrm{I}} U_\theta^\dagger \right) \end{aligned}$$

$$\begin{aligned} &= i\left(U_\theta \rho^{\mathrm{I}} U_\theta^\dagger U_\theta H^{\mathrm{I}} U_\theta^\dagger - U_\theta H^{\mathrm{I}} U_\theta^\dagger U_\theta \rho^{\mathrm{I}} U_\theta^\dagger\right) \\ &= i\left(\rho^{\mathrm{M}} H^{\mathrm{M}} - H^{\mathrm{M}} \rho^{\mathrm{M}}\right) \\ &= i\left[\rho^{\mathrm{M}}, H^{\mathrm{M}}\right], \end{aligned} \tag{C.42}$$

with

$$H^{\mathrm{M}} = U_\theta H^{\mathrm{I}} U_\theta^\dagger = \frac{1}{2}\begin{bmatrix} 0 & \Omega \\ \Omega & 0 \end{bmatrix}. \tag{C.43}$$

For the first two terms, one obtains

$$\begin{aligned} \frac{\partial U_\theta}{\partial t}\rho^{\mathrm{I}} U_\theta^\dagger + U_\theta \rho^{\mathrm{I}} \frac{\partial U_\theta^\dagger}{\partial t} &= -i\begin{bmatrix} 0 & 0 \\ \frac{\partial\theta}{\partial t}\rho_{\mathrm{eg}}^{\mathrm{M}} & \frac{\partial\theta}{\partial t}\rho_{\mathrm{ee}}^{\mathrm{M}} \end{bmatrix} + i\begin{bmatrix} 0 & \frac{\partial\theta}{\partial t}\rho_{\mathrm{ge}}^{\mathrm{M}} \\ 0 & \frac{\partial\theta}{\partial t}\rho_{\mathrm{ee}}^{\mathrm{M}} \end{bmatrix} \\ &= -i\begin{bmatrix} 0 & 0 \\ 0 & \frac{\partial\theta}{\partial t} \end{bmatrix}\rho^{\mathrm{M}} + i\rho^{\mathrm{M}}\begin{bmatrix} 0 & 0 \\ 0 & \frac{\partial\theta}{\partial t} \end{bmatrix} \\ &= i\left[\rho^{\mathrm{M}}, H_\theta\right], \end{aligned} \tag{C.44}$$

with

$$H_\theta = \begin{bmatrix} 0 & 0 \\ 0 & \frac{\partial\theta}{\partial t} \end{bmatrix}. \tag{C.45}$$

Putting all the terms together, one finds the evolution of the density matrix in the rotating-phase picture as

$$\frac{\partial \rho^{\mathrm{M}}}{\partial t} = i\left[\rho^{\mathrm{M}}, H^{\mathrm{M}} + H_\theta\right] = i\left[\rho^{\mathrm{M}}, H_{\mathrm{eff}}\right], \tag{C.46}$$

with the effective Hamiltonian given as

$$H_{\mathrm{eff}} = \begin{bmatrix} 0 & \Omega/2 \\ \Omega/2 & \frac{\partial\theta}{\partial t} \end{bmatrix}. \tag{C.47}$$

From this effective Hamiltonian one can see that the change of the phase with time gives the time-dependent instantaneous frequency detuning in this coupled system:

$$\Delta_\theta(t) = -\frac{\partial\theta}{\partial t}. \tag{C.48}$$

Because $\mathbf{k}\cdot\mathbf{x}$ and ϕ_0 are constant quantities which are independent of time for each atom, one could have

$$\Delta_\theta(t) = \Delta - \frac{\partial\phi}{\partial t}. \tag{C.49}$$

The time-dependent phase function $\phi(\mathbf{x}, t)$, can be written it in a polynomial form as

$$\phi(\mathbf{x}, t) = \phi^{(0)}(\mathbf{x}) + \phi^{(1)}(\mathbf{x})\, t + \phi^{(2)}(\mathbf{x})\, t^2 + ... \tag{C.50}$$

One may notice that, the first term $\phi^{(0)}$ refers to a constant phase which is independent of

time. Because the derivative of this term gives zero in the rotating-phase picture, it does not change the physics in this case. One could also absorb the other two constant-phase terms $\mathbf{k}\cdot\mathbf{x}$ and ϕ_0 into $\phi^{(0)}$. The second term $\phi^{(1)}$ can be regarded as a frequency shift of the carrier frequency. If we take the reference carrier frequency to be resonant with the two-level system, we have $\Delta = 0$ and $\phi^{(1)}$ exactly refers to the detuning between the two-level system and light field. For the third term, $\phi^{(2)}$ corresponds to a chirp in the light pulse. So, in principle, the detuning Δ, the constant phase ϕ_0 and the time-independent phase $\mathbf{k}\cdot\mathbf{x}$ can be absorbed into a single phase term ϕ.

$$\theta(\mathbf{x},t) = \theta^{(0)}(\mathbf{x}) + \theta^{(1)}(\mathbf{x})\,t + \theta^{(2)}(\mathbf{x})\,t^2 + ..., \tag{C.51}$$

with

$$\theta(\mathbf{x})^{(0)} = \phi(\mathbf{x})^{(0)} + \mathbf{k}\cdot\mathbf{x} + \phi_0, \tag{C.52}$$

$$\theta(\mathbf{x})^{(1)} = \phi(\mathbf{x})^{(1)} - \Delta, \tag{C.53}$$

$$\theta(\mathbf{x})^{(\mathrm{n})} = \phi(\mathbf{x})^{(\mathrm{n})} \qquad \text{for all } n \geq 2. \tag{C.54}$$

Then, the dynamics of the system can be fully described by the effective Hamiltonian

$$H_{\mathrm{eff}} = \begin{bmatrix} 0 & \Omega/2 \\ \Omega/2 & \frac{\partial\theta}{\partial t} \end{bmatrix}. \tag{C.55}$$

Appendix D

More on Maxwell–Bloch equations

In the Maxwell–Bloch equations given by Eqs. (2.151–2.157), the amplitude and phase of the light field is treated separately. This procedure has the advantages in e.g. defining the Rabi frequency in Eqs. (2.113 and 2.125), obtaining the rate equations in Eq. (2.196) and Eq. (2.197) and analyzing the light amplification and absorption based on simple properties of atomic coherences. In particular, in the rotating-phase picture, the Hamiltonian in Eq. (2.125) gives clear physics on the interaction between the atom and a chirped light pulse with a time-dependent detuning [113]. Nevertheless, Eqs. (2.151–2.157) have problems in numerical simulations. The evolution of the phase of the light, $\phi(x,t)$, includes a $1/\mathcal{E}(x,t)$ term that leads to singularities when $\mathcal{E}(x,t) \to 0$. Furthermore, treating the amplitude and phase separately results in two wave propagation equations that makes the analytical treatment more complicated.

In this Appendix, we account the amplitude and phase in terms of a single complex function and derive the corresponding Maxwell–Bloch equations used in Chapters 5–7. In order to solve these equations numerically, the Maxwell–Bloch equations in terms of its real and imaginary parts of the light field are also derived.

D.1 The light field as a complex function

By defining two complex vector functions

$$\boldsymbol{\mathcal{E}}_{\mathrm{c}}(x,t) = \boldsymbol{\mathcal{E}}(x,t)\, e^{i\phi(x,t)}, \tag{D.1}$$
$$\boldsymbol{\mathcal{P}}_{\mathrm{c}}(x,t) = \boldsymbol{\mathcal{P}}(x,t)\, e^{i\phi(x,t)}, \tag{D.2}$$

the electric field and the polarization is

$$\mathbf{E}^{(+)}(\mathbf{r},t) = \boldsymbol{\mathcal{E}}_{\mathrm{c}}(x,t)\, e^{i(kx-\omega_0 t)}, \tag{D.3}$$
$$\mathbf{P}^{(+)}(\mathbf{r},t) = \boldsymbol{\mathcal{P}}_{\mathrm{c}}(x,t)\, e^{i(kx-\omega_0 t)}. \tag{D.4}$$

This means

$$\frac{\partial \boldsymbol{\mathcal{E}}_{\mathrm{c}}}{\partial t} = \frac{\partial \mathcal{E}}{\partial t} e^{i\phi} + i\frac{\partial \phi}{\partial t}\mathcal{E} e^{i\phi}, \tag{D.5}$$
$$\frac{\partial \boldsymbol{\mathcal{E}}_{\mathrm{c}}}{\partial x} = \frac{\partial \mathcal{E}}{\partial x} e^{i\phi} + i\frac{\partial \phi}{\partial x}\mathcal{E} e^{i\phi}. \tag{D.6}$$

and

$$\frac{\partial \mathcal{E}}{\partial t} + c\frac{\partial \mathcal{E}}{\partial x} + \frac{\partial \phi}{\partial t}\mathcal{E} + c\frac{\partial \phi}{\partial x}\mathcal{E} = \left(\frac{\partial \boldsymbol{\mathcal{E}}_{\mathrm{c}}}{\partial t} + c\frac{\partial \boldsymbol{\mathcal{E}}_{\mathrm{c}}}{\partial x}\right) e^{-i\phi}. \tag{D.7}$$

From Eq. (2.52), we obtain the evolution equation of the complex field in the the slowly varying envelope approximation as:

$$\frac{\partial \boldsymbol{\mathcal{E}}_{\mathrm{c}}}{\partial t}+c\frac{\partial \boldsymbol{\mathcal{E}}_{\mathrm{c}}}{\partial x}=\frac{i\mu_0\omega_0 c^2}{2}\boldsymbol{\mathcal{P}}_{\mathrm{c}}. \tag{D.8}$$

Again, using the definition $\boldsymbol{\mathcal{E}}=\mathcal{E}\hat{\epsilon}$, one can multiply the conjugate of the polarization vector, $\hat{\epsilon}^*$, to each side of the equation to obtain the scalar equation:

$$\frac{\partial \mathcal{E}_{\mathrm{c}}}{\partial t}+c\frac{\partial \mathcal{E}_{\mathrm{c}}}{\partial x}=\frac{i\mu_0\omega_0 c^2}{2}\boldsymbol{\mathcal{P}}_{\mathrm{c}}\cdot\hat{\epsilon}^*, \tag{D.9}$$

with $\mathcal{E}_{\mathrm{c}}$ and $\mathcal{P}_{\mathrm{c}}$ being complex scalar functions. Separating $\mathcal{E}_{\mathrm{c}}$ into a real and an imaginary part:

$$\mathcal{E}_{\mathrm{c}}=\mathcal{E}_{\mathrm{a}}+i\mathcal{E}_{\mathrm{b}} \tag{D.10}$$

one obtains a new set of wave propagation equations given as:

$$\frac{\partial \mathcal{E}_{\mathrm{a}}}{\partial t}+c\frac{\partial \mathcal{E}_{\mathrm{a}}}{\partial x} = -\frac{\mu_0\omega_0 c^2}{2}\mathrm{Im}[\boldsymbol{\mathcal{P}}_{\mathrm{c}}\cdot\hat{\epsilon}^*], \tag{D.11}$$

$$\frac{\partial \mathcal{E}_{\mathrm{b}}}{\partial t}+c\frac{\partial \mathcal{E}_{\mathrm{b}}}{\partial x} = \frac{\mu_0\omega_0 c^2}{2}\mathrm{Re}[\boldsymbol{\mathcal{P}}_{\mathrm{c}}\cdot\hat{\epsilon}^*]. \tag{D.12}$$

Similarly, in retarded time we have

$$\frac{\partial \mathcal{E}_{\mathrm{c}}}{\partial x'}=\frac{i\mu_0\omega_0 c}{2}\boldsymbol{\mathcal{P}}_{\mathrm{c}}\cdot\hat{\epsilon}^*, \tag{D.13}$$

or, in a different form

$$\frac{\partial \mathcal{E}_{\mathrm{a}}}{\partial x'} = -\frac{\mu_0\omega_0 c}{2}\mathrm{Im}[\boldsymbol{\mathcal{P}}_{\mathrm{c}}\cdot\hat{\epsilon}^*], \tag{D.14}$$

$$\frac{\partial \mathcal{E}_{\mathrm{b}}}{\partial x'} = \frac{\mu_0\omega_0 c}{2}\mathrm{Re}[\boldsymbol{\mathcal{P}}_{\mathrm{c}}\cdot\hat{\epsilon}^*]. \tag{D.15}$$

The complex light fields have the following relations with the amplitude and phase of the light field.

$$\mathcal{E}_{\mathrm{c}}(x,t) = \mathcal{E}(x,t)\,e^{i\phi(x,t)}, \tag{D.16}$$

and

$$\mathcal{E}_{\mathrm{a}}(x,t) = \mathcal{E}(x,t)\cos(\phi(x,t)), \tag{D.17}$$

$$\mathcal{E}_{\mathrm{b}}(x,t) = \mathcal{E}(x,t)\sin(\phi(x,t)). \tag{D.18}$$

D.2 The xi picture

Apart from switching to the rotating-phase picture to obtain a completely positive coupling strength given by the Rabi frequency Ω (see Sec. 2.3), one can also change to

another picture with a complex coupling strength where the phase $\phi(x,t)$ of the light field is included. In the following, we call this newly defined picture the xi picture.

With Eq. (D.1) and Eq. (2.113), the complex coupling strength can be written as:

$$\begin{aligned} \Omega_{\mathrm{c}}(x,t) &= e\langle \mathrm{e}|\,\mathbf{r}\,|\mathrm{g}\rangle\,\boldsymbol{\mathcal{E}}_{\mathrm{c}}(x,t)\,e^{i\phi_0}, \\ \Omega_{\mathrm{c}}^{*}(x,t) &= e\langle \mathrm{g}|\,\mathbf{r}\,|\mathrm{e}\rangle\,\boldsymbol{\mathcal{E}}_{\mathrm{c}}^{*}(x,t)\,e^{-i\phi_0}, \end{aligned} \tag{D.19}$$

which has the relation with the Rabi frequency as:

$$\begin{aligned} \Omega_{\mathrm{c}}(x,t) &= \Omega(x,t)\,e^{i\phi(x,t)} = \mu\mathcal{E}e^{i\phi(x,t)}, \\ \Omega_{\mathrm{c}}^{*}(x,t) &= \Omega(x,t)\,e^{-i\phi(x,t)} = \mu\mathcal{E}e^{-i\phi(x,t)}. \end{aligned}$$

They can also be separate into a real and an imaginary part

$$\Omega_{\mathrm{c}} = \Omega_{\mathrm{a}} + i\Omega_{\mathrm{b}}, \tag{D.20}$$

with

$$\Omega_{\mathrm{a}} = \mu\mathcal{E}_{\mathrm{a}}, \tag{D.21}$$

$$\Omega_{\mathrm{b}} = \mu\mathcal{E}_{\mathrm{b}}. \tag{D.22}$$

In the interaction picture, the Hamiltonian is given as

$$H^{\mathrm{I}} = \frac{1}{2}\begin{bmatrix} 0 & \Omega_{\mathrm{c}}^{*}e^{-i\xi(x,t)} \\ \Omega_{\mathrm{c}}e^{i\xi(x,t)} & 0 \end{bmatrix}, \tag{D.23}$$

and

$$\xi(x,t) = kx - \Delta t + \phi_0. \tag{D.24}$$

Similarly to the procedures adopted in Appx. C, using the unitary transformation

$$U_{\mathrm{xi}} = \begin{bmatrix} 1 & 0 \\ 0 & e^{-i\xi(x,t)} \end{bmatrix}, \tag{D.25}$$

the Hamiltonian changes to

$$H^{\mathrm{xi}} = U_{\mathrm{xi}}H^{\mathrm{I}}U_{\mathrm{xi}}^{\dagger} = \frac{1}{2}\begin{bmatrix} 0 & \Omega_{\mathrm{c}}^{*} \\ \Omega_{\mathrm{c}} & 0 \end{bmatrix}, \tag{D.26}$$

and the wave function has the form

$$\left|\psi^{\mathrm{xi}}\right\rangle = U_{\mathrm{xi}}\left|\psi^{\mathrm{I}}\right\rangle = \begin{bmatrix} 1 & 0 \\ 0 & e^{-i\xi} \end{bmatrix}\begin{bmatrix} C_{\mathrm{g}} \\ C_{\mathrm{e}} \end{bmatrix} = \begin{bmatrix} C_{\mathrm{g}} \\ C_{\mathrm{e}}e^{-i\xi} \end{bmatrix}. \tag{D.27}$$

The relations between the coefficients in the interaction picture and in the xi picture is given by

$$C_{\mathrm{g}}^{\mathrm{xi}} = C_{\mathrm{g}} = c_{\mathrm{g}},$$

$$C_{\rm e}^{\rm xi} = C_{\rm e}e^{-i\xi} = c_{\rm e}e^{i\omega_{\rm a}t-i\xi}. \tag{D.28}$$

Therefore, the density matrix $\rho^{\rm xi}$ in the xi picture has the form

$$\rho^{\rm xi} = U_{\rm xi}\rho^{\rm I}U_{\rm xi}^{\dagger} = \begin{bmatrix} \rho_{\rm gg}^{\rm I} & \rho_{\rm ge}^{\rm I}e^{i\xi} \\ \rho_{\rm eg}^{\rm I}e^{-i\xi} & \rho_{\rm ee}^{\rm I} \end{bmatrix}, \tag{D.29}$$

where one can have the following relations for the density matrix elements in the xi picture, the interaction picture and the Schrödinger picture

$$\rho_{\rm ge}^{\rm xi} = \rho_{\rm ge}^{\rm I}e^{i\xi} = \rho_{\rm ge}e^{-i\omega_{\rm a}t+i\xi}, \tag{D.30}$$
$$\rho_{\rm eg}^{\rm xi} = \rho_{\rm eg}^{\rm I}e^{-i\xi} = \rho_{\rm eg}e^{i\omega_{\rm a}t-i\xi}, \tag{D.31}$$
$$\rho_{\rm gg}^{\rm xi} = \rho_{\rm gg}^{\rm I} = \rho_{\rm gg}, \tag{D.32}$$
$$\rho_{\rm ee}^{\rm xi} = \rho_{\rm ee}^{\rm I} = \rho_{\rm ee}. \tag{D.33}$$

The corresponding evolution equation of the density matrix in this xi picture is

$$\frac{\partial\rho^{\rm xi}}{\partial t} = i\left[\rho^{\rm xi}, H_{\rm eff}^{\rm xi}\right], \tag{D.34}$$

with the effective Hamiltonian given as

$$H_{\rm eff}^{\rm xi} = \begin{bmatrix} 0 & \Omega_{\rm c}^{*}/2 \\ \Omega_{\rm c}/2 & \frac{\partial\xi}{\partial t} \end{bmatrix} = \begin{bmatrix} 0 & \Omega_{\rm c}^{*}/2 \\ \Omega_{\rm c}/2 & -\Delta \end{bmatrix}. \tag{D.35}$$

Here, $\Omega_{\rm c}$ in the off-diagonal term is a complex function.

D.3 Polarization in the xi picture

With the relations

$$\rho_{\rm ge} = \rho_{\rm ge}^{\rm xi}e^{i\omega_{\rm a}t-i\xi} = \rho_{\rm ge}^{\rm xi}e^{i(\omega_0 t-kx-\phi_0)}, \tag{D.36}$$
$$\rho_{\rm eg} = \rho_{\rm eg}^{\rm xi}e^{-i\omega_{\rm a}t+i\xi} = \rho_{\rm eg}^{\rm xi}e^{-i(\omega_0 t-kx-\phi_0)}, \tag{D.37}$$

we can obtain the polarization in the xi picture as

$$\begin{aligned} \mathbf{P} &= -ne\left\langle {\rm e}\right|\mathbf{r}\left|{\rm g}\right\rangle\rho_{\rm ge}^{\rm xi}e^{i(\omega_0 t-kx-\phi_0)} \\ &\quad -ne\left\langle {\rm g}\right|\mathbf{r}\left|{\rm e}\right\rangle\rho_{\rm eg}^{\rm xi}e^{-i(\omega_0 t-kx-\phi_0)} \\ &= \mathbf{P}^{(+)}(x,t)+\mathbf{P}^{(-)}(x,t), \end{aligned} \tag{D.38}$$

with

$$\mathbf{P}^{(+)}(x,t) = -ne\left\langle {\rm g}\right|\mathbf{r}\left|{\rm e}\right\rangle\rho_{\rm eg}^{\rm xi}e^{-i(\omega_0 t-kx-\phi_0)},$$
$$\mathbf{P}^{(-)}(x,t) = -ne\left\langle {\rm e}\right|\mathbf{r}\left|{\rm g}\right\rangle\rho_{\rm ge}^{\rm xi}e^{i(\omega_0 t-kx-\phi_0)}.$$

Because we also have the relation

$$\mathbf{P}^{(+)}(x,t) = \frac{1}{2}\boldsymbol{\mathcal{P}}_{\mathrm{c}}(x,t)\, e^{i(kx-\omega_0 t)}, \tag{D.39}$$

we immediately arrive at

$$\boldsymbol{\mathcal{P}}_{\mathrm{c}}(x,t) = -2ne\,\langle \mathrm{g}|\,\mathbf{r}\,|\mathrm{e}\rangle\,\rho_{\mathrm{eg}}^{\mathrm{xi}} e^{i\phi_0}, \tag{D.40}$$

and

$$\boldsymbol{\mathcal{P}}_{\mathrm{c}}\cdot\hat{\epsilon}^{*} = -2n\mu\rho_{\mathrm{eg}}^{\mathrm{xi}}. \tag{D.41}$$

Thus, the evolution equation of the slowly varying scalar envelope is given as

$$\frac{\partial \mathcal{E}_{\mathrm{c}}}{\partial t} + c\frac{\partial \mathcal{E}_{\mathrm{c}}}{\partial x} = -i\mu_0 n\mu\omega_0 c\rho_{\mathrm{eg}}^{\mathrm{xi}}, \tag{D.42}$$

or, equivalently,

$$\frac{\partial \mathcal{E}_{\mathrm{a}}}{\partial t} + c\frac{\partial \mathcal{E}_{\mathrm{a}}}{\partial x} = \mu_0 n\mu\omega_0 c\mathrm{Im}[\rho_{\mathrm{eg}}^{\mathrm{xi}}], \tag{D.43}$$

$$\frac{\partial \mathcal{E}_{\mathrm{b}}}{\partial t} + c\frac{\partial \mathcal{E}_{\mathrm{b}}}{\partial x} = -\mu_0 n\mu\omega_0 c\mathrm{Re}[\rho_{\mathrm{eg}}^{\mathrm{xi}}]. \tag{D.44}$$

D.4 Maxwell-Bloch equation in the xi picture

Similar to Eq. (2.133), in the xi picture, the evolution equation of the density matrix including decay and decoherence processes is given as

$$\dot{\rho}^{\mathrm{xi}} = i\left[\rho^{\mathrm{xi}}, H_{\mathrm{eff}}^{\mathrm{xi}}\right] + \Gamma\begin{bmatrix} \rho_{\mathrm{ee}}^{\mathrm{xi}} & -\frac{1}{2}\rho_{\mathrm{ge}}^{\mathrm{xi}} \\ -\frac{1}{2}\rho_{\mathrm{eg}}^{\mathrm{xi}} & -\rho_{\mathrm{ee}}^{\mathrm{xi}} \end{bmatrix} + \beta\begin{bmatrix} 0 & -\frac{1}{2}\rho_{\mathrm{ge}}^{\mathrm{xi}} \\ -\frac{1}{2}\rho_{\mathrm{eg}}^{\mathrm{xi}} & 0 \end{bmatrix}.. \tag{D.45}$$

Considering that

$$\begin{aligned}
&\left[\rho^{\mathrm{xi}}, H_{\mathrm{eff}}^{\mathrm{xi}}\right] \\
=& \begin{bmatrix} \rho_{\mathrm{gg}}^{\mathrm{xi}} & \rho_{\mathrm{ge}}^{\mathrm{xi}} \\ \rho_{\mathrm{eg}}^{\mathrm{xi}} & \rho_{\mathrm{ee}}^{\mathrm{xi}} \end{bmatrix}\begin{bmatrix} 0 & \Omega_{\mathrm{c}}^{*}/2 \\ \Omega_{\mathrm{c}}/2 & -\Delta \end{bmatrix} - \begin{bmatrix} 0 & \Omega_{\mathrm{c}}^{*}/2 \\ \Omega_{\mathrm{c}}/2 & -\Delta \end{bmatrix}\begin{bmatrix} \rho_{\mathrm{gg}}^{\mathrm{xi}} & \rho_{\mathrm{ge}}^{\mathrm{xi}} \\ \rho_{\mathrm{eg}}^{\mathrm{xi}} & \rho_{\mathrm{ee}}^{\mathrm{xi}} \end{bmatrix} \\
=& \begin{bmatrix} \frac{\Omega_{\mathrm{c}}}{2}\rho_{\mathrm{ge}}^{\mathrm{xi}} & \frac{\Omega_{\mathrm{c}}^{*}}{2}\rho_{\mathrm{gg}}^{\mathrm{xi}} - \Delta\rho_{\mathrm{ge}}^{\mathrm{xi}} \\ \frac{\Omega_{\mathrm{c}}}{2}\rho_{\mathrm{ee}}^{\mathrm{xi}} & \frac{\Omega_{\mathrm{c}}^{*}}{2}\rho_{\mathrm{eg}}^{\mathrm{xi}} - \Delta\rho_{\mathrm{ee}}^{\mathrm{xi}} \end{bmatrix} - \begin{bmatrix} \frac{\Omega_{\mathrm{c}}^{*}}{2}\rho_{\mathrm{eg}}^{\mathrm{xi}} & \frac{\Omega_{\mathrm{c}}^{*}}{2}\rho_{\mathrm{ee}}^{\mathrm{xi}} \\ \frac{\Omega_{\mathrm{c}}}{2}\rho_{\mathrm{gg}}^{\mathrm{xi}} - \Delta\rho_{\mathrm{eg}}^{\mathrm{xi}} & \frac{\Omega_{\mathrm{c}}}{2}\rho_{\mathrm{ge}}^{\mathrm{xi}} - \Delta\rho_{\mathrm{ee}}^{\mathrm{xi}} \end{bmatrix} \\
=& \begin{bmatrix} \frac{1}{2}\left(\Omega_{\mathrm{c}}\rho_{\mathrm{ge}}^{\mathrm{xi}} - \Omega_{\mathrm{c}}^{*}\rho_{\mathrm{eg}}^{\mathrm{xi}}\right) & \frac{\Omega_{\mathrm{c}}^{*}}{2}\left(\rho_{\mathrm{gg}}^{\mathrm{xi}} - \rho_{\mathrm{ee}}^{\mathrm{xi}}\right) - \Delta\rho_{\mathrm{ge}}^{\mathrm{xi}} \\ \frac{\Omega_{\mathrm{c}}}{2}\left(\rho_{\mathrm{ee}}^{\mathrm{xi}} - \rho_{\mathrm{gg}}^{\mathrm{xi}}\right) + \Delta\rho_{\mathrm{eg}}^{\mathrm{xi}} & \frac{1}{2}\left(\Omega_{\mathrm{c}}^{*}\rho_{\mathrm{eg}}^{\mathrm{xi}} - \Omega_{\mathrm{c}}\rho_{\mathrm{ge}}^{\mathrm{xi}}\right) \end{bmatrix},
\end{aligned} \tag{D.46}$$

one obtains the differential equation for each density matrix element as:

$$\dot{\rho}_{\mathrm{gg}}^{\mathrm{xi}} = \frac{i}{2}\left(\Omega_{\mathrm{c}}\rho_{\mathrm{ge}}^{\mathrm{xi}} - \Omega_{\mathrm{c}}^{*}\rho_{\mathrm{eg}}^{\mathrm{xi}}\right) + \Gamma\rho_{\mathrm{ee}}^{\mathrm{xi}}, \tag{D.47}$$

$$\dot{\rho}^{\mathrm{xi}}_{\mathrm{ge}} = i\frac{\Omega^*_{\mathrm{c}}}{2}\left(\rho^{\mathrm{xi}}_{\mathrm{gg}} - \rho^{\mathrm{xi}}_{\mathrm{ee}}\right) - i\Delta\rho^{\mathrm{xi}}_{\mathrm{ge}} - \frac{\gamma}{2}\rho^{\mathrm{xi}}_{\mathrm{ge}}, \tag{D.48}$$

$$\dot{\rho}^{\mathrm{xi}}_{\mathrm{eg}} = i\frac{\Omega_{\mathrm{c}}}{2}\left(\rho^{\mathrm{xi}}_{\mathrm{ee}} - \rho^{\mathrm{xi}}_{\mathrm{gg}}\right) + i\Delta\rho^{\mathrm{xi}}_{\mathrm{eg}} - \frac{\gamma}{2}\rho^{\mathrm{xi}}_{\mathrm{eg}}, \tag{D.49}$$

$$\dot{\rho}^{\mathrm{xi}}_{\mathrm{ee}} = \frac{i}{2}\left(\Omega^*_{\mathrm{c}}\rho^{\mathrm{xi}}_{\mathrm{eg}} - \Omega_{\mathrm{c}}\rho^{\mathrm{xi}}_{\mathrm{ge}}\right) - \Gamma\rho^{\mathrm{xi}}_{\mathrm{ee}}. \tag{D.50}$$

where we used $\gamma = \Gamma + \beta$. Together with the wave propagation equation

$$\frac{\partial \mathcal{E}_{\mathrm{c}}}{\partial t} + c\frac{\partial \mathcal{E}_{\mathrm{c}}}{\partial x} = -i\mu_0 n\mu\omega_0 c\rho^{\mathrm{xi}}_{\mathrm{eg}}, \tag{D.51}$$

one arrives to the Maxwell-Bloch equations in the xi picture. Besides, compared to the results in book of Scully and Zubairy (page 163) [107], there is a sign difference in the Bloch equations, which is because of the extra sign in defining the elementary charge e. The same difference also applies to the definition of the dipole moment and the Rabi frequency.

D.5 Maxwell-Bloch equation with real functions

As defined before, one can rewrite the complex function into a real and an imaginary part (neglect the superscript xi)

$$\begin{aligned}\Omega_{\mathrm{c}} &= \Omega_{\mathrm{a}} + i\Omega_{\mathrm{b}},\\ \rho_{\mathrm{eg}} &= a + ib,\\ \rho_{\mathrm{ge}} &= a - ib,\\ \mathcal{E}_{\mathrm{c}} &= \mathcal{E}_{\mathrm{a}} + i\mathcal{E}_{\mathrm{b}}.\end{aligned}$$

This results in the following Bloch equations:

$$\dot{\rho}_{\mathrm{gg}} = \Omega_{\mathrm{a}}b - \Omega_{\mathrm{b}}a + \Gamma\rho_{\mathrm{ee}}, \tag{D.52}$$

$$\dot{a} = -\frac{\Omega_{\mathrm{b}}}{2}\left(\rho_{\mathrm{ee}} - \rho_{\mathrm{gg}}\right) - \Delta b - \frac{\gamma}{2}a, \tag{D.53}$$

$$\dot{b} = \frac{\Omega_{\mathrm{a}}}{2}\left(\rho_{\mathrm{ee}} - \rho_{\mathrm{gg}}\right) + \Delta a - \frac{\gamma}{2}b, \tag{D.54}$$

$$\dot{\rho}_{\mathrm{ee}} = -\Omega_{\mathrm{a}}b + \Omega_{\mathrm{b}}a - \Gamma\rho_{\mathrm{ee}}. \tag{D.55}$$

Using the relation $\Omega_{\mathrm{a}} = \mu\mathcal{E}_{\mathrm{a}}$ and $\Omega_{\mathrm{b}} = \mu\mathcal{E}_{\mathrm{b}}$, one obtains the Maxwell-Bloch equations in terms of the real and imaginary part of the light as:

$$\dot{\rho}_{\mathrm{gg}} = \mu\mathcal{E}_{\mathrm{a}}b - \mu\mathcal{E}_{\mathrm{b}}a + \Gamma\rho_{\mathrm{ee}}, \tag{D.56}$$

$$\dot{a} = -\frac{\mu\mathcal{E}_{\mathrm{b}}}{2}\left(\rho_{\mathrm{ee}} - \rho_{\mathrm{gg}}\right) - \Delta b - \frac{\gamma}{2}a, \tag{D.57}$$

$$\dot{b} = \frac{\mu\mathcal{E}_{\mathrm{a}}}{2}\left(\rho_{\mathrm{ee}} - \rho_{\mathrm{gg}}\right) + \Delta a - \frac{\gamma}{2}b, \tag{D.58}$$

$$\dot{\rho}_{\mathrm{ee}} = -\mu\mathcal{E}_{\mathrm{a}}b + \mu\mathcal{E}_{\mathrm{b}}a - \Gamma\rho_{\mathrm{ee}}, \tag{D.59}$$

and

$$\frac{\partial \mathcal{E}_{\rm a}}{\partial t} + c\frac{\partial \mathcal{E}_{\rm a}}{\partial x} = \mu_0 n \mu \omega_0 c b, \tag{D.60}$$

$$\frac{\partial \mathcal{E}_{\rm b}}{\partial t} + c\frac{\partial \mathcal{E}_{\rm b}}{\partial x} = -\mu_0 n \mu \omega_0 c a, \tag{D.61}$$

where we used $\mathrm{Im}[\rho_{\rm ge}] = -b$. Comparing these differential equations with the equations we obtained in Sec. 2.4, it has a main advantage in numerical simulations: there is no possibility for singularity to appear in the equations above.

Appendix E

More on multipole transitions

In this Appendix, we explain more details on multipole light-matter interaction, based on Walther Johnson's book on *Atomic structure theory* [115]

E.1 Multipole expansion of the electromagnetic field

Assuming a plane wave, $\boldsymbol{A}(\boldsymbol{r},t) = \boldsymbol{A}(\boldsymbol{r},\omega)\, e^{-i\omega t} + h.c.$, the vector potential can be given as

$$\boldsymbol{A}(\boldsymbol{r},\omega) \;=\; \mathcal{A}\hat{\epsilon} e^{i\boldsymbol{kr}}.$$

The scalar quantity $\mathcal{A}$ is the amplitude of the field for which we assume $\mathcal{A} = 1$ in the following. The vector $\hat{\epsilon}$ refers to the polarization of the field.

To proceed, we expand the vector potential $\boldsymbol{A}(\boldsymbol{r},\omega)$ in the basis of vector spherical harmonics $\boldsymbol{Y}_{JLM}(\hat{r})$ as [115]

$$\boldsymbol{A}(\boldsymbol{r},\omega) \;=\; \sum_{JLM} A_{JLM} \boldsymbol{Y}_{JLM}(\hat{r}), \tag{E.1}$$

with $\hat{r} = (\cos\phi\sin\theta, \sin\phi\sin\theta, \cos\theta)$ the unit vector, and the vector spherical harmonics

$$\boldsymbol{Y}_{JLM}(\hat{r}) \;=\; \sum_{\sigma} C(L,1,J,M-\sigma,\sigma,M) Y_{LM-\sigma}(\hat{r}) \boldsymbol{\xi}_{\sigma}. \tag{E.2}$$

The $Y_{LM}(\hat{r})$ are the spherical harmonics and the vectors $\boldsymbol{\xi}_{\sigma}$ are the unit spherical vectors defined by

$$\boldsymbol{\xi}_1 \;=\; -\frac{1}{\sqrt{2}} \begin{bmatrix} 1 \\ i \\ 0 \end{bmatrix}, \boldsymbol{\xi}_0 = \begin{bmatrix} 0 \\ 0 \\ 1 \end{bmatrix}, \boldsymbol{\xi}_{-1} = \frac{1}{\sqrt{2}} \begin{bmatrix} 1 \\ -i \\ 0 \end{bmatrix}. \tag{E.3}$$

The coefficients A_{JLM} can be obtained by adopting the orthogonality relations between different vector spherical harmonics:

$$\int \mathrm{d}\Omega \boldsymbol{Y}^*_{J'L'M'}(\hat{r}) \boldsymbol{Y}_{JLM}(\hat{r}) = \int_0^{2\pi} \mathrm{d}\phi \int_0^{\pi} \mathrm{d}\theta \boldsymbol{Y}^*_{J'L'M'}(\theta,\phi) \boldsymbol{Y}_{JLM}(\theta,\phi) = \delta_{J'J}\delta_{L'L}\delta_{M'M}.$$

This results in

$$\begin{aligned} A_{JLM} \;&=\; \int \mathrm{d}\Omega \left(\boldsymbol{Y}^*_{JLM}(\hat{r}) \cdot \boldsymbol{A}(\boldsymbol{r},\omega)\right) \\ &=\; \int \mathrm{d}\Omega \left(\boldsymbol{Y}^*_{JLM}(\hat{r}) \cdot \hat{\epsilon}\right) e^{i\boldsymbol{kr}}. \end{aligned} \tag{E.4}$$

Considering that a plane wave can be expanded in the basis of spherical Bessel functions $j_l(kr)$ as

$$e^{i\boldsymbol{kr}} = 4\pi \sum_{lm} i^l j_l(kr) Y^*_{lm}(\hat{k}) Y_{lm}(\hat{r}), \tag{E.5}$$

the coefficients A_{JLM} can be rewritten as

$$\begin{aligned}
A_{JLM} &= \int \mathrm{d}\Omega \left(\boldsymbol{Y}^*_{JLM}(\hat{r}) \cdot \hat{\epsilon}\right) \left(4\pi \sum_{lm} i^l j_l(kr) Y^*_{lm}(\hat{k}) Y_{lm}(\hat{r})\right) \\
&= 4\pi \sum_{lm} i^l Y^*_{lm}(\hat{k}) \int \mathrm{d}\Omega \left(\boldsymbol{Y}^*_{JLM}(\hat{r}) \cdot Y_{lm}(\hat{r})\right) \cdot \hat{\epsilon} j_l(kr) \\
&= 4\pi \sum_{lm} i^l Y^*_{lm}(\hat{k}) \int \mathrm{d}\Omega \left(\sum_{\sigma} C(L,1,J,M-\sigma,\sigma,M) Y^*_{LM-\sigma}(\hat{r}) \boldsymbol{\xi}^*_{\sigma} \cdot Y_{lm}(\hat{r})\right) \cdot \hat{\epsilon} j_l(kr) \\
&= 4\pi \sum_{lm} i^l Y^*_{lm}(\hat{k}) \left(\sum_{\sigma} C(L,1,J,M-\sigma,\sigma,M) \delta_{Ll} \delta_{M-\sigma m} \boldsymbol{\xi}^*_{\sigma}\right) \cdot \hat{\epsilon} j_l(kr) \\
&= 4\pi i^L \left(\sum_{\sigma} C(L,1,J,M-\sigma,\sigma,M) Y^*_{lm}(\hat{k}) \boldsymbol{\xi}^*_{\sigma}\right) \cdot \hat{\epsilon} j_L(kr) \\
&= 4\pi i^L \left(\boldsymbol{Y}^*_{JLM}(\hat{k}) \cdot \hat{\epsilon}\right) j_L(kr).
\end{aligned}$$

Therefore, the vector potential can be written as

$$\begin{aligned}
\boldsymbol{A}(\boldsymbol{r},\omega) &= 4\pi \sum_{JLM} i^L \left(\boldsymbol{Y}^*_{JLM}(\hat{k}) \cdot \hat{\epsilon}\right) j_L(kr) \boldsymbol{Y}_{JLM}(\hat{r}) \\
&= 4\pi \sum_{JLM} i^L \left(\boldsymbol{Y}^*_{JLM}(\hat{k}) \cdot \hat{\epsilon}\right) \boldsymbol{a}_{JLM}(\boldsymbol{r}),
\end{aligned}$$

with

$$\boldsymbol{a}_{JLM}(\boldsymbol{r}) = j_L(kr) \boldsymbol{Y}_{JLM}(\hat{r}). \tag{E.6}$$

Introducing the transformation for the spherical vector harmonics

$$\boldsymbol{Y}_{JJ-1M}(\hat{r}) = \sqrt{\frac{J}{2J+1}} \boldsymbol{Y}^{(-1)}_{JM}(\hat{r}) + \sqrt{\frac{J+1}{2J+1}} \boldsymbol{Y}^{(1)}_{JM}(\hat{r}), \tag{E.7}$$

$$\boldsymbol{Y}_{JJM}(\hat{r}) = \boldsymbol{Y}^{(0)}_{JM}(\hat{r}), \tag{E.8}$$

$$\boldsymbol{Y}_{JJ+1M}(\hat{r}) = -\sqrt{\frac{J+1}{2J+1}} \boldsymbol{Y}^{(-1)}_{JM}(\hat{r}) + \sqrt{\frac{J}{2J+1}} \boldsymbol{Y}^{(1)}_{JM}(\hat{r}), \tag{E.9}$$

one obtains

$$\boldsymbol{A}(\boldsymbol{r},\omega) = 4\pi \sum_{JM\lambda} i^{J-\lambda} \left(\boldsymbol{Y}^{(\lambda)*}_{JM}(\hat{k}) \cdot \hat{\epsilon}\right) \boldsymbol{a}^{(\lambda)}_{JM}(\boldsymbol{r}), \tag{E.10}$$

with the multipole potentials $\boldsymbol{a}^{(\lambda)}_{JM}(\boldsymbol{r})$ given by

$$\boldsymbol{a}^{(0)}_{JM}(\boldsymbol{r}) = \boldsymbol{a}_{JJM}(\boldsymbol{r}), \tag{E.11}$$

$$\boldsymbol{a}^{(1)}_{JM}(\boldsymbol{r}) = \sqrt{\frac{J+1}{2J+1}}\boldsymbol{a}_{JJ-1M}(\boldsymbol{r}) - \sqrt{\frac{J}{2J+1}}\boldsymbol{a}_{JI+1M}(\boldsymbol{r}). \tag{E.12}$$

Consider that $\boldsymbol{Y}^{(-1)*}_{JM}(\hat{k}) = \hat{k}Y^{(\lambda)*}_{JM}(\hat{k})$ and

$$\boldsymbol{Y}^{(-1)*}_{JM}(\hat{k})\cdot\hat{\epsilon} = Y^{(\lambda)*}_{JM}(\hat{k})\left(\hat{k}\cdot\hat{\epsilon}\right) = 0, \tag{E.13}$$

only terms with $\lambda = 0$ and $\lambda = 1$ remain in the multipole expansion, with $\lambda = 0$ corresponding to the magnetic multipole potential and $\lambda = 1$ corresponding to the electric multipole potential. All information referring to the polarization $\hat{\epsilon}$, propagation direction $\hat{k}$ and field strength $\mathcal{A}$ are included in the expansion coefficients $\boldsymbol{Y}^{(\lambda)*}_{JM}(\hat{k})\cdot\hat{\epsilon}$.

Moreover, with the definition in Eq. (E.6), the expression of the multipole potential can be rewritten in the basis of spherical vector harmonics as [115]

$$\boldsymbol{a}^{(0)}_{JM}(\boldsymbol{r}) = j_J(kr)\boldsymbol{Y}^{(0)}_{JM}(\hat{r}), \tag{E.14}$$

$$\boldsymbol{a}^{(1)}_{JM}(\boldsymbol{r}) = \left[j'_J(kr) + \frac{j_J(kr)}{kr}\right]\boldsymbol{Y}^{(1)}_{JM}(\hat{r}) + \sqrt{J(J+1)}\frac{j_J(kr)}{kr}\boldsymbol{Y}^{(-1)}_{JM}(\hat{r}). \tag{E.15}$$

To derive these equations, the following identities for spherical Bessel functions

$$j_{n-1}(z) = \frac{n+1}{z}j_n(z) + j'_n(z), \tag{E.16}$$

$$j_{n+1}(z) = \frac{n}{z}j_n(z) - j'_n(z), \tag{E.17}$$

and

$$j'_n(z) = \frac{d}{dz}j_n(z), \tag{E.18}$$

have been used.

One can examine that the multipole potentials $\boldsymbol{a}^{(\lambda)}_{JM}(\boldsymbol{r})$ satisfy the Helmholtz equation

$$\nabla^2\boldsymbol{a}^{(\lambda)}_{JM}(\boldsymbol{r}) + k^2\boldsymbol{a}^{(\lambda)}_{JM}(\boldsymbol{r}) = 0 \tag{E.19}$$

and the transverality condition

$$\boldsymbol{\nabla}\cdot\boldsymbol{a}^{(\lambda)}_{JM}(\boldsymbol{r}) = 0. \tag{E.20}$$

E.2 Multipole transition operators

For the calculation of the Einstein A coefficient, one needs to proceed with the calculation of the multipole transition operator

$$\left[T^{(\lambda)}_{JM}\right]_{ba} = \int \mathrm{d}\boldsymbol{r}\psi^\dagger_b\boldsymbol{\alpha}\cdot\boldsymbol{a}^{(\lambda)}_{JM}(\boldsymbol{r})\psi_a. \tag{E.21}$$

In the nonrelativistic limit, the wave function is calculated from the Schrödinger equation. In the following, we do not refer to any specific wave function. Instead, we only

consider the interaction Hamiltonian for multipole transitions

$$\left[H_{JM}^{(\lambda)}\right]_{ba} = \boldsymbol{\alpha}\cdot\boldsymbol{a}_{JM}^{(\lambda)}(\boldsymbol{r}). \tag{E.22}$$

E.2.1 Gauge invariance

For an electron interacting with an external field with vector potential $\boldsymbol{A}(\boldsymbol{r},t)$ and scalar potential $\phi(\boldsymbol{r},t)$ given by

$$\boldsymbol{A}(\boldsymbol{r},t) = \boldsymbol{A}(\boldsymbol{r},\omega)\,e^{-i\omega t}+h.c, \tag{E.23}$$
$$\phi(\boldsymbol{r},t) = \phi(\boldsymbol{r},\omega)\,e^{-i\omega t}+h.c, \tag{E.24}$$

the interaction Hamiltonian is given by

$$h_{\mathrm{I}}(\boldsymbol{r},t) = h_{\mathrm{I}}(\boldsymbol{r},\omega)\,e^{-i\omega t}+h.c, \tag{E.25}$$

with

$$h_{\mathrm{I}}(\boldsymbol{r},\omega) = e\left\{-c\boldsymbol{\alpha}\cdot\boldsymbol{A}(\boldsymbol{r},\omega)+\phi(\boldsymbol{r},\omega)\right\}. \tag{E.26}$$

Introducing scalar gauge function

$$G(\boldsymbol{r},t) = G(\boldsymbol{r},\omega)\,e^{-i\omega t}+h.c, \tag{E.27}$$

with $G(\boldsymbol{r},\omega)$ satisfying the Helmholtz equation

$$\nabla^2 G(\boldsymbol{r},\omega)+k^2 G(\boldsymbol{r},\omega)=0, \tag{E.28}$$

one can perform the gauge transformation for the external fields

$$\boldsymbol{A}'(\boldsymbol{r},t) = \boldsymbol{A}(\boldsymbol{r},t)+\boldsymbol{\nabla}G(\boldsymbol{r},t), \tag{E.29}$$
$$\phi'(\boldsymbol{r},t) = \phi(\boldsymbol{r},t)-\frac{\partial}{\partial t}G(\boldsymbol{r},t), \tag{E.30}$$

which gives

$$\boldsymbol{A}'(\boldsymbol{r},\omega) = \boldsymbol{A}(\boldsymbol{r},\omega)+\boldsymbol{\nabla}G(\boldsymbol{r},\omega), \tag{E.31}$$
$$\phi'(\boldsymbol{r},\omega) = \phi(\boldsymbol{r},\omega)+i\omega G(\boldsymbol{r},\omega). \tag{E.32}$$

This procedure can be followed in the multipole expansion, with the gauge function defined as

$$G(\boldsymbol{r},\omega) = 4\pi\sum_{JM\lambda} i^{J-\lambda}\left(\boldsymbol{Y}_{JM}^{(\lambda)*}(\hat{k})\cdot\hat{\epsilon}\right)g_{JM}^{(\lambda)}(\boldsymbol{r}), \tag{E.33}$$

where the $g_{JM}^{(\lambda)}(\boldsymbol{r})$ is the multipole gauge functions. Because the expansion coefficients are $\boldsymbol{r}$-independent, one can immediately recognize that $g_{JM}^{(\lambda)}(\boldsymbol{r})$ should satisfy the Helmholtz equation. Therefore, the gauge transformation for the multipole potential is given as

$$\boldsymbol{a}'^{(\lambda)}_{JM}(\hat{r}) = \boldsymbol{a}_{JM}^{(\lambda)}(\boldsymbol{r})+\boldsymbol{\nabla}g_{JM}^{(\lambda)}(\boldsymbol{r}), \tag{E.34}$$
$$\phi'^{(\lambda)}_{JM}(\boldsymbol{r}) = \phi_{JM}^{(\lambda)}(\boldsymbol{r})+i\omega g_{JM}^{(\lambda)}(\boldsymbol{r}). \tag{E.35}$$

E.2.1.1 Length gauge

Considering that the gauge function can be any function that satisfies the Helmholtz equation, one can design $G(\boldsymbol{r},\omega)$ by neglecting any term of its multipole components. One of the choices is to drop all the magnetic multipole terms with $\lambda = 0$, and keep only the electric multipole terms. This can be done by setting $g^{(0)}_{JM}(\boldsymbol{r}) = 0$ for all J and M to give

$$G(\boldsymbol{r},\omega) = 4\pi \sum_{JM} i^{J-1} \left(\boldsymbol{Y}^{(1)*}_{JM}(\hat{k}) \cdot \hat{\epsilon} \right) g^{(1)}_{JM}(\boldsymbol{r}). \tag{E.36}$$

This means that one only performs gauge transformation for the electric multipole potential, and the magnetic multipole potential remains unchanged:

$$\boldsymbol{a}'^{(0)}_{JM}(\hat{r}) = \boldsymbol{a}^{(0)}_{JM}(\boldsymbol{r}), \tag{E.37}$$

$$\phi'^{(0)}_{JM}(\boldsymbol{r}) = \phi^{(0)}_{JM}(\boldsymbol{r}). \tag{E.38}$$

Furthermore, we assume $g^{(1)}_{JM}(\boldsymbol{r})$ to be

$$g^{(1)}_{JM}(\boldsymbol{r}) = -\frac{1}{k}\sqrt{\frac{J+1}{J}} j_J(kr) Y_{JM}(\hat{r}). \tag{E.39}$$

Then

$$\begin{aligned}
\boldsymbol{\nabla} g^{(1)}_{JM}(\boldsymbol{r}) &= -\frac{1}{k}\sqrt{\frac{J+1}{J}} \boldsymbol{\nabla} \left(j_J(kr) Y_{JM}(\hat{r}) \right) \\
&= -\frac{1}{k}\sqrt{\frac{J+1}{J}} \left[\left(\boldsymbol{\nabla} j_J(kr) \right) Y_{JM}(\hat{r}) + j_J(kr) \left(\boldsymbol{\nabla} Y_{JM}(\hat{r}) \right) \right] \\
&= -\frac{1}{k}\sqrt{\frac{J+1}{J}} \left[\left(j'_J(kr) \cdot k \cdot \hat{r} \right) Y_{JM}(\hat{r}) + j_J(kr) \left(\frac{\sqrt{J(J+1)}}{r} \boldsymbol{Y}^{(1)}_{JM}(\hat{r}) \right) \right] \\
&= -\sqrt{\frac{J+1}{J}} j'_J(kr) \boldsymbol{Y}^{(1)}_{JM}(\hat{r}) - (J+1)\frac{j_J(kr)}{kr} \boldsymbol{Y}^{(1)}_{JM}(\hat{r}).
\end{aligned}$$

Substituting this into the gauge transformation and using the fact that $\phi(\boldsymbol{r},t) = 0$ before the transformation, one obtains

$$\boldsymbol{a}'^{(1)}_{JM}(\hat{r}) = -j_{J+1}(kr) \left[\boldsymbol{Y}^{(1)}_{JM}(\hat{r}) - \frac{\sqrt{J+1}}{J} \boldsymbol{Y}^{(-1)}_{JM}(\hat{r}) \right], \tag{E.40}$$

$$\phi'^{(1)}_{JM}(\boldsymbol{r}) = -ic\frac{\sqrt{J+1}}{J} j_J(kr) Y_{JM}(\hat{r}). \tag{E.41}$$

With this gauge transformation we arrive to then length gauge. Accordingly, the multipole transition operators are given as

$$h_{\mathrm{I}}(\boldsymbol{r},\omega) = -ec \left\{ \boldsymbol{\alpha} \cdot \boldsymbol{a}'^{(1)}_{JM}(\hat{r}) - \frac{1}{c} \phi'^{(1)}_{JM}(\boldsymbol{r}) \right\}. \tag{E.42}$$

If the wavelength of the external field is much larger than to the size of the atom, it

holds $kr \ll 1$. In this case,

$$\begin{aligned}
\lim_{kr\to 0} \boldsymbol{a}'^{(1)}_{JM}(\hat{r}) &= \frac{(kr)^{J+1}}{(2J+3)!!}\left[\boldsymbol{Y}^{(1)}_{JM}(\hat{r}) - \frac{\sqrt{J+1}}{J}\boldsymbol{Y}^{(-1)}_{JM}(\hat{r})\right], \\
\lim_{kr\to 0} \frac{1}{c}\phi'^{(1)}_{JM}(\boldsymbol{r}) &= i\sqrt{\frac{J+1}{J}}\frac{(kr)^J}{(2J+1)!!}Y_{JM}(\hat{r}).
\end{aligned}$$

Here we can see that the vector potential scales has a lower of kr-order than the scalar potential, e.g. it is smaller in the long-wavelength limit, such that

$$\begin{aligned}
\lim_{kr\to 0}\left\{\boldsymbol{\alpha}\cdot\boldsymbol{a}'^{(1)}_{JM}(\hat{r}) - \frac{1}{c}\phi'^{(1)}_{JM}(\boldsymbol{r})\right\} &= \lim_{kr\to 0}\frac{1}{c}\phi'^{(1)}_{JM}(\boldsymbol{r}) \\
&= i\sqrt{\frac{J+1}{J}}\frac{(kr)^J}{(2J+1)!!}Y_{JM}(\hat{r}) \\
&= i\sqrt{\frac{(2J+1)(J+1)}{4\pi J}}\frac{k^J}{(2J+1)!!}Q_{JM}(\boldsymbol{r}),
\end{aligned}$$

with the electric J-pole moment operator $Q_{JM}(\boldsymbol{r})$ being defined in a spherical basis

$$Q_{JM}(\boldsymbol{r}) = r^J C_{JM}(\hat{r}),$$

and

$$C_{JM}(\hat{r}) = \sqrt{\frac{4\pi}{2J+1}}Y_{JM}(\hat{r}).$$

For the magnetic multipole transitions,

$$\begin{aligned}
\lim_{kr\to 0}\boldsymbol{a}'^{(0)}_{JM}(\hat{r}) &= \lim_{kr\to 0}\boldsymbol{a}^{(0)}_{JM}(\hat{r}) \\
&= \lim_{kr\to 0}\left\{j_J(kr)\boldsymbol{Y}^{(0)}_{JM}(\hat{r})\right\} \\
&= \frac{(kr)^J}{(2J+1)!!}\boldsymbol{Y}^{(0)}_{JM}(\hat{r}).
\end{aligned}$$

Therefore, the following holds

$$\lim_{kr\to 0}\left\{\boldsymbol{\alpha}\cdot\boldsymbol{a}'^{(0)}_{JM}(\hat{r})\right\} = \frac{(kr)^J}{(2J+1)!!}\left\{\boldsymbol{\alpha}\cdot\boldsymbol{Y}^{(0)}_{JM}(\hat{r})\right\}.$$

E.2.2 Multipole transition operators

No matter which gauge we are considering, the multipole interaction can be rewritten as

$$\begin{aligned}
\left\{\boldsymbol{\alpha}\cdot\boldsymbol{a}'^{(\lambda)}_{JM}(\hat{r}) - \frac{1}{c}\phi'^{(\lambda)}_{JM}(\boldsymbol{r})\right\} &= \sqrt{\frac{(2J+1)(J+1)}{4\pi J}}\frac{k^J}{(2J+1)!!}q^{(\lambda)}_{JM}(\boldsymbol{r}), \\
&= \sqrt{\frac{(2J+1)(J+1)}{4\pi J}}t^{(\lambda)}_{JM}(\boldsymbol{r}),
\end{aligned}$$

with $t^{(\lambda)}_{JM}(\boldsymbol{r})$ being the dimensionless multipole-transition operator and $q^{(\lambda)}_{JM}(\boldsymbol{r},\omega)$ the frequency-dependent multipole-moment operators. These two kinds of operators satisfy the following relation:

$$q^{(\lambda)}_{JM}(\boldsymbol{r}) \;=\; \frac{(2J+1)!!}{k^J} t^{(\lambda)}_{JM}(\boldsymbol{r}),$$

With such definition, we know that

$$t^{(\lambda)}_{JM}(\boldsymbol{r}) \;=\; \sqrt{\frac{4\pi J}{(2J+1)(J+1)}} \left\{ \boldsymbol{\alpha}\cdot \boldsymbol{a}'^{(\lambda)}_{JM}(\hat{r}) - \frac{1}{c}\phi'^{(\lambda)}_{JM}(\boldsymbol{r}) \right\}.$$

For $\lambda = 0$, the transition operators are

$$t^{(0)}_{JM}(\boldsymbol{r}) \;=\; \sqrt{\frac{4\pi J}{(2J+1)(J+1)}} j_J(kr) \left\{ \boldsymbol{\alpha}\cdot \boldsymbol{Y}^{(0)}_{JM}(\hat{r}) \right\}. \tag{E.43}$$

For $\lambda = 1$, we have

$$\begin{aligned} t^{(1)}_{JM}(\boldsymbol{r}) \;=\; & -\sqrt{\frac{4\pi J}{(2J+1)(J+1)}} j_{J+1}(kr) \left\{ \boldsymbol{\alpha}\cdot \boldsymbol{Y}^{(1)}_{JM}(\hat{r}) - \frac{\sqrt{J+1}}{J} \boldsymbol{\alpha}\cdot \boldsymbol{Y}^{(-1)}_{JM}(\hat{r}) \right\} \\ & + i\sqrt{\frac{4\pi J}{(2J+1)(J+1)}} \frac{\sqrt{J+1}}{J} j_J(kr) Y_{JM}(\hat{r}). \end{aligned} \tag{E.44}$$

Remember that the Einstein A coefficient is

$$A_{ba} \;=\; \frac{\alpha}{2\pi}\omega \left\langle |T_{ba}|^2 \right\rangle = 8\pi\alpha\omega \sum_{JM\lambda} \left| \left[T^{(\lambda)}_{JM} \right]_{ba} \right|^2,$$

with

$$\begin{aligned} \left[T^{(\lambda)}_{JM} \right]_{ba} \;&=\; \int \mathrm{d}\boldsymbol{r} \psi^\dagger_b \left\{ \boldsymbol{\alpha}\cdot \boldsymbol{a}'^{(\lambda)}_{JM}(\hat{r}) - \frac{1}{c}\phi'^{(\lambda)}_{JM}(\boldsymbol{r}) \right\} \psi_a \\ &=\; \sqrt{\frac{(2J+1)(J+1)}{4\pi J}} \int \mathrm{d}\boldsymbol{r} \psi^\dagger_b t^{(\lambda)}_{JM}(\boldsymbol{r}) \psi_a, \end{aligned}$$

and with the matrix elements

$$\int \mathrm{d}\boldsymbol{r} \psi^\dagger_b t^{(\lambda)}_{JM}(\boldsymbol{r}) \psi_a \;=\; \left\langle \psi_b \right| t^{(\lambda)}_{JM}(\boldsymbol{r}) \left| \psi_a \right\rangle$$

Here, the Dirac wave function can be written in spherical coordinates as [115]

$$\psi^\dagger_b(\boldsymbol{r}) \;=\; \frac{1}{r} \left[-iP_{n_b\kappa_b}(r)\Omega^\dagger_{\kappa_b m_b}(\hat{r}), Q_{n_b\kappa_b}(r)\Omega^\dagger_{-\kappa_b m_b}(\hat{r}) \right], \tag{E.45}$$

$$\psi_a(\boldsymbol{r}) \;=\; \frac{1}{r} \begin{bmatrix} iP_{n_a\kappa_a}(r)\Omega_{\kappa_a m_a}(\hat{r}) \\ Q_{n_a\kappa_a}(r)\Omega_{-\kappa_a m_a}(\hat{r}) \end{bmatrix}, \tag{E.46}$$

with the radial functions $P_{n_a\kappa_a}(r)$ and $Q_{n_a\kappa_a}(r)$, and the spherical spinor $\Omega_{\kappa_a m_a}(\hat{r})$. Then we know that for $\lambda = 0$, the matrix element is

$$
\begin{aligned}
& \int \mathrm{d}\boldsymbol{r}\psi_b^\dagger t_{JM}^{(0)}(\boldsymbol{r})\psi_a \\
= & \int \mathrm{d}\boldsymbol{r}\left\{\frac{1}{r}\left[-iP_{n_b\kappa_b}(r)\Omega_{\kappa_b m_b}^\dagger(\hat{r}), Q_{n_b\kappa_b}(r)\Omega_{-\kappa_b m_b}^\dagger(\hat{r})\right]\right. \\
& \left.\times\sqrt{\frac{4\pi J}{(2J+1)(J+1)}}j_J(kr)\begin{bmatrix} 0, \boldsymbol{\sigma}\cdot\boldsymbol{Y}_{JM}^{(0)}(\hat{r}) \\ \boldsymbol{\sigma}\cdot\boldsymbol{Y}_{JM}^{(0)}(\hat{r}), 0 \end{bmatrix}\frac{1}{r}\begin{bmatrix} iP_{n_a\kappa_a}(r)\Omega_{\kappa_a m_a}(\hat{r}) \\ Q_{n_a\kappa_a}(r)\Omega_{-\kappa_a m_a}(\hat{r}) \end{bmatrix}\right\} \\
= & \int r^2\mathrm{d}r\int\sin\theta\mathrm{d}\theta\int\mathrm{d}\phi\left\{\sqrt{\frac{4\pi J}{(2J+1)(J+1)}}j_J(kr)\frac{1}{r^2}\right. \\
& \left.\times\left[-iP_{n_b\kappa_b}(r)\Omega_{\kappa_b m_b}^\dagger(\hat{r}), Q_{n_b\kappa_b}(r)\Omega_{-\kappa_b m_b}^\dagger(\hat{r})\right]\begin{bmatrix} 0, \boldsymbol{\sigma}\cdot\boldsymbol{Y}_{JM}^{(0)}(\hat{r}) \\ \boldsymbol{\sigma}\cdot\boldsymbol{Y}_{JM}^{(0)}(\hat{r}), 0 \end{bmatrix}\begin{bmatrix} iP_{n_a\kappa_a}(r)\Omega_{\kappa_a m_a}(\hat{r}) \\ Q_{n_a\kappa_a}(r)\Omega_{-\kappa_a m_a}(\hat{r}) \end{bmatrix}\right\} \\
= & \int \mathrm{d}r\int\sin\theta\mathrm{d}\theta\int\mathrm{d}\phi\left\{\sqrt{\frac{4\pi J}{(2J+1)(J+1)}}j_J(kr)\right. \\
& \left.\times\left[Q_{n_b\kappa_b}(r)\Omega_{-\kappa_b m_b}^\dagger(\hat{r})\boldsymbol{\sigma}\cdot\boldsymbol{Y}_{JM}^{(0)}(\hat{r}), -iP_{n_b\kappa_b}(r)\Omega_{\kappa_b m_b}^\dagger(\hat{r})\boldsymbol{\sigma}\cdot\boldsymbol{Y}_{JM}^{(0)}(\hat{r})\right]\begin{bmatrix} iP_{n_a\kappa_a}(r)\Omega_{\kappa_a m_a}(\hat{r}) \\ Q_{n_a\kappa_a}(r)\Omega_{-\kappa_a m_a}(\hat{r}) \end{bmatrix}\right\} \\
= & \int \mathrm{d}r\int\sin\theta\mathrm{d}\theta\int\mathrm{d}\phi\sqrt{\frac{4\pi J}{(2J+1)(J+1)}}j_J(kr) \\
& \times i\left\{Q_{n_b\kappa_b}(r)\Omega_{-\kappa_b m_b}^\dagger(\hat{r})\boldsymbol{\sigma}\cdot\boldsymbol{Y}_{JM}^{(0)}(\hat{r})P_{n_a\kappa_a}(r)\Omega_{\kappa_a m_a}(\hat{r})\right. \\
& \left.-P_{n_b\kappa_b}(r)\Omega_{\kappa_b m_b}^\dagger(\hat{r})\boldsymbol{\sigma}\cdot\boldsymbol{Y}_{JM}^{(0)}(\hat{r})Q_{n_a\kappa_a}(r)\Omega_{-\kappa_a m_a}(\hat{r})\right\} \\
= & \int\sin\theta\mathrm{d}\theta\int\mathrm{d}\phi\sqrt{\frac{4\pi J}{(2J+1)(J+1)}} \\
& \times i\int\mathrm{d}r j_J(kr)\left\{Q_{n_b\kappa_b}(r)\Omega_{-\kappa_b m_b}^\dagger(\hat{r})\boldsymbol{\sigma}\cdot\boldsymbol{L}\frac{1}{\sqrt{J(J+1)}}Y_{JM}(\hat{r})P_{n_a\kappa_a}(r)\Omega_{\kappa_a m_a}(\hat{r})\right. \\
& \left.-P_{n_b\kappa_b}(r)\Omega_{\kappa_b m_b}^\dagger(\hat{r})\boldsymbol{\sigma}\cdot\boldsymbol{L}\frac{1}{\sqrt{J(J+1)}}Y_{JM}(\hat{r})Q_{n_a\kappa_a}(r)\Omega_{-\kappa_a m_a}(\hat{r})\right\} \\
= & \int\sin\theta\mathrm{d}\theta\int\mathrm{d}\phi\sqrt{\frac{4\pi}{(2J+1)(J+1)^2}} \\
& \times i\int\mathrm{d}r j_J(kr)\left\{Q_{n_b\kappa_b}(r)\Omega_{-\kappa_b m_b}^\dagger(\hat{r})\left(\kappa_b-1\right)Y_{JM}(\hat{r})P_{n_a\kappa_a}(r)\Omega_{\kappa_a m_a}(\hat{r})\right. \\
& \left.-P_{n_b\kappa_b}(r)\Omega_{\kappa_b m_b}^\dagger(\hat{r})\left(-\kappa_b-1\right)Y_{JM}(\hat{r})Q_{n_a\kappa_a}(r)\Omega_{-\kappa_a m_a}(\hat{r})\right\} \\
= & \int\sin\theta\mathrm{d}\theta\int\mathrm{d}\phi\sqrt{\frac{4\pi}{(2J+1)}}\Omega_{-\kappa_b m_b}^\dagger(\hat{r})Y_{JM}(\hat{r})\Omega_{\kappa_a m_a}(\hat{r}) \\
& \times i\int\mathrm{d}r\frac{\kappa_b+\kappa_a}{(J+1)}j_J(kr)\left\{Q_{n_b\kappa_b}(r)P_{n_a\kappa_a}(r)+P_{n_b\kappa_b}(r)Q_{n_a\kappa_a}(r)\right\} \\
= & i\sqrt{\frac{4\pi}{(2J+1)}}\left\langle-\kappa_b m_b\right|Y_{JM}(\hat{r})\left|\kappa_a m_a\right\rangle\times\int\mathrm{d}r\frac{\kappa_b+\kappa_a}{(J+1)}j_J(kr)\left\{Q_{n_b\kappa_b}(r)P_{n_a\kappa_a}(r)+P_{n_b\kappa_b}(r)Q_{n_a\kappa_a}(r)\right\} \\
= & i\left\langle-\kappa_b m_b\right|C_{JM}(\hat{r})\left|\kappa_a m_a\right\rangle\times\int\mathrm{d}r\frac{\kappa_b+\kappa_a}{(J+1)}j_J(kr)\left\{Q_{n_b\kappa_b}(r)P_{n_a\kappa_a}(r)+P_{n_b\kappa_b}(r)Q_{n_a\kappa_a}(r)\right\}
\end{aligned}
$$

$$
\begin{aligned}
&= i(-1)^{-\kappa_b - m_b} \begin{pmatrix} -\kappa_b, J, \kappa_a \\ -m_b, M, m_a \end{pmatrix} \langle -\kappa_b | \, | C_J(\hat{r}) | \, | \kappa_a \rangle \\
&\quad \times \int \mathrm{d}r \frac{\kappa_b + \kappa_a}{(J+1)} j_J(kr) \left\{ Q_{n_b\kappa_b}(r) P_{n_a\kappa_a}(r) + P_{n_b\kappa_b}(r) Q_{n_a\kappa_a}(r) \right\}
\end{aligned}
$$

with the reduced matrix elements

$$
\langle l_1 | \, | C_J(\hat{r}) | \, | l_2 \rangle = (-1)^{l_b} \sqrt{(2l_1+1)(2l_2+1)} \begin{pmatrix} l_1, J, l_2 \\ 0, 0, 0 \end{pmatrix}. \tag{E.47}
$$

If we define the following reduced matrix element

$$
\begin{aligned}
&\langle \psi_b \parallel t_J^{(0)}(\boldsymbol{r}) \parallel \psi_a \rangle \\
&= \langle -\kappa_b \parallel C_J(\hat{r}) \parallel \kappa_a \rangle \int \mathrm{d}r \frac{\kappa_b + \kappa_a}{(J+1)} j_J(kr) \left\{ Q_{n_b\kappa_b}(r) P_{n_a\kappa_a}(r) + P_{n_b\kappa_b}(r) Q_{n_a\kappa_a}(r) \right\},
\end{aligned}
$$

one will have

$$
\langle \psi_b | \, t_{JM}^{(0)}(\boldsymbol{r}) \, | \psi_a \rangle = i(-1)^{-\kappa_b - m_b} \begin{pmatrix} -\kappa_b, J, \kappa_a \\ -m_b, M, m_a \end{pmatrix} \langle \psi_b \parallel t_J^{(0)}(\boldsymbol{r}) \parallel \psi_a \rangle . \tag{E.48}
$$

Let us Set

$$
A_{ba} = \left[A_J^{(\lambda)} \right]_{ba},
$$

with

$$
\begin{aligned}
\left[A_J^{(\lambda)} \right]_{ba} &= 8\pi\alpha\omega \sum_M \left| \left[T_{JM}^{(\lambda)} \right]_{ba} \right|^2 \\
&= 2\alpha\omega \frac{[J]}{[J_a]} \frac{J+1}{J} \left| \langle \psi_b \parallel t_J^{(\lambda)}(\boldsymbol{r}) \parallel \psi_a \rangle \right|^2 \\
&= 2\alpha\omega \frac{(2J+1)}{[J_a]} \frac{J+1}{J} \frac{k^{2J}}{[(2J+1)!!]^2} \left| \langle \psi_b \parallel q_J^{(\lambda)}(\boldsymbol{r}) \parallel \psi_a \rangle \right|^2 \\
&= 2\alpha\omega \frac{(J+1)(2J+1)k^{2J}}{J[(2J+1)!!]^2} \frac{\left| \langle \psi_b \parallel q_J^{(\lambda)}(\boldsymbol{r}) \parallel \psi_a \rangle \right|^2}{[J_a]}
\end{aligned} \tag{E.49}
$$

By introducing the definition of the line strength of a J-pole λ-transition

$$
\left[S_J^{(\lambda)} \right]_{ba} = \left| \langle \psi_b \parallel q_J^{(\lambda)}(\boldsymbol{r}) \parallel \psi_a \rangle \right|^2, \tag{E.50}
$$

we have the following relation between the line strength and the Einstein A coefficient:

$$
\left[A_J^{(\lambda)} \right]_{ba} = 2\alpha\omega \frac{(J+1)(2J+1)k^{2J}}{J[(2J+1)!!]^2} \frac{\left[S_J^{(\lambda)} \right]_{ba}}{[J_a]}. \tag{E.51}
$$

Furthermore, we introduce the oscillator strength for a transition $a \to b$:

$$\begin{aligned}
\left[f_{JM}^{(\lambda)}\right]_{ab} &= \frac{4\pi mc^2}{\hbar\omega_{ba}} \left| \langle \psi_b | \, \boldsymbol{\alpha} \cdot \boldsymbol{a}'^{(\lambda)}_{JM}(\hat{r}) - \frac{1}{c}\phi'^{(\lambda)}_{JM}(\boldsymbol{r}) \, |\psi_a\rangle \right|^2 \\
&= \frac{4\pi mc^2}{\hbar\omega_{ba}} \left| \langle n_b, \kappa_b, m_b | \, \boldsymbol{\alpha} \cdot \boldsymbol{a}'^{(\lambda)}_{JM}(\hat{r}) - \frac{1}{c}\phi'^{(\lambda)}_{JM}(\boldsymbol{r}) \, |n_a, \kappa_a, m_a\rangle \right|^2 \\
&= \frac{4\pi mc^2}{\hbar\omega_{ba}} \left| \langle n_b, \kappa_b, m_b | \sqrt{\frac{(2J+1)(J+1)}{4\pi J}} \frac{k^J}{(2J+1)!!} q^{(\lambda)}_{JM}(\boldsymbol{r}) \, |n_a, \kappa_a, m_a\rangle \right|^2 \\
&= \frac{4\pi mc^2}{\hbar\omega_{ba}} \left| \langle n_b, \kappa_b, m_b | \sqrt{\frac{(2J+1)(J+1)}{4\pi J}} t^{(\lambda)}_{JM}(\boldsymbol{r}) \, |n_a, \kappa_a, m_a\rangle \right|^2 .
\end{aligned}$$

This means that

$$\begin{aligned}
\left[f_{JM}^{(\lambda)}\right]_{ab} &= \frac{4\pi mc^2}{\hbar\omega_{ba}} \frac{(2J+1)(J+1)}{4\pi J} \frac{k^{2J}}{[(2J+1)!!]^2} \left| \langle n_b, \kappa_b, m_b | \, q^{(\lambda)}_{JM}(\boldsymbol{r}) \, |n_a, \kappa_a, m_a\rangle \right|^2 \\
&= \frac{4\pi mc^2}{\hbar\omega_{ba}} \frac{(2J+1)(J+1)}{4\pi J} \left| \langle n_b, \kappa_b, m_b | \, t^{(\lambda)}_{JM}(\boldsymbol{r}) \, |n_a, \kappa_a, m_a\rangle \right|^2 . \qquad \text{(E.52)}
\end{aligned}$$

When the transition happens between degenerate states, the transition energy ω is the same for all the M under given J, one cannot distinguish which m_b and m_a contribute to the emission. Thus, one needs to collect oscillator strengths from all the transition channels and average over the initial substates, which gives the average oscillator strength for a single transition. This is called the reduced oscillator strength:

$$\begin{aligned}
\left[\bar{f}_J^{(\lambda)}\right]_{ba} &= \frac{1}{[J_a]} \sum_{m_a, m_b} \left[f_{JM}^{(\lambda)}\right]_{ba} \\
&= -\frac{4\pi mc^2}{\hbar\omega} \frac{(2J+1)(J+1)}{4\pi J} \frac{k^{2J}}{[(2J+1)!!]^2} \frac{1}{[J_a]} \sum_{m_a, m_b} \left| \langle n_b, \kappa_b, m_b | \, q^{(\lambda)}_{JM}(\boldsymbol{r}) \, |n_a, \kappa_a, m_a\rangle \right|^2 ,
\end{aligned} \qquad \text{(E.53)}$$

where we have assumed $\langle \psi_a|$ to be the excited state and $\langle \psi_b|$ the ground state ($\omega_{ba} = -\omega$). Concerning that the line strength is defined by

$$\begin{aligned}
\left[S_J^{(\lambda)}\right]_{ba} &= \sum_{m_a, m_b} \left| \langle n_b, \kappa_b, m_b | \, q^{(\lambda)}_{JM}(\boldsymbol{r}) \, |n_a, \kappa_a, m_a\rangle \right|^2 \\
&= \frac{[(2J+1)!!]^2}{k^{2J}} \sum_{m_a, m_b} \left| \langle n_b, \kappa_b, m_b | \, t^{(\lambda)}_{JM}(\boldsymbol{r}) \, |n_a, \kappa_a, m_a\rangle \right|^2 , \qquad \text{(E.54)}
\end{aligned}$$

one obtains

$$\begin{aligned}
\left[\bar{f}_J^{(\lambda)}\right]_{ba} &= -\frac{4\pi mc^2}{\hbar\omega} \frac{(2J+1)(J+1)}{4\pi J} \frac{k^{2J}}{[(2J+1)!!]^2} \frac{\left[S_J^{(\lambda)}\right]_{ba}}{[J_a]} \\
&= -\frac{mc^2}{\hbar\omega} \frac{(2J+1)(J+1)}{J} \frac{k^{2J}}{[(2J+1)!!]^2} \frac{\left[S_J^{(\lambda)}\right]_{ba}}{[J_a]} . \qquad \text{(E.55)}
\end{aligned}$$

This results in the general relation between the Einstein A coefficient and the reduced

oscillator strength:

$$\left[A_J^{(\lambda)}\right]_{ba} = -2\alpha\frac{\hbar\omega^2}{mc^2}\left[\bar{f}_J^{(\lambda)}\right]_{ba}. \tag{E.56}$$

This relations can also be verified through atomic structure codes [105].

E.3 Nonrelativistic limit

In the Pauli approximation, the wave functions are given by [115]

$$\psi_b^\dagger(\boldsymbol{r}) \approx \phi_b^*(\boldsymbol{r})\left[1, \frac{\boldsymbol{\sigma}\cdot\boldsymbol{p}}{2mc}\right], \qquad \psi_a(\boldsymbol{r}) \approx \begin{bmatrix} 1 \\ \frac{\boldsymbol{\sigma}\cdot\boldsymbol{p}}{2mc} \end{bmatrix}\phi_a(\boldsymbol{r}). \tag{E.57}$$

where we have used the relation $\boldsymbol{\sigma}^* = \boldsymbol{\sigma}$, and the $\phi_a(\boldsymbol{r})$ and $\phi_b(\boldsymbol{r})$ are scaler wave functions.

Therefore,

$$\begin{aligned}
\left[T_{JM}^{(\lambda)}\right]_{ba} &= \int \mathrm{d}\boldsymbol{r}\phi_b^*(\boldsymbol{r})\left[1, \frac{\boldsymbol{\sigma}\cdot\boldsymbol{p}}{2mc}\right]\begin{bmatrix} 0, \boldsymbol{\sigma}\cdot\boldsymbol{a}_{JM}^{(\lambda)}(\boldsymbol{r}) \\ \boldsymbol{\sigma}\cdot\boldsymbol{a}_{JM}^{(\lambda)}(\boldsymbol{r}), 0 \end{bmatrix}\begin{bmatrix} 1 \\ \frac{\boldsymbol{\sigma}\cdot\boldsymbol{p}}{2mc} \end{bmatrix}\phi_a(\boldsymbol{r}) \\
&= \int \mathrm{d}\boldsymbol{r}\phi_b^*(\boldsymbol{r})\left[\frac{(\boldsymbol{\sigma}\cdot\boldsymbol{p})\left(\boldsymbol{\sigma}\cdot\boldsymbol{a}_{JM}^{(\lambda)}(\boldsymbol{r})\right)}{2mc}, \boldsymbol{\sigma}\cdot\boldsymbol{a}_{JM}^{(\lambda)}(\boldsymbol{r})\right]\begin{bmatrix} 1 \\ \frac{\boldsymbol{\sigma}\cdot\boldsymbol{p}}{2mc} \end{bmatrix}\phi_a(\boldsymbol{r}) \\
&= \frac{1}{2mc}\int \mathrm{d}\boldsymbol{r}\phi_b^*(\boldsymbol{r})\left((\boldsymbol{\sigma}\cdot\boldsymbol{p})\left(\boldsymbol{\sigma}\cdot\boldsymbol{a}_{JM}^{(\lambda)}(\boldsymbol{r})\right) + \left(\boldsymbol{\sigma}\cdot\boldsymbol{a}_{JM}^{(\lambda)}(\boldsymbol{r})\right)(\boldsymbol{\sigma}\cdot\boldsymbol{p})\right)\phi_a(\boldsymbol{r}).
\end{aligned}$$

Using the relation

$$(\boldsymbol{\sigma}\cdot\boldsymbol{a})(\boldsymbol{\sigma}\cdot\boldsymbol{b}) = \boldsymbol{a}\cdot\boldsymbol{b} + i\boldsymbol{\sigma}\cdot[\boldsymbol{a}\times\boldsymbol{b}], \tag{E.58}$$

one has

$$\begin{aligned}
&\left((\boldsymbol{\sigma}\cdot\boldsymbol{p})\left(\boldsymbol{\sigma}\cdot\boldsymbol{a}_{JM}^{(\lambda)}(\boldsymbol{r})\right) + \left(\boldsymbol{\sigma}\cdot\boldsymbol{a}_{JM}^{(\lambda)}(\boldsymbol{r})\right)(\boldsymbol{\sigma}\cdot\boldsymbol{p})\right) \\
= \;& \boldsymbol{p}\cdot\boldsymbol{a}_{JM}^{(\lambda)}(\boldsymbol{r}) + \boldsymbol{a}_{JM}^{(\lambda)}(\boldsymbol{r})\cdot\boldsymbol{p} + i\boldsymbol{\sigma}\cdot\left(\boldsymbol{p}\times\boldsymbol{a}_{JM}^{(\lambda)}(\boldsymbol{r}) + \boldsymbol{a}_{JM}^{(\lambda)}(\boldsymbol{r})\times\boldsymbol{p}\right)
\end{aligned} \tag{E.59}$$

E.3.1 Nonrelativistic results: magnetic multipole transition

The magnetic multipole potentials are given by

$$\begin{aligned}
\boldsymbol{a}_{JM}^{(0)}(\boldsymbol{r}) &= j_J(kr)\boldsymbol{Y}_{JM}^{(0)}(\hat{r}) = j_J(kr)\frac{1}{\sqrt{J(J+1)}}\boldsymbol{L}Y_{JM}(\hat{r}) \\
&= \frac{1}{i\hbar\sqrt{J(J+1)}}\boldsymbol{L}\left(j_J(kr)Y_{JM}(\hat{r})\right) \\
&= \frac{1}{i\hbar\sqrt{J(J+1)}}\boldsymbol{L}f,
\end{aligned} \tag{E.60}$$

with

$$f = j_J(kr)Y_{JM}(\hat{r}).$$

Therefore, the magnitude of the matrix element is

$$\begin{aligned} & \left((\boldsymbol{\sigma}\cdot\boldsymbol{p})\left(\boldsymbol{\sigma}\cdot\boldsymbol{a}^{(0)}_{JM}(\boldsymbol{r})\right)+\left(\boldsymbol{\sigma}\cdot\boldsymbol{a}^{(0)}_{JM}(\boldsymbol{r})\right)(\boldsymbol{\sigma}\cdot\boldsymbol{p})\right) \\ = & \frac{1}{i\hbar\sqrt{J(J+1)}}\left\{\boldsymbol{p}\cdot(\boldsymbol{L}f)+(\boldsymbol{L}f)\cdot\boldsymbol{p}+i\boldsymbol{\sigma}\cdot[\boldsymbol{p}\times(\boldsymbol{L}f)+(\boldsymbol{L}f)\times\boldsymbol{p}]\right\}. \end{aligned} \tag{E.61}$$

In the following, we will calculate these terms one by one. Firstly,

$$\begin{aligned} \boldsymbol{p}\cdot(\boldsymbol{L}f) &= \boldsymbol{p}\cdot[(\boldsymbol{r}\times\boldsymbol{p})f]=-\hbar^2\boldsymbol{\nabla}\cdot[(\boldsymbol{r}\times\boldsymbol{\nabla})f], \\ (\boldsymbol{L}f)\cdot\boldsymbol{p} &= \boldsymbol{p}\cdot[(\boldsymbol{r}\times\boldsymbol{p})f]=-\hbar^2[(\boldsymbol{r}\times\boldsymbol{\nabla})f]\cdot\boldsymbol{\nabla}, \\ \boldsymbol{p}\times(\boldsymbol{L}f) &= -\hbar^2\boldsymbol{\nabla}\times[(\boldsymbol{r}\times\boldsymbol{\nabla})f], \\ (\boldsymbol{L}f)\times\boldsymbol{p} &= -\hbar^2[(\boldsymbol{r}\times\boldsymbol{\nabla})f]\times\boldsymbol{\nabla}. \end{aligned}$$

The first terms can be calculated as

$$\begin{aligned} \boldsymbol{\nabla}\cdot[(\boldsymbol{r}\times\boldsymbol{\nabla})f] &= \partial_i\left[\varepsilon^i_{jk}\left(r^j\partial^k f\right)\right] \\ &= \varepsilon^i_{jk}\partial_i\left[r^j\left(\partial^k f\right)\right] \\ &= \varepsilon^i_{jk}(\delta_{ij}+r^j\partial_i)\left(\partial^k f\right) \\ &= \varepsilon^i_{ik}\left(\partial^k f\right)+\varepsilon^i_{jk}r^j\partial_i\left(\partial^k f\right) \\ &= 0-\varepsilon^k_{ji}r^j\partial_i\left(\partial^k f\right) \\ &= -(\boldsymbol{r}\times\boldsymbol{\nabla})\cdot(\boldsymbol{\nabla}f), \end{aligned}$$

the second term gives

$$\begin{aligned} [(\boldsymbol{r}\times\boldsymbol{\nabla})f]\cdot\boldsymbol{\nabla} &= \left[\varepsilon^i_{jk}\left(r^j\partial^k f\right)\right]\partial_i \\ &= \varepsilon^i_{jk}r^j\left(\partial^i\frac{\partial f}{\partial_k}-\frac{\partial^2 f}{\partial_k\partial_i}\right) \\ &= -\varepsilon^k_{ji}r^j\partial^i\frac{\partial f}{\partial_k}-\varepsilon^i_{jk}r^j\frac{\partial^2 f}{\partial_k\partial_i} \\ &= -(\boldsymbol{r}\times\boldsymbol{\nabla})\cdot(\boldsymbol{\nabla}f)-0 \\ &= -(\boldsymbol{r}\times\boldsymbol{\nabla})\cdot(\boldsymbol{\nabla}f). \end{aligned} \tag{E.62}$$

The third term reads

$$\begin{aligned} \boldsymbol{\nabla}\times[(\boldsymbol{r}\times\boldsymbol{\nabla})f] &= \varepsilon^i_{jk}\partial^i\varepsilon^k_{mn}\left[r^m(\partial^n f)\right]\cdot\hat{e}_i \\ &= \varepsilon^i_{jk}\varepsilon^k_{mn}\partial^j\left[r^m(\partial^n f)\right]\cdot\hat{e}_i \\ &= \varepsilon^i_{jk}\varepsilon^k_{mn}(\delta_{jm}+r^m\partial^j)(\partial^n f)\cdot\hat{e}_i \\ &= \varepsilon^i_{jk}\varepsilon^k_{jn}(\partial^n f)\cdot\hat{e}_i+\varepsilon^i_{jk}\varepsilon^k_{mn}r^m\partial^j(\partial^n f)\cdot\hat{e}_i \\ &= -\varepsilon^i_{jk}\varepsilon^n_{jk}(\partial^n f)\cdot\hat{e}_i+\varepsilon^i_{jk}\varepsilon^k_{mn}r^m\left[\frac{\partial^2 f}{\partial_j\partial_n}+\frac{\partial f}{\partial_n}\partial^j\right]\cdot\hat{e}_i \end{aligned}$$

$$
\begin{aligned}
&= -2\delta_{in}(\partial^n f)\cdot\hat{e}_i + \varepsilon^i_{jk}\varepsilon^k_{mn} r^m \left(\frac{\partial^2 f}{\partial_j \partial_n}\right)\cdot\hat{e}_i + \varepsilon^i_{jk}\varepsilon^k_{mn} r^m \left(\frac{\partial f}{\partial_n}\partial^j\right)\cdot\hat{e}_i \\
&= -2\boldsymbol{\nabla} f + \varepsilon^i_{jk}\varepsilon^k_{mn} r^m \left(\frac{\partial^2 f}{\partial_j \partial_n}\right)\cdot\hat{e}_i + \varepsilon^i_{jk}\varepsilon^k_{mn} r^m \left(\frac{\partial f}{\partial_n}\partial^j\right)\cdot\hat{e}_i.
\end{aligned}
\tag{E.63}
$$

The fourth term represents

$$
\begin{aligned}
[(\boldsymbol{r}\times\boldsymbol{\nabla})f]\times\boldsymbol{\nabla} &= \varepsilon^i_{jk}\left(\varepsilon^j_{mn} r^m(\partial^n f)\right)\partial^k\cdot\hat{e}_i \\
&= \varepsilon^i_{kj}\left(\varepsilon^k_{mn} r^m(\partial^n f)\right)\partial^j\cdot\hat{e}_i \\
&= -\varepsilon^i_{jk}\left(\varepsilon^k_{mn} r^m(\partial^n f)\right)\partial^j\cdot\hat{e}_i.
\end{aligned}
$$

Thus also use

$$
\boldsymbol{\nabla}\times[(\boldsymbol{r}\times\boldsymbol{\nabla})f] + [(\boldsymbol{r}\times\boldsymbol{\nabla})f]\times\boldsymbol{\nabla} = -2\boldsymbol{\nabla} f + \varepsilon^i_{jk}\varepsilon^k_{mn} r^m\left(\frac{\partial^2 f}{\partial_j\partial_n}\right)\cdot\hat{e}_i. \tag{E.64}
$$

Furthermore,

$$
\begin{aligned}
\varepsilon^i_{jk}\varepsilon^k_{mn} r^m\left(\frac{\partial^2 f}{\partial_j\partial_n}\right)\cdot\hat{e}_i &= -\varepsilon^k_{ji}\varepsilon^k_{mn} r^m\left(\frac{\partial^2 f}{\partial_j\partial_n}\right)\cdot\hat{e}_i \\
&= -(\delta_{jm}\delta_{in}-\delta_{jn}\delta_{im}) r^m\left(\frac{\partial^2 f}{\partial_j\partial_n}\right)\cdot\hat{e}_i \\
&= -r^m\left(\frac{\partial^2 f}{\partial_m\partial_n}\right)\cdot\hat{e}_n + r^m\left(\frac{\partial^2 f}{\partial_n\partial_n}\right)\cdot\hat{e}_m \\
&= -\left(\partial_n r^m\frac{\partial f}{\partial_m} - \delta_{nm}\frac{\partial f}{\partial_m}\right)\cdot\hat{e}_n + \boldsymbol{r}\cdot\nabla^2 f \\
&= -\partial_n\left(r\frac{\partial f}{\partial r}\right)\hat{e}_n + \boldsymbol{\nabla} f + \boldsymbol{r}\cdot\nabla^2 f \\
&= -\boldsymbol{\nabla}\left(r\frac{\partial f}{\partial r}\right) + \boldsymbol{\nabla} f + \boldsymbol{r}\cdot\nabla^2 f.
\end{aligned}
$$

Thus Eq. (E.64)can be rewritten as

$$
\boldsymbol{\nabla}\times[(\boldsymbol{r}\times\boldsymbol{\nabla})f] + [(\boldsymbol{r}\times\boldsymbol{\nabla})f]\times\boldsymbol{\nabla} = -\boldsymbol{\nabla} f - \boldsymbol{\nabla}\left(r\frac{\partial f}{\partial r}\right) + \boldsymbol{r}\cdot\nabla^2 f. \tag{E.65}
$$

To proceed, we calculate

$$
\begin{aligned}
\nabla^2 f &= \nabla^2\cdot[j_J(kr)Y_{JM}(\hat{r})] \\
&= \frac{1}{r^2}\left(\frac{\partial}{\partial r}\left(r^2\frac{\partial}{\partial r}\right) - \frac{\boldsymbol{L}^2}{\hbar^2}\right)\cdot[j_J(kr)Y_{JM}(\hat{r})] \\
&= \frac{1}{r^2}\left\{\left[\frac{\partial}{\partial r}\left(r^2\frac{\partial}{\partial r}\right)j_J(kr)\right]Y_{JM}(\hat{r}) - \frac{j_J(kr)}{\hbar^2}\boldsymbol{L}^2 Y_{JM}(\hat{r})]\right\},
\end{aligned}
$$

with

$$\begin{aligned}
&\frac{\partial}{\partial r}\left(r^2\frac{\partial}{\partial r}\right)j_J(kr)\\
=\;&\frac{\partial}{\partial r}\left(r^2\frac{\partial}{\partial r}j_J(kr)\right)\\
=\;&\frac{\partial}{\partial z}z^2\left(\frac{\partial}{\partial z}j_J(z)\right)\\
=\;&\frac{\partial}{\partial z}z^2\left(\frac{J}{z}j_J(z)-j_{J+1}(z)\right)\\
=\;&2z\left(\frac{J}{z}j_J(z)-j_{J+1}(z)\right)+z^2\left(-\frac{J}{z^2}j_J(z)+\frac{J}{z}j'_J(z)-j'_{J+1}(z)\right)\\
=\;&2z\left(\frac{J}{z}j_J(z)-j_{J+1}(z)\right)+z^2\left[-\frac{J}{z^2}j_J(z)+\frac{J}{z}\left(\frac{J}{z}j_J(z)-j_{J+1}(z)\right)\right.\\
&\qquad\left.-\left(\frac{J+1}{z}j_{J+1}(z)-j_{J+2}(z)\right)\right]\\
=\;&J(J+1)j_J(z)-z(J+4)j_{J+1}(z)+z^2j_{J+2}(z)\\
=\;&J(J+1)j_J(kr)-kr(J+4)j_{J+1}(kr)+(kr)^2j_{J+2}(kr),
\end{aligned}\tag{E.66}$$

and

$$\frac{j_J(kr)}{\hbar^2}\boldsymbol{L}^2Y_{JM}(\hat{r}) \;=\; J(J+1)j_J(kr)Y_{JM}(\hat{r}).$$

Thus we obtain

$$\nabla^2 f \;=\; \frac{1}{r^2}\left(-kr(J+4)j_{J+1}(kr)+(kr)^2j_{J+2}(kr)\right)Y_{JM}(\hat{r}).$$

The other term can be reformulated as

$$\begin{aligned}
r\frac{\partial f}{\partial r} &= r\frac{\partial}{\partial r}j_J(kr)Y_{JM}(\hat{r})\\
&= z\frac{\partial}{\partial z}j_J(z)Y_{JM}(\hat{r})\\
&= z\left(\frac{J}{z}j_J(z)-j_{J+1}(z)\right)Y_{JM}(\hat{r})\\
&= \left(Jj_J(z)-zj_{J+1}(z)\right)Y_{JM}(\hat{r})\\
&= \left(Jj_J(kr)-krj_{J+1}(kr)\right)Y_{JM}(\hat{r}).
\end{aligned}$$

in the long wavelength-approximation, $kr \ll 1$, one has

$$\begin{aligned}
r\frac{\partial f}{\partial r} &= \left(Jj_J(kr)-krj_{J+1}(kr)\right)Y_{JM}(\hat{r})\\
&= Jj_J(kr)Y_{JM}(\hat{r}) = Jf
\end{aligned}$$

and

$$\boldsymbol{\nabla}\left(r\frac{\partial f}{\partial r}\right) \;\approx\; J\boldsymbol{\nabla}f \gg \boldsymbol{r}\cdot\nabla^2 f. \tag{E.67}$$

Therefore, $\boldsymbol{r}\cdot\nabla^2 f$ can be taken to be zero. This yields the result

$$\boldsymbol{\nabla}\times[(\boldsymbol{r}\times\boldsymbol{\nabla})f]+[(\boldsymbol{r}\times\boldsymbol{\nabla})f]\times\boldsymbol{\nabla} \approx -(J+1)\boldsymbol{\nabla}f. \tag{E.68}$$

All together, we have

$$\begin{aligned}
&\left((\boldsymbol{\sigma}\cdot\boldsymbol{p})\left(\boldsymbol{\sigma}\cdot\boldsymbol{a}^{(0)}_{JM}(\boldsymbol{r})\right)+\left(\boldsymbol{\sigma}\cdot\boldsymbol{a}^{(0)}_{JM}(\boldsymbol{r})\right)(\boldsymbol{\sigma}\cdot\boldsymbol{p})\right)\\
=&\ \frac{1}{i\hbar\sqrt{J(J+1)}}\left\{\boldsymbol{p}\cdot(\boldsymbol{L}f)+(\boldsymbol{L}f)\cdot\boldsymbol{p}+i\boldsymbol{\sigma}\left[\boldsymbol{p}\times(\boldsymbol{L}f)+(\boldsymbol{L}f)\times\boldsymbol{p}\right]\right\}\\
=&\ \frac{\hbar^2}{i\hbar\sqrt{J(J+1)}}\left\{2(\boldsymbol{r}\times\boldsymbol{\nabla})+i(J+1)\boldsymbol{\sigma}\right\}\cdot(\boldsymbol{\nabla}f)\\
=&\ \frac{1}{\sqrt{J(J+1)}}\left\{-i\hbar 2(\boldsymbol{r}\times\boldsymbol{\nabla})+\hbar(J+1)\boldsymbol{\sigma}\right\}\cdot(\boldsymbol{\nabla}f)\\
=&\ \frac{1}{\sqrt{J(J+1)}}\left\{2\boldsymbol{L}+(J+1)2\boldsymbol{S}\right\}\cdot(\boldsymbol{\nabla}f)\\
=&\ \sqrt{\frac{J+1}{J}}\left\{\frac{2}{J+1}\boldsymbol{L}+2\boldsymbol{S}\right\}\cdot(\boldsymbol{\nabla}f),
\end{aligned}$$

where we have used the relation $\boldsymbol{S}=\frac{1}{2}\hbar\boldsymbol{\sigma}$ for the spin operator. Therefore Therefore,

$$\begin{aligned}
\left[T^{(0)}_{JM}\right]_{ba} &= \frac{1}{2mc}\int \mathrm{d}\boldsymbol{r}\phi^*_b(\boldsymbol{r})\left((\boldsymbol{\sigma}\cdot\boldsymbol{p})\left(\boldsymbol{\sigma}\cdot\boldsymbol{a}^{(\lambda)}_{JM}(\boldsymbol{r})\right)+\left(\boldsymbol{\sigma}\cdot\boldsymbol{a}^{(\lambda)}_{JM}(\boldsymbol{r})\right)(\boldsymbol{\sigma}\cdot\boldsymbol{p})\right)\phi_a(\boldsymbol{r})\\
&= \frac{1}{2mc}\int \mathrm{d}\boldsymbol{r}\phi^*_b(\boldsymbol{r})\sqrt{\frac{J+1}{J}}\left\{\frac{2}{J+1}\boldsymbol{L}+2\boldsymbol{S}\right\}\cdot(\boldsymbol{\nabla}f)\,\phi_a(\boldsymbol{r}).
\end{aligned}$$

E.3.2 Nonrelativistic results: electric multipole transition

For simplicity, we just start with the long-wavelength approximation $kr\ll 1$. Then,

$$\begin{aligned}
\lim_{kr\to 0}\left\{\boldsymbol{\alpha}\cdot\boldsymbol{a}'^{(1)}_{JM}(\hat{r})-\frac{1}{c}\phi'^{(1)}_{JM}(\boldsymbol{r})\right\} &= \lim_{kr\to 0}\frac{1}{c}\phi'^{(1)}_{JM}(\boldsymbol{r})\\
&= i\sqrt{\frac{J+1}{J}}\frac{(kr)^J}{(2J+1)!!}Y_{JM}(\hat{r}).\\
&= i\sqrt{\frac{(2J+1)(J+1)}{4\pi J}}\frac{k^J}{(2J+1)!!}Q_{JM}(\boldsymbol{r}),
\end{aligned}$$

and thus

$$\begin{aligned}
\left[T^{(1)}_{JM}\right]_{ba} &= -\int \mathrm{d}\boldsymbol{r}\phi^*_b(\boldsymbol{r})\left[1,\frac{\boldsymbol{\sigma}\cdot\boldsymbol{p}}{2mc}\right]\frac{1}{c}\phi'^{(1)}_{JM}(\boldsymbol{r})\begin{bmatrix}1\\ \frac{\boldsymbol{\sigma}\cdot\boldsymbol{p}}{2mc}\end{bmatrix}\phi_a(\boldsymbol{r})\\
&= -\frac{1}{2mc}\int \mathrm{d}\boldsymbol{r}\phi^*_b(\boldsymbol{r})\left\{\frac{1}{c}\phi'^{(1)}_{JM}(\boldsymbol{r})+\frac{\boldsymbol{\sigma}\cdot\boldsymbol{p}}{2mc}\frac{1}{c}\phi'^{(1)}_{JM}(\boldsymbol{r})\frac{\boldsymbol{\sigma}\cdot\boldsymbol{p}}{2mc}\right\}\phi_a(\boldsymbol{r})\\
&\approx -\frac{1}{2mc}\int \mathrm{d}\boldsymbol{r}\phi^*_b(\boldsymbol{r})\left\{\frac{1}{c}\phi'^{(1)}_{JM}(\boldsymbol{r})\right\}\phi_a(\boldsymbol{r})\\
&= -\frac{1}{2mc}\int \mathrm{d}\boldsymbol{r}\phi^*_b(\boldsymbol{r})\left\{i\sqrt{\frac{(2J+1)(J+1)}{4\pi J}}\frac{k^J}{(2J+1)!!}Q_{JM}(\boldsymbol{r})\right\}\phi_a(\boldsymbol{r}).
\end{aligned}$$

Appendix F

Collisions between two charged particles

This Appendix follows the treatment of reference [146–148] on charged particle collisions.

F.1 Elastic two-body collisions

The basic laws for two-body collisions are momentum and energy conservation

$$m_1\boldsymbol{v}_1 + m_2\boldsymbol{v}_2 = m_1\boldsymbol{v}_1' + m_2\boldsymbol{v}_2', \tag{F.1}$$

$$\frac{1}{2}m_1\boldsymbol{v}_1^2 + \frac{1}{2}m_2\boldsymbol{v}_2^2 = \frac{1}{2}m_1\boldsymbol{v}_1'^{\,2} + \frac{1}{2}m_2\boldsymbol{v}_2'^{\,2} + \Delta E. \tag{F.2}$$

For elastic collisions, $\Delta E = 0$, and for inelastic collisions $\Delta E \neq 0$. By introducing center-of-mass coordinate

$$\boldsymbol{R} = \frac{m_1\boldsymbol{r}_1 + m_2\boldsymbol{r}_2}{m_1 + m_2}, \tag{F.3}$$

with $\boldsymbol{r}_1$ and $\boldsymbol{r}_2$ the displacements of particle 1 and particle 2, one can obtain the velocity of the center-of-mass,

$$\boldsymbol{v}_{\rm c} = \dot{\boldsymbol{R}} = \frac{m_1\boldsymbol{v}_1 + m_2\boldsymbol{v}_2}{m_1 + m_2}. \tag{F.4}$$

This quantity is important because it is conserved during any collision

$$\boldsymbol{v}_{\rm c}' = \frac{m_1\boldsymbol{v}_1' + m_2\boldsymbol{v}_2'}{m_1 + m_2} = \boldsymbol{v}_{\rm c}. \tag{F.5}$$

Therefore, one can go to the center-of-mass coordinates with the mathematical description of the two conservation laws

$$M\boldsymbol{v}_{\rm c} = M\boldsymbol{v}_{\rm c}', \tag{F.6}$$

$$\frac{1}{2}M\boldsymbol{v}_{\rm c}^2 + E_{\rm r} = \frac{1}{2}M\boldsymbol{v}_{\rm c}^2 + E_{\rm r}' + \Delta E, \tag{F.7}$$

with the residual energy $E_{\rm r}$ defined as

$$\begin{aligned} E_{\rm r} &= \frac{1}{2}m_1\boldsymbol{v}_1^2 + \frac{1}{2}m_2\boldsymbol{v}_2^2 - \frac{1}{2}M\boldsymbol{v}_{\rm c}^2 \\ &= \frac{1}{2}\frac{m_1m_2}{m_1 + m_2}(\boldsymbol{v}_1 - \boldsymbol{v}_2)^2 \\ &= \frac{1}{2}\mu_{12}\boldsymbol{v}_{12}^2. \end{aligned} \tag{F.8}$$

$\mu_{12} = \frac{m_1 m_2}{m_1+m_2}$ is the reduced mass and $\boldsymbol{v}_{12} = \boldsymbol{v}_1 - \boldsymbol{v}_2$ is the relative velocity for particle 1 with respect to particle 2. From the energy conservation law, one can notice another advantage of center-of-mass coordinates in describing the collisions between two particles: for elastic collisions, $E_{\rm r} = E'_{\rm r}$ means

$$\boldsymbol{v}_{12}^2 \quad = \quad \boldsymbol{v}'_{12}{}^2. \tag{F.9}$$

The magnitude of the relative velocity is also conversed before and after the collision. Only the direction of the relative velocity may be changed under collisions. This leads us to adopt a relative coordinate by assuming that one of the particle is fixed and only consider the moving of the other particles whose (relative) speed does change before and after the collision. Only the direction of motion particle is changed after collision with the fixed particle.

In general, as mentioned above, there are several choices of coordinates to describe the two-body collision problem. It can be the laboratory coordinate, the center-of-mass coordinate, the relative coordinate where particle 1 is fixed, the relative coordinates where particle 2 is fixed, and so on. The first two coordinates (laboratory and center-of-mass) are always convenient because they satisfy Galilean transformation and does not change before and after the collisions. For the other two relative coordinates with respect to particle 1 or particle 2, one should always be careful for collisional problems because the momentum conservation law is violated. That is, though the energy is still conserved,

$$\frac{1}{2} m_1 \boldsymbol{v}_{12}^2 \quad = \quad \frac{1}{2} m_1 \boldsymbol{v}'_{12}{}^2,$$

but

$$m_1 \boldsymbol{v}_{12} \quad \neq \quad m_1 \boldsymbol{v}'_{12}, \quad \text{or} \quad m_2 \boldsymbol{v}_{21} \neq m_2 \boldsymbol{v}'_{21}.$$

The reason is that the velocity of each of the particles has been changed after the collision, so the transformations from a laboratory coordinate to the relative coordinates, before and after collision, are different. Any physical law adopted in laboratory coordinates should account for extra coordinate transformation terms.

However, there is one extreme case where the relative coordinate becomes equivalent to the center-of-mass coordinate. This is true when the masses of the two particles are different from each other by orders of magnitude. As an example, we assume $m_1 \ll m_2$. Because during the collision $r_1 \sim r_2$, then

$$\boldsymbol{R} \quad = \quad \frac{m_1 \boldsymbol{r}_1 + m_2 \boldsymbol{r}_2}{m_1 + m_2} \approx \frac{m_2 \boldsymbol{r}_2}{m_1} = \boldsymbol{r}_2. \tag{F.10}$$

F.1.1 Change in relative velocity

Assuming that the relative velocity is along the $\hat{z}$ direction, $\boldsymbol{v}_{12} = v_{12}\hat{z}$, the relative velocity after the collision can be written in the form

$$\boldsymbol{v}'_{12} \quad = \quad v_{12}(\sin\theta\cos\phi\hat{x} + \sin\theta\sin\phi\hat{y} + \cos\theta\hat{z}). \tag{F.11}$$

This gives the change in relative velocity as

$$\Delta\boldsymbol{v}_{12} \quad = \quad \boldsymbol{v}'_{12} - \boldsymbol{v}_{12} = v_{12}(\sin\theta\cos\phi\hat{x} + \sin\theta\sin\phi\hat{y} + (\cos\theta - 1)\hat{z}). \tag{F.12}$$

F.1.2 Change in momentum

According to momentum conservation, the momentum of particle 1 has been changed by

$$\Delta \boldsymbol{p}_1 = m_1(\boldsymbol{v}_1' - \boldsymbol{v}_1) = -m_2(\boldsymbol{v}_2' - \boldsymbol{v}_2) = -\Delta \boldsymbol{p}_2.$$

Considering that

$$\boldsymbol{v}_1 = \boldsymbol{v}_{12} - \boldsymbol{v}_2, \qquad \boldsymbol{v}_1' = \boldsymbol{v}_{12}' - \boldsymbol{v}_2'$$

one has

$$\begin{aligned} \Delta \boldsymbol{p}_1 &= m_1(\boldsymbol{v}_1' - \boldsymbol{v}_1) \\ &= m_1(\boldsymbol{v}_{12}' - \boldsymbol{v}_{12}) + m_1(\boldsymbol{v}_2' - \boldsymbol{v}_2) \\ &= m_1 \Delta \boldsymbol{v}_{12} + \frac{m_1}{m_2} m_2(\boldsymbol{v}_2' - \boldsymbol{v}_2) \\ &= m_1 \Delta \boldsymbol{v}_{12} - \frac{m_1}{m_2} \Delta \boldsymbol{p}_1. \end{aligned}$$

This means that

$$\left(1 + \frac{m_1}{m_2}\right) \Delta \boldsymbol{p}_1 = m_1 \Delta \boldsymbol{v}_{12},$$

and

$$\Delta \boldsymbol{p}_1 = \frac{m_1 m_2}{m_1 + m_2} \Delta \boldsymbol{v}_{12} = \mu_{12} \Delta \boldsymbol{v}_{12} = -\Delta \boldsymbol{p}_2.$$

The relations above account for the total momentum transfer between the two particles during the collision.

F.1.3 Change in energy

To calculate the energy transfered between the two particles after the collision, one first has the relation

$$\begin{aligned} \Delta E_1 &= \frac{1}{2} m_1 \boldsymbol{v}_1^2 - \frac{1}{2} m_1 \boldsymbol{v}_1'^{\,2} \\ &= \frac{1}{2} m_1 (\boldsymbol{v}_1 + \boldsymbol{v}_1')(\boldsymbol{v}_1 - \boldsymbol{v}_1') \\ &= -\frac{1}{2} \Delta \boldsymbol{p}_1 (\boldsymbol{v}_1 + \boldsymbol{v}_1'). \end{aligned} \tag{F.13}$$

Similarly, for particle 2, we have

$$\Delta E_2 = -\frac{1}{2} \Delta \boldsymbol{p}_2 (\boldsymbol{v}_2 + \boldsymbol{v}_2') = \frac{1}{2} \Delta \boldsymbol{p}_1 (\boldsymbol{v}_2 + \boldsymbol{v}_2') = -\Delta E_1. \tag{F.14}$$

We can notice that, on the one hand

$$m_1\Delta E_1 - m_2\Delta E_2 = m_1\Delta E_1 + m_2\Delta E_1 = M\Delta E_1,$$

on the other hand

$$\begin{aligned} m_1\Delta E_1 - m_2\Delta E_2 &= -\frac{m_1}{2}\Delta\boldsymbol{p}_1(\boldsymbol{v}_1+\boldsymbol{v}_1') - \frac{m_2}{2}\Delta\boldsymbol{p}_1(\boldsymbol{v}_2+\boldsymbol{v}_2') \\ &= -\frac{1}{2}\Delta\boldsymbol{p}_1\left(m_1\boldsymbol{v}_1 + m_2\boldsymbol{v}_2 + m_1\boldsymbol{v}_1' + m_2\boldsymbol{v}_2'\right) \\ &= -\frac{1}{2}\Delta\boldsymbol{p}_1\left(M\boldsymbol{v}_\mathrm{c} + M\boldsymbol{v}_\mathrm{c}'\right) \\ &= -\Delta\boldsymbol{p}_1 M\boldsymbol{v}_\mathrm{c}. \end{aligned}$$

Combining the two results, one obtains the energy transfer between the two particles as

$$\Delta E_1 = -\Delta\boldsymbol{p}_1\boldsymbol{v}_\mathrm{c} = -\boldsymbol{v}_\mathrm{c}\mu_{12}\Delta\boldsymbol{v}_{12} = -\Delta E_2.$$

F.2 Differential cross section

For the collision of two charged-particles with Coulomb interaction, the differential scattering cross section is given by the Rutherford formula [146–148]

$$\sigma_{12} = \frac{b_\perp^2}{4\sin^4\frac{\theta}{2}}, \tag{F.15}$$

with

$$b_\perp = \frac{Z_1 Z_2 e^2}{4\pi\varepsilon_0\mu_{12}v_{12}^2}, \tag{F.16}$$

Z_1, Z_2 are the charges of the two particles, $\mu_{12} = \frac{m_1 m_2}{m_1+m_2}$ is the reduced mass, and v_{12} is the relative velocity between the two particles.

From this formula, one can notice that the differential cross section goes to infinity either for small scattering angles or for small relative velocities. Small scattering angles correspond to large impact parameters which is always the case for long-range interactions like Coulomb potential. To remove this singularity, one needs to take the screening effect into consideration. In a plasma, the potential decays approximately according to

$$U(r) \propto \frac{e^{-r/\lambda_\mathrm{D}}}{r}, \quad \text{instead of} \quad \frac{1}{r}.$$

Interaction for distances outside of the Debye radius λ_D is negligible because of the screening effect.

The reason for large differential cross sections at small relative velocities is that the interaction time for small velocities is much longer than that for large velocities. Thus, the scattering is more efficient than in the large velocity case. This can be seen from the relatively larger impact parameter $b_\perp$ for 90° scattering. However, the calculation is based on the impact approximation where we assume that the time for scattering is much shorter than the other time scales. Thus, the cross section calculated here is not correct for very small relative velocity which breaks down the impact approximation. To avoid such problems, one needs a cut-off at the small velocity edge. One of the possible

ways is to assume that the Debye radius is much larger than $b_\perp$, giving the lower limit of the relative velocity.

We should know that this is the differential cross section for a given impact parameter and shooting velocity. Corresponding to each scattering, there are changes in different physical quantities like energy, momentum, phase, inner-state transition and scattered particle number, etc. For each physical quantity, one needs to calculate the effective total scattering cross section separately. Each of them corresponds to a relaxiation process with different time scales (as the rate of change during the collision for different quantities may be different). For example, elastic scattering usually leads to transfer of momentum and energy between the two particles. If one of the particles is more massive than the other and can be treated as fixed at the original point during the collision process, there is approximately no energy transfer and only momentum transfer is prominent.

F.3 Total cross section for number of particles being scattered

The most simple calculation is the calculation of the total cross section for the number of scattered particles at a given relative shooting velocity, which is just the integration of the differential cross section (thus integral over impact parameters). In free space, one has to integrate θ from 0 to π:

$$\begin{aligned}
\sigma_{12}^{\mathrm{n}} &= \int \mathrm{d}\Omega\sigma_{12} \\
&= 2\pi\int_0^\pi \frac{b_\perp^2}{4\sin^4\frac{\theta}{2}}\sin\theta\mathrm{d}\theta \\
&= 2\pi\int_0^\pi \frac{b_\perp^2}{4\sin^4\frac{\theta}{2}}\left(2\cos\frac{\theta}{2}\sin\frac{\theta}{2}\right)\mathrm{d}\theta \\
&= 8\pi\int_0^\pi \frac{b_\perp^2}{4\sin^3\frac{\theta}{2}}\mathrm{d}\left(\sin\frac{\theta}{2}\right) \\
&= -\pi\left.\frac{b_\perp^2}{\sin^2\frac{\theta}{2}}\right|_0^\pi \\
&= \pi b_\perp^2\left(\frac{1}{\sin^2\frac{0}{2}}-1\right)=\infty. \qquad \text{(F.17)}
\end{aligned}$$

For Coulomb potential scattering, the total cross section for the number of particles scattered diverges because the long-range Coulomb interacting makes $\sigma\to\infty$ when $\theta\to 0$. This long-range potential scatters all the particles no matter how far they would be.

When the two charged particles are immersed in a plasma, the Debye screening sets an upper limit of the interaction to be approximately the Debye radius λ_{D}. Particle distances larger than the Debye radius lead to no interaction at all. This upper limit of interaction distance sets the lower limit for the scattering angle. Then, the corresponding total cross section for scattered particles is given as

$$\begin{aligned}
\sigma_{12}^{\mathrm{n}} &= -\pi\left.\frac{b_\perp^2}{\sin^2\frac{\theta}{2}}\right|_{\theta_{\min}(b_{\max})}^{\pi} \\
&= -\pi\left.\frac{b_\perp^2}{\sin^2\frac{\theta}{2}}\right|_{\theta_{\min}(\lambda_{\mathrm{D}})}^{\pi}
\end{aligned}$$

$$= \pi b_\perp^2 \left(\frac{1}{\sin^2 \frac{\theta_{\min}(\lambda_D)}{2}} - 1 \right). \tag{F.18}$$

Using the relation between the scattering angle and the impact parameter

$$\tan\frac{\theta}{2} = \frac{b_\perp}{b},$$

one has $\sin\frac{\theta_{\min}}{2} \approx \frac{b_\perp}{\lambda_D}$ when $\lambda_D \gg b_\perp$. This gives

$$\begin{aligned} \sigma_{12}^{n} &= \pi b_\perp^2 \left(\frac{\lambda_D^2}{b_\perp^2} - 1 \right) \\ &= \pi \left(\lambda_D^2 - b_\perp^2 \right). \end{aligned} \tag{F.19}$$

The reason we have a cross section of $\pi\left(\lambda_D^2 - b_\perp^2\right)$ instead of $\pi\lambda_D^2$ may come from our approximation $\sin\frac{\theta_{\min}}{2} \approx \frac{b_\perp}{\lambda_D}$. Because $\lambda_D \gg b_\perp$, one could continue to use approximation and get

$$\sigma_{12}^{n} = \pi\lambda_D^2 \tag{F.20}$$

which means that the total cross section for the number of particles being scattered is just the area of the full ineraction range. One can also calculate the cross section for backward scattering which accounts for all the particles scattered into $(\pi/2, \pi)$:

$$\begin{aligned} \sigma_{12}^{n'} &= \pi b_\perp^2 \left(\frac{1}{\sin^2 \frac{\pi}{4}} - 1 \right) \\ &= \pi b_\perp^2. \end{aligned} \tag{F.21}$$

F.4 Total cross section for momentum transfer

During each collision, there is momentum transfer between the two particles. To calculate the effective total cross section for momentum transfer, one should first calculate the momentum transfer for each specific collision characterized by the impact parameter, velocity and particle species. Subsequently average over different velocities when thermal effects are taken into consideration.

F.4.1 Momentum transfer: single velocity

First consider the case of a particle beam in which that all the particles are moving in a single direction with fixed velocity. Scatterings of these particles with the target particles lead to momentum loss. Assume the relative velocity before collision is along $\hat{\boldsymbol{z}}$, and the scattering is elastic $v_{12} = v'_{12}$. One will have the relative velocity after the collision as

$$\boldsymbol{v}'_{12} = v_{12} \left(\sin\theta\cos\phi\hat{\boldsymbol{x}} + \sin\theta\sin\phi\hat{\boldsymbol{y}} + \cos\theta\hat{\boldsymbol{z}} \right); \tag{F.22}$$

then the corresponding momentum transfer is

$$\Delta \boldsymbol{p}_1 = \mu_{12}\left(\boldsymbol{v}'_{12} - \boldsymbol{v}_{12}\right) = \mu_{12}\Delta \boldsymbol{v}_{12} = -\Delta \boldsymbol{p}_2,$$

with the changes in relative velocity given as

$$\Delta \boldsymbol{v}_{12} = v_{12}\left(\sin\theta\cos\phi\hat{\boldsymbol{x}} + \sin\theta\sin\phi\hat{\boldsymbol{y}} + (\cos\theta - 1)\hat{\boldsymbol{z}}\right).$$

Based on this knowledge, the total momentum change of particle 1 after collision with different impact parameters is given as

$$\begin{aligned}\langle \Delta \boldsymbol{p}_1 \rangle &= \int_0^{\pi} \sin\theta \mathrm{d}\theta \int_0^{2\pi} \mathrm{d}\phi \sigma_{12}\mu_{12}\Delta \boldsymbol{v}_{12} \\ &= -2\pi \int_0^{\pi} \sin\theta \mathrm{d}\theta \sigma_{12}\mu_{12}v_{12}(\cos\theta - 1)\hat{\boldsymbol{z}} \\ &= -2\pi p_{12} \int_0^{\pi} \sigma_{12}(\cos\theta - 1)\sin\theta \mathrm{d}\theta \hat{\boldsymbol{z}}.\end{aligned}$$

The momentum transfer from particle 1 to particle 2 is

$$\langle \Delta \boldsymbol{p}_2 \rangle = 2\pi p_{12} \int_0^{\pi} \sigma_{12}(\cos\theta - 1)\sin\theta \mathrm{d}\theta \hat{\boldsymbol{z}}.$$

We can see that, for a given incident velocity, the effective momentum changes is just along the incident direction. All the transverse momentum changes are averaged out to be zero. For a given relative velocity, the relative momentum transfer rate is

$$\frac{\langle \Delta \boldsymbol{p}_2 \rangle}{p_{12}} = 2\pi \int_0^{\pi} \sigma_{12}(\cos\theta - 1)\sin\theta \mathrm{d}\theta \hat{\boldsymbol{z}}.$$

This leads to the definition of the effective cross section for momentum transfer as

$$\sigma_{12}^{\mathrm{m}} = \frac{\langle \Delta p_2 \rangle}{p_{12}} = 2\pi \int_0^{\pi} \sigma_{12}(\cos\theta - 1)\sin\theta \mathrm{d}\theta.$$

This can be fully evaluated as

$$\begin{aligned}\sigma_{12}^{\mathrm{m}} &= 2\pi \int_0^{\pi} \sigma_{12}(1 - \cos\theta)\sin\theta \mathrm{d}\theta \\ &= 2\pi \int_0^{\pi} \frac{b_{\perp}^2}{4\sin^4\frac{\theta}{2}} \left(2\sin^2\frac{\theta}{2}\right)\left(2\cos\frac{\theta}{2}\sin\frac{\theta}{2}\right)\mathrm{d}\theta \\ &= 2\pi b_{\perp}^2 \int_0^{\pi} \frac{1}{\sin\frac{\theta}{2}}\cos\frac{\theta}{2}\mathrm{d}\theta \\ &= 4\pi b_{\perp}^2 \left(\ln \sin\frac{\theta}{2}\right)\Big|_0^{\pi} \\ &= 4\pi b_{\perp}^2 \left(\ln \sin\frac{\pi}{2} - \ln 0\right) = \infty.\end{aligned}$$

Again, we notice that the effective cross section for momentum transfer is divergent for the long-range Coulomb interaction. If the particles are immersed in a plasma, similarly

to the previous subsection, one will have a finite cross section due to screening

$$\begin{aligned}\sigma_{12}^{\mathrm{m}} &= 4\pi b_{\perp}^2 \left(\ln \sin\frac{\theta}{2}\right)\Big|_{\theta_{\min}(\lambda_{\mathrm{D}})}^{\pi} \\ &= -4\pi b_{\perp}^2 \ln \left(\sin\frac{\theta_{\min}(\lambda_{\mathrm{D}})}{2}\right) \\ &= 4\pi b_{\perp}^2 \ln\Lambda, \end{aligned} \tag{F.23}$$

with

$$\ln\Lambda \approx \ln\frac{\lambda_{\mathrm{D}}}{b_{\perp}} \approx \ln\left(\frac{T^{3/2}}{e^2 n^{1/2}}\right) \tag{F.24}$$

being the Coulomb logarithm which has $\ln\Lambda \sim (10 \sim 20)$. We know that, on the one hand, the scattering cross section σ_{12} for particles with large distances (thus smaller scattering angles) are dominant compared to short-distance scattering; one the other hand, large distances lead to smaller scattering angles, thus a lower efficiency for modifications of the scattering particles (the term $1-\cos\theta$ for momentum transfer in the integral). When this two factors are multiplied, the contribution of the effective scattering cross section for large distances (thus small angles) tends to be reduced. However, even though it is reduced, the contribution of the total momentum transfer under long-range Coulomb potential is still dominant and render the total effective cross section divergent. So, one needs to include the screening effect in the plasma case which gives a finite cross section. Comparing to the cross section for the total number of particles scattered in Eq. (F.20), one can find that the effective cross section for momentum transfer is significantly reduced. One can calculate the ratio as

$$\frac{\sigma_{12}^{\mathrm{m}}}{\sigma_{12}^{\mathrm{n}}} = \frac{4\pi b_{\perp}^2 \ln\Lambda}{4\pi\lambda_{\mathrm{D}}^2} = \frac{b_{\perp}^2}{\lambda_{\mathrm{D}}^2}\ln\Lambda = \frac{b_{\perp}^2}{\lambda_{\mathrm{D}}^2}\ln\frac{\lambda_{\mathrm{D}}}{b_{\perp}} \approx 10\frac{b_{\perp}^2}{\lambda_{\mathrm{D}}^2}. \tag{F.25}$$

The effective cross section obtained above is the transfer rate of momentum under single scattering. Now we can calculate the effective momentum loss rate of particle 1 under a given relative velocity after a propagation distance of $\mathrm{d}l$. Before this, we first calculate the total momentum loss along $\hat{\boldsymbol{z}}$ after propagating through $\mathrm{d}l$,

$$\langle\Delta p_1\rangle_{\mathrm{d}t} = -p_{12}n_2\sigma_{12}^{\mathrm{m}}\mathrm{d}l = -p_{12}n_2\sigma_{12}^{\mathrm{m}}v_{12}\mathrm{d}t,$$

with $\mathrm{d}l = v_{12}\mathrm{d}t$. The minus sign refers to loss of momentum. The accuracy of this definition of $\mathrm{d}l$ holds if the momentum loss rate is infinitesimal so that one can treat v_{12} constant during the time duration $\mathrm{d}t$. Because the momentum of shooting particle is $p_1 = m_1 v_{12}$, one has the following equations for momentum loss of the shooting particle as

$$\frac{\mathrm{d}p_1}{\mathrm{d}t} = \frac{\langle\Delta p_1\rangle_{\mathrm{d}t}}{\mathrm{d}t} = -\nu_{12}p_1, \tag{F.26}$$

with ν_{12} the momentum loss rate given as

$$\nu_{12} = n_2\sigma_{12}^{\mathrm{m}}v_{12}\frac{\mu_{12}}{m_1}. \tag{F.27}$$

However, this definition of the momentum loss rate is not strict because both v_{12} and

σ_{12}^{m} are momentum dependent. The loss rate for a given relative velocity is nonlinear, and

$$\begin{aligned}\nu_{12} &= n_2 v_{12}\frac{\mu_{12}}{m_1}4\pi b_\perp^2\ln\Lambda \\ &= 4\pi n_2 v_{12}\frac{\mu_{12}}{m_1}\left(\frac{Z_1 Z_2 e^2}{4\pi\varepsilon_0\mu_{12}v_{12}^2}\right)^2\ln\Lambda \\ &= \frac{n_2 Z_1^2 Z_2^2 e^4}{4\pi\varepsilon_0^2 m_1\mu_{12}v_{12}^3}\ln\Lambda. \end{aligned} \tag{F.28}$$

We can see that the momentum loss rate in collision is smaller for collisions of large velocities than for that with lower velocities.

For electron-electron scattering, electron-ion scattering, ion-electron scattering and ion-ion scattering, the reduced masses are

$$\begin{aligned}\mu_{\mathrm{ee}} &= \frac{m_{\mathrm{e}}m_{\mathrm{e}}}{m_{\mathrm{e}}+m_{\mathrm{e}}} = \frac{m_{\mathrm{e}}}{2}, \\ \mu_{\mathrm{ei}} &= \mu_{\mathrm{ie}} = \frac{m_{\mathrm{e}}m_{\mathrm{i}}}{m_{\mathrm{e}}+m_{\mathrm{i}}} \approx m_{\mathrm{e}}, \\ \mu_{\mathrm{ii}} &= \frac{m_{\mathrm{i}}m_{\mathrm{i}}}{m_{\mathrm{i}}+m_{\mathrm{i}}} = \frac{m_{\mathrm{i}}}{2}, \end{aligned}$$

respectively, So, the corresponding effective loss rates are

$$\nu_{\mathrm{ee}} = \frac{n_{\mathrm{e}}e^4}{2\pi\varepsilon_0^2 m_{\mathrm{e}}^2 v_{\mathrm{ee}}^3}\ln\Lambda, \tag{F.29}$$

$$\nu_{\mathrm{ei}} = \frac{n_{\mathrm{i}}Z_{\mathrm{i}}^2 e^4}{4\pi\varepsilon_0^2 m_{\mathrm{e}}^2 v_{\mathrm{ei}}^3}\ln\Lambda, \tag{F.30}$$

$$\nu_{\mathrm{ie}} = \frac{n_{\mathrm{e}}Z_{\mathrm{i}}^2 e^4}{4\pi\varepsilon_0^2 m_{\mathrm{e}}m_{\mathrm{i}} v_{\mathrm{ie}}^3}\ln\Lambda, \tag{F.31}$$

$$\nu_{\mathrm{ii}} = \frac{n_{\mathrm{i}}Z_{\mathrm{i}}^4 e^4}{2\pi\varepsilon_0^2 m_{\mathrm{i}}^2 v_{\mathrm{ii}}^3}\ln\Lambda, \tag{F.32}$$

respectively.

F.4.2 Momentum transfer: thermal effects

In the previous Sections, all the particles in the beam are assumed to be identical and moving along the same direction. Besides the macroscopic drift velocity $\boldsymbol{v}_{\mathrm{d}}$, in reality, microscopically the particles in the beam are moving with different velocities in both magnitude and direction. It is the drift velocity that gives the macroscopic flow of the particle beam. Then, one can calculate how the collisions with target particles may lead to a macroscopic momentum loss of the particle flow.

Let us assume the distribution of the microscopic relative velocity is given by a Maxwell-Boltzmann distribution,

$$f(\boldsymbol{v}) = \sqrt{\left(\frac{\mu_{12}}{2\pi k_{\mathrm{B}}T}\right)^3}\, e^{-\frac{\mu_{12}}{2k_{\mathrm{B}}T}(\boldsymbol{v}-\boldsymbol{v}_{\mathrm{d}})^2}. \tag{F.33}$$

The total momentum change after a propagation distance of $\mathrm{d}l$ is given by

$$\langle \Delta \mathrm{P}_1 \rangle_{\mathrm{d}t}^{\mathrm{th}} = n_1 \langle \Delta p_1 \rangle_{\mathrm{d}t}^{\mathrm{th}} = n_1 \int \langle \Delta p_1 \rangle_{\mathrm{d}t} f(\boldsymbol{v}) \mathrm{d}^3 \boldsymbol{v}. \tag{F.34}$$

For the Maxwell-Boltzmann distribution, one can define the thermal velocity

$$v_{\mathrm{th}} = \sqrt{\frac{k_{\mathrm{B}} T}{\mu_{12}}} \tag{F.35}$$

to get

$$f(\boldsymbol{v}) = \frac{1}{(2\pi)^{3/2} v_{\mathrm{th}}^3} e^{-\frac{1}{2v_{\mathrm{th}}^2}(\boldsymbol{v}-\boldsymbol{v}_{\mathrm{d}})^2}. \tag{F.36}$$

By defining $\boldsymbol{u} = \boldsymbol{v}/v_{\mathrm{th}}$ and $\boldsymbol{u}_{\mathrm{d}} = \boldsymbol{v}_{\mathrm{d}}/v_{\mathrm{th}}$, one obtains

$$f(\boldsymbol{u}) = \frac{1}{(2\pi)^{3/2} v_{\mathrm{th}}^3} e^{-\frac{1}{2}(\boldsymbol{u}-\boldsymbol{u}_{\mathrm{d}})^2}. \tag{F.37}$$

Thus, with $f(\boldsymbol{v})\mathrm{d}^3\boldsymbol{v} = v_{\mathrm{th}}^3 f(\boldsymbol{u})\mathrm{d}^3\boldsymbol{u}$ the total momentum change $\langle \Delta \mathrm{P}_1 \rangle_{\mathrm{d}t}^{\mathrm{th}}$ can be written as

$$\langle \Delta \mathrm{P}_1 \rangle_{\mathrm{d}t}^{\mathrm{th}} = n_1 v_{\mathrm{th}}^3 \int \langle \Delta p_1 \rangle_{\mathrm{d}t} f(\boldsymbol{u}) \mathrm{d}^3 \boldsymbol{u}. \tag{F.38}$$

In principle, the drift velocity is much smaller than the typical thermal velocity, $\boldsymbol{u}_{\mathrm{d}} \ll 1$, so we can approximate

$$f(\boldsymbol{u}) \approx \frac{1}{(2\pi)^{3/2} v_{\mathrm{th}}^3} e^{-\frac{1}{2}\boldsymbol{u}^2}(1 + \boldsymbol{u} \cdot \boldsymbol{u}_{\mathrm{d}}). \tag{F.39}$$

Setting the drift velocity to be along $\hat{\boldsymbol{z}}$, the corresponding momentum loss along $\hat{\boldsymbol{z}}$ is given as

$$\begin{aligned}
\langle \Delta \mathrm{P}_1^z \rangle_{\mathrm{d}t}^{\mathrm{th}} &= n_1 v_{\mathrm{th}} \int \langle \Delta p_1^z \rangle_{\mathrm{d}t} f(\boldsymbol{u}) \mathrm{d}^3 \boldsymbol{u} \\
&= -n_1 v_{\mathrm{th}}^3 \mathrm{d}t \int p_{12}^z n_2 \sigma_{12}^{\mathrm{m}} v_{12} f(\boldsymbol{u}) \mathrm{d}^3 \boldsymbol{u} \\
&= -v_{\mathrm{th}}^3 \mathrm{d}t \int p_{12}^z \frac{n_1 n_2 Z_1^2 Z_2^2 e^4}{4\pi\varepsilon_0^2 \mu_{12}^2 v_{12}^3} \ln\Lambda f(\boldsymbol{u}) \mathrm{d}^3 \boldsymbol{u} \\
&= -v_{\mathrm{th}}^3 \mathrm{d}t \int p_{12}^z \frac{n_1 n_2 Z_1^2 Z_2^2 e^4}{4\pi\varepsilon_0^2 \mu_{12}^2 v_{12}^3} \ln\Lambda \frac{1 + \boldsymbol{u} \cdot \boldsymbol{u}_{\mathrm{d}}}{(2\pi)^{3/2} v_{\mathrm{th}}^3} e^{-\frac{1}{2}\boldsymbol{u}^2} \mathrm{d}^3 \boldsymbol{u} \\
&= -\mathrm{d}t \int \mu_{12} v_{12}^z \frac{n_1 n_2 Z_1^2 Z_2^2 e^4}{4\pi\varepsilon_0^2 \mu_{12}^2 v_{12}^3} \ln\Lambda \frac{1 + u_z u_{\mathrm{d}}}{(2\pi)^{3/2}} e^{-\frac{1}{2}\boldsymbol{u}^2} \mathrm{d}^3 \boldsymbol{u},
\end{aligned}$$

or

$$\begin{aligned}
\frac{\langle \Delta \mathrm{P}_1^z \rangle_{\mathrm{d}t}^{\mathrm{th}}}{\mathrm{d}t} &= -\int \mu_{12} v_{12}^z \frac{n_1 n_2 Z_1^2 Z_2^2 e^4}{4\pi\varepsilon_0^2 \mu_{12}^2 v_{12}^3} \ln\Lambda \frac{1 + u_z u_{\mathrm{d}}}{(2\pi)^{3/2}} e^{-\frac{1}{2}u^2} \mathrm{d}^3 \boldsymbol{u} \\
&= -\int n_1 m_1 v_{12}^z \nu_{12}(v_{\mathrm{th}}) \frac{v_{\mathrm{th}}^3}{v_{12}^3} \frac{1 + u_z u_{\mathrm{d}}}{(2\pi)^{3/2}} e^{-\frac{1}{2}u^2} \mathrm{d}^3 \boldsymbol{u}
\end{aligned}$$

$$
\begin{aligned}
&= -\int n_1 m_1 \nu_{12}(v_{\rm th}) \frac{v_{\rm th}^4}{v_{12}^3} \frac{u_z + u_z^2 u_{\rm d}}{(2\pi)^{3/2}} e^{-\frac{1}{2}u^2} {\rm d}^3\boldsymbol{u} \\
&= -\frac{n_1 m_1 \nu_{12}(v_{\rm th}) v_{\rm th}}{(2\pi)^{3/2}} \int \frac{u_z + u_z^2 u_{\rm d}}{u^3} e^{-\frac{1}{2}u^2} {\rm d}^3\boldsymbol{u},
\end{aligned}
$$

where $u_z = v_{12}^z / v_{\rm th}$, $u = v_{12}/v_{\rm th}$, and

$$
\nu_{12}(v_{\rm th}) = \frac{n_2 Z_1^2 Z_2^2 e^4}{4\pi\varepsilon_0^2 m_1 \mu_{12} v_{12}^3} \ln\Lambda. \tag{F.40}
$$

To continue the integration of the momentum change, one should notice that there is no sign for v_{12} (thus u), because it originates from our former calculation of the loss rate. However, u_z has signs indicating the particles are shooting the target from -$\hat{\boldsymbol{z}}$ or $\hat{\boldsymbol{z}}$. Then one can see that the first integral is

$$
\int \frac{u_z}{u^3} e^{-\frac{1}{2}u^2} {\rm d}^3\boldsymbol{u} = 0,
$$

and the average momentum change only depends on the term containing the drift effect:

$$
\begin{aligned}
\frac{\langle \Delta {\rm P}_1^z \rangle_{{\rm d}t}^{\rm th}}{{\rm d}t} &= -\frac{n_1 m_1 \nu_{12}(v_{\rm th}) v_{\rm th}}{(2\pi)^{3/2}} \int \frac{u_z^2 u_{\rm d}}{u^3} e^{-\frac{1}{2}u^2} {\rm d}^3\boldsymbol{u} \\
&= -\frac{n_1 m_1 v_{\rm d} \nu_{12}(v_{\rm th})}{(2\pi)^{3/2}} \int \frac{u_z^2}{u^3} e^{-\frac{1}{2}u^2} {\rm d}^3\boldsymbol{u}.
\end{aligned}
$$

Here, the integral can be calculated as

$$
\begin{aligned}
\int \frac{u_z^2}{u^3} e^{-\frac{1}{2}u^2} {\rm d}^3\boldsymbol{u} &= \frac{1}{3}\int \frac{u^2}{u^3} e^{-\frac{1}{2}u^2} {\rm d}^3\boldsymbol{u} \\
&= \frac{1}{3}\int \frac{1}{u} e^{-\frac{1}{2}u^2} {\rm d}^3\boldsymbol{u} \\
&= \frac{1}{3}\int_0^\infty \frac{4\pi u^2}{u} e^{-\frac{1}{2}u^2} {\rm d}u \\
&= \frac{4\pi}{3}\int_0^\infty u e^{-\frac{1}{2}u^2} {\rm d}u \\
&= \frac{4\pi}{3}.
\end{aligned}
$$

For a beam of particle of 1 shooting on a target of particles 2, the total drift momentum of particle 1 is given as ${\rm P}_1^{\rm d} = n_1 p_1^{\rm d} = n_1 m_1 v_1^{\rm d}$. So we know that

$$
\frac{\langle \Delta {\rm P}_1^z \rangle_{{\rm d}t}^{\rm th}}{{\rm d}t} = -\frac{{\rm P}_1^{\rm d} \nu_{12}(v_{\rm th})}{(2\pi)^{3/2}} \frac{4\pi}{3}.
$$

This gives the momentum loss equation for the drift momentum as

$$
\frac{\langle \Delta {\rm P}_1^z \rangle_{{\rm d}t}^{\rm th}}{{\rm d}t} = -\bar{\nu}_{12}^{\rm m} {\rm P}_1^{\rm d}, \tag{F.41}
$$

with the average loss rate of the drift momentum as

$$\bar{\nu}_{12}^{\mathrm{m}} = \frac{2}{3(2\pi)^{1/2}}\nu_{12}(v_{\mathrm{th}}). \tag{F.42}$$

The averaged momentum loss rate is approximately the loss rate under collisions with thermal velocity.

For electron-electron scattering, electron-ion scattering, ion-electron scattering and ion-ion scattering, the thermal velocities are

$$\begin{aligned} v_{\text{ee-th}} &= \sqrt{\frac{2k_{\mathrm{B}}T}{m_{\mathrm{e}}}}, \\ v_{\text{ei-th}} &= v_{\text{ie-th}} = \sqrt{\frac{k_{\mathrm{B}}T}{m_{\mathrm{e}}}}, \\ v_{\text{ii-th}} &= \sqrt{\frac{2k_{\mathrm{B}}T}{m_{\mathrm{i}}}}, \end{aligned}$$

respectively. Thus, the averaged loss rate for each types of collisions are

$$\bar{\nu}_{\mathrm{ee}}^{\mathrm{m}} = \frac{n_{\mathrm{e}}e^4\ln\Lambda}{6\pi^{\frac{3}{2}}\varepsilon_0^2 m_{\mathrm{e}}^{\frac{1}{2}}(k_{\mathrm{B}}T)^{\frac{3}{2}}}, \tag{F.43}$$

$$\bar{\nu}_{\mathrm{ei}}^{\mathrm{m}} = \frac{n_{\mathrm{i}}Z_{\mathrm{i}}^2e^4\ln\Lambda}{6\sqrt{2}\pi^{\frac{3}{2}}\varepsilon_0^2 m_{\mathrm{e}}^{\frac{1}{2}}(k_{\mathrm{B}}T)^{\frac{3}{2}}}, \tag{F.44}$$

$$\bar{\nu}_{\mathrm{ie}}^{\mathrm{m}} = \frac{n_{\mathrm{e}}Z_{\mathrm{i}}^2e^4m_{\mathrm{e}}^{\frac{1}{2}}\ln\Lambda}{6\sqrt{2}\pi^{\frac{3}{2}}\varepsilon_0^2 m_{\mathrm{i}}(k_{\mathrm{B}}T)^{\frac{3}{2}}}, \tag{F.45}$$

$$\bar{\nu}_{\mathrm{ii}}^{\mathrm{m}} = \frac{n_{\mathrm{i}}Z_{\mathrm{i}}^4e^4\ln\Lambda}{6\pi^{\frac{3}{2}}\varepsilon_0^2 m_{\mathrm{i}}^{\frac{1}{2}}(k_{\mathrm{B}}T)^{\frac{3}{2}}} \tag{F.46}$$

If the ion-ion scatterings are collisions between two different ions, the corresponding loss rate is

$$\bar{\nu}_{\mathrm{ij}}^{\mathrm{m}} = \frac{n_{\mathrm{i}}\mu_{\mathrm{ij}}^{\frac{1}{2}}Z_{\mathrm{i}}^2Z_{\mathrm{j}}^2e^4\ln\Lambda}{6\sqrt{2}\pi^{\frac{3}{2}}\varepsilon_0^2 m_{\mathrm{i}}(k_{\mathrm{B}}T)^{\frac{3}{2}}}. \tag{F.47}$$

For a neutral plasma, one can approximately take $n_{\mathrm{e}} = n_{\mathrm{i}}Z_{\mathrm{i}}$, thus one has the following approximate relation:

$$\bar{\nu}_{\mathrm{ee}}^{\mathrm{m}} : \bar{\nu}_{\mathrm{ei}}^{\mathrm{m}} : \bar{\nu}_{\mathrm{ie}}^{\mathrm{m}} : \bar{\nu}_{\mathrm{ii}}^{\mathrm{m}} = 1 : Z_{\mathrm{i}} : Z_{\mathrm{i}}^2\frac{m_{\mathrm{e}}}{m_{\mathrm{i}}} : Z_{\mathrm{i}}^3\sqrt{\frac{m_{\mathrm{e}}}{m_{\mathrm{i}}}}. \tag{F.48}$$

Thus, if Z_{i} is not too large compared to $\sqrt{m_{\mathrm{i}}/m_{\mathrm{e}}} \approx 43$, one will have

$$\bar{\nu}_{\mathrm{ei}}^{\mathrm{m}} \sim Z_{\mathrm{i}}\bar{\nu}_{\mathrm{ee}}^{\mathrm{m}} \gg \bar{\nu}_{\mathrm{ii}}^{\mathrm{m}} \gg \bar{\nu}_{\mathrm{ie}}^{\mathrm{m}}. \tag{F.49}$$

F.5 Total cross section for energy transfer

We know that for a single collision, the energy transfer is given as

$$\Delta E_1 = -\boldsymbol{v}_{\rm c}\mu_{12}\Delta\boldsymbol{v}_{12}.$$

For given a configuration of $\boldsymbol{v}_{\rm c}$ and $\boldsymbol{v}_{12}$ (thus given $\boldsymbol{v}_1$ and $\boldsymbol{v}_2$), the impact factor may change from collision to collision. Therefore, similar as in the case of momentum transfer, the energy transfer averaged over different impact factors is given as

$$\begin{aligned}
\langle\Delta E_1\rangle &= -\int_0^\pi \sin\theta{\rm d}\theta\int_0^{2\pi}{\rm d}\phi\sigma_{12}\Delta E_1 \\
&= -\int_0^\pi \sin\theta{\rm d}\theta\int_0^{2\pi}{\rm d}\phi\sigma_{12}\boldsymbol{v}_{\rm c}\mu_{12}\Delta\boldsymbol{v}_{12} \\
&= -2\pi\int_0^\pi \sin\theta{\rm d}\theta\sigma_{12}\boldsymbol{v}_{\rm c}\mu_{12}v_{12}(\cos\theta-1)\hat{z} \\
&= -2\pi\mu_{12}\int_0^\pi \sin\theta(\cos\theta-1){\rm d}\theta\sigma_{12}\boldsymbol{v}_{\rm c}\cdot\boldsymbol{v}_{12} \\
&= -4\pi\mu_{12}b_\perp^2\ln\Lambda\boldsymbol{v}_{\rm c}\cdot\boldsymbol{v}_{12},
\end{aligned}$$

where we have used the relation $\boldsymbol{v}_{12}=v_{12}\hat{z}$. One should mention that $\langle\Delta E_1\rangle$ has a unit of energy per area. After a time of ${\rm d}t$, there would be $n_2\sigma_{12}v_{12}{\rm d}t$ total collisions, and

$$\langle\Delta E_1\rangle_{{\rm d}t} = -4\pi\mu_{12}n_2b_\perp^2\ln\Lambda\boldsymbol{v}_{\rm c}\cdot\boldsymbol{v}_{12}v_{12}{\rm d}t.$$

To proceed, we calculate the term in the integral through

$$\begin{aligned}
\boldsymbol{v}_{\rm c}\cdot\boldsymbol{v}_{12} &= \frac{m_1\boldsymbol{v}_1+m_2\boldsymbol{v}_2}{m_1+m_2}(\boldsymbol{v}_1-\boldsymbol{v}_2) \\
&= \frac{1}{m_1+m_2}[m_1\boldsymbol{v}_1^2-m_2\boldsymbol{v}_2^2+(m_2-m_1)\boldsymbol{v}_1\cdot\boldsymbol{v}_2] \\
&= \frac{2}{m_1+m_2}[E_1-E_2+\frac{1}{2}(m_2-m_1)\boldsymbol{v}_1\cdot\boldsymbol{v}_2].
\end{aligned}$$

Considering the thermal effect, one needs to average over different configurations of $\boldsymbol{v}_1$ and $\boldsymbol{v}_2$:

$$\begin{aligned}
\langle\Delta E_1\rangle_{{\rm d}t}^{\rm th} &= \int{\rm d}\boldsymbol{v}_1\int{\rm d}\boldsymbol{v}_2 f(\boldsymbol{v}_1,\boldsymbol{v}_2)\langle\Delta E_1\rangle_{{\rm d}t} \\
&= -4\pi\mu_{12}n_2\ln\Lambda\int{\rm d}\boldsymbol{v}_1\int{\rm d}\boldsymbol{v}_2 b_\perp^2 f(\boldsymbol{v}_1,\boldsymbol{v}_2)\boldsymbol{v}_{\rm c}\cdot\boldsymbol{v}_{12}v_{12}{\rm d}t,
\end{aligned}$$

with $f(\boldsymbol{v}_1,\boldsymbol{v}_2)$ being the distribution function of the two particles. Usually, this distribution is isotropic over different directions. Therefore, the thermal average would give $\left\langle b_\perp^2(\boldsymbol{v}_1\cdot\boldsymbol{v}_2)v_{12}\right\rangle^{\rm th}=0$ because $b_\perp$ and v_{12} do not depend on the angle between $\boldsymbol{v}_1$ and $\boldsymbol{v}_2$. One can just take

$$\left\langle b_\perp^2(\boldsymbol{v}_{\rm c}\cdot\boldsymbol{v}_{12})v_{12}\right\rangle^{\rm th} = \frac{2}{m_1+m_2}\left\langle b_\perp^2(E_1-E_2)v_{12}\right\rangle^{\rm th}.$$

This means that

$$\begin{aligned}\langle \Delta E_1 \rangle_{\mathrm{d}t}^{\mathrm{th}} &= \int \mathrm{d}\boldsymbol{v}_1 \int \mathrm{d}\boldsymbol{v}_2 f(\boldsymbol{v}_1, \boldsymbol{v}_2) \langle \Delta E_1 \rangle_{\mathrm{d}t} \\ &= -\frac{8\pi m_1 m_2}{(m_1+m_2)^2} n_2 \ln\Lambda \int \mathrm{d}\boldsymbol{v}_1 \int \mathrm{d}\boldsymbol{v}_2 f(\boldsymbol{v}_1, \boldsymbol{v}_2) b_\perp^2 (E_1 - E_2) v_{12} \mathrm{d}t.\end{aligned}$$

As an approximation, let us assume particle 2 moves slowly compared to particle 1, and $E_1 \gg E_2$, then

$$\begin{aligned}\langle \Delta E_1 \rangle_{\mathrm{d}t}^{\mathrm{th}} &\approx -\frac{8\pi m_1 m_2}{(m_1+m_2)^2} n_2 \ln\Lambda \int \mathrm{d}\boldsymbol{v}_1 f(\boldsymbol{v}_1) b_\perp^2 E_1 v_1 \mathrm{d}t \\ &\approx -\frac{8\pi m_1 m_2}{(m_1+m_2)^2} n_2 \ln\Lambda \int \mathrm{d}v_1 f(v_1) b_\perp^2 E_1 v_1 \mathrm{d}t.\end{aligned}$$

With

$$f(v_1) = 4\pi v_1^2 \sqrt{\left(\frac{m_1}{2\pi k_{\mathrm{B}} T}\right)^3} e^{-\frac{m_1}{2k_{\mathrm{B}}T} v_1^2}, \tag{F.50}$$

and

$$b_\perp = \frac{Z_1 Z_2 e^2}{4\pi\varepsilon_0 \mu_{12} v_1^2}, \tag{F.51}$$

one can write

$$\begin{aligned}\frac{\langle \Delta E_1 \rangle_{\mathrm{d}t}^{\mathrm{th}}}{\mathrm{d}t} &\approx -\frac{32\pi^2 m_1 m_2}{(m_1+m_2)^2} n_2 \ln\Lambda \sqrt{\left(\frac{m_1}{2\pi k_{\mathrm{B}} T}\right)^3} \\ &\qquad \times \int \mathrm{d}v_1 v_1^2 e^{-\frac{m_1}{2k_{\mathrm{B}}T} v_1^2} \left(\frac{Z_1 Z_2 e^2}{4\pi\varepsilon_0 \mu_{12} v_1^2}\right)^2 \frac{1}{2} m_1 v_1^2 v_1 \\ &= -\frac{16\pi^2 m_1^2 m_2}{(m_1+m_2)^2} n_2 \ln\Lambda \sqrt{\left(\frac{m_1}{2\pi k_{\mathrm{B}} T}\right)^3} \left(\frac{Z_1 Z_2 e^2}{4\pi\varepsilon_0 \mu_{12}}\right)^2 \int \mathrm{d}v_1 v_1 e^{-\frac{m_1}{2k_{\mathrm{B}}T} v_1^2}.\end{aligned} \tag{F.52}$$

Setting $u = \sqrt{\frac{m_1}{2k_{\mathrm{B}}T}} v$, the integral gives

$$\begin{aligned}&\sqrt{\left(\frac{m_1}{2\pi k_{\mathrm{B}} T}\right)^3} \int v_1 e^{-\frac{m_1}{2k_{\mathrm{B}}T} v_1^2} \mathrm{d}v_1 \\ &= \frac{1}{2\pi} \sqrt{\frac{m_1}{2\pi k_{\mathrm{B}} T}} \int u e^{-u^2} \mathrm{d}u \\ &= \frac{1}{\pi} \sqrt{\frac{m_1}{2\pi k_{\mathrm{B}} T}} \frac{1}{2} \\ &= \frac{1}{\pi^{3/2}} \sqrt{\frac{m_1}{8 k_{\mathrm{B}} T}} \\ &= \frac{1}{\pi^2} \frac{1}{\langle v_1 \rangle_{\mathrm{th}}},\end{aligned} \tag{F.53}$$

with the average velocity given by

$$\langle v_1 \rangle_{\rm th} = \sqrt{\frac{8k_{\rm B}T}{\pi m_1}}.$$

Then

$$\begin{aligned} \frac{\langle \Delta E_1 \rangle_{{\rm d}t}^{\rm th}}{{\rm d}t} &= -\frac{16\pi^2 m_1^2 m_2}{(m_1+m_2)^2} n_2 \ln\Lambda \left(\frac{Z_1 Z_2 e^2}{4\pi\varepsilon_0 \mu_{12}}\right)^2 \frac{1}{\pi^2} \frac{1}{\langle v_1 \rangle_{\rm th}} \\ &= -\frac{n_2 Z_1^2 Z_2^2 e^4 \ln\Lambda}{\pi^2 \varepsilon_0^2 m_2 \langle v_1 \rangle_{\rm th}}. \end{aligned} \tag{F.54}$$

The result is interesting because it is inversely proportional to the velocity of the shooting particle: the higher energy the shooting particle has, the less energy it loses during the collision.

Furthermore, we can use the relation between average velocity and average kinetic energy:

$$\langle v_1 \rangle_{\rm th} = 2\sqrt{\frac{2}{3}\langle v_1^2 \rangle_{\rm th}} = 2\sqrt{\frac{2}{3}\frac{2\langle E_1 \rangle_{\rm th}}{m_1}}. \tag{F.55}$$

Substituting it into the above equation, one obtains

$$\begin{aligned} \frac{\langle \Delta E_1 \rangle_{{\rm d}t}^{\rm th}}{{\rm d}t} &= -\frac{n_2 Z_1^2 Z_2^2 e^4 \ln\Lambda}{4\pi^2 \varepsilon_0^2 m_2} \sqrt{\frac{3m_1}{\langle E_1 \rangle_{\rm th}}} \\ &= -\frac{n_2 Z_1^2 Z_2^2 e^4 \ln\Lambda}{4\pi^2 \varepsilon_0^2 m_2} \sqrt{\frac{3m_1}{\langle E_1 \rangle_{\rm th}^3}} \langle E_1 \rangle_{\rm th}. \end{aligned} \tag{F.56}$$

For electron-electron collision, this yields

$$\begin{aligned} \frac{\langle \Delta E_{\rm e} \rangle_{\rm e\text{-}e}}{{\rm d}t} &= -\frac{n_{\rm e} e^4 \ln\Lambda}{4\pi^2 \varepsilon_0^2 m_{\rm e}} \sqrt{\frac{3m_{\rm e}}{\langle E_{\rm e} \rangle_{\rm th}^3}} \langle E_{\rm e} \rangle_{\rm th} \\ &= -\frac{n_{\rm e} e^4 \ln\Lambda}{\pi^2 \varepsilon_0^2 m_{\rm e} \langle v_{\rm e} \rangle_{\rm th}}. \end{aligned} \tag{F.57}$$

For electron-ion collision where the ion is the target particle 2,

$$\begin{aligned} \frac{\langle \Delta E_{\rm e} \rangle_{\rm e\text{-}i}}{{\rm d}t} &= -\frac{n_{\rm i} Z_{\rm i}^2 e^4 \ln\Lambda}{4\pi^2 \varepsilon_0^2 m_{\rm i}} \sqrt{\frac{3m_{\rm e}}{\langle E_{\rm e} \rangle_{\rm th}^3}} \langle E_{\rm e} \rangle_{\rm th} \\ &= -\frac{n_{\rm i} Z_{\rm i}^2 e^4 \ln\Lambda}{\pi^2 \varepsilon_0^2 m_{\rm i} \langle v_{\rm e} \rangle_{\rm th}}. \end{aligned} \tag{F.58}$$

Usually, the neutrality of plasma gives $n_{\rm e} = n_{\rm i} Z_{\rm i}$, therefore

$$\frac{\langle \Delta E_{\rm e} \rangle_{\rm e\text{-}e}}{{\rm d}t} : \frac{\langle \Delta E_{\rm e} \rangle_{\rm e\text{-}i}}{{\rm d}t} = \frac{1}{m_{\rm e}} : \frac{Z_{\rm i}}{2m_{\rm i}} \approx \frac{m_{\rm i}}{m_{\rm e}}, \tag{F.59}$$

where we assume highly charged ions for which $Z_{\rm i}$ is approximately the atomic number of the ion. The ratio between the energy transfer rates for electron-electron and electron-ion

collisions indicates that thermalization times between hot electrons and cold electrons are almost 4000 times shorter than the thermalization times between hot electrons and cold ions.

F.6 Phase shift: collisional broadening and shift

During collision processes, when the scattering particles fly by the targets, the interaction potential between the two particles stark shifts the eigenstates of the targets, atoms or ions. The changes in eigenstates and energies modify the evolution of the target in free space, giving rise to both spectral broadening and frequency shift.

We start with the total Hamiltonian for a target particle (emitter) interacting with the surrounding perturbers:

$$H = H_0 + U, \tag{F.60}$$

with H_0 being the Hamiltonian of the free emitter, with the eigenstates

$$H_0 \left|\psi_n\right\rangle = E_n \left|\psi_n\right\rangle, \tag{F.61}$$

and U being the sum of the interaction Hamiltonian of the emitter with all the perturbers:

$$U = \sum_i U_i(b, v; t), \tag{F.62}$$

where each interaction is time dependent, and also depends on a specific impact parameter and shooting velocity. Let us assume the wave function is

$$\left|\Psi\right\rangle = \sum_n c_n \left|\psi_n\right\rangle \tag{F.63}$$

In the interaction picture, the evolution of the wave function follows the equation

$$i\hbar \frac{\partial}{\partial t} \left|\Psi\right\rangle_{\mathrm{I}} = U_{\mathrm{I}} \left|\Psi\right\rangle_{\mathrm{I}}, \tag{F.64}$$

with

$$\left|\Psi\right\rangle_{\mathrm{I}} = e^{-iH_0 t/\hbar} \left|\Psi\right\rangle = \sum_n c_n e^{-iE_n t/\hbar} \left|\psi_n\right\rangle = \sum_n C_n \left|\psi_n\right\rangle.$$

therefore, wave function in the interaction picture and

$$U_{\mathrm{I}} = e^{-iH_0 t/\hbar} U e^{iH_0 t/\hbar} \tag{F.65}$$

being the Hamiltonian in the interaction picture. Thus, the time-dependent wave function can be integrated as

$$\left|\Psi(t)\right\rangle_{\mathrm{I}} = e^{-iU_{\mathrm{I}} t/\hbar} \left|\Psi(0)\right\rangle_{\mathrm{I}}, \tag{F.66}$$

Or, in other way,

$$\left|\Psi(t)\right\rangle_{\mathrm{I}} = \left|\Psi(0)\right\rangle_{\mathrm{I}} + \int_0^t U_{\mathrm{I}}(t_1) \left|\Psi(t_1)\right\rangle_{\mathrm{I}} \mathrm{d}t_1$$

$$
\begin{aligned}
&= |\Psi(0)\rangle_{\rm I} + \int_0^t U_{\rm I}(t_1)\,|\Psi(0)\rangle_{\rm I}\,{\rm d}t_1 \\
&\quad + \int_0^t {\rm d}t_1 \int_0^{t_1} {\rm d}t_2 U_{\rm I}(t_1)U_{\rm I}(t_2)\,|\Psi(0)\rangle_{\rm I} \\
&\quad + \int_0^t {\rm d}t_1 \int_0^{t_1} {\rm d}t_2 \int_0^{t_2} {\rm d}t_3 U_{\rm I}(t_1)U_{\rm I}(t_2)U_{\rm I}(t_3)\,|\Psi(0)\rangle_{\rm I} \\
&\quad + ... \qquad \text{(F.67)}
\end{aligned}
$$

In the following, we assume that the duration of a single collision process is significantly smaller compared to other time scales. After some time duration Δs sufficiently large compared to the collision time, but sufficiently small compared to the other physical processes, one can calculate the wave function as

$$
\begin{aligned}
&|\Psi(\Delta s)\rangle_{\rm I} - |\Psi(0)\rangle_{\rm I} \\
&= \left[\int_0^{\Delta s} {\rm d}t_1 U_{\rm I}(t_1) + \int_0^{\Delta s} {\rm d}t_1 \int_0^{t_1} {\rm d}t_2 U_{\rm I}(t_1)U_{\rm I}(t_2)\right. \\
&\quad \left. + \int_0^{\Delta s} {\rm d}t_1 \int_0^{t_1} {\rm d}t_2 \int_0^{t_2} {\rm d}t_3 U_{\rm I}(t_1)U_{\rm I}(t_2)U_{\rm I}(t_3) + ...\right] |\Psi(0)\rangle_{\rm I}\,.
\end{aligned}
$$

Because the time duration for each scattering events is much smaller than Δs, one can divide the Δs into time segments $[n, n+1)\delta s$ so that within each segment there is only one single collision. Then we have

$$
\begin{aligned}
&|\Psi(\Delta s)\rangle_{\rm I} - |\Psi(0)\rangle_{\rm I} \\
&= \sum_i f_i \Delta s \left[\int_0^{\delta s} {\rm d}t U_{{\rm I}i}(t) + \int_0^{\delta s} {\rm d}t_1 \int_0^{t_1} {\rm d}t_2 U_{{\rm I}i}(t_1)U_{{\rm I}i}(t_2)\right. \\
&\quad \left. + \int_0^{\delta s} {\rm d}t_1 \int_0^{t_1} {\rm d}t_2 \int_0^{t_2} {\rm d}t_3 U_{{\rm I}i}(t_1)U_{{\rm I}i}(t_2)U_{{\rm I}i}(t_3) + ...\right] |\Psi(0)\rangle_{\rm I}\,,
\end{aligned}
$$

with f_i being the collision frequencies for a specific type of collision. Here we assume that there are only two-body collisions, and all collisions involving more than two particles are neglected. This means that $U_{{\rm I}i}(t_1)$ and $U_{{\rm I}j}(t_2)$ do not overlap, and

$$
U_{\rm I}(t_1)U_{\rm I}(t_2) = \sum_{ij} U_{{\rm I}i}(t_1)U_{{\rm I}j}(t_2) \approx \sum_i U_{{\rm I}i}(t_1)U_{{\rm I}i}(t_2).
$$

If we assume the scattering process does not change the internal state of the perturber and emitter, U will commute with H_0 and $U_{\rm I} = U$. So we can further written:

$$
\begin{aligned}
&|\Psi(\Delta s)\rangle_{\rm I} - |\Psi(0)\rangle_{\rm I} \\
&= \sum_i f_i \Delta s \left[\frac{1}{i\hbar}\int_0^{\delta s} {\rm d}t U_i(t)\right. \\
&\quad \left. + \left(\frac{1}{i\hbar}\right)^2 \int_0^{\delta s} {\rm d}t_1 \int_0^{t_1} {\rm d}t_2 U_i(t_1)U_i(t_2) + ...\right] |\Psi(0)\rangle_{\rm I} \\
&= \sum_i f_i (S_i - 1)\Delta s\,|\Psi(0)\rangle_{\rm I}\,,
\end{aligned}
$$

with the scattering matrix S given as

$$\begin{aligned} S_i &= 1 + \frac{1}{i\hbar}\int_0^{\delta s} \mathrm{d}t U_i(t) + \left(\frac{1}{i\hbar}\right)^2 \int_0^{\delta s} \mathrm{d}t_1 \int_0^{t_1} \mathrm{d}t_2 U_i(t_1)U_i(t_2) \\ &\quad + \left(\frac{1}{i\hbar}\right)^3 \int_0^{\delta s} \mathrm{d}t_1 \int_0^{t_1} \mathrm{d}t_2 \int_0^{t_2} \mathrm{d}t_3 U_i(t_1)U_i(t_2)U_i(t_3) + ... \end{aligned}$$

In a given time segment, δs is much larger than the collision time, $U_i(t) = 0$ for a given collision event. Thus one can extend the integral to infinity to get the strictly defined S-matrix

$$\begin{aligned} S_i &= 1 + \frac{1}{i\hbar}\int_{-\infty}^{\infty} \mathrm{d}t U_i(t) + \left(\frac{1}{i\hbar}\right)^2 \int_{-\infty}^{\infty} \mathrm{d}t_1 \int_{-\infty}^{t_1} \mathrm{d}t_2 U_i(t_1)U_i(t_2) \\ &\quad + \left(\frac{1}{i\hbar}\right)^3 \int_{-\infty}^{\infty} \mathrm{d}t_1 \int_{-\infty}^{t_1} \mathrm{d}t_2 \int_{-\infty}^{t_2} \mathrm{d}t_3 U_i(t_1)U_i(t_2)U_i(t_3) + ... \end{aligned}$$

Then we will have

$$\frac{|\Psi(\Delta s)\rangle_{\mathrm{I}} - |\Psi(0)\rangle_{\mathrm{I}}}{\Delta s} = \sum_i f_i(S_i - 1)\,|\Psi(0)\rangle_{\mathrm{I}}$$

Or, equivalently

$$i\hbar\frac{\partial}{\partial s}\,|\Psi(s)\rangle_{\mathrm{I}} = i\hbar\sum_i f_i(S_i - 1)\,|\Psi(s)\rangle_{\mathrm{I}}$$

One can define an effective non-Hermite Hamiltonian

$$\mathcal{H} = i\hbar\sum_i f_i(S_i - 1) \tag{F.68}$$

with

$$\frac{1}{i\hbar}\mathcal{H} = w + id \tag{F.69}$$

Here, w corresponds to the spectral broadening operator, and d corresponds to the energy shift operator. Then, calculation of the collisional broadening and shift is equivalent to the calculation of the scattering matrix for each collision event, as shown in Sec. 4.2.

Appendix G

Light propagation in resonant media

When a light interacts with a dense medium, the nonlinear dispersion and significant absorption/amplification become prominent. The the wave propagation equations in the slowly varying envelope approximation derived in Chapter 2 and Appx. D may breaks down. Therefore, in this Appendix, a more elaborated consideration of the slowly varying envelope approximation of the light propagation equations is presented in the frequency space. As we show later, the frequency-domain approach reveals much more information than the time-domain approach.

It is well known in nonlinear optics that (see Sec. G.3), when nonlinear dispersion (group velocity dispersion) becomes significant, some higher-order time derivatives must be included [109] [there is only first-order time-derivative in Eq. (2.52) and Eq. (2.57)]. This phenomenon is crucial because when light-matter interaction is close to resonance, it does lead to nonlinear dispersion. Therefore, we examined the conditions for a SVEA approach to holds in describing resonant light-matter interactions in Sec. G.4.

G.1 Light propagation equation

In this Section, we first recall the equations describing the propagation of light in matter discussed in Sec. 2.1.1, then derive the propagation equation of the electric field in both time domain and frequency domain.

G.1.1 Light propagation in time domain

For a source-free medium, e.g. without free charges, free currents and magnetizations, the corresponding Maxwell equations for the electric field $\mathbf{E}$ and magnetic field $\mathbf{B}$ are [108]

$$\nabla \cdot \mathbf{D} = 0, \tag{G.1}$$

$$\nabla \cdot \mathbf{B} = 0, \tag{G.2}$$

$$\nabla \times \mathbf{E} = -\frac{\partial \mathbf{B}}{\partial t}, \tag{G.3}$$

$$\nabla \times \mathbf{B} = \mu_0 \frac{\partial \mathbf{D}}{\partial t}, \tag{G.4}$$

with the displacement field $\mathbf{D}$ defined by

$$\mathbf{D}(\mathbf{r}, t) = \varepsilon_0 \mathbf{E}(\mathbf{r}, t) + \mathbf{P}(\mathbf{r}, t). \tag{G.5}$$

Here, $\mathbf{P}$ is the polarization field. Combining these equations, one obtains the propagation equation for the electric field

$$\nabla^2\mathbf{E} - \nabla(\nabla\cdot\mathbf{E}) - \frac{1}{c^2}\frac{\partial^2\mathbf{E}}{\partial t^2} = \mu_0\frac{\partial^2\mathbf{P}}{\partial t^2}. \tag{G.6}$$

Usually, in most media, the term $\nabla(\nabla\cdot\mathbf{E}) \neq 0$. In general, it does not hold. The polarization field is induced by the electric field, therefore, it may depend on $\mathbf{E}$ either linearly or nonlinearly. For convenience, we rewrite the above definitions as

$$\mathbf{D} = \varepsilon_0\mathbf{E} + \mathbf{P}_{(1)} + \mathbf{P}_{\mathrm{NL}} = \varepsilon_{(1)}\mathbf{E} + \mathbf{P}_{\mathrm{NL}}, \tag{G.7}$$

with $\mathbf{P}_{(1)}$ the linear polarization in $\mathbf{E}$,

$$\varepsilon_{(1)}\mathbf{E} = \varepsilon_0\mathbf{E} + \mathbf{P}_{(1)}, \tag{G.8}$$

and $\mathbf{P}_{\mathrm{NL}}$ the nonlinear polarization in $\mathbf{E}$. The quantity $\varepsilon_{(1)} = n_{(1)}^2\varepsilon_0$ is the linear permitivity with $n_{(1)}$ being the linear refractive index. Then, $\nabla\cdot\mathbf{D} = 0$ means

$$\varepsilon_{(1)}\nabla\cdot\mathbf{E} = -\mathbf{E}\cdot\nabla\varepsilon_{(1)} - \nabla\cdot\mathbf{P}_{\mathrm{NL}}. \tag{G.9}$$

In a nonlinear medium [109], one usually has $\nabla\cdot\mathbf{P}_{\mathrm{NL}} \neq 0$, therefore, $\nabla\cdot\mathbf{E} \neq 0$. But in this Appendix, we not consider such a case. If the nonlinear polarization $\mathbf{P}_{\mathrm{NL}}$ is weak and the first-order permitivity $\varepsilon_{(1)}$ does not change with space, one can neglect this term and set $\nabla\cdot\mathbf{E} = 0$. Under such conditions, one could have the well known propagation equation for the electric field:

$$\nabla^2\mathbf{E} - \frac{1}{c^2}\frac{\partial^2\mathbf{E}}{\partial t^2} = \mu_0\frac{\partial^2\mathbf{P}}{\partial t^2}. \tag{G.10}$$

In the following, we only consider the case where $\nabla(\nabla\cdot\mathbf{E}) = 0$ and Eq. (G.10) holds. One should always keep in mind that this condition may not be satisfied for some specific cases, such as in nonlinear optics.

G.1.2 Light propagation in frequency domain

By introducing the Fourier transform

$$\hat{\mathbf{P}}(\mathbf{r},\omega) = \frac{1}{\sqrt{2\pi}}\int_{-\infty}^{\infty}\mathbf{P}(\mathbf{r},t)\mathrm{e}^{-i\omega t}dt,$$
$$\hat{\mathbf{E}}(\mathbf{r},\omega) = \frac{1}{\sqrt{2\pi}}\int_{-\infty}^{\infty}\mathbf{E}(\mathbf{r},t)\mathrm{e}^{-i\omega t}dt,$$

and substituting these relation into Eq. (G.10), one obtains the propagation equation in frequency domain as

$$\nabla^2\hat{\mathbf{E}} + \frac{\omega^2}{c^2}\hat{\mathbf{E}} = -\mu_0\omega^2\hat{\mathbf{P}}. \tag{G.11}$$

Compared to Eq. (G.10), there is no time derivative any more. This reduces the partial differential equation to an ordinary differential equation and simplifies the calculations if one knows the expression of polarization in frequency domain.

G.2 Linear polarization

For linear polarization $\mathbf{P}_{\rm NL} = 0$, one usually has

$$\mathbf{P}(\mathbf{r},t) = \mathbf{P}_{(1)}(\mathbf{r},t) + \mathbf{P}_{\rm NL}(\mathbf{r},t) = \epsilon\varepsilon_0\mathbf{E}(\mathbf{r},t).$$

Then the displacement field is

$$\begin{aligned}\mathbf{D}(\mathbf{r},t) &= \varepsilon_0\mathbf{E}(\mathbf{r},t) + \mathbf{P}(\mathbf{r},t)\\ &= \varepsilon_0\mathbf{E}(\mathbf{r},t) + \epsilon\varepsilon_0\mathbf{E}(\mathbf{r},t)\\ &= \varepsilon_{(1)}\mathbf{E}(\mathbf{r},t),\end{aligned}$$

where $\varepsilon_{(1)} = (1+\epsilon)\varepsilon_0 = n_{(1)}^2\varepsilon_0$ with $n_{(1)}$ being the refractive index. For convenience, we use n instead of $n_{(1)}$ to represent the refractive index without specifying whether it is a linear or nonlinear index. The propagation equation becomes

$$\nabla^2\mathbf{E} - \frac{1}{c^2}\frac{\partial^2\mathbf{E}}{\partial t^2} = \mu_0\epsilon\varepsilon_0\frac{\partial^2\mathbf{E}}{\partial t^2}. \tag{G.12}$$

Re-arranging the terms in the equation gives

$$\nabla^2\mathbf{E} - \frac{n^2}{c^2}\frac{\partial^2\mathbf{E}}{\partial t^2} = 0. \tag{G.13}$$

However, the relation $\mathbf{P} = \epsilon\varepsilon_0\mathbf{E}$ between polarization field and electric field in time domain is correct only if the refractive index is constant for all frequencies constituting to the electric field. A more general relation between $\mathbf{P}$ and $\mathbf{E}$ is given as

$$\mathbf{P}(\mathbf{r},t) = \varepsilon_0\int_{-\infty}^{t}\chi(\mathbf{r},t-t')\mathbf{E}(\mathbf{r},t')dt' = \varepsilon_0\int_{-\infty}^{\infty}\chi(\mathbf{r},t-t')\mathbf{E}(\mathbf{r},t')dt', \tag{G.14}$$

with

$$\chi(\mathbf{r},t-t') = 0 \qquad \text{for} \qquad t' > t. \tag{G.15}$$

This is a convolution of the electric field and the material response function $\chi(\mathbf{r},t)$. Using the convolution theorem, one has a linear relation between the electric field and polarization field for different frequencies

$$\hat{\mathbf{P}}(\mathbf{r},\omega) = \varepsilon_0\hat{\chi}(\mathbf{r},\omega)\hat{\mathbf{E}}(\mathbf{r},\omega), \tag{G.16}$$

with

$$\hat{\chi}(\mathbf{r},\omega) = \frac{1}{\sqrt{2\pi}}\int_{-\infty}^{\infty}\chi(\mathbf{r},t)\mathrm{e}^{-i\omega t}dt. \tag{G.17}$$

It indicates that, the medium responses differently to different frequencies: or, in other words, the refractive index and the absorption/amplification coefficient are frequency-dependent:

$$n(\mathbf{r},\omega) = n_1(\mathbf{r},\omega) + in_2(\mathbf{r},\omega) = \sqrt{1+\hat{\chi}(\mathbf{r},\omega)}, \tag{G.18}$$

with n_1 being the refractive index and n_2 the absorption coefficient if $n_2 > 0$, amplification coefficient if $n_2 < 0$. In the following, we call n the complex refractive index, where its real part corresponds to the refractive index of matter and the imaginary part corresponds to the absorption/amplification coefficient.

In this Appendix, we only consider the polarization where there is no interplay between different frequency components. In Chapter 7, a more complex polarization field defined by Eq. (7.13) and Eq. (7.19) is used. Here we only consider the polarization field defined according to Eq. (G.14).

G.2.1 Instantaneous response

If the medium responses to an external electric field instantaneously, the corresponding linear response function is a Dirac δ-function,

$$\chi(\mathbf{r}, t - t') = \chi_0 \delta(t - t'), \tag{G.19}$$

which gives a frequency-independent response

$$\hat{\chi}(\mathbf{r}, \omega) = \chi_0. \tag{G.20}$$

Then one has

$$\begin{aligned} \mathbf{P}(\mathbf{r}, t) &= \varepsilon_0 \int_{-\infty}^{t} \chi(\mathbf{r}, t - t') \mathbf{E}(\mathbf{r}, t') \\ &= \varepsilon_0 \int_{-\infty}^{t} \chi_0 \delta(t - t') \mathbf{E}(\mathbf{r}, t') \\ &= \varepsilon_0 \chi_0 \mathbf{E}(\mathbf{r}, t), \end{aligned} \tag{G.21}$$

and

$$\hat{\mathbf{P}}(\mathbf{r}, \omega) = \chi_0 \varepsilon_0 \hat{\mathbf{E}}(\mathbf{r}, \omega), \tag{G.22}$$

with $\epsilon = \chi_0$ being a constant.

In reality, the instantaneous response refers to the case when the duration T of the electric field is much longer than the time scale τ of the response function. Compared to T, τ is infinitely small and can be taken to be instantaneous. In this situation, the envelop of the electric field varies so slowly in the duration τ that one can approximately assume $\mathbf{E}(\mathbf{r}, t') = \mathbf{E}(\mathbf{r}, t)$, and take it out of the integral:

$$\begin{aligned} \mathbf{P}(\mathbf{r}, t) &= \varepsilon_0 \int_{-\infty}^{t} \chi(\mathbf{r}, t - t') \mathbf{E}(\mathbf{r}, t') dt' \\ &= \varepsilon_0 \mathbf{E}(\mathbf{r}, t) \int_{-\infty}^{t} \chi(\mathbf{r}, t - t') dt' \\ &= \chi_0 \varepsilon_0 \mathbf{E}(\mathbf{r}, t), \end{aligned} \tag{G.23}$$

with

$$\chi_0 = \int_{-\infty}^{t} \chi(\mathbf{r}, t - t') dt' = \int_{0}^{\infty} \chi(\mathbf{r}, t_1) dt_1.$$

In frequency domain, this corresponds to the case when the bandwidth of the electric field is much narrower than the linewidth of the medium such that $\hat{\chi}(\mathbf{r},\omega)$ does not change significantly within the bandwidth of $\hat{\mathbf{E}}(\mathbf{r},\omega)$. Then, the propagation equation is given as

$$\nabla^2\mathbf{E} - \frac{1}{c^2}\frac{\partial^2\mathbf{E}}{\partial t^2} = \mu_0\chi_0\varepsilon_0\frac{\partial^2\mathbf{E}}{\partial t^2}.$$

This equation can be rewritten as

$$\nabla^2\mathbf{E} - \frac{n^2}{c^2}\frac{\partial^2\mathbf{E}}{\partial t^2} = 0,$$

with

$$n = \sqrt{1+\chi_0}.$$

The solution to this equation is

$$\mathbf{E}(\mathbf{r},t) = \frac{1}{\sqrt{2\pi}}\int_{-\infty}^{\infty} d\omega\hat{\mathbf{E}}(0,\omega)e^{i(\omega t-\mathbf{k}(\omega)\cdot\mathbf{r})}, \tag{G.24}$$

with $\hat{\mathbf{E}}(0,\omega)$ being the input spectrum at $\mathbf{r}=\mathbf{0}$. The wave number $\mathbf{k}(\omega)$ and the frequency ω satisfy the linear dispersion relation

$$k(\omega) = \frac{n}{c}\omega. \tag{G.25}$$

In general, the susceptibility χ_0 could be a complex value, thus one has a complex refractive index. However, in this subsection, we assume there is no absorption or amplification, thus n is a real number.

Given a frequency ω_0, one can rewrite the dispersion relation as

$$k(\omega) = k_0 + k_1(\omega-\omega_0), \tag{G.26}$$

with $k_0 = \frac{n}{c}\omega_0$ and $k_1 = \frac{n}{c}$. The phase velocity for ω_0 is

$$v_{\mathrm{p}}(\omega_0) = \frac{\omega_0}{k_0} = \frac{c}{n}, \tag{G.27}$$

and the group velocity for ω_0 is

$$v_{\mathrm{g}}(\omega_0) = \left(\frac{\mathrm{d}k(\omega)}{\mathrm{d}\omega}\bigg|_{\omega=\omega_0}\right)^{-1} = \frac{1}{k_1} = \frac{c}{n}. \tag{G.28}$$

Because the medium responses equally to every frequency, the phase velocity and group velocity are equal to each other and have no dependence on a specific frequency.

G.2.2 Finite-time response

If the medium has a finite response time which is comparable to the time duration of the light pulse, it will response differently to different frequencies. This can be seen

explicitly in the frequency domain, where the light propagation equation in Eq. (G.11) changes to be

$$\nabla^2\hat{\mathbf{E}}(\mathbf{r},\omega)+\frac{\omega^2}{c^2}\hat{\mathbf{E}}(\mathbf{r},\omega) \quad = \quad -\mu_0\varepsilon_0\omega^2\hat{\chi}(\mathbf{r},\omega)\hat{\mathbf{E}}(\mathbf{r},\omega).$$

Reorganizing the terms above, one obtains

$$\nabla^2\hat{\mathbf{E}}(\mathbf{r},\omega)+k^2(\mathbf{r},\omega)\hat{\mathbf{E}}(\mathbf{r},\omega) \quad = \quad 0, \tag{G.29}$$

with the dispersion relation

$$k(\mathbf{r},\omega) \quad = \quad \frac{\omega}{c}\sqrt{1+\hat{\chi}(\mathbf{r},\omega)}=\frac{\omega}{c}n(\mathbf{r},\omega). \tag{G.30}$$

Here we still keep the dispersion relation $k(\mathbf{r},\omega)$ position dependent. This corresponds to a position-dependent complex refractive index $n(\mathbf{r},\omega)$.

Usually, the dispersion relation only accounts for the real refractive index which only refers to phase changes in the light field, the changes of amplitudes are not included in the dispersion relation. However, for the sake of simplicity, we define the dispersion relation in a more general way so that it includes changes in both phase and amplitude. This refers to a complex refractive index, thus complex wave number k.

If the refractive index changes periodically in space as $n(\mathbf{r},\omega)=n(\mathbf{r}+\mathbf{r}_0,\omega)$, then Eq. (G.29) is similar to the equations for electrons moving in a periodic lattice described by Bloch band theory. This is the situation in photonic crystals.

In the following, we assume that the medium is homogeneous, the susceptibility $\hat{\chi}$, thus the dispersion and refractive index, are independent of $\mathbf{r}$. Then we have

$$\nabla^2\hat{\mathbf{E}}(\mathbf{r},\omega)+k^2(\omega)\hat{\mathbf{E}}(\mathbf{r},\omega) \quad = \quad 0, \tag{G.31}$$

with the dispersion relation

$$k(\omega) \quad = \quad \frac{\omega}{c}\sqrt{1+\hat{\chi}(\omega)}=\frac{\omega}{c}n(\omega). \tag{G.32}$$

The ordinary differential equation Eq. (G.31) can be easily solved to get

$$\hat{\mathbf{E}}(\mathbf{r},\omega) \quad = \quad \hat{\mathbf{E}}(\mathbf{0},\omega)e^{-i\mathbf{k}(\omega)\cdot\mathbf{r}}. \tag{G.33}$$

In time domain, one has

$$\mathbf{E}(\mathbf{r},t)=\frac{1}{\sqrt{2\pi}}\int_{-\infty}^{\infty}d\omega\hat{\mathbf{E}}(\mathbf{0},\omega)e^{i(\omega t-\mathbf{k}(\omega)\cdot\mathbf{r})}. \tag{G.34}$$

This means that, for linear dispersion, as long as one knows the input spectrum $\hat{\mathbf{E}}(\mathbf{0},\omega)$ at $\mathbf{r}=\mathbf{0}$ and the dispersion relation $\mathbf{k}(\omega)$, one can immediately get the corresponding output spectrum through Eq. (G.33), and get the pulse function through Eq. (G.34). The dispersion relation $\mathbf{k}(\omega)$ can be obtained either by a theoretical calculation of the susceptibility $\chi(\omega)$ through light-matter interaction, or by experimentally measuring the complex refractive index $n(\omega)$.

Nevertheless, assuming $n(\omega)$ [thus $k(\omega)$] being a real function, there are only phase changes in the spectrum and the amplitude of the power spectrum remains unaffected.

One can again write the dispersion in form of a Taylor series around ω_0

$$k(\omega) = k_0 + k_1\tilde{\omega} + \frac{k_2}{2!}\tilde{\omega}^2 + \frac{k_3}{3!}\tilde{\omega}^3 + ..., \tag{G.35}$$

with $\tilde{\omega} = \omega - \omega_0$, and

$$k_0 = \frac{\omega_0}{c}\sqrt{1+\hat{\chi}(\omega_0)} = \frac{\omega_0}{c}n(\omega_0). \tag{G.36}$$

With this relation, one can easily get the frequency-dependent phase velocity

$$v_\mathrm{p}(\omega_0) = \frac{\omega_0}{k_0} = \frac{c}{n(\omega_0)}, \tag{G.37}$$

and frequency-dependent group velocity

$$\begin{aligned} v_\mathrm{g}(\omega_0) &= \left(\frac{\mathrm{d}k(\omega)}{\mathrm{d}\omega}\bigg|_{\omega=\omega_0}\right)^{-1} \\ &= \left(\frac{\mathrm{d}}{\mathrm{d}\omega}\frac{\omega n(\omega)}{c}\bigg|_{\omega=\omega_0}\right)^{-1} \\ &= \frac{c}{n(\omega_0)+\omega_0\left.\frac{\mathrm{d}n(\omega)}{\mathrm{d}\omega}\right|_{\omega=\omega_0}}. \end{aligned}$$

Both the phase velocity and group velocity are different from frequency to frequency with a frequency-dependent refractive index. For a given frequency ω_0, the group velocity is equal to the phase velocity only if $\left.\frac{\mathrm{d}n(\omega)}{\mathrm{d}\omega}\right|_{\omega=\omega_0} = 0$. This either refers to a frequency-independent constant refractive index, or to the extrema on the curve of a frequency-dependent refractive index.

More generally, we have the relations

$$v_\mathrm{p}(\omega) = \frac{c}{n(\omega)}, \tag{G.38}$$

$$v_\mathrm{g}(\omega) = \frac{c}{n(\omega)+\omega\frac{\mathrm{d}n(\omega)}{\mathrm{d}\omega}}, \tag{G.39}$$

and

$$v_\mathrm{g}(\omega)\begin{cases} < v_\mathrm{p}(\omega), & \text{if } \frac{\mathrm{d}n(\omega)}{\mathrm{d}\omega} > 0, \\ = v_\mathrm{p}(\omega), & \text{if } \frac{\mathrm{d}n(\omega)}{\mathrm{d}\omega} = 0, \\ > v_\mathrm{p}(\omega), & \text{if } \frac{\mathrm{d}n(\omega)}{\mathrm{d}\omega} < 0. \end{cases} \tag{G.40}$$

These relations reveal that the group velocity can be smaller, equal to or larger than the phase velocity, depending on whether the refractive index increases or decreases when ω gets larger. For $\frac{\mathrm{d}n(\omega)}{\mathrm{d}\omega} > 0$, high frequencies have larger refractive indices, thus their phase velocities are smaller compared to those with lower frequencies. As a results, the group velocity becomes smaller than the phase velocity and vise versa.

Another conclusion from the finite-time response is that there always exists chirp phenomenon because of the frequency-dependent phase velocity.

G.2.2.1 Linear dispersion

However, even when the phase velocity is frequency-dependent, the group velocity can still be frequency-independent if all the higher-order terms beyond linear dispersion in Eq. (G.35) vanish. In details, this means

$$k(\omega) \quad = \quad k_0 + k_1\tilde{\omega} = \omega_0\left(\frac{1}{v_{\rm p}(\omega_0)} - \frac{1}{v_{\rm g}}\right) + \frac{\omega}{v_{\rm g}}, \tag{G.41}$$

with

$$v_{\rm g}(\omega_0) = \frac{1}{k_1} = v_{\rm g}. \tag{G.42}$$

The corresponding refractive index for linear dispersion is an inversely proportional function given by

$$n(\omega) = \frac{ck(\omega)}{\omega} = \frac{\omega_0}{\omega}\left(\frac{c}{v_{\rm p}(\omega_0)} - \frac{c}{v_{\rm g}}\right) + \frac{c}{v_{\rm g}}, \tag{G.43}$$

with the derivative

$$\omega\frac{{\rm d}n(\omega)}{{\rm d}\omega} = -n(\omega) + \frac{c}{v_{\rm g}}, \tag{G.44}$$

and

$$v_{\rm g}(\omega) \quad = \quad v_{\rm g} = v_{\rm g}(\omega_0). \tag{G.45}$$

Therefore, we should keep in mind that a linear dispersion relation does not imply a linear refractive index.

Compared to the linear dispersion in Eq. (G.25) for instantaneous response, there is a finite intercept at $\omega = \omega_0$ in Eq. (G.41). This gives rise to an offset between group velocity and phase velocity, as well as a frequency-dependent refractive index. In particular, the phase velocity for linear dispersion can be calculated as

$$v_{\rm p}(\omega) \quad = \quad \frac{\omega}{k(\omega)} = \frac{1}{\frac{\omega_0}{\omega}\left(\frac{1}{v_{\rm p}(\omega_0)} - \frac{1}{v_{\rm g}}\right) + \frac{1}{v_{\rm g}}}. \tag{G.46}$$

One can check the behavior of the phase velocity in two extremes

$$v_{\rm p}(\omega) = \begin{cases} v_{\rm g}, & \text{if } \omega \gg \omega_0, \\ \frac{\omega}{\omega_0}\frac{v_{\rm p}(\omega_0)v_{\rm g}}{v_{\rm g} - v_{\rm p}(\omega_0)}, & \text{if } \omega \ll \omega_0. \end{cases} \tag{G.47}$$

For this linear dispersion, the group velocity is frequency-independent and it is always faster than (or equal to) the phase velocity, indicating superluminal propagation for such kind of materials. This conclusion can also be derived from the frequency dependent refractive index which is inversely proportional to ω.

G.2.2.2 Second-order dispersion

As we have discussed before, the group velocity is universal for all frequencies if the material has a linear dispersion relation. When higher-order dispersions are significant, one expects the group velocity to be frequency-dependent. This phenomenon is called group velocity dispersion (GVD) [109] or group delay dispersion (GDD) [113],

$$GVD(\omega) = \frac{\mathrm{d}^2}{\mathrm{d}\omega^2} k(\omega). \tag{G.48}$$

If all the terms beyond second order in Eq. (G.41) are negligible, one has

$$k(\omega) = k_0 + k_1\tilde{\omega} + \frac{k_2}{2}\tilde{\omega}^2,$$

with the

$$GVD(\omega) = k_2. \tag{G.49}$$

Nevertheless, this second-order dispersion gives rise to a frequency-dependent group velocity when the light propagates through the medium.

G.3 Nonlinear polarization

As we discussed before, for a homogeneous medium with linear polarization only, the dispersion $k(\omega)$ is $\mathbf{r}$-independent. The propagation equation is exactly solvable for any given input spectrum $\hat{\mathbf{E}}(\mathbf{0},\omega)$, provided that we know the dispersion relation [either theoretically from $\chi(\omega)$ or experimentally from $n(\omega)$]. However, when nonlinear polarization sets in, it may change the dispersion relation to be $\mathbf{r}$-dependent again, which prohibits the analytical calculations. More precisely, a specific dispersion relation may not even exist because the nonlinear term is not explicitly expressed in frequency domain by Fourier transform. (the Fourier transform has advantages only for linear systems.)

In this Section, we tackle this problem from two aspects: one is a perturbative treatment where the nonlinear polarization term is much smaller compared to the linear term so that it does not change the dispersion relation obtained from linear polarization too much; the other one is a non-perturbative treatment in which nonlinear polarization is comparable to linear polarization, and one should solve Eq. (G.10) or Eq. (G.11) exactly.

G.3.1 Perturbative treatment

Going back to the beginning of this Appendix, the polarization can be separated into a linear term and a small nonlinear term

$$\mathbf{P}(\mathbf{r},t) \;=\; \mathbf{P}_{(1)}(\mathbf{r},t) + \mathbf{P}_{\mathrm{NL}}(\mathbf{r},t),$$

with the linear polarization term satisfying

$$\mathbf{P}_{(1)}(\mathbf{r},t) \;=\; \varepsilon_0 \int_{-\infty}^{t} \chi_{(1)}(\mathbf{r},t-t')\mathbf{E}(\mathbf{r},t'), \tag{G.50}$$

and

$$\hat{\mathbf{P}}_{(1)}(\mathbf{r},\omega) = \varepsilon_0\hat{\chi}_{(1)}(\mathbf{r},\omega)\hat{\mathbf{E}}(\mathbf{r},\omega). \tag{G.51}$$

One can see that, because of the convolution there, when we discuss linear polarization, it is more accurate and convenient in the language of frequency space instead of the time domain. In the following, we still assume that the linear susceptibility $\hat{\chi}_{(1)}(\mathbf{r},\omega) = \hat{\chi}_{(1)}(\omega)$ is independent of the position $\mathbf{r}$. Then we can adopt the propagation equation in Eq. (G.10) and rewrite it as

$$\nabla^2\mathbf{E} - \frac{1}{c^2}\frac{\partial^2\mathbf{E}}{\partial t^2} = \mu_0\frac{\partial^2\mathbf{P}_{(1)}}{\partial t^2} + \mu_0\frac{\partial^2\mathbf{P}_{\rm NL}}{\partial t^2}. \tag{G.52}$$

Similarly, in frequency domain with

$$\hat{\mathbf{P}}_{\rm NL}(\mathbf{r},\omega) = \frac{1}{\sqrt{2\pi}}\int_{-\infty}^{\infty}\mathbf{P}_{\rm NL}(\mathbf{r},t)\mathrm{e}^{-i\omega t}dt,$$

Eq. (G.11) changes to be

$$\nabla^2\hat{\mathbf{E}} + \frac{\omega^2}{c^2}\hat{\mathbf{E}} = -\mu_0\omega^2\hat{\mathbf{P}}_{(1)} - \mu_0\omega^2\hat{\mathbf{P}}_{\rm NL}. \tag{G.53}$$

This can be simplified by substituting Eq. (G.51) into the equations above,

$$\nabla^2\hat{\mathbf{E}} + \frac{\omega^2}{c^2}\left(1+\hat{\chi}_{(1)}\right)\hat{\mathbf{E}} = -\mu_0\omega^2\hat{\mathbf{P}}_{\rm NL}. \tag{G.54}$$

As defined before, we use

$$k^2(\omega) = \frac{\omega^2}{c^2}\left(1+\hat{\chi}_{(1)}\right) \tag{G.55}$$

to represent the dispersion from linear polarization. Accordingly, the propagation equation becomes

$$\nabla^2\hat{\mathbf{E}} + k^2(\omega)\hat{\mathbf{E}} = -\mu_0\omega^2\hat{\mathbf{P}}_{\rm NL}. \tag{G.56}$$

To get this equation from the exact one given in Eq. (G.6), two approximations are adopted: firstly, the linear polarization field is homogeneous; secondly, the nonlinear polarization field is small and can be treated perturbatively. If $\hat{\mathbf{P}}_{\rm NL}$ is comparable to $\hat{\mathbf{P}}_{(1)}$, it at least should be homogeneous as well.

The solutions for $\hat{\mathbf{P}}_{\rm NL} = 0$ have been given in Sec. G.2, with

$$\begin{aligned}\hat{\mathbf{E}}(\mathbf{r},\omega) &= \hat{\mathbf{E}}(\mathbf{0},\omega)e^{-i\mathbf{k}(\omega)\cdot\mathbf{r}},\\ \mathbf{E}(\mathbf{r},t) &= \frac{1}{\sqrt{2\pi}}\int_{-\infty}^{\infty}d\omega\hat{\mathbf{E}}(\mathbf{0},\omega)e^{i(\omega t-\mathbf{k}(\omega)\cdot\mathbf{r})}.\end{aligned}$$

When $\hat{\mathbf{P}}_{\rm NL} \neq 0$, there are no general solutions to Eq. (G.54) or Eq. (G.56). One can not get the spectrum $\hat{\mathbf{E}}(\mathbf{r},\omega)$ at $\mathbf{r}$ directly. To proceed, we first write the electric field in its

general form,

$$\mathbf{E}(\mathbf{r},t) = \frac{1}{\sqrt{2\pi}}\int_{-\infty}^{\infty} d\omega \hat{\mathbf{E}}(\mathbf{r},\omega)e^{i\omega t},$$

with $\hat{\mathbf{E}}(\mathbf{r},\omega)$ being an unknown function. However, no matter what kind of polarization is present, one can always write the spectrum at $\mathbf{r}$ as a multiplication of the spectrum at $\mathbf{r}=\mathbf{0}$ and a modification function

$$\hat{\mathbf{E}}(\mathbf{r},\omega) = \hat{\mathbf{E}}(\mathbf{0},\omega)e^{-i\beta(\mathbf{r},\omega)\cdot\mathbf{r}}. \tag{G.57}$$

In such a way, the time-dependent electric field reads

$$\mathbf{E}(\mathbf{r},t) = \frac{1}{\sqrt{2\pi}}\int_{-\infty}^{\infty} d\omega \hat{\mathbf{E}}(\mathbf{0},\omega)e^{i(\omega t-\beta(\mathbf{r},\omega)\cdot\mathbf{r})}. \tag{G.58}$$

Compared to the linear-polarization-only case, the $\mathbf{r}$-independent dispersion relation $\mathbf{k}(\omega)$ is replaced by a new dispersion relation $\beta(\mathbf{r},\omega)$ which may depend on $\mathbf{r}$ even for a homogeneous medium. The task remains is to solve or measure $\beta(\mathbf{r},\omega)$.

G.3.1.1 Slowly varying envelope approximation I

In order to proceed further in understanding, we separate the total dispersion into a linear-polarization contribution and a nonlinear-polarization contribution,

$$\beta(\mathbf{r},\omega) = \mathbf{k}(\omega) + [\beta(\mathbf{r},\omega)-\mathbf{k}(\omega)]. \tag{G.59}$$

We thus have

$$\begin{aligned}\mathbf{E}(\mathbf{r},t) &= \frac{1}{\sqrt{2\pi}}\int_{-\infty}^{\infty} d\omega \hat{\mathbf{E}}(\mathbf{0},\omega)e^{i(\omega t-\mathbf{k}(\omega)\cdot\mathbf{r})}e^{-i(\beta(\mathbf{r},\omega)-\mathbf{k}(\omega))\cdot\mathbf{r}} \\ &= \frac{1}{\sqrt{2\pi}}\int_{-\infty}^{\infty} d\omega \hat{\boldsymbol{\mathcal{A}}}(\mathbf{r},\omega)e^{i(\omega t-\mathbf{k}(\omega)\cdot\mathbf{r})},\end{aligned} \tag{G.60}$$

with

$$\hat{\boldsymbol{\mathcal{A}}}(\mathbf{r},\omega) = \hat{\mathbf{E}}(\mathbf{0},\omega)e^{-i(\beta(\mathbf{r},\omega)-\mathbf{k}(\omega))\cdot\mathbf{r}}. \tag{G.61}$$

The spectrum at position $\mathbf{r}$ is

$$\hat{\mathbf{E}}(\mathbf{r},\omega) = \hat{\boldsymbol{\mathcal{A}}}(\mathbf{r},\omega)e^{-i\mathbf{k}(\omega)\cdot\mathbf{r}}. \tag{G.62}$$

If $|\hat{\mathbf{P}}_{\mathrm{NL}}| \ll |\hat{\mathbf{P}}_{(1)}|$, one would expect that the new dispersion function $\beta(\mathbf{r},\omega)$ will not deviate from $\mathbf{k}(\omega)$ too much,

$$|\beta(\mathbf{r},\omega)-\mathbf{k}(\omega)| \ll \mathbf{1}. \tag{G.63}$$

Then $\hat{\boldsymbol{\mathcal{A}}}(\mathbf{r},\omega)$ would be slowly varying in space $\mathbf{r}$. Although they look similar to each other, the new function $\hat{\boldsymbol{\mathcal{A}}}(\mathbf{r},\omega)$ defined here is not the envelope function. Therefore, a slowly varying $\hat{\boldsymbol{\mathcal{A}}}(\mathbf{r},\omega)$ does not mean that the evolution of the spectrum is also slow as it is propagating through the medium. There are contributions from $\mathbf{k}(\omega)$ that stand for light absorption/amplification.

With Eq. (G.62), the spatial derivative of the spectrum is given as

$$\nabla^2\hat{\mathbf{E}} = \left(\nabla^2\hat{\boldsymbol{\mathcal{A}}} - i2\mathbf{k}(\omega)\nabla\cdot\hat{\boldsymbol{\mathcal{A}}} - k^2(\omega)\hat{\boldsymbol{\mathcal{A}}}\right)e^{-i\mathbf{k}(\omega)\cdot\mathbf{r}}.$$

Substituting into the propagation equation in Eq. (G.56), the $k^2(\omega)$ terms cancel with each other and give

$$\left(\nabla^2\hat{\boldsymbol{\mathcal{A}}} - i2\mathbf{k}(\omega)\nabla\cdot\hat{\boldsymbol{\mathcal{A}}}\right)e^{-i\mathbf{k}(\omega)\cdot\mathbf{r}} = -\mu_0\omega^2\hat{\mathbf{P}}_{\mathrm{NL}}. \tag{G.64}$$

We should mention that Eq. (G.64) is equivalent to Eq. (G.56) without any further approximation. For a slowly varying $\hat{\boldsymbol{\mathcal{A}}}(\mathbf{r},\omega)$ in space, one has

$$\left|\nabla^2\hat{\boldsymbol{\mathcal{A}}}\right| \ll \left|2\mathbf{k}(\omega)\nabla\cdot\hat{\boldsymbol{\mathcal{A}}}\right|.$$

Dropping the second-order derivative in space, one obtains the propagation equation for the slowly varying field:

$$i2\mathbf{k}(\omega)\nabla\cdot\hat{\boldsymbol{\mathcal{A}}}e^{-i\mathbf{k}(\omega)\cdot\mathbf{r}} = \mu_0\omega^2\hat{\mathbf{P}}_{\mathrm{NL}}. \tag{G.65}$$

Compared to Eq. (G.56), the second-order differential equation has been reduced to a first-order differential equation. However, both Eq. (G.56) and Eq. (G.65) have the same problem in finding a general solution in frequency space: the explicit form of the spectrum $\hat{\mathbf{P}}_{\mathrm{NL}}$, in general, is not available.

Going back to time domain from Eq. (G.65) is also complicated. There is no explicit relation between the two fields $\mathbf{E}(\mathbf{r},t)$ and $\boldsymbol{\mathcal{A}}(\mathbf{r},t)$ defined in time domain as

$$\mathbf{E}(\mathbf{r},t) = \frac{1}{\sqrt{2\pi}}\int_{-\infty}^{\infty} d\omega\hat{\boldsymbol{\mathcal{A}}}(\mathbf{r},\omega)e^{i(\omega t-\mathbf{k}(\omega)\cdot\mathbf{r})},$$

and

$$\boldsymbol{\mathcal{A}}(\mathbf{r},t) = \frac{1}{\sqrt{2\pi}}\int_{-\infty}^{\infty} d\omega\hat{\boldsymbol{\mathcal{A}}}(\mathbf{r},\omega)e^{i\omega t}.$$

Therefore, general analytical calculations for such an approach is applicable neither in time domain nor in frequency domain. So, one needs to find a new function that can make the inverse Fourier transform of the propagation equation available.

G.3.1.2 Slowly varying envelope approximation II

The difficulties for solving the slowly varying field above mainly come from the frequency-dependent relation between $\hat{\boldsymbol{\mathcal{A}}}(\mathbf{r},\omega)$ and $\mathbf{E}(\mathbf{r},\omega)$ in Eq. (G.62). This cue indicates that we should separate the dispersion $\mathbf{k}(\omega)$ into two parts ,

$$\mathbf{k}(\omega) = \mathbf{k}_0 + \mathbf{C}(\tilde{\omega}), \tag{G.66}$$

with $\mathbf{k}_0$ being the frequency-independent term and

$$\mathbf{C}(\tilde{\omega}) = \mathbf{k}_1\tilde{\omega} + \frac{\mathbf{k}_2}{2!}\tilde{\omega}^2 + \frac{\mathbf{k}_3}{3!}\tilde{\omega}^3 + ..., \tag{G.67}$$

the frequency-dependent term. Accordingly, one defines another field $\hat{\boldsymbol{\mathcal{E}}}(\mathbf{r},\omega)$ that satisfies

$$\hat{\mathbf{E}}(\mathbf{r},\omega) = \hat{\boldsymbol{\mathcal{E}}}(\mathbf{r},\omega)e^{-i\mathbf{k}_0\cdot\mathbf{r}}, \tag{G.68}$$

and

$$\hat{\boldsymbol{\mathcal{E}}}(\mathbf{r},\omega) = \hat{\boldsymbol{\mathcal{A}}}(\mathbf{r},\omega)e^{-i\mathbf{C}(\tilde{\omega})\cdot\mathbf{r}} = \hat{\mathbf{E}}(\mathbf{0},\omega)e^{-i(\beta(\mathbf{r},\omega)-\mathbf{k}_0)\cdot\mathbf{r}}. \tag{G.69}$$

Then we can express the electric field in time domain as

$$\mathbf{E}(\mathbf{r},t) = \frac{1}{\sqrt{2\pi}}\int_{-\infty}^{\infty} d\omega\hat{\boldsymbol{\mathcal{E}}}(\mathbf{r},\omega)e^{i(\omega t-\mathbf{k}_0\cdot\mathbf{r})} = \boldsymbol{\mathcal{E}}(\mathbf{r},t)e^{i(\omega_0 t-\mathbf{k}_0\cdot\mathbf{r})}, \tag{G.70}$$

with $\boldsymbol{\mathcal{E}}(\mathbf{r},t)$ the envelope function under frequency ω_0. It is an inverse Fourier transform of $\hat{\boldsymbol{\mathcal{E}}}(\mathbf{r},\omega)$ with the frequency being shifted by ω_0:

$$\boldsymbol{\mathcal{E}}(\mathbf{r},t) = \frac{1}{\sqrt{2\pi}}\int_{-\infty}^{\infty} d\tilde{\omega}\hat{\boldsymbol{\mathcal{E}}}(\mathbf{r},\tilde{\omega})e^{i\tilde{\omega}t}, \tag{G.71}$$

where $\tilde{\omega} = \omega - \omega_0$. With this new field representing the envelope function, Eq. (G.64) is replaced by

$$\left(\nabla^2\hat{\boldsymbol{\mathcal{E}}} - i2\mathbf{k}_0\nabla\cdot\hat{\boldsymbol{\mathcal{E}}}\right)e^{-i\mathbf{k}_0\cdot\mathbf{r}} + \left[k^2(\omega) - k_0^2\right]\hat{\boldsymbol{\mathcal{E}}}e^{-i\mathbf{k}_0\cdot\mathbf{r}} = -\mu_0\omega^2\hat{\mathbf{P}}_{\mathrm{NL}}. \tag{G.72}$$

Considering that the dispersion term is $k^2(\omega) = k_0^2 + 2\mathbf{k}_0\cdot\mathbf{C}(\tilde{\omega}) + \mathrm{C}^2(\tilde{\omega})$, Eq. (G.72) can be rewritten in the language of $\tilde{\omega}$ as

$$\left(\nabla^2\hat{\boldsymbol{\mathcal{E}}} - i2\mathbf{k}_0\nabla\cdot\hat{\boldsymbol{\mathcal{E}}}\right)e^{-i\mathbf{k}_0\cdot\mathbf{r}} + \left[2\mathbf{k}_0\cdot\mathbf{C}(\tilde{\omega}) + \mathrm{C}^2(\tilde{\omega})\right]\hat{\boldsymbol{\mathcal{E}}}e^{-i\mathbf{k}_0\cdot\mathbf{r}} = -\mu_0(\omega_0+\tilde{\omega})^2\hat{\mathbf{P}}_{\mathrm{NL}} \tag{G.73}$$

Furthermore, from Eq. (G.69), the first-order derivative of $\hat{\boldsymbol{\mathcal{E}}}$ yields

$$\nabla\cdot\hat{\boldsymbol{\mathcal{E}}} = \nabla\cdot\hat{\boldsymbol{\mathcal{A}}}e^{-i\mathbf{C}(\tilde{\omega})\cdot\mathbf{r}} - i\mathbf{C}(\tilde{\omega})\cdot\hat{\boldsymbol{\mathcal{E}}}, \tag{G.74}$$

and the second-order derivative of $\hat{\boldsymbol{\mathcal{E}}}$ gives

$$\nabla^2\hat{\boldsymbol{\mathcal{E}}} = \left(\nabla^2\hat{\boldsymbol{\mathcal{A}}} - i2\mathbf{C}(\tilde{\omega})\nabla\cdot\hat{\boldsymbol{\mathcal{A}}}\right)e^{-i\mathbf{C}(\tilde{\omega})\cdot\mathbf{r}} - C^2(\tilde{\omega})\hat{\boldsymbol{\mathcal{E}}}. \tag{G.75}$$

We first substitute the second-order derivative into Eq. (G.73) and multiply $e^{i\mathbf{k}_0\cdot\mathbf{r}}$ to both sides of the equation, resulting in

$$\begin{aligned}&\left(\nabla^2\hat{\boldsymbol{\mathcal{A}}} - i2\mathbf{C}(\tilde{\omega})\nabla\cdot\hat{\boldsymbol{\mathcal{A}}}\right)e^{-i(\mathbf{k}_0+\mathbf{C}(\tilde{\omega}))\cdot\mathbf{r}} - 2i\mathbf{k}_0\left[\nabla\cdot\hat{\boldsymbol{\mathcal{E}}} + i\mathbf{C}(\tilde{\omega})\cdot\hat{\boldsymbol{\mathcal{E}}}\right]e^{-i\mathbf{k}_0\cdot\mathbf{r}}\\ =\ & -\mu_0(\omega_0+\tilde{\omega})^2\hat{\mathbf{P}}_{\mathrm{NL}}.\end{aligned} \tag{G.76}$$

Then using the relation from the first-order derivatives $\nabla\cdot\hat{\boldsymbol{\mathcal{A}}}e^{-i\mathbf{C}(\tilde{\omega})\cdot\mathbf{r}} = \nabla\cdot\hat{\boldsymbol{\mathcal{E}}} + i\mathbf{C}(\tilde{\omega})\cdot\hat{\boldsymbol{\mathcal{E}}}$, one obtains the equation

$$\left(\nabla^2\hat{\boldsymbol{\mathcal{A}}} - i2\mathbf{C}(\tilde{\omega})\nabla\cdot\hat{\boldsymbol{\mathcal{A}}}\right)e^{-ik(\omega)\cdot\mathbf{r}} - i2\mathbf{k}_0\nabla\cdot\hat{\boldsymbol{\mathcal{A}}}e^{-ik(\omega)\cdot\mathbf{r}} = -\mu_0\omega^2\hat{\mathbf{P}}_{\mathrm{NL}}. \tag{G.77}$$

This equation is the same equation we derived before in Eq. (G.64). The only difference is that we have separated the dispersion $k(\omega)$ into a frequency-dependent part $\mathbf{C}(\tilde{\omega})$ and a frequency-independent part k_0.

Again, until now, all the derivations are accurate. Eq. (G.77) is equivalent to Eq. (G.56). To proceed, we make further approximations. However, unlike what we have done for Eq. (G.64) where only a slowly varying $\hat{\boldsymbol{\mathcal{A}}}$ is considered, here we also assume

$$|\mathbf{C}(\tilde{\omega})| \quad \ll \quad k_0, \text{ or, equivalently, } \tilde{\omega} \ll \omega_0. \tag{G.78}$$

These two extra approximations mean

$$-i2\mathbf{k}_0\nabla\cdot\hat{\boldsymbol{\mathcal{A}}}e^{-ik(\omega)\cdot\mathbf{r}} \quad = \quad -\mu_0\omega^2\hat{\mathbf{P}}_{\rm NL}, \tag{G.79}$$

or

$$\nabla\cdot\hat{\boldsymbol{\mathcal{E}}} + i\mathbf{C}(\tilde{\omega})\cdot\hat{\boldsymbol{\mathcal{E}}} \quad = \quad -i\frac{\mu_0\omega^2}{2k_0^2}\mathbf{k}_0\cdot\hat{\mathbf{P}}_{\rm NL}e^{i\mathbf{k}_0\cdot\mathbf{r}}. \tag{G.80}$$

As $\tilde{\omega} \ll \omega_0$, one can approximate

$$\omega^2 = (\omega_0+\tilde{\omega})^2 \approx \omega_0^2. \tag{G.81}$$

This results in the well-known propagation equation for a slowly varying envelope

$$\nabla\cdot\hat{\boldsymbol{\mathcal{E}}} + i\mathbf{C}(\tilde{\omega})\cdot\hat{\boldsymbol{\mathcal{E}}} \quad = \quad -i\frac{\mu_0\omega_0^2}{2k_0^2}\mathbf{k}_0\cdot\hat{\mathbf{P}}_{\rm NL}e^{i\mathbf{k}_0\cdot\mathbf{r}}. \tag{G.82}$$

In time domain, one has by inverse Fourier transform

$$\nabla\boldsymbol{\mathcal{E}} + \hat{C}\boldsymbol{\mathcal{E}} \quad = \quad -i\frac{\mu_0\omega_0^2}{2k_0^2}\mathbf{k}_0\cdot\boldsymbol{\mathcal{P}}_{\rm NL}, \tag{G.83}$$

with the operator $\hat{C}$ given as

$$\hat{C} \quad = \quad \sum_{s=1}^{\infty}(-i)^{s+1}\frac{k_{\rm s}}{s!}\frac{\partial^s}{\partial t^s} = k_1\frac{\partial}{\partial t} - i\frac{k_2}{2}\frac{\partial^2}{\partial t^2} - \frac{k_3}{6}\frac{\partial^3}{\partial t^3} + ..., \tag{G.84}$$

and the time-domain envelope of the nonlinear polarization field

$$\mathbf{P}_{\rm NL} \quad = \quad \boldsymbol{\mathcal{P}}_{\rm NL}e^{i(\omega_0 t - \mathbf{k}_0\cdot\mathbf{r})}. \tag{G.85}$$

From $\hat{C}$ we know that, in frequency space, a higher-order dispersion corresponds to higher-order terms in the Taylor series of $k(\omega)$; in time domain, they are represented by higher-order time derivatives of the envelope function.

Considering the case of light propagating along $\hat{z}$, the propagation equation is reduced to be

$$\frac{\partial\mathcal{E}}{\partial z} + \hat{C}\mathcal{E} \quad = \quad -i\frac{\mu_0\omega_0^2}{2k_0}\mathcal{P}_{\rm NL}. \tag{G.86}$$

If there is only s linear dispersion and all the higher-order dispersions are not significant,

one has

$$\frac{\partial \mathcal{E}}{\partial z} + k_1 \frac{\partial \mathcal{E}}{\partial t} = -i\frac{\mu_0 \omega_0^2}{2k_0}\mathcal{P}_{\mathrm{NL}}, \tag{G.87}$$

with $k_1 = 1/v_{\mathrm{g}}$. We know that the group velocity is independent of the frequency under linear dispersion, and one can transform to retarded time coordinates with

$$\tau = t - \frac{z}{v_{\mathrm{g}}}, \qquad z' = z.$$

Because

$$\begin{aligned} \frac{\partial}{\partial t} &= \frac{\partial}{\partial \tau}, \\ \frac{\partial}{\partial z} &= -k_1 \frac{\partial}{\partial \tau} + \frac{\partial}{\partial z'}, \end{aligned}$$

the propagation equation in retarded time is given as

$$\frac{\partial \mathcal{E}}{\partial z'} = -i\frac{\mu_0 \omega_0^2}{2k_0}\mathcal{P}_{\mathrm{NL}}. \tag{G.88}$$

We can see that the contributions from the group velocity terms have been canceled.

When higher-order dispersion are involved, the time derivatives change to be

$$\frac{\partial^s}{\partial t^s} = \frac{\partial^s}{\partial \tau^s}.$$

So, the propagation equation in Eq. (G.86) in retarded time domain is given as

$$\frac{\partial \mathcal{E}}{\partial z'} + \sum_{s=2}^{\infty} (-i)^{s+1} \frac{k_{\mathrm{s}}}{s!} \frac{\partial^s}{\partial \tau^s} a = -i\frac{\mu_0 \omega_0^2}{2k_0}\mathcal{P}_{\mathrm{NL}}. \tag{G.89}$$

We know that higher-order dispersions lead to group velocity dispersion. Therefore, for different carrier frequencies, the retarded time $\tau(\omega) = t - \frac{z}{v_{\mathrm{g}}(\omega)}$ would be different. However, for $\tilde{\omega} \ll \omega_0$, one can take $\tau(\omega) = \tau$ for all the frequency components within this narrow bandwidth.

As a summary of all the approximations we made until now, we list

1.

$$\nabla \cdot \mathbf{E} = 0 \text{ for } \begin{cases} \mathbf{P}_{(1)} \text{ being homogeneous and } \mathbf{P}_{\mathrm{NL}} \text{being small,} \\ \text{or} \\ \text{both } \mathbf{P}_{(1)} \text{ and } \mathbf{P}_{\mathrm{NL}} \text{ being homogeneous;} \end{cases} \tag{G.90}$$

2.

$$\nabla^2 \hat{\boldsymbol{\mathcal{A}}} = 0 \text{ for } \begin{cases} \mathbf{P}_{\mathrm{NL}} \text{ being small, such that } \beta(\mathbf{r},\omega) - \mathbf{k}(\omega) \ll \mathbf{1}, \\ \text{or} \\ \text{both } \mathbf{P}_{(1)} \text{ and } \mathbf{P}_{\mathrm{NL}} \text{ being homogeneous } [\beta(\mathbf{r},\omega) = \beta(\omega)]; \end{cases} \tag{G.91}$$

3.

$$C(\tilde{\omega})\nabla \cdot \hat{\boldsymbol{\mathcal{A}}} = 0 \text{ for } \begin{cases} |C(\tilde{\omega})| \ll k_0 \text{ or } \tilde{\omega} \ll \omega_0, \\ \text{or} \\ \mathbf{k}(\omega) \approx \mathbf{k_0} \text{ or } \tilde{\omega} \ll \omega_{\mathbf{0}}. \end{cases} \tag{G.92}$$

Especially, the condition $\tilde{\omega} \ll \omega_0$ indicates that the bandwidth of the light field should be much smaller compared to the carrier frequency.

G.3.1.3 Slowly varying envelope approximation III

The propagation equation above is only applicable to a light field with a slowly varying envelope. In other words, the relative bandwidth is much smaller than one. For ultrashort pulses, especially few-cycle pulses, the relative bandwidth becomes closer to unity. Eq. (G.86) and Eq. (G.89) are not sufficient to describe the propagation effects anymore. We need to look for a different approach beyond the slowly varying envelope approximation, or beyond narrow bandwidth approximation.

This can be started by taking into account the first-order dispersion in $k(\omega)$:

$$\mathbf{k}(\omega) = \mathbf{k}_0 + \mathbf{k}_1\tilde{\omega} + \mathbf{F}(\tilde{\omega}), \tag{G.93}$$

with

$$\mathbf{F}(\tilde{\omega}) = \frac{\mathbf{k}_2}{2!}\tilde{\omega}^2 + \frac{\mathbf{k}_3}{3!}\tilde{\omega}^3 + ... \tag{G.94}$$

Then, Eq. (G.68) is replaced by

$$\hat{\mathbf{E}}(\mathbf{r},\omega) \;=\; \hat{\boldsymbol{\mathcal{B}}}(\mathbf{r},\omega)e^{-i(\mathbf{k}_0+\mathbf{k}_1\tilde{\omega})\cdot\mathbf{r}}, \tag{G.95}$$

with

$$\hat{\boldsymbol{\mathcal{B}}}(\mathbf{r},\omega) \;=\; \hat{\boldsymbol{\mathcal{E}}}(\mathbf{r},\omega)e^{i\tilde{\omega}\mathbf{k}_1\cdot\mathbf{r}} = \hat{\boldsymbol{\mathcal{A}}}(\mathbf{r},\omega)e^{-i\mathbf{F}(\tilde{\omega})\cdot\mathbf{r}} = \hat{\mathbf{E}}(\mathbf{0},\omega)e^{-i(\beta(\mathbf{r},\omega)-\mathbf{k}_0-\mathbf{k}_1\tilde{\omega})\cdot\mathbf{r}}. \tag{G.96}$$

Then substituting Eq. (G.95) into Eq. (G.56), the Eq. (G.64) and Eq. (G.72) are replaced

by

$$\begin{aligned} &\left(\nabla^2\hat{\boldsymbol{\mathcal{B}}} - i2(\mathbf{k}_0+\mathbf{k}_1\tilde{\omega})\nabla\cdot\hat{\boldsymbol{\mathcal{B}}}\right)e^{-i(\mathbf{k}_0+\mathbf{k}_1\tilde{\omega})\cdot\mathbf{r}} + \left[k^2(\omega) - (\mathbf{k}_0+\mathbf{k}_1\tilde{\omega})^2\right]\hat{\boldsymbol{\mathcal{B}}}e^{-i(\mathbf{k}_0+\mathbf{k}_1\tilde{\omega})\cdot\mathbf{r}} \\ = \;& -\mu_0\omega^2\hat{\mathbf{P}}_{\rm NL}. \end{aligned} \tag{G.97}$$

Following the same procedure for $\hat{\boldsymbol{\mathcal{E}}}$, one obtains another form of Eq. (G.64) and Eq. (G.77):

$$\left(\nabla^2\hat{\boldsymbol{\mathcal{A}}} - i2\mathbf{F}(\tilde{\omega})\nabla\cdot\hat{\boldsymbol{\mathcal{A}}}\right)e^{-i\mathbf{k}(\omega)\cdot\mathbf{r}} - i2(\mathbf{k}_0+\mathbf{k}_1\tilde{\omega})\nabla\cdot\hat{\boldsymbol{\mathcal{A}}}e^{-i\mathbf{k}(\omega)\cdot\mathbf{r}} = -\mu_0\omega^2\hat{\mathbf{P}}_{\rm NL}. \tag{G.98}$$

Similar to Eq. (G.77), the propagation equation Eq. (G.98) is also accurate without any approximation.

If all the higher-order dispersions are perturbative,

$$|\mathbf{F}(\tilde{\omega})| \ll k_0 + k_1\tilde{\omega}, \tag{G.99}$$

one can drop the first term in Eq. (G.98) and obtain

$$-i2(\mathbf{k}_0+\mathbf{k}_1\tilde{\omega})\nabla\cdot\hat{\boldsymbol{\mathcal{A}}}e^{-i\mathbf{k}(\omega)\cdot\mathbf{r}} = -\mu_0\omega^2\hat{\mathbf{P}}_{\rm NL}. \tag{G.100}$$

With $\nabla\cdot\hat{\boldsymbol{\mathcal{A}}} = \left(\nabla\cdot\hat{\boldsymbol{\mathcal{B}}} + i\mathbf{F}(\tilde{\omega})\cdot\hat{\boldsymbol{\mathcal{B}}}\right)e^{i\mathbf{F}(\tilde{\omega})\cdot\mathbf{r}}$, one gets

$$\nabla\cdot\hat{\boldsymbol{\mathcal{B}}} + i\mathbf{F}(\tilde{\omega})\cdot\hat{\boldsymbol{\mathcal{B}}} = -i\frac{\mu_0\omega^2}{2(k_0+k_1\tilde{\omega})^2}(\mathbf{k}_0+\mathbf{k}_1\tilde{\omega})\cdot\hat{\mathbf{P}}_{\rm NL}e^{i(\mathbf{k}_0+\mathbf{k}_1\tilde{\omega})\cdot\mathbf{r}}. \tag{G.101}$$

The complex forms in $\tilde{\omega}$ on the right-hand-side of the above equation makes it difficult to have a simple inverse Fourier transform. Therefore, we need further approximations based on

$$\begin{aligned} k_0 + k_1\tilde{\omega} &= \frac{\omega_0}{v_{\rm p}(\omega_0)} + \frac{\tilde{\omega}}{v_{\rm g}(\omega_0)} \\ &\approx \frac{1}{v_{\rm p}(\omega_0)}(\omega_0+\tilde{\omega}) \\ &= \frac{k_0}{\omega_0}(\omega_0+\tilde{\omega}). \end{aligned} \tag{G.102}$$

This argument is satisfied when $v_{\rm g}(\omega_0) \approx v_{\rm p}(\omega_0)$ or $\omega_0 \gg \tilde{\omega}$ is fulfilled. Then, one has

$$\nabla\cdot\hat{\boldsymbol{\mathcal{B}}} + \mathbf{F}(\tilde{\omega})\cdot\hat{\boldsymbol{\mathcal{B}}} = -\frac{i\mu_0\omega_0}{2k_0}\frac{(\omega_0+\tilde{\omega})}{(k_0+k_1\tilde{\omega})}(\mathbf{k}_0+\mathbf{k}_1\tilde{\omega})\cdot\hat{\mathbf{P}}_{\rm NL}e^{i(\mathbf{k}_0+\mathbf{k}_1\tilde{\omega})\cdot\mathbf{r}}. \tag{G.103}$$

By introducing another polarization field

$$\hat{\mathbf{Q}}_{\rm NL} = \frac{1}{(k_0+k_1\tilde{\omega})}(\mathbf{k}_0+\mathbf{k}_1\tilde{\omega})\cdot\hat{\mathbf{P}}_{\rm NL}e^{i\tilde{\omega}\mathbf{k}_1\cdot\mathbf{r}}, \tag{G.104}$$

the propagation equation is changed to a form

$$\nabla\cdot\hat{\boldsymbol{\mathcal{B}}} + \mathbf{F}(\tilde{\omega})\cdot\hat{\boldsymbol{\mathcal{B}}} = -\frac{i\mu_0\omega_0}{2k_0}(\omega_0+\tilde{\omega})\hat{\mathbf{Q}}_{\rm NL}\mathbf{e}^{\mathbf{i}\mathbf{k}_0\cdot\mathbf{r}}, \tag{G.105}$$

which can be easily transformed to the time domain:

$$\nabla \cdot \boldsymbol{\mathcal{B}} + \hat{\mathbf{F}} \cdot \boldsymbol{\mathcal{B}} = -\frac{i\mu_0\omega_0}{2k_0}\left(\omega_0 - i\frac{\partial}{\partial t}\right)\mathbf{Q}_{\rm NL}e^{i\mathbf{k}_0\cdot\mathbf{r}}. \tag{G.106}$$

The differential operator $\hat{F}$ is defined by

$$\hat{F} = \sum_{s=2}^{\infty}(-i)^{s+1}\frac{k_{\rm s}}{s!}\frac{\partial^s}{\partial t^s} = -i\frac{k_2}{2}\frac{\partial^2}{\partial t^2} - \frac{k_3}{6}\frac{\partial^3}{\partial t^3} + ..., \tag{G.107}$$

and the new polarization field in time domain is given as

$$\begin{aligned}\mathbf{Q}_{\rm NL}(\mathbf{r},t) &= \frac{1}{\sqrt{2\pi}}\int_{-\infty}^{\infty}d\tilde{\omega}\hat{\mathbf{Q}}_{\rm NL}(\mathbf{r},\tilde{\omega})\mathbf{e}^{\mathbf{i}\tilde{\omega}\mathbf{t}} \\ &= \frac{1}{\sqrt{2\pi}}\int_{-\infty}^{\infty}d\tilde{\omega}\hat{\mathbf{P}}_{\rm NL}(\mathbf{r},\tilde{\omega}).e^{i\tilde{\omega}\mathbf{k}_1\cdot\mathbf{r}}e^{i\tilde{\omega}t}.\end{aligned} \tag{G.108}$$

We know how to obtain $\mathbf{Q}_{\rm NL}(\mathbf{r},t)$ in terms of $\hat{\mathbf{P}}_{\rm NL}(\mathbf{r},t)$, however, there is no explicit relation between $\mathbf{Q}_{\rm NL}(\mathbf{r},t)$ and $\mathbf{P}_{\rm NL}(\mathbf{r},t)$.

In the one dimensional case,

$$\frac{\partial}{\partial z}\mathcal{B} + \hat{\rm D}\mathcal{B} = -\frac{i\mu_0\omega_0}{2k_0}\left(\omega_0 - i\frac{\partial}{\partial t}\right)Q_{\rm NL}e^{ik_0z}. \tag{G.109}$$

Compared to the equation obtained before, there is a time-derivative term for the nonlinear polarization. The group-velocity term is absent in a sense that we are in the retarded-time domain. This would be more clear if we notice the similarity between Eq. (G.109) and Eq. (G.89) in a way that, if we take

$$(\omega_0+\tilde{\omega})^2 = \omega_0^2 + 2\omega_0\tilde{\omega} + \tilde{\omega}^2 \approx \omega_0^2 + 2\omega_0\tilde{\omega} \tag{G.110}$$

instead of the approximation in Eq. (G.81), we find that Eq. (G.89) is replaced by

$$\frac{\partial}{\partial z'}a + \hat{\rm F}_\tau a = -\frac{i\mu_0\omega_0}{2k_0}\left(\omega_0 - i2\frac{\partial}{\partial \tau}\right)P_{\rm NL}e^{ik_0z}, \tag{G.111}$$

with

$$\hat{F}_\tau = \sum_{s=2}^{\infty}(-i)^{s+1}\frac{k_{\rm s}}{s!}\frac{\partial^s}{\partial \tau^s} = -i\frac{k_2}{2}\frac{\partial^2}{\partial \tau^2} - \frac{k_3}{6}\frac{\partial^3}{\partial \tau^3} + ... \tag{G.112}$$

The only difference is that there is a factor of 2 in the time derivative of nonlinear polarization in Eq. (G.111) compared to the term in Eq. (G.109).

G.3.2 Non-perturbative treatment

In the derivations before, we are working with slowly varying approximation in three different approaches, all of which are limited by the condition

$$\begin{aligned}|\beta(\omega) - \mathbf{k}(\omega)| &\ll |2\mathbf{k}(\omega)|, \text{ for } \hat{\boldsymbol{\mathcal{A}}}, \\ |\beta(\omega) - \mathbf{k}(\omega)|, |2\mathbf{C}(\tilde{\omega})| &\ll |2\mathbf{k}_0|, \text{ for } \hat{\boldsymbol{\mathcal{E}}}, \\ |\beta(\omega) - \mathbf{k}(\omega)|, |2\mathbf{F}(\tilde{\omega})| &\ll |2(\mathbf{k}_0 + \mathbf{k}_1\tilde{\omega})|, \text{ for } \hat{\boldsymbol{\mathcal{B}}}.\end{aligned}$$

These conditions are satisfied only if the nonlinear polarization is small compared to the linear polarization so that it does not change the dispersion of linear polarization too much.

However, either when nonlinear polarization is comparable to linear polarization, or when nonlinear dispersion is comparable to linear dispersion, the approximation will not be available any more. Depending on whether the total polarization can be separated into linear and nonlinear parts, one should solve the following equations directly:

$$\begin{aligned}
\nabla^2\hat{\mathbf{E}}+\frac{\omega^2}{c^2}\hat{\mathbf{E}} &= -\mu_0\omega^2\hat{\mathbf{P}}, \text{ for non-separable } \mathbf{P}\\
\nabla^2\mathbf{E}-\frac{1}{c^2}\frac{\partial^2\mathbf{E}}{\partial t^2} &= \mu_0\frac{\partial^2\mathbf{P}}{\partial t^2}, \text{ for non-separable } \mathbf{P}\\
&\text{and}\\
\nabla^2\hat{\mathbf{E}}+k^2(\omega)\hat{\mathbf{E}} &= -\mu_0\omega^2\hat{\mathbf{P}}_{\mathrm{NL}}, \text{ for separable } \mathbf{P}
\end{aligned}$$

G.4 Two-level system

From Sec. G.3.1.2 we know that the slowly varying envelope approximation holds only if $C(\omega)\ll k_0$. In the following, we check how this argument can be fulfilled when light is interacting with a set of two-level atoms. We assume that the light is linearly polarized and is propagating along $\hat{z}$.

The electric and polarization fields can be written in an integral of all their frequency components

$$\begin{aligned}
\mathrm{E}(z,t) &= \frac{1}{\sqrt{2\pi}}\int_{-\infty}^{\infty}d\omega\hat{\mathrm{E}}(z,\omega)e^{i\omega t},\\
\mathrm{P}(z,t) &= \frac{1}{\sqrt{2\pi}}\int_{-\infty}^{\infty}d\omega\hat{\mathrm{P}}(z,\omega)e^{i\omega t}.
\end{aligned}$$

Introducing a carrier frequency ω_0 and the corresponding envelope functions

$$\begin{aligned}
\mathrm{E}(z,t) &= \mathcal{E}(z,t)e^{i(\omega_0 t-k_0 z)}=\frac{1}{\sqrt{2\pi}}\int_{-\infty}^{\infty}\mathrm{d}\tilde{\omega}\hat{\mathcal{E}}(z,\tilde{\omega})e^{i\tilde{\omega}t}e^{i(\omega_0 t-k_0 z)},\\
\mathrm{P}(z,t) &= \mathcal{P}(z,t)e^{i(\omega_0 t-k_0 z)}=\frac{1}{\sqrt{2\pi}}\int_{-\infty}^{\infty}\mathrm{d}\tilde{\omega}\hat{\mathcal{P}}(z,\tilde{\omega})e^{i\tilde{\omega}t}e^{i(\omega_0 t-k_0 z)},
\end{aligned}$$

with $\tilde{\omega}=\omega-\omega_0$, we know the relations between the full spectrum and the envelope spectrum to be

$$\begin{aligned}
\hat{\mathrm{E}}(z,\omega) &= \hat{\mathcal{E}}(z,\tilde{\omega})e^{-ik_0 z},\\
\hat{\mathrm{P}}(z,\omega) &= \hat{\mathcal{P}}(z,\tilde{\omega})e^{-ik_0 z}.
\end{aligned}$$

In the following, we see how these relations may be broken if we introduce the slowly varying envelope approximation.

For two-level systems, if the populations of the two levels do not change significantly and can be taken as constants during interacting with the light field, the situation corresponds to the weak-field case as discussed in Chapter 6, and the system can be

described by linear polarization theory

$$\begin{aligned} \mathrm{P}(z,t) &= \varepsilon_0 \int_{-\infty}^{t} \chi(t-t')\mathrm{E}(z,t'), \\ \hat{\mathrm{P}}(z,\omega) &= \varepsilon_0 \hat{\chi}(\omega)\hat{\mathrm{E}}(z,\omega). \end{aligned}$$

Because the different frequency components are decoupled, from Eq. (G.33) we know that the accurate spectrum is given by

$$\hat{\mathrm{E}}(z,\omega) = \hat{\mathrm{E}}(0,\omega)e^{-i\frac{\omega}{c}\sqrt{1+\hat{\chi}(\omega)}z}. \tag{G.113}$$

However, if the populations change vastly during the interaction with light (see Chapter 7), all the frequencies are coupled to each other, and an analytical solution becomes difficult. In this situation, numerical simulations become important to understand the physics of light propagating in the medium. When the propagation distance is short (several wavelengths $z \sim \lambda$), one can just solve

$$\frac{\partial^2 \mathrm{E}(z,t)}{\partial z^2} - \frac{1}{c^2}\frac{\partial^2 \mathrm{E}(z,t)}{\partial t^2} = \mu_0 \frac{\partial^2 \mathrm{P}(z,t)}{\partial t^2}$$

together with the Bloch equations numerically and obtain an accurate result. However, if the length of the medium is long compared to the wavelength ($z \gg \lambda$), this approach is time consuming. Instead, one can solve equations for the envelope of the fields. Therefore, it is important to verify the slowly varying envelope approximation under given conditions.

G.4.1 SVEA

Usually, the light propagation equation under slowly varying envelope approximation is given by

$$\frac{\partial \mathcal{E}(z,t)}{\partial z} + \frac{1}{c}\frac{\partial \mathcal{E}(z,t)}{\partial t} = -i\frac{\mu_0\omega_0 c}{2}\mathcal{P}(z,t).$$

Compared to Eq. (G.83), all the higher-order dispersion effects have been neglected. In frequency domain, one has

$$\frac{\partial \hat{\mathcal{E}}(z,\tilde{\omega})}{\partial z} + i\frac{\tilde{\omega}}{c}\hat{\mathcal{E}}(z,\tilde{\omega}) = -i\frac{\mu_0\omega_0 c}{2}\hat{\mathcal{P}}(z,\tilde{\omega}). \tag{G.114}$$

We also only consider the linear polarization case

$$\hat{\mathcal{P}}(z,\tilde{\omega}) = \varepsilon_0 \hat{\chi}(\tilde{\omega})\hat{\mathcal{E}}(z,\tilde{\omega}).$$

This relation gives the propagation equation for the spectrum as

$$\frac{\partial \hat{\mathcal{E}}(z,\tilde{\omega})}{\partial z} = -\frac{i}{c}\left(\tilde{\omega} + \frac{\hat{\chi}(\tilde{\omega})\omega_0}{2}\right)\hat{\mathcal{E}}(z,\tilde{\omega}). \tag{G.115}$$

Therefore, the spectrum of the envelope function is solved as

$$\hat{\mathcal{E}}(z,\tilde{\omega}) = \hat{\mathcal{E}}(0,\tilde{\omega})e^{-\frac{i}{c}\left(\tilde{\omega}+\frac{\hat{\chi}(\tilde{\omega})\omega_0}{2}\right)z}.$$

Then, the full spectrum is recovered by

$$\begin{aligned}\hat{\mathrm{E}}(z,\omega) &= \hat{\mathcal{E}}(z,\tilde{\omega})e^{-ik_0 z} \\ &= \hat{\mathcal{E}}(0,\tilde{\omega})e^{-\frac{i}{c}\left(\tilde{\omega}+\frac{\hat{\chi}(\tilde{\omega})\omega_0}{2}\right)z}e^{-ik_0 z} \\ &= \hat{\mathrm{E}}(0,\tilde{\omega})e^{-\frac{i}{c}\left(\omega-\omega_0+\frac{\hat{\chi}(\tilde{\omega})\omega_0}{2}\right)z}e^{-ik_0 z} \\ &= \hat{\mathrm{E}}(0,\tilde{\omega})e^{-\frac{i}{c}\left(\omega+\frac{\hat{\chi}(\tilde{\omega})\omega_0}{2}\right)z}e^{i\frac{\omega_0}{c}z-ik_0 z}.\end{aligned}$$

Because $ck_0 = \omega_0$, and $\hat{\chi}(\omega) = \hat{\chi}(\tilde{\omega})$ for a given ω, one has

$$\hat{\mathrm{E}}(z,\omega) = \hat{\mathrm{E}}(0,\omega)e^{-\frac{i}{c}\left(\omega+\frac{\hat{\chi}(\omega)\omega_0}{2}\right)z} \tag{G.116}$$

In order to compare this spectrum to the accurate results in Eq. (G.113), one can expand the exponent in the accurate spectrum as

$$\sqrt{1+\hat{\chi}(\omega)} = 1+\frac{\hat{\chi}(\omega)}{2}-\frac{\hat{\chi}(\omega)^2}{8}+\frac{\hat{\chi}(\omega)^3}{16}+.... \tag{G.117}$$

When $\hat{\chi}(\omega) \ll 1$, one can only keep the first-order term,

$$\hat{\mathrm{E}}(z,\omega) = \hat{\mathrm{E}}(0,\omega)e^{-i\frac{\omega}{c}\left(1+\frac{\hat{\chi}(\omega)}{2}\right)z}. \tag{G.118}$$

Comparing the spectra in Eq. (G.116) and Eq. (G.118), one finds that they are almost the same, except for different frequency multipliers in front of the susceptibility.

Based on these results, a comparison between the accurate spectrum and the approximate spectrum can be performed based on whether the condition $\hat{\chi}(\omega) \ll 1$ is fulfilled or not.

Firstly, if $\hat{\chi}(\omega) \ll 1$ holds, the amplitudes of the spectrum can be approximated by the first-order term. However, the phase of the spectrum will be modified by higher-order terms at larger propagation distance because $\frac{\hat{\chi}(\omega)^2}{8}z \approx 1$ for large z. For the first order of $\hat{\chi}(\tilde{\omega})$ in Eq. (G.118), one has

$$\frac{\omega}{c}\frac{\hat{\chi}(\tilde{\omega})}{2}z = \frac{2\pi}{\lambda}\frac{\hat{\chi}(\tilde{\omega})}{2}z = \pi\frac{z}{\lambda}\hat{\chi}(\tilde{\omega}). \tag{G.119}$$

The effect of polarization shows up for a propagation distance

$$z = \frac{1}{\pi\hat{\chi}(\tilde{\omega})}\lambda. \tag{G.120}$$

If we have $\hat{\chi}(\tilde{\omega}) \sim 10^{-2}$, one has $z \sim 10^2\lambda$. Then, the second order term $-\frac{\hat{\chi}(\tilde{\omega})^2}{8}$ will be of effect for $z \sim 10^4\lambda$.

Secondly, if $\hat{\chi}(\omega) \gtrsim 1$, all the higher-order terms in Eq. (G.117)must be taken into account, and the slowly varying envelope approximation breaks down.

G.4.2 Susceptibility

The susceptibility is given as

$$\hat{\chi}(\tilde{\omega}) = -i\frac{\wp^2 n_{\mathcal{E}}}{\varepsilon_0\hbar}\Delta N\frac{1}{i\tilde{\omega}+\gamma}, \tag{G.121}$$

with $\Delta N \approx 1$ being the population inversion per atom. At resonance, one has

$$\hat{\chi}(0) = \frac{\wp^2 n_{\mathcal{E}}}{\varepsilon_0\hbar}\frac{i}{\gamma}. \tag{G.122}$$

Using relation

$$\gamma = \frac{8\pi^2\wp^2\omega_0^3}{3\varepsilon_0\hbar c^3}, \tag{G.123}$$

one obtains

$$\hat{\chi}(0) = \frac{3c^3}{8\pi^2\omega_0^3}n_{\mathcal{E}} = \frac{3\pi c^3}{\nu_0^3}n_{\mathcal{E}}. \tag{G.124}$$

The peak value of the susceptibility is proportional to the atomic density $n_{\mathcal{E}}$. For $\nu_0 = 3\times10^{15}$ Hz, $\hat{\chi}(0) = 1$ gives $n_{\mathcal{E}} = \frac{1}{3\pi}\times10^{21}$ m^{-3} or $n_{\mathcal{E}} = \frac{1}{3\pi}\times10^{15}$ cm^{-3}. For idea gas with concentration 1 mol per 22.4 L, the typical atom number density is around $\frac{6.02\times10^{23}}{22.4}\mathrm{L}^{-1} = 2.7\times10^{19}$ cm^{-3}.

For our X-ray lasing scheme, a photon energy of 920 eV gives a frequency $\nu_0 = 2.22\times10^{17}$ Hz, the corresponding atomic density is $n_{\mathcal{E}} = 4.3\times10^{19}$ cm^{-3}. The ionic density used in our simulation with $n_{\mathrm{ion}} = 3.5\times10^{18}$ cm^{-3} gives a ratio of 0.13 compared to $n_{\mathcal{E}}$. This means that slowly varying approximation in such a system is applicable.

G.5 Summary

In particular, the SVEA is valid only if the polarization field is small compared to the electric field of the light pulses that the dispersion (refractive index and loss/gain coefficient) does not change significantly. The differences between the results from SVEA and the accurate solution are discussed for two-level system. It shows that, for photon energy around 920 eV, SVEA is applicable when the density of the medium is well below 2.7×10^{19} cm^{-3}. For our X-ray lasing scheme with ionic density around 3.5×10^{18} cm^{-3}, SVEA is still a good approximation for the light propagation.

Bibliography

[1] J. P. Gordon, H. J. Zeiger, and C. H. Townes, "Molecular Microwave Oscillator and New Hyperfine Structure in the Microwave Spectrum of NH_3," Phys. Rev. **95**, 282 (1954).

[2] A. L. Schawlow and C. H. Townes, "Infrared and Optical Masers," Phys. Rev. **112**, 1940 (1958).

[3] T. H. Maiman, "Stimulated optical radiation in ruby," Nature **187**, 493 (1960).

[4] W. T. Silfvast, *Laser fundamentals* (Cambridge University Press, 2004).

[5] K. F. Renk, *Basics of laser physics* (Springer, 2012).

[6] M. Bertolotti, *Masers and lasers: an historical approach* (CRC Press, 2015).

[7] R. C. Elton, *X-ray Lasers* (Acadenic, 1990).

[8] J. J. Rocca, "Table-top soft x-ray lasers," Rev. Sci. Instrum. **70**, 3799 (1999).

[9] H. Daido, "Review of soft x-ray laser researches and developments," Rep. Prog. Phys. **65**, 1513 (2002).

[10] P. Jaeglé, *Coherent sources of XUV radiation* (Springer, 2006).

[11] S. Suckewer and P. Jaegle, "X-Ray laser: past, present, and future," Laser Phys. Lett. **6**, 411 (2009).

[12] D. Attwood and A. Sakdinawat, *X-rays and extreme ultraviolet radiation: principles and applications* (Cambridge University Press, 2017).

[13] D. L. Matthews, P. L. Hagelstein, M. D. Rosen, M. J. Eckart, N. M. Ceglio, A. U. Hazi, H. Medecki, B. J. MacGowan, J. E. Trebes, B. L. Whitten, E. M. Campbell, C. W. Hatcher, A. M. Hawryluk, R. L. Kauffman, L. D. Pleasance, G. Rambach, J. H. Scofield, G. Stone, and T. A. Weaver, "Demonstration of a Soft X-Ray Amplifier," Phys. Rev. Lett. **54**, 110 (1985).

[14] M. Rosen, P. Hagelstein, D. Matthews, E. Campbell, A. Hazi, B. Whitten, B. MacGowan, R. Turner, R. Lee, G. Charatis, *et al.*, "Exploding-foil technique for achieving a soft x-ray laser," Phys. Rev. Lett. **54**, 106 (1985).

[15] S. Suckewer, C. Skinner, H. Milchberg, C. Keane, and D. Voorhees, "Amplification of stimulated soft x-ray emission in a confined plasma column," Phys. Rev. Lett. **55**, 1753 (1985).

[16] H. Kapteyn, R. Lee, and R. Falcone, "Observation of a short-wavelength laser pumped by Auger decay," Phys. Rev. Lett. **57**, 2939 (1986).

[17] C. Chenais-Popovics, R. Corbett, C. Hooker, M. Key, G. Kiehn, C. Lewis, G. Pert, C. Regan, S. Rose, S. Sadaat, *et al.*, "Laser amplification at 18.2 nm in recombining plasma from a laser-irradiated carbon fiber," Phys. Rev. Lett. **59**, 2161 (1987).

[18] T. Lee, E. McLean, and R. Elton, "Soft x-ray lasing in neonlike germanium and copper plasmas," Phys. Rev. Lett. **59**, 1185 (1987).

[19] A. Carillon, H. Chen, P. Dhez, L. Dwivedi, J. Jacoby, P. Jaegle, G. Jamelot, J. Zhang, M. Key, A. Kidd, *et al.*, "Saturated and near-diffraction-limited operation of an XUV laser at 23.6 nm," Phys. Rev. Lett. **68**, 2917 (1992).

[20] B. MacGowan, L. Da Silva, D. Fields, C. Keane, J. Koch, R. London, D. L. Matthews, S. Maxon, S. Mrowka, A. Osterheld, *et al.*, "Short wavelength x-ray laser research at the Lawrence Livermore National Laboratory," Phys. Fluids B **4**, 2326 (1992).

[21] J. Rocca, V. Shlyaptsev, F. Tomasel, O. Cortazar, D. Hartshorn, and J. Chilla, "Demonstration of a discharge pumped table-top soft-x-ray laser," Phys. Rev. Lett. **73**, 2192 (1994).

[22] Y. Nagata, K. Midorikawa, S. Kubodera, M. Obara, H. Tashiro, and K. Toyoda, "Soft-x-ray amplification of the Lyman-α transition by optical-field-induced ionization," Phys. Rev. Lett. **71**, 3774 (1993).

[23] D. Korobkin, C. Nam, S. Suckewer, and A. Goltsov, "Demonstration of soft X-ray lasing to ground state in Li III," Phys. Rev. Lett. **77**, 5206 (1996).

[24] M. Duguay and P. Rentzepis, "Some Approaches to vacuum UV and x-ray lasers," Appl. Phys. Lett. **10**, 350 (1967).

[25] H. C. Kapteyn, "Photoionization-pumped x-ray lasers using ultrashort-pulse excitation," Appl. Opt. **31**, 4931 (1992).

[26] T. Axelrod, "Inner-shell photoionization-pumped x-ray lasers. Sulfur," Phys. Rev. A **13**, 376 (1976).

[27] G. L. Strobel, D. C. Eder, R. A. London, M. D. Rosen, R. W. Falcone, and S. Gordon, "Innershell photoionized x-ray laser schemes," in *Short-Pulse High-Intensity Lasers and Applications II*, Vol. 1860 (International Society for Optics and Photonics, 1993) pp. 157–167.

[28] J. Zhao, Q. Dong, S. Wang, L. Zhang, and J. Zhang, "X-ray lasers from Inner-shell transitions pumped by the Free-electron laser," Opt. Express **16**, 3546 (2008).

[29] N. Rohringer and R. London, "Atomic inner-shell x-ray laser pumped by an x-ray free-electron laser," Phys. Rev. A **80**, 013809 (2009).

[30] N. Rohringer, D. Ryan, R. A. London, M. Purvis, F. Albert, J. Dunn, J. D. Bozek, C. Bostedt, A. Graf, R. Hill, *et al.*, "Atomic inner-shell X-ray laser at 1.46 nanometres pumped by an X-ray free-electron laser," Nature **481**, 488 (2012).

[31] H. Yoneda, Y. Inubushi, K. Nagamine, Y. Michine, H. Ohashi, H. Yumoto, K. Yamauchi, H. Mimura, H. Kitamura, T. Katayama, *et al.*, "Atomic inner-shell laser at 1.5-ångströ mwavelength pumped by an X-ray free-electron laser," Nature **524**, 446 (2015).

[32] E. L. Saldin, E. Schneidmiller, and M. V. Yurkov, *The physics of free electron lasers* (Springer Science & Business Media, 2000).

[33] Z. Huang and K.-J. Kim, "Review of x-ray free-electron laser theory," Phys. Rev. Accel. Beams **10**, 034801 (2007).

[34] J. Als-Nielsen and D. McMorrow, *Elements of modern X-ray physics* (John Wiley & Sons, 2011).

[35] C. Pellegrini, A. Marinelli, and S. Reiche, "The physics of x-ray free-electron lasers," Rev. Mod. Phys. **88**, 015006 (2016).

[36] J. M. Madey, "Stimulated emission of bremsstrahlung in a periodic magnetic field," J. Appl. Phys **42**, 1906 (1971).

[37] D. A. Deacon, L. Elias, J. M. Madey, G. Ramian, H. Schwettman, and T. I. Smith, "First operation of a free-electron laser," Phys. Rev. Lett. **38**, 892 (1977).

[38] A. Kondratenko and E. Saldin, "Generating of coherent radiation by a relativistic electron beam in an ondulator," Part. Accel. **10**, 207 (1980).

[39] C. Pellegrini, "The history of X-ray free-electron lasers," Eur. Phys. J. H **37**, 659 (2012).

[40] R. Bonifacio, C. Pellegrini, and L. Narducci, "Collective instabilities and high-gain regime free electron laser," in *AIP Conference Proceedings*, Vol. 118 (AIP, 1984) pp. 236–259.

[41] J. Murphy and C. Pellegrini, "Generation of high-intensity coherent radiation in the soft-x-ray and vacuum-ultraviolet region," J. Opt. Soc. Am. B **2**, 259 (1985).

[42] C. Pellegrini, "Progress toward a soft X-ray FEL," Nucl. Instrum. Methods A **272**, 364 (1988).

[43] M. Hogan, C. Pellegrini, J. Rosenzweig, S. Anderson, P. Frigola, A. Tremaine, C. Fortgang, D. Nguyen, R. Sheffield, J. Kinross-Wright, *et al.*, "Measurements of Gain Larger than 10^5 at 12 μm in a Self-Amplified Spontaneous-Emission Free-Electron Laser," Phys. Rev. Lett. **81**, 4867 (1998).

[44] S. Milton, E. Gluskin, N. Arnold, C. Benson, W. Berg, S. Biedron, M. Borland, Y.-C. Chae, R. Dejus, P. Den Hartog, *et al.*, "Exponential gain and saturation of a self-amplified spontaneous emission free-electron laser," Science **292**, 2037 (2001).

[45] V. Ayvazyan, N. Baboi, I. Bohnet, R. Brinkmann, M. Castellano, P. Castro, L. Catani, S. Choroba, A. Cianchi, M. Dohlus, *et al.*, "Generation of GW radiation pulses from a VUV free-electron laser operating in the femtosecond regime," Phys. Rev. Lett. **88**, 104802 (2002).

[46] V. Ayvazyan, N. Baboi, I. Bohnet, R. Brinkmann, M. Castellano, P. Castro, L. Catani, S. Choroba, A. Cianchi, M. Dohlus, *et al.*, "A new powerful source for coherent VUV radiation: Demonstration of exponential growth and saturation at the TTF free-electron laser," Eur. Phys. J. D **20**, 149 (2002).

[47] V. Ayvazyan, N. Baboi, J. Bähr, V. Balandin, B. Beutner, A. Brandt, I. Bohnet, A. Bolzmann, R. Brinkmann, O. Brovko, *et al.*, "First operation of a free-electron laser generating GW power radiation at 32 nm wavelength," Eur. Phys. J. D **37**, 297 (2006).

[48] W. a. Ackermann, G. Asova, V. Ayvazyan, A. Azima, N. Baboi, J. Bähr, V. Balandin, B. Beutner, A. Brandt, A. Bolzmann, *et al.*, "Operation of a free-electron laser from the extreme ultraviolet to the water window," Nat. Photonics **1**, 336 (2007).

[49] M. E. Couprie, "New generation of light sources: Present and future," J. Electron Spectrosc. Relat. Phenom. **196**, 3 (2014).

[50] P. Emma, R. Akre, J. Arthur, R. Bionta, C. Bostedt, J. Bozek, A. Brachmann, P. Bucksbaum, R. Coffee, F.-J. Decker, *et al.*, "First lasing and operation of an ångstrom-wavelength free-electron laser," Nat. Photonics **4**, 641 (2010).

[51] T. Ishikawa, H. Aoyagi, T. Asaka, Y. Asano, N. Azumi, T. Bizen, H. Ego, K. Fukami, T. Fukui, Y. Furukawa, *et al.*, "A compact X-ray free-electron laser emitting in the sub-ångström region," Nat. Photonics **6**, 540 (2012).

[52] E. Allaria, R. Appio, L. Badano, W. Barletta, S. Bassanese, S. Biedron, A. Borga, E. Busetto, D. Castronovo, P. Cinquegrana, *et al.*, "Highly coherent and stable pulses from the FERMI seeded free-electron laser in the extreme ultraviolet," Nat. Photonics **6**, 699 (2012).

[53] H.-S. Kang, C.-K. Min, H. Heo, C. Kim, H. Yang, G. Kim, I. Nam, S. Y. Baek, H.-J. Choi, G. Mun, *et al.*, "Hard X-ray free-electron laser with femtosecond-scale timing jitter," Nat. Photonics **11**, 708 (2017).

[54] C. J. Milne, T. Schietinger, M. Aiba, A. Alarcon, J. Alex, A. Anghel, V. Arsov, C. Beard, P. Beaud, S. Bettoni, *et al.*, "SwissFEL: The Swiss X-ray free electron laser," Appl. Sci. **7**, 720 (2017).

[55] D. Wang, "Soft X-ray Free Electron Laser at SINAP," (2016).

[56] M. Altarelli, R. Brinkmann, M. Chergui, W. Decking, B. Dobson, S. Düsterer, G. Grübel, W. Graeff, H. Graafsma, J. Hajdu, *et al.*, "The European x-ray free-electron laser," Technical Design Report, DESY **97**, 1 (2007).

[57] C. Bostedt, H. N. Chapman, J. T. Costello, J. R. C. López-Urrutia, S. Düsterer, S. W. Epp, J. Feldhaus, A. Föhlisch, M. Meyer, T. Möller, *et al.*, "Experiments at FLASH," Nucl. Instrum. Methods A **601**, 108 (2009).

[58] M. N. Piancastelli, M. Simon, and K. Ueda, "Present trends and future perspectives for atomic and molecular physics at the new X-ray light sources," J. Electron Spectrosc. Relat. Phenom. **181**, 98 (2010).

[59] J. Feldhaus, M. Krikunova, M. Meyer, T. Möller, R. Moshammer, A. Rudenko, T. Tschentscher, and J. Ullrich, "AMO science at the FLASH and European XFEL free-electron laser facilities," J. Phys. B **46**, 164002 (2013).

[60] P. Bucksbaum and J. Glownia, "Ultrafast AMO physics at the LCLS x-ray FEL," in *EPJ Web of Conferences*, Vol. 57 (EDP Sciences, 2013) p. 04001.

[61] C. Bostedt, J. Bozek, P. Bucksbaum, R. Coffee, J. Hastings, Z. Huang, R. Lee, S. Schorb, J. Corlett, P. Denes, *et al.*, "Ultra-fast and ultra-intense x-ray sciences: first results from the Linac Coherent Light Source free-electron laser," J. Phys. B **46**, 164003 (2013).

[62] E. Seddon, J. Clarke, D. Dunning, C. Masciovecchio, C. Milne, F. Parmigiani, D. Rugg, J. Spence, N. Thompson, K. Ueda, *et al.*, "Short-wavelength free-electron laser sources and science: a review," Rep. Prog. Phys. **80**, 115901 (2017).

[63] W. Helml, A. Maier, W. Schweinberger, I. Grguraš, P. Radcliffe, G. Doumy, C. Roedig, J. Gagnon, M. Messerschmidt, S. Schorb, *et al.*, "Measuring the temporal structure of few-femtosecond free-electron laser X-ray pulses directly in the time domain," Nat. Photonics **8**, 950 (2014).

[64] S. Krinsky and R. Gluckstern, "Analysis of statistical correlations and intensity spiking in the self-amplified spontaneous-emission free-electron laser," Phys. Rev. Accel. Beams **6**, 050701 (2003).

[65] E. L. Saldin, E. A. Schneidmiller, and M. Yurkov, "Statistical and coherence properties of radiation from x-ray free-electron lasers," New J. Phys. **12**, 035010 (2010).

[66] A. McPherson, G. Gibson, H. Jara, U. Johann, T. S. Luk, I. McIntyre, K. Boyer, and C. K. Rhodes, "Studies of multiphoton production of vacuum-ultraviolet radiation in the rare gases," J. Opt. Soc. Am. B **4**, 595 (1987).

[67] M. Ferray, A. L'Huillier, X. Li, L. Lompre, G. Mainfray, and C. Manus, "Multiple-harmonic conversion of 1064 nm radiation in rare gases," J. Phys. B **21**, L31 (1988).

[68] K. Midorikawa, "High-order harmonic generation and attosecond science," Japanese J. Appl. Phys **50**, 090001 (2011).

[69] S. Corde, K. T. Phuoc, G. Lambert, R. Fitour, V. Malka, A. Rousse, A. Beck, and E. Lefebvre, "Femtosecond x rays from laser-plasma accelerators," Rev. Mod. Phys. **85**, 1 (2013).

[70] B. Dromey, M. Zepf, A. Gopal, K. Lancaster, M. Wei, K. Krushelnick, M. Tatarakis, N. Vakakis, S. Moustaizis, R. Kodama, *et al.*, "High harmonic generation in the relativistic limit," Nat. Phys. **2**, 456 (2006).

[71] B. Dromey, S. Kar, C. Bellei, D. Carroll, R. Clarke, J. Green, S. Kneip, K. Markey, S. Nagel, P. Simpson, *et al.*, "Bright multi-keV harmonic generation from relativistically oscillating plasma surfaces," Phys. Rev. Lett. **99**, 085001 (2007).

[72] T. Popmintchev, M.-C. Chen, D. Popmintchev, P. Arpin, S. Brown, S. Ališauskas, G. Andriukaitis, T. Balčiunas, O. D. Mücke, A. Pugzlys, *et al.*, "Bright coherent ultrahigh harmonics in the keV X-ray regime from mid-infrared femtosecond lasers," Science **336**, 1287 (2012).

[73] J. Miao, T. Ishikawa, I. K. Robinson, and M. M. Murnane, "Beyond crystallography: Diffractive imaging using coherent x-ray light sources," Science **348**, 530 (2015).

[74] C. Lyu, S. M. Cavaletto, C. H. Keitel, and Z. Harman, "Narrow-band hard-x-ray lasing," arXiv:1801.02503 (2018).

[75] B. W. Adams, C. Buth, S. M. Cavaletto, J. Evers, Z. Harman, C. H. Keitel, A. Pálffy, A. Picón, R. Röhlsberger, Y. Rostovtsev, *et al.*, "X-ray quantum optics," J. Mod. Opt. **60**, 2 (2013).

[76] F. Vagizov, V. Antonov, Y. Radeonychev, R. Shakhmuratov, and O. Kocharovskaya, "Coherent control of the waveforms of recoilless γ-ray photons," Nature **508**, 80 (2014).

[77] K. P. Heeg, A. Kaldun, C. Strohm, P. Reiser, C. Ott, R. Subramanian, D. Lentrodt, J. Haber, H.-C. Wille, S. Goerttler, *et al.*, "Spectral narrowing of x-ray pulses for precision spectroscopy with nuclear resonances," Science **357**, 375 (2017).

[78] J. Haber, X. Kong, C. Strohm, S. Willing, J. Gollwitzer, L. Bocklage, R. Rüffer, A. Pálffy, and R. Röhlsberger, "Rabi oscillations of X-ray radiation between two nuclear ensembles," Nat. Photonics **11**, 720 (2017).

[79] S. M. Cavaletto, Z. Harman, C. Ott, C. Buth, T. Pfeifer, and C. H. Keitel, "Broadband high-resolution X-ray frequency combs," Nat. Photonics **8**, 520 (2014).

[80] E. P. Kanter, B. Krässig, Y. Li, A. M. March, P. Ho, N. Rohringer, R. Santra, S. H. Southworth, L. F. DiMauro, G. Doumy, C. A. Roedig, N. Berrah, L. Fang, M. Hoener, P. H. Bucksbaum, S. Ghimire, D. A. Reis, J. D. Bozek, C. Bostedt, M. Messerschmidt, and L. Young, "Unveiling and Driving Hidden Resonances with High-Fluence, High-Intensity X-Ray Pulses," Phys. Rev. Lett. **107**, 233001 (2011).

[81] G. Doumy, C. Roedig, S.-K. Son, C. I. Blaga, A. D. DiChiara, R. Santra, N. Berrah, C. Bostedt, J. D. Bozek, P. H. Bucksbaum, J. P. Cryan, L. Fang, S. Ghimire, J. M. Glownia, M. Hoener, E. P. Kanter, B. Krässig, M. Kuebel, M. Messerschmidt, G. G. Paulus, D. A. Reis, N. Rohringer, L. Young, P. Agostini, and L. F. DiMauro, "Nonlinear Atomic Response to Intense Ultrashort X Rays," Phys. Rev. Lett. **106**, 083002 (2011).

[82] S. Bernitt, G. V. Brown, J. K. Rudolph, R. Steinbrügge, A. Graf, M. Leutenegger, S. W. Epp, S. Eberle, K. Kubiček, V. Mäckel, M. C. Simon, E. Träbert, E. W. Magee, C. Beilmann, N. Hell, S. Schippers, A. Müller, S. M. Kahn, A. Surzhykov, Z. Harman, C. H. Keitel, J. Clementson, F. S. Porter, W. Schlotter, J. J. Turner, J. Ullrich, P. Beiersdorfer, and J. R. Crespo López-Urrutia, "An unexpectedly low oscillator strength as the origin of the Fexvii emission problem," Nature **492**, 225 (2012).

[83] A. Authier, *Early days of X-ray crystallography* (OUP Oxford, 2013).

[84] C. Hammond and C. Hammond, *The Basics of Cristallography and Diffraction*, Vol. 214 (Oxford, 2001).

[85] J. D. Watson and F. H. Crick, "Molecular Structure of Nucleic Acids: A Structure for Deoxyribose Nucleic Acid," Nature **171**, 737 (1953).

[86] G. N. Hounsfield, "Computed medical imaging," Med. Phys. **7**, 283 (1980).

[87] D. Paganin, *Coherent X-ray optics* (Oxford University Press on Demand, 2006).

[88] S. Aoki, Y. Ichihara, and S. Kikuta, "X-ray hologram obtained by using synchrotron radiation," Japanese J. Appl. Phys **11**, 1857 (1972).

[89] I. McNulty, J. Kirz, C. Jacobsen, E. H. Anderson, M. R. Howells, and D. P. Kern, "High-resolution imaging by Fourier transform X-ray holography," Science **256**, 1009 (1992).

[90] M. Tegze and G. Faigel, "X-ray holography with atomic resolution," Nature **380**, 49 (1996).

[91] G. Faigel and M. Tegze, "X-ray holography," Rep. Prog. Phys. **62**, 355 (1999).

[92] J. Miao, P. Charalambous, J. Kirz, and D. Sayre, "Extending the methodology of X-ray crystallography to allow imaging of micrometre-sized non-crystalline specimens," Nature **400**, 342 (1999).

[93] S. M. Cavaletto, C. Buth, Z. Harman, E. P. Kanter, S. H. Southworth, L. Young, and C. H. Keitel, "Resonance fluorescence in ultrafast and intense x-ray free-electron-laser pulses," Phys. Rev. A **86**, 033402 (2012).

[94] P. Willmott, *An introduction to synchrotron radiation: techniques and applications* (John Wiley & Sons, 2011).

[95] H. N. Chapman, A. Barty, M. J. Bogan, S. Boutet, M. Frank, S. P. Hau-Riege, S. Marchesini, B. W. Woods, S. Bajt, W. H. Benner, *et al.*, "Femtosecond diffractive imaging with a soft-X-ray free-electron laser," Nat. Phys. **2**, 839 (2006).

[96] H. N. Chapman, S. P. Hau-Riege, M. J. Bogan, S. Bajt, A. Barty, S. Boutet, S. Marchesini, M. Frank, B. W. Woods, W. H. Benner, *et al.*, "Femtosecond time-delay X-ray holography," Nature **448**, 676 (2007).

[97] R. Moshammer, Y. Jiang, L. Foucar, A. Rudenko, T. Ergler, C. Schröter, S. Lüdemann, K. Zrost, D. Fischer, J. Titze, *et al.*, "Few-photon multiple ionization of Ne and Ar by strong free-electron-laser pulses," Phys. Rev. Lett. **98**, 203001 (2007).

[98] G. Lambert, T. Hara, D. Garzella, T. Tanikawa, M. Labat, B. Carre, H. Kitamura, T. Shintake, M. Bougeard, S. Inoue, *et al.*, "Injection of harmonics generated in gas in a free-electron laser providing intense and coherent extreme-ultraviolet light," Nat. Phys. **4**, 296 (2008).

[99] J. Amann, W. Berg, V. Blank, F.-J. Decker, Y. Ding, P. Emma, Y. Feng, J. Frisch, D. Fritz, J. Hastings, *et al.*, "Demonstration of self-seeding in a hard-X-ray free-electron laser," Nat. Photonics **6**, 693 (2012).

[100] D. Ratner, R. Abela, J. Amann, C. Behrens, D. Bohler, G. Bouchard, C. Bostedt, M. Boyes, K. Chow, D. Cocco, F. J. Decker, Y. Ding, C. Eckman, P. Emma, D. Fairley, Y. Feng, C. Field, U. Flechsig, G. Gassner, J. Hastings, P. Heimann, Z. Huang, N. Kelez, J. Krzywinski, H. Loos, A. Lutman, A. Marinelli, G. Marcus, T. Maxwell, P. Montanez, S. Moeller, D. Morton, H. D. Nuhn, N. Rodes, W. Schlotter, S. Serkez, T. Stevens, J. Turner, D. Walz, J. Welch, and J. Wu, "Experimental Demonstration of a Soft X-Ray Self-Seeded Free-Electron Laser," Phys. Rev. Lett. **114**, 054801 (2015).

[101] S. Huang, Y. Ding, Y. Feng, E. Hemsing, Z. Huang, J. Krzywinski, A. A. Lutman, A. Marinelli, T. J. Maxwell, and D. Zhu, "Generating Single-Spike Hard X-Ray Pulses with Nonlinear Bunch Compression in Free-Electron Lasers," Phys. Rev. Lett. **119**, 154801 (2017).

[102] K.-J. Kim, Y. Shvyd'ko, and S. Reiche, "A Proposal for an X-Ray Free-Electron Laser Oscillator with an Energy-Recovery Linac," Phys. Rev. Lett. **100**, 244802 (2008).

[103] O. Larroche, D. Ros, A. Klisnick, A. Sureau, C. Möller, and H. Guennou, "Maxwell-Bloch modeling of x-ray-laser-signal buildup in single-and double-pass configurations," Phys. Rev. A **62**, 043815 (2000).

[104] C. Weninger and N. Rohringer, "Transient-gain photoionization x-ray laser," Phys. Rev. A **90**, 063828 (2014).

[105] K. Dyall, I. Grant, C. Johnson, F. Parpia, and E. Plummer, "GRASP: A general-purpose relativistic atomic structure program," Comput. Phys. Commun. **55**, 425 (1989).

[106] H.-K. Chung, M. Chen, W. Morgan, Y. Ralchenko, and R. Lee, "FLYCHK: Generalized population kinetics and spectral model for rapid spectroscopic analysis for all elements," High Energy Density Phys. **1**, 3 (2005).

[107] M. O. Scully and M. S. Zubairy, *Quantum optics* (Cambridge University Press, 1997).

[108] J. D. Jackson, *Electrodynamics* (Wiley Online Library, 1975).

[109] A. Weiner, *Ultrafast optics* (John Wiley & Sons, 2011).

[110] J. J. Sakurai and J. Napolitano, *Modern quantum mechanics* (Pearson Education, London, 2006).

[111] K. Blum, *Density matrix theory and applications* (Springer Science & Business Media, 1981).

[112] D. F. Walls and G. J. Milburn, *Quantum optics* (Springer Science & Business Media, 2007).

[113] M. Wollenhaupt, T. Bayer, and T. Baumert, "Control of ultrafast electron dynamics with shaped femtosecond laser pulses: from atoms to solids," in *Ultrafast Dynamics Driven by Intense Light Pulses* (Springer, 2016) pp. 63–122.

[114] C. J. Foot, *Atomic physics* (Oxford University Press, 2005).

[115] W. R. Johnson, *Atomic structure theory* (Springer, 2007).

[116] R. A. Satten, "Effects of atomic quadrupole moments upon the index of refraction," J. Chem. Phys. **26**, 766 (1957).

[117] A. Buckingham and M. Dunn, "Optical activity of oriented molecules," J. Chem. Soc. A **0**, 1988 (1971).

[118] E. Graham, J. Pierrus, and R. Raab, "Multipole moments and Maxwell's equations," J. Phys. B **25**, 4673 (1992).

[119] R. I. Slavchov and T. I. Ivanov, "Quadrupole terms in the Maxwell equations: Born energy, partial molar volume, and entropy of ions," J. Chem. Phys. **140**, 074503 (2014).

[120] R. I. Slavchov, "Quadrupole terms in the Maxwell equations: Debye-Hückel theory in quadrupolarizable solvent and self-salting-out of electrolytes," J. Chem. Phys. **140**, 074503 (2014).

[121] H. R. Griem, A. C. Kolb, and K. Shen, "Stark broadening of hydrogen lines in a plasma," Phys. Rev. **116**, 4 (1959).

[122] H. R. Griem and K. Shen, "Stark broadening of hydrogenic ion lines in a plasma," Phys. Rev. **122**, 1490 (1961).

[123] H. Griem, M. Baranger, A. Kolb, and G. Oertel, "Stark broadening of neutral helium lines in a plasma," Phys. Rev. **125**, 177 (1962).

[124] H. R. Griem, "Electron-Impact Broadening of Isolated Ion Lines," Phys. Rev. Lett. **17**, 509 (1966).

[125] H. R. Griem, *Spectral line broadening in Plasmas* (Acadamic, New York, 1974).

[126] H. R. Griem, *Principles of plasma spectroscopy* (Cambridge University Press, 2005).

[127] G. Peach, "Collisional broadening of spectral lines," in *Springer Handbook of Atomic, Molecular, and Optical Physics* (Springer, 2006) pp. 875–888.

[128] H. A. Bethe and E. E. Salpeter, *Quantum mechanics of one-and two-electron atoms* (Springer Science & Business Media, 1957).

[129] H. F. Beyer and V. P. Shevelko, *Introduction to the physics of highly charged ions* (CRC Press, 2003).

[130] J. Holtsmark, Ann. Phys. (Leipzig) **58**, 577 (1919).

[131] J. A. Koch, B. J. MacGowan, L. B. Da Silva, D. L. Matthews, J. H. Underwood, P. J. Batson, and S. Mrowka, "Observation of gain-narrowing and saturation behavior in Se x-ray laser line profiles," Phys. Rev. Lett. **68**, 3291 (1992).

[132] T. Tanimoto, H. Habara, R. Kodama, M. Nakatsutsumi, K. A. Tanaka, K. Lancaster, J. Green, R. Scott, M. Sherlock, P. A. Norreys, *et al.*, "Measurements of fast electron scaling generated by petawatt laser systems," Phys. Plasmas **16**, 062703 (2009).

[133] P. Nilson, J. Davies, W. Theobald, P. Jaanimagi, C. Mileham, R. Jungquist, C. Stoeckl, I. Begishev, A. Solodov, J. Myatt, *et al.*, "Time-resolved measurements of hot-electron equilibration dynamics in high-intensity laser interactions with thin-foil solid targets," Phys. Rev. Lett. **108**, 085002 (2012).

[134] Y. Ping, R. Shepherd, B. Lasinski, M. Tabak, H. Chen, H. Chung, K. Fournier, S. Hansen, A. Kemp, D. Liedahl, *et al.*, "Absorption of short laser pulses on solid targets in the ultrarelativistic regime," Phys. Rev. Lett. **100**, 085004 (2008).

[135] C. Danson, D. Hillier, N. Hopps, and D. Neely, "Petawatt class lasers worldwide," High Power Laser Sci. Eng. **3** (2015).

[136] V. Krainov and M. Smirnov, "Cluster beams in the super-intense femtosecond laser pulse," Phys. Rep. **370**, 237 (2002).

[137] A. Pálffy, J. Evers, and C. H. Keitel, "Electric-dipole-forbidden nuclear transitions driven by super-intense laser fields," Phys. Rev. C **77**, 044602 (2008).

[138] H. R. Griem and K. Y. Shen, "Stark Broadening of Hydrogenic Ion Lines in a Plasma," Phys. Rev. **122**, 1490 (1961).

[139] S. Bastiani-Ceccotti, N. Kontogiannopoulos, J.-R. Marques, S. Tzortzakis, L. Lecherbourg, F. Thais, I. Matsushima, O. Peyrusse, and C. Chenais-Popovics, "Analysis of the X-ray and time-resolved XUV emission of laser produced Xe and Kr plasmas," High Energy Density Phys. **3**, 20 (2007).

[140] S. Bastiani-Ceccotti, A.-C. Bourgaux, C. Bowen, F. Dorchies, F. Gilleron, J.-R. Marquès, J.-C. Pain, V. Silvert, and T. Vinci, "Analysis of X-ray and Thomson scattering data from non-LTE Nb and Ta plasmas," High Energy Density Phys. **16**, 41 (2015).

[141] D. Hoarty, N. Sircombe, P. Beiersdorfer, C. D. Brown, M. Hill, L. R. Hobbs, S. James, J. Morton, E. Hill, M. Jeffery, *et al.*, "Modelling K shell spectra from short pulse heated buried microdot targets," High Energy Density Phys. **23**, 178 (2017).

[142] O. Peyrusse, "A superconfiguration model for broadband spectroscopy of non-LTE plasmas," J. Phys. B **33**, 4303 (2000).

[143] "http://aphysics2.lanl.gov/cgi-bin/ION/runlanl08f.pl," LANL Atomic Physics Codes .

[144] J. Olivero and R. Longbothum, "Empirical fits to the Voigt line width: A brief review," J. Quant. Spectrosc. Radiat. Transf. **17**, 233 (1977).

[145] E. Graham and R. Raab, "Light propagation in cubic and other anisotropic crystals," Proc. R. Soc. Lond. A **430**, 593 (1990).

[146] P. Gibbon, *Short pulse laser interactions with matter* (World Scientific Publishing Company, 2004).

[147] T. J. M. Boyd and J. J. Sanderson, *The physics of plasmas* (Cambridge University Press, 2003).

[148] W. Kruer, *The Physics Of Laser Plasma Interactions (Frontiers in Physics)* (Westview Press, 2003).

Acknowledgements

I would like to thank my supervisor Honorarprof. Christoph H. Keitel for providing me such a good chance to work in his excellent group at the Max-Plank-Institute für Kernphysik. Looking at the contents of this thesis, I can not imaging how it may look like without the advise from him and the other group members. Discussing with him is always fruitful and pleasant. Back in the autumn of 2014 when we first had the idea of this project, Christoph was the one who insisted mostly to use a density-matrix theory instead of the rate equations to study the lasing process, which became the main part of Chapter 2. Now we know clearly that the rate-equation approach is not applicable in describing our transient lasers. Furthermore, it is also him who pointed out the significance of spectral broadening effects in plasmas, leading to our discussions in Chapter 4. Besides, his generous financial support on attending conferences and summer schools has engaged me with the opportunity to broaden visions in the X-ray and the ultrafast science. All these are lifelong resources for my scientific career in the future. Vielen Dank.

I am very grateful for Zoltán Harman and Stefano M. Cavaletto who have kept giving endless support during the last four years, both in science and in life. They conceived the underlying scheme of this project and engaged in almost every single aspect of the thesis. Even now, in such a sunny weekend, they are still proofreading some of the Chapters for me. So many times we got together to discuss and solve the puzzles encountered in physics. Their cautious attitude in work and perseverance in faith impressed and encouraged me from time to time.

I am always enlightened by Zoltán's broad background, brilliant ideas and insistence in achieving goals. Just to list a few, in the very beginning of this project, we are looking for a gain medium based on highly charged ions in the EBIT. However, the ion density turned out to be too low, then he suggested to use ions in laser-produced plasmas that I could never think of. Furthermore, when we realized that the $E1$ transitions from Ne^{8+} only provides a 4-fold reduction in bandwidth compared to other schemes, again, it is him who proposed to use heavier elements like Ar, Kr and Xe with $E2$ and $M2$ transitions, which makes our lasing scheme more superior than others. His endeavor on this project encouraged me to keep moving forward. In particular, Zoltán trained me the atomic structure calculations. Books, references and atomic structure codes suggested by him had become the mathematical and physical foundations of this thesis.

Stefano and I had plenty of discussions on the Maxwell–Bloch equations and their analytical solutions. For a time, I was confused about different variants of these equations. Our discussions made the theory clear to us. When we had problems in analyzing our numerical results, Stefano had spent a lot of time to discuss with me. In particular, he encouraged me to find approximate analytical solutions which turned out to be very insightful and inspired the contents discussed in the last two Chapters of this thesis.

Moreover, I am very appreciate the help from Zoltán and Stefano on improving my English writing. And I promise you I will become better. Working with them, it is like a journey to the wild world. At the beginning you may not foresee what you will experience. But at the end, you will know it is the struggles that bring you to this fantastic vision. They are my tutors, but they are more like my friends.

In the work presented in this thesis, I also received help from Jonas Gunst, Matteo Tamburini, Suo Tang and Yuanbin Wu on the subject of laser-produced plasma. I would like to thank them for their efforts. Particularly, I would like to thank Yuangbin Wu for teaching me FLYCHK simulations. Besides, I would also like to thank Jörg Evers for introducing me to the nonlinear wave propagation equations, thank Xiangjin Kong and Bin Yang for discussions about quantum optics, and thank Bastian Sikora for proofreading parts of the thesis.

I am very proud to be a member of Zoltán's group, as we always support each other. I would like to thank Zoltán, Stefano, Natalia Oreshkina, Vincent Debierre, Halil Cakir, Niklas Michel, Bastian Sikora and Siddhartha Chattopadhyay for their kind help in proofreading our manuscript before submission. I am also very grateful for their help in presenting our work at group seminars.

I would like to thank Alessandro Angioi, Shikha Bhadoria, Jiří Daněk, Niklas Michel, Bastian Sikora, Pavlo Bilous, Maitreyi Sangal, Archana Sampath and Sergei Kobzak, for their friendly help in the daily life. Thank Sibel Babacan and Zoila Eisenhauer for their work on office documents and computers.

I would also like to thank Jianxing Li, Meng Wen, Luling Jin, Yue-Yue Chen, Suo Tang, Xiangjin Kong, Lida Zhang, Yuanbin Wu, Yifan Liu, Yonghao Mi, Ruoyu Liu, Zuoye Liu, Huipeng Kang, Yanwei Li, Xueguang Ren, Ni Cui and Helen Poon. They provide me a pleasant life in living in Heidelberg.

Lastly, special thanks are given to my love Li Han, my parents Yongju Xu and Jicheng Lyu for their selfless support.